Modal Analysis Applied to the Stability Study of Hydroelectric Systems with Modular Structures

THÈSE N^{O} 6780 (2015)

PRÉSENTÉE LE 6 NOVEMBRE 2015

À LA FACULTÉ DES SCIENCES ET TECHNIQUES DE L'INGÉNIEUR
GROUPE DE SCIENTIFIQUES STI
PROGRAMME DOCTORAL EN ENERGIE

ÉCOLE POLYTECHNIQUE FÉDÉRALE DE LAUSANNE

POUR L'OBTENTION DU GRADE DE DOCTEUR ÈS SCIENCES

PAR

Pedro Camilo DE OLIVEIRA E SILVA

acceptée sur proposition du jury:

Prof. A. Rufer, président du jury
Dr B. Kawkabani, directeur de thèse
Prof. E. da Costa Bortoni, rapporteur
Dr A. Schwery, rapporteur
Dr R. Cherkaoui, rapporteur

ÉCOLE POLYTECHNIQUE
FÉDÉRALE DE LAUSANNE

Suisse
2015

Tout notre raisonnement
se réduit à céder au sentiment.
— Blaise Pascal

A meus pais, que me deram vida, amor e muito mais.

Abstract

Power plants experience distinct dynamic behaviors according to the primary source of energy. Whereas thermal power plants have a slow dynamic, modern renewables such as wind and solar PV are subject to very fast variations, due to environmental factors. Therefore, their availability is not guaranteed.

Consequently, it is opportune to take advantage of the intrinsic flexibility of hydropower plants for balancing fast variations caused by modern renewable sources, in order to keep stability and reliability of the power grid. On the other hand, the use of hydropower plants as means of compensating constant variations between electricity generation and consumption leads to off-design operation. Such condition may cause instabilities or undesirable oscillations in the power plant whose origin lies in the hydraulic system. Furthermore, small hydropower plants play a major role in the development of emerging countries, where they may be frequently subjected to islanded or isolated operation. In such context, operating conditions are more critical in terms of reliability and stability.

Considering these factors, one can readily understand the importance of predicting the dynamic behavior of power plants under various scenarios and different operating modes. This requires precise, comprehensive mathematical models and efficient computational tools, which are appropriate for planning new installations and better exploiting the existing ones.

Thereupon, the purpose of the present work is the development of a novel tool for small-signal stability analysis of hydroelectric systems, with comprehensive modeling of both electrical and hydraulic elements of a hydropower plant. This tool is implemented in SIMSEN, a fully modular, efficient, user-friendly software developed at EPFL, for the simulation of electrical

power networks and hydroelectric systems.

The originality of this new tool lies not only on the exhaustive and detailed modeling of electrical and hydraulic systems (a multi-physics representation). It lies also on the fact that it is a modular tool, capable of treating systems with any given topology, with automatic generation of the full set of differential equations, based on circuits easily built in an user-friendly GUI.

Another distinctive characteristic of the present work is that small-signal models of electrical elements are based on *a,b,c*-phase variables, different from the traditional *d,q,o*-axis representation. The procedure to be followed for the derivation of such models is presented in this document.

Furthermore, case studies performed with this tool show that substantial interactions happen between electrical, mechanical, hydraulic and regulation elements. These interactions can be either positive or detrimental to the stability of the system. In case of adverse interactions, unstable behaviors may occur. Such instabilities cannot be predicted without a comprehensive, multi-physics model. These conflicting interactions are presented, and their consequences and possible solutions are discussed in this document.

Keywords: Small-signal stability, eigenanalysis, eigenvalues, eigenvectors, modal analysis, hydroelectric power, hydropower plants, power system stability, power system dynamics.

Résumé

Les centrales électriques subissent des comportements dynamiques distincts selon leur source d'énergie primaire. Alors que les centrales thermiques ont une dynamique lente, les énergies renouvelables modernes, telles que l'éolienne et la solaire photovoltaïque, sont soumises à des variations très rapides dues à des facteurs environnementaux. Leur disponibilité n'est donc pas garantie.

Par conséquent, il est opportun de profiter de la flexibilité intrinsèque des centrales hydroélectriques pour compenser les variations rapides causés par les sources renouvelables modernes, afin de maintenir la stabilité et la fiabilité du réseau électrique. D'autre part, l'utilisation des centrales hydroélectriques comme un moyen de compenser les variations constantes entre production et consommation d'électricité conduit à des points de fonctionnement hors des plages habituelles. Cette condition peut provoquer des instabilités ou des oscillations indésirables dans la centrale, dont l'origine se trouve dans le système hydraulique. En outre, les petites centrales hydroélectriques jouent un rôle majeur dans le développement des pays émergents, où elles peuvent être souvent soumises à des fonctionnements en îlotage ou isolés. Dans ce contexte, les conditions de fonctionnement sont plus critiques en termes de fiabilité et de stabilité.

Compte tenu de ces facteurs, l'importance de prévoir le comportement dynamique des centrales, soumises à divers scénarios et à différents modes de fonctionnement, est manifeste. Pour ce faire, des modèles mathématiques précis et complets sont nécessaires, ainsi que des outils informatiques performants, appropriés à la planification de nouvelles centrales et à une exploitation plus efficace des aménagements existants.

Ainsi, le but de ce travail est le développement d'un nouvel outil informatique d'analyse de stabilité aux petites perturbations appliqué à des systèmes hydroélectriques, avec une modélisation exhaustive des éléments électriques et hydrauliques qui composent un aménagement de cette nature. Cet outil est implémenté dans SIMSEN, un logiciel à structure entièrement modulaire, performant et convivial, développé à l'EPFL pour la simulation des réseaux électriques et des systèmes hydroélectriques.

L'originalité de ce nouvel outil réside non seulement dans la modélisation exhaustive et détaillée des systèmes électriques et hydrauliques (une représentation multi-physique). Elle se situe aussi dans le fait qu'il s'agit d'un outil à structure modulaire, capable de traiter des systèmes avec des topologies a priori quelconques, avec génération automatique du système d'équations différentielles correspondant, basé sur des circuits facilement structurés à travers une interface graphique conviviale.

Une autre caractéristique distinctive de ce travail est que les modèles des éléments électriques développés pour l'analyse de la stabilité aux petites perturbations sont basés sur les coordonnées de phases *a,b,c*, ce qui diffère de la représentation traditionnelle dans les axes *d,q,o*. La procédure à suivre pour la mise en place de ces modèles est présentée dans ce document.

En outre, des études de cas effectuées avec cet outil montrent que d'importantes interactions ont lieu entre les éléments électriques, mécaniques, hydrauliques et de régulation. Ces interactions peuvent être soit positives, soit nuisibles à la stabilité du système. En cas d'interactions défavorables, des comportements instables peuvent se produire. Il n'est pas possible de prévoir ces instabilités sans un modèle multi-physique complet. Dans ce travail, ces interactions problématiques sont présentées. De plus, leurs conséquences et solutions possibles sont étudiées.

Mots clefs : Analyse de la stabilité aux petites variations, valeurs propres, vecteurs propres, analyse modale, énergie hydroélectrique, centrales hydroélectriques, stabilité des réseaux électriques, dynamique des réseaux électriques.

Acknowledgements

The realization of this work has only been possible due to the support of numerous people. I would therefore like to express my gratitude to all those that have contributed.

I would like to thank first Dr. Basile Kawkabani for giving me the opportunity to join his research group and for seeing in me the capacity for accomplishing this work. I also would like to thank him for his guidance and availability, and for all the hours we spent together on enriching discussions when problems arose.

I gratefully acknowledge the members of the jury, Prof. Alfred Rufer from EPFL, Prof. Edson da Costa Bortoni from UNIFEI (Brazil), Dr. Alexander Schwery from Alstom Renewable Ltd (Switzerland) and Dr. Rachid Cherkaoui from EPFL, for kindly accepting to evaluate this work and for their comments and suggestions, which allowed me to improve the final version of this document.

I would like to express my sincere gratitude to the companies that funded this research for making it possible, namely EOS Holding SA, Alstom Renewable Power (Switzerland) Ltd, Andritz Hydro AG and Voith Hydro Holding GmbH & Co. KG.

I am indebted to Mr. Patrick Grillot and Mr. Jean-Louis Drommi for their important contribution in one of the case studies presented in this document, which considerably enriched this work.

I am grateful to Dr. Christophe Nicolet, Dr. Sébastien Alligné and Dr. Antoine Béguin, from Power Vision Engineering, for the fruitful and pleasant collaboration during these years, as well as for the words of encouragement all along. Thanks to Christophe for all his rich and

pertinent suggestions, and also for being my "coach" on the comprehension and interpretation of hydraulic phenomena. Thanks to Seb for helping me many times to unfold intricate results and for his advices concerning the structure of this document. And thanks to Antoine for giving me a number of simple but truly perceptive suggestions, which helped solving problems that looked rather complicated.

I would like to thank Philippe Allenbach for his fundamental contribution to the implementation of the models developed during this work in SIMSEN, and also for all the interesting and entertaining discussions during the coffee breaks.

All along my doctoral studies, I shared many moments, courses, duties, doubts, meals and laughter with my colleague and friend Michel Han. Thank you Michel for being there all the time, for the technical and non-technical discussions, for keeping me good company, for helping me improve *mon français* and for making me discover the hardest face of *Le Moléson*, which I will never forget.

I am also grateful to Dr. André Hodder for all the advices he gave me, for the times he helped me to better understand intricacies related to electrical machines, and also for giving me the opportunity of working with him as a teaching assistant in many lab courses. In these courses, I had the pleasure to work in collaboration with Sylvain Robert and Stéphane Burri. I would like to thank both of them for sharing their time, experience and stories with me.

In addition, I would like to thank all those people in EPFL that directly or indirectly helped me and motivated me, either with words or attitudes that made me go on when I thought I had exhausted my forces.

While I was writing this document, I was fortunate enough to have three persons going through it (either partially or totally) with very attentive eyes, looking for my mistakes in order to make it better. Therefore, I feel very indebted to my little sister Heloísa, as well as to Adrien L. and Catherine S. I thank you sincerely for this great help. Many thanks to Catherine S. also for having encouraged and supported me all along the development of this work.

On a more personal note, I would like to thank my friends with whom I shared many coffees and meals at EPFL, and/or good moments in Lausanne: Ricardo Padilha, Joana & Mark, Laurence & Rafael, Maria & Catatau, Montse & Marcelão, Reni & Alê, Simona & Pietro, Didier, and Camillo. Thank you to my friend Antônio "Conselheiro" for his interest in my research and for keeping in touch. I could not forget my friend Dayana, whom I deeply thank for her loyal and patient friendship. Many thanks to my friends in Brazil with whom I shared great times during holidays in my hometown, Sete Lagoas: Laura, Sheila, Lu & Gustavo, Bill, Boró, Muri and Caio. Thanks also to Anay from São Paulo for giving me attention and consoling words many times during difficult moments, and to Carina from Taubaté for being frequently

(virtually) present.

Many thanks to my housemates Anouk, Sam, Elisabeth and Nuria, for their good company and the funny moments along these years, for tolerating me during the final stretch of this work and also for cooking me dinner when I had no time whatsoever for doing so.

I am also very grateful to my friends of GEEPE for receiving me with open arms, for treating me always warmly and kindly, for praying for me, for trusting me and for understanding my constant absence in the last few months. Special thanks to "my" group of Thursday evenings for always being there for me and for everything they taught me. I also would like to thank my friends Ane, Sérgio and Luciana from Basel for their companionship since we met; Glória, André, Letícia, Sofia and Nikita from Biel for their friendship and the good times we spent together; Gorete, Walda & Mario, Carol & Galo from Winterthur, and Isabel and Luciana from St.-Gallen, for having me with much affection as part of their families, just as I have them as my second family, here in Switzerland; Jorge Godinho and Antônia Helena from Brasília for their constant guidance, patience and friendship.

I am deeply thankful to my parents, my sisters and their husbands, and my nieces and nephews, for whom I leave here a few words in Portuguese: *Pai e mãe, muito obrigado por todo o carinho e apoio, por tudo o que me ensinaram para que eu me tornasse a pessoa que sou e pelos sábios conselhos tão valiosos que vocês sempre me deram para que eu chegasse até aqui. Mesmo que vocês não o entendam, este trabalho e todo o empenho que coloquei nele são dedicados a vocês. Luciana; Marília, Fernando, Bela, Lica e Dedé; Carola, Daniel, Lulu, João e Larinha; Laura, Demetrius, Cissa e Álvaro; Heloísa, o carinho de vocês, o interesse pelo meu sucesso e bem-estar sempre me deram mais forças para continuar caminhando sempre, mesmo nos momentos de maior dificuldade. O apoio que vocês me deram desde o dia em que lhes contei sobre meu desejo de encarar esse desafio foi muito importante. Muito obrigado do fundo do meu coração!*

Last, but by no means least, I would like to thank my dearest, *minha lindinha*, Tatiana for giving me happiness and lull during the most tempestuous times of my life.

Lausanne, September 18, 2015 Pedro Camilo de Oliveira e Silva

Contents

Abstract i

Résumé iii

Acknowledgements v

I Introduction 1

1 Introduction, Context and Purpose 3

1.1 Power Sector Evolution 3

1.2 Reliability of Power Networks and the Role of Hydropower 4

1.3 Concepts on Power System Stability 6

1.3.1 Physical and Theoretical Definition of Power System Stability 6

1.3.2 Classification of Power System Stability 7

1.3.3 Interactions Between Hydroelectric Machinery and the Power Grid . . . 10

1.4 Description of the Present Work 12

1.4.1 Purpose 12

1.4.2 Methodology 14

1.4.3 Structure of the Document 15

2 State of the Art 19

2.1 Eigenvalues Computation Methods for Small-Signal Stability 19

2.2 Small-Signal Multi-Physics Models for Stability Assessment 21

2.3 Power Systems Softwares with Eigenanalysis Capabilities 24

2.4 Eigenanalysis Capabilities in SIMSEN 25

II Theoretical Approach **27**

3 Small-Signal Stability **29**
3.1 Lyapunov Stability 29
3.2 Eigenanalysis: An Intuitive Example 31
3.3 Concepts on Small-Signal Stability 32
3.3.1 Linearized State-Space Representation 33
3.3.2 Eigensolution of the Linearized System 34
3.3.3 Participation Factors 37
3.3.4 Eigenvalue Sensitivity 38
3.3.5 Eigenanalysis and Transfer Functions 38

4 Small-Signal Modeling of Electrical Elements **41**
4.1 Time-Domain Models of Electrical Elements in SIMSEN 41
4.2 Extension of Eigenanalysis Concepts to Nonautonomous Systems 43
4.3 Small-Signal Electrical Models for SIMSEN based on *a,b,c*-Phase Coordinates . 44
4.4 Proposed Modeling Procedure Applied to the Salient-Pole Synchronous Machine 48

5 Validation of the Small-Signal Models **53**
5.1 Small-Signal Electrical Models Based on *a,b,c*-Phase Coordinates 53
5.2 Construction of System Matrices in SIMSEN 53
5.3 Salient-Pole Synchronous Machine 54
5.4 Wound-Rotor Induction Machine 59
5.5 Power Transformers 62
5.6 RL and RLC Loads 65
5.7 Transmission Lines 68
5.8 Voltage Regulators 70
5.9 Power System Stabilizer 73

6 Modeling of Hydraulic Elements **77**
6.1 General 77
6.2 Hydroacoustic Model of a Pipe 77
6.3 Francis Turbine Model 80
6.4 Model of a Surge Tank 82
6.5 Model of the Turbine Governor 83
6.6 Linearization of the Hydraulic Models 83

III Case Studies **87**

7 Stability Issues and Solutions for an Islanded Hydropower Plant **89**
7.1 Introduction . . . 89
7.2 Case Study Description . . . 90
7.2.1 Electrical Subsystem . . . 90
7.2.2 Hydraulic Subsystem . . . 91
7.2.3 Possible Scenarios . . . 93
7.3 Eigenanalysis of the Electrical System . . . 93
7.3.1 The Regular Scenario . . . 93
7.3.2 The Intermediate Scenario . . . 94
7.3.3 The Critical Scenario . . . 94
7.3.4 Contribution of the PSS to the Stability of the Local Mode . . . 96
7.4 Eigenanalysis of the Hydraulic System . . . 99
7.5 Eigenanalysis of the Complete Hydroelectric System . . . 100
7.5.1 Interactions between the Hydraulic and the Electrical Subsystems . . . 101
7.5.2 Contribution of the Turb. Governor to the Stability of the Local Mode . . . 102
7.5.3 Interaction between the Turbine Governor and the PSS . . . 106
7.6 Concluding Remarks . . . 109

8 Power Fluctuations in an Existing Hydropower Plant **111**
8.1 Introduction . . . 111
8.2 Case Study Description . . . 112
8.2.1 Electrical Model . . . 112
8.2.2 Hydraulic Model . . . 113
8.2.3 Problems Encountered During Operation . . . 114
8.3 Validation of the Electrical Model . . . 115
8.4 Eigenanalysis of the Electrical System at Part Load Condition . . . 120
8.5 Eigenanalysis of the Hydraulic System at Part Load Condition . . . 126
8.6 Hydroelectric System Eigenanalysis at Part Load Condition . . . 130
8.7 Concluding Remarks . . . 135

IV Conclusions **137**

9 Summary, Conclusions and Perspectives **139**
9.1 Summary . . . 139
9.2 Conclusions . . . 141
9.3 Contributions of the Present Work . . . 141
9.4 Perspectives . . . 143

9.4.1 Other Standard Types of Regulators 143
9.4.2 Parametric Studies through Eigenvalue Sensitivity 143
9.4.3 Extension to other Renewable Energy Systems 144

V Appendices **145**

A Small-Signal Models Based on *a,b,c*-Phase Coordinates **147**
A.1 Salient-Pole Synchronous Machine 147
A.1.1 Stator Equations 147
A.1.2 Rotor Equations 151
A.1.3 Mechanical Equations 152
A.2 Wound-Rotor Induction Machine 153
A.2.1 Stator Equations 153
A.2.2 Rotor Equations 156
A.2.3 Mechanical Equations 158
A.3 Power Transformers 159
A.3.1 Vector Group *Yy0* 159
A.3.2 Vector Group *Yd5* 161
A.3.3 Vector Group *Yd11* 162
A.4 Electrical Loads 163
A.4.1 RL Series Load 163
A.4.2 RLC Series Load 163
A.5 Transmission Lines 164
A.5.1 RL Transmission Line 164
A.5.2 π-Section Model of Transmission Line 164
A.6 Voltage Regulators 168
A.6.1 IEEE ST1A 168
A.6.2 Unitrol® 169
A.6.3 Voltage Input (Δu_m) 170
A.7 Power System Stabilizer IEEE PSS2B 170

Bibliography **182**

List of Symbols **183**

List of Figures **193**

List of Tables **197**

Curriculum Vitae **201**

Part I

Introduction

1 Introduction, Context and Purpose

1.1 Power Sector Evolution

The power sector is in constant evolution and the worldwide demand for electricity is in permanent expansion. Consequently, electricity is the fastest-growing final form of energy throughout the world, and sustaining the growth of its supply is essential. Nonetheless, the development of the electricity market is also driven by concerns for environmental issues, especially reduction of flue-gas emissions from fossil-fuel combustion; furthermore, this expansion is also affected by the need of replacement of retired power plants along the years.

Current energy policies and investments promote the expansion of renewable power generation in many OECD countries, while the growth of several emerging economies keeps relying on traditional sources (fossil fuels). In fact, growth and transformations in the power sector are fundamental and universal, but the way they happen varies according to current and new policies, distribution of investments and how authorities tackle the issues, thus driving market trends.

The "New Policies Scenario"[a] proposed by the International Energy Agency (IEA) in its *World Energy Outlook 2014* indicates that over the period of 2012-2040 world electricity demand is forecasted to increase with an average ratio of 2.1% per year. Power capacity additions correspond to 7200 GW, whereas retirements add up to 2450 GW. As a result, the worldwide installed capacity rises from 5950 GW in 2013 to 10700 GW in 2040 [37].

[a] This scenario admits an evolution of the overall energy market considering policies adopted from mid-2014 and also other pertinent policy proposals yet to be accepted, which establish new targets for factors such as reduction of carbon emission, development of renewable energy and improved energy efficiency [37].

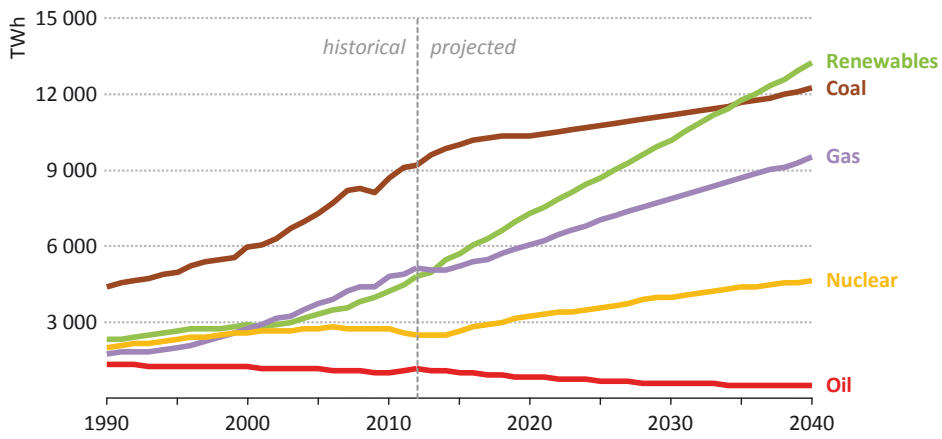

Figure 1.1: Worldwide electricity generation forecast by source [37].

This growth is followed by a compelling change in the mix of power sources. Although the use of coal keeps increasing, its share in the electricity mix decreases considerably. Renewable sources, hydropower included, almost triple until 2040, and also gas and nuclear have their participation increased in the mix. As a result, renewable sources tend to surpass coal, turning into the biggest source of electricity [37, 82] (see figure 1.1).

Nonetheless, these general trends conceal important information about the development of electricity markets in different regions. Figure 1.2 shows that neither the penetration of renewable sources nor the reduction of fossil fuel power plants are the same in all regions. Also, the worldwide fossil fuel share reduction is to be compensated mostly by the adoption of modern renewable technologies, such as wind, solar PV and others. Simultaneously, hydropower tends to preserve its share, which means that it keeps increasing in terms of absolute values of installed capacity. Indeed, hydropower has an important role to play in the context of the modern electricity sector concerning the operational stability of power networks.

1.2 Reliability of Power Networks and the Role of Hydropower

Depending on the source of energy, power plants may present distinct dynamic behaviors. Thermal power plants (which shall remain as the major contribution to the electricity sector) have a slow dynamic and are not able to compensate sudden changes in power production or consumption. On the other hand, modern renewables such as wind and solar PV do not have guaranteed availability, since they depend on environmental factors. For this reason, they shall represent a source of disturbances for power networks. Figure 1.3, adapted from [25], illustrates the high intermittency of wind and solar PV installation in Germany over a period of seven months in 2010. Despite of an installed capacity of over 36 GW, the maximum peak power is 20 GW. Also, the volatility of the energy production of both sources is clear.

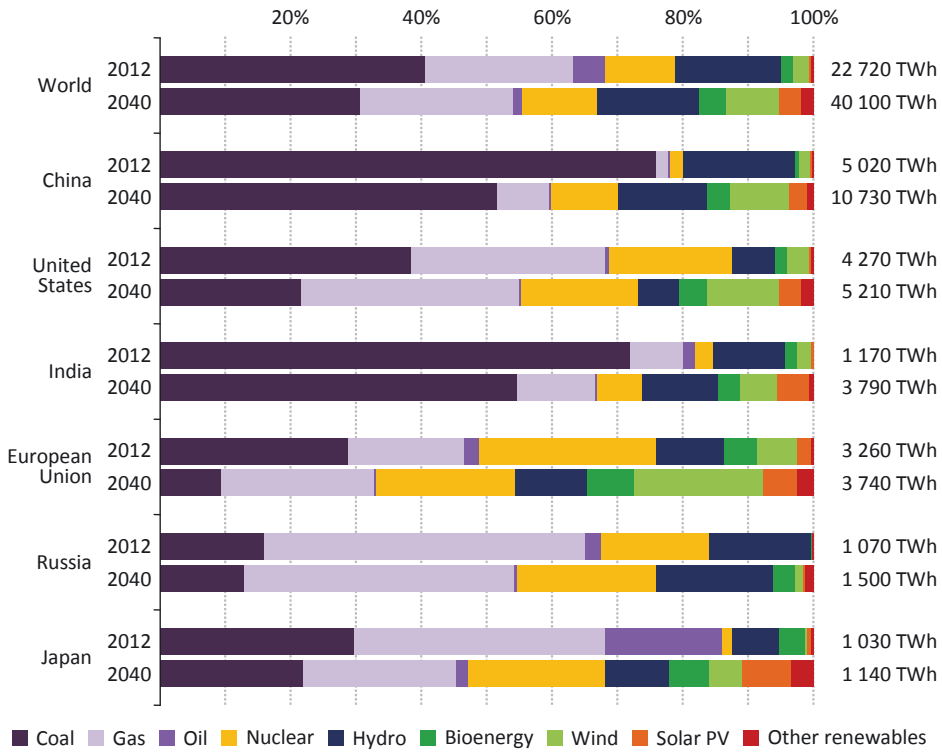

Figure 1.2: Share of energy production by source and by region [37].

Consequently, in order to keep the stability and reliability of the power grid, it is opportune to take profit of the intrinsic flexibility of hydropower plants. Indeed, this type of power plant is capable of withstanding rapid set-point variations of active and reactive power. Therefore, hydropower plants are able to compensate for fast variations caused by renewable sources, thus contributing to frequency and voltage stability of the power grid. In addition, excessive power production can be stored by pump-storage power plants. Furthermore, small hydropower plants play a major role in emerging countries, where they are used for rural and township electrification of remote regions [69].

Nevertheless, the exploitation of hydropower plants to counterbalance constant variations of electricity generation and consumption leads to off-design operation. This condition may provoke instabilities or undesirable oscillations, as pulsations originated in the hydraulic system may propagate in the electrical system, deteriorating the dynamic behavior of the power plant. Thus, care must be taken on the parametrization of controllers of hydropower units, in order to obtain an effective contribution to the stability of power grids.

Turbine governors, automatic voltage regulators (AVR) and power system stabilizers (PSS) must correctly interact with the rest of the system, either contributing to frequency and voltage stability or active and reactive power flow. Consequently, their parameter sets must be in consonance with the operating mode of the power plant.

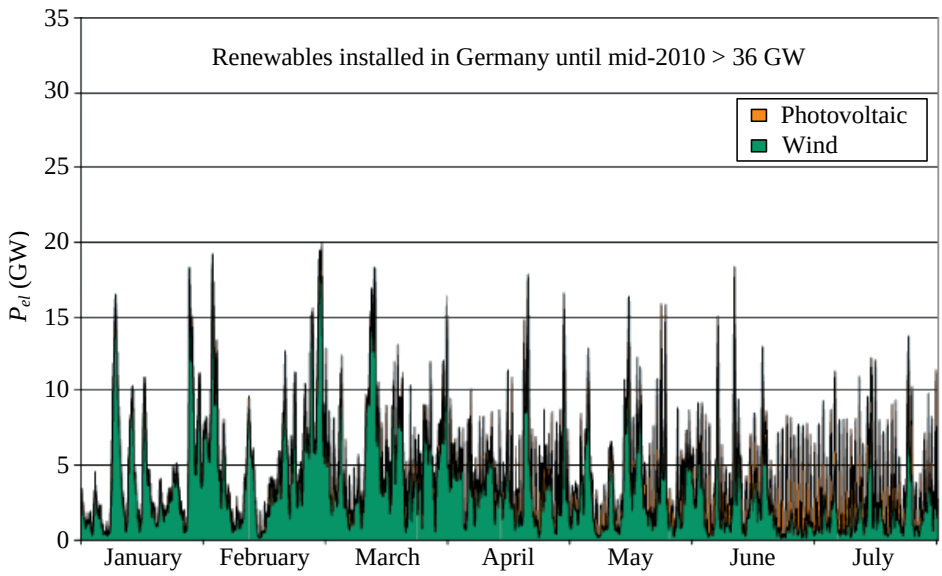

Figure 1.3: Intermittency of wind and solar PV in Germany in 2010 [25].

Three different operating modes are common: (i) interconnected operation – when the power plant is connected to a large power system; (ii) islanded operation – when the power plant and its surrounding network have a weak connection (low short-circuit power) with the power grid and with no tie-line connections to neighboring systems; (iii) isolated operation – when the power plant is responsible for feeding a local network without any connection with a large power grid.

Considering all these factors, one can readily understand the importance of predicting the behavior of power plants under various scenarios of the energy market and different operating modes. This requires precise mathematical models and efficient computational tools. Furthermore, if the focus is put on the stability of hydropower plants, hydraulic, mechanical, electrical and regulation elements must be represented properly, so that phenomena arising from the interaction of these subsystems are correctly represented.

1.3 Concepts on Power System Stability

1.3.1 Physical and Theoretical Definition of Power System Stability

Power system stability has been a topic of major concern in the context of operation of electrical networks for almost one hundred years, following the expansion of the first electrical systems feeding metropolitan areas [24, 99]. Ever since then, a number of forms of instability have come forth as a consequence of the growth of power networks. They have originated some distinct fields of investigation in the scope of power system stability.

As defined by the *IEEE/CIGRÉ Joint Task Force on Stability Terms and Definitions*, "power system stability is the ability of an electric power system, for a given initial operating condition, to regain a state of operating equilibrium after being subjected to a physical disturbance, with most system variables bounded so that practically the entire system remains intact" [52].

This physically-based definition means that the system does not necessarily recover its initial equilibrium state. Indeed, disturbances are likely to cause changes in the topology of the network, thus modifying voltage levels and power flows. However, the final steady state operating point must lay inside the rated limits of all devices (transmission lines, transformers, generators, etc.), so that the new equilibrium point is continuously acceptable. Otherwise, additional disturbances may happen to the system [4].

These conditions are closely related to the definition of asymptotic stability from dynamic nonlinear systems theory. According to this definition, an equilibrium point is asymptotically stable if: (a) all solutions starting at nearby points stay nearby; and (b) all solutions starting at nearby points not only stay nearby, but also tend to the equilibrium point as time approaches infinity [48]. The first condition intuitively expresses stability in the sense of Lyapunov. These concepts are dealt with in depth in chapter 3, section 3.1.

1.3.2 Classification of Power System Stability

Even though power system stability is a single problem, it is convenient to divide it in categories according to three main criteria [51, 52]:

1. The physical nature of the instability, indicated by the variables in which instability is manifested;

2. The magnitude of the disturbance, which determines the method of calculation and prediction of stability;

3. The devices, processes and time span that are taken into account in order to determine stability.

In the sense of criterion 1, the stability problem may be classified as *rotor angular stability*, *frequency stability* and *voltage stability*. Regarding aspect 2., the stability problem may be of *small disturbance (signal)* or *large disturbance (signal)* type. And considering criterion 3., especially with respect to the time span, it can be defined as a *short-term* or a *long-term* phenomenon. Short-term phenomena happen in a time range of several seconds, whereas long-term phenomena involve events occurring in a time range up to several minutes.

Rotor Angular or Synchronous Stability

Rotor angular stability is related to the ability of synchronous machines of an interconnected power system to remain in synchronism following a given disturbance. Instabilities that may arise can be of two different forms: aperiodic or nonoscillatory instabilities resulting from a lack of synchronizing torque, and periodic or oscillatory instabilities resulting from a lack of damping torque [4, 51, 52].

In general, rotor angular stability deals with phenomena in the time frame of a few seconds up to a few tens of seconds, being a short-term stability problem.

It is convenient to divide the analysis of rotor angular stability in two subcategories:

- *Small-disturbance* (or *small-signal*) *rotor angle stability* deals with the ability of the power system to maintain synchronism when subjected to disturbances of small amplitudes, frequently resulting from small variations in power consumption and generation. A small disturbance means that the system can be linearized around its operating point without major loss of information so that linear systems analysis techniques can be applied. As a consequence, small-signal stability is strongly dependent upon the initial equilibrium point of the system.
  Small-disturbance stability is mainly a question of damping of oscillations, which may be of local or global nature. Local problems are related to a specific part of the system and involve rotor angle oscillations of a power plant against the rest of the system (*local plant mode oscillations*) or oscillations between generators close to each other (*inter-machine or interplant mode oscillations*). As a whole, these two types of oscillations are also known as *electro-mechanical mode oscillations* and their frequency range is most commonly of 0.7 to 2.0 Hz.
  Local problems may also be caused by the presence of control and regulation elements, either due to inappropriate tuning of parameters (*control mode oscillations*) or to improper interactions with the turbine-generator shaft system (*torsional mode oscillations*).
  Global problems are related to interactions among large groups of generators, thus involving an extensive part of the system (*interarea mode oscillations*). Typically, a very low frequency mode (0.1 to 0.3 Hz) happens, involving all the generators of the system, which is basically split into two areas swinging against each other. Also, higher frequency modes (0.4 to 0.7 Hz) may occur, related to subgroups of generators oscillating against each other [51].
  This method of stability analysis is based on the calculation of eigenvalues and eigenvectors of the system. The concepts related to small-signal stability are presented in more detail in chapter 3.

- *Large-disturbance rotor angle stability* or *transient stability* deals with the ability of the power system to maintain synchronism when subjected to substantial disturbances, such as short-circuits in a transmission line or close to a generator. In this case, the system response undergoes large variations and the stability depends not only upon the initial equilibrium point, but also upon the duration and the severity of the disturbance [52].

Frequency Stability

Frequency stability is related to the ability of a power system to maintain steady frequency after being subjected to a severe disturbance leading to a considerable imbalance between power consumption and generation. Essentially, the system must be able to recover equilibrium between load and generation, with minimum loss of load [52].

Several distinct devices and mechanisms with different time characteristics are involved in frequency instabilities. For this reason, frequency stability is distinguished between short-term and long-term events. The former involves elements such as protections and generator controls, whereas the latter is related to characteristics of prime movers, boilers and reactors [4].

Voltage Stability

Voltage stability is related to the ability of a power system to keep steady voltage levels at all buses of the system following a disturbance. As it is the case with rotor angular stability, disturbances can be large, such as loss of generation and system faults, or small, *e.g.* incremental variations in consumption/generation of power [4].

Phenomena related to voltage stability may be of either short-term or long-term nature. Short-term voltage stability depends on fast dynamics of components such as HVDC converters, induction motors and other electronically controlled loads. Long-term voltage stability is affected by components with slower action, as transformers with tap changers and generator current limiters [51].

Instabilities may occur in the form of gradual uncontrolled rise or fall of voltages of several buses of the system, possibly resulting in voltage collapse of a large part of it. The development of such phenomena can happen over a time range of several minutes and may result in loss of load, outage of components of the network due to tripping of the protection system and even loss of synchronism of some generators [52].

Aspects exclusively related to frequency and voltage stability analysis are out of the scope of the present work, since these are two very specific and broad fields of study.

Figure 1.4 summarizes the classification and definitions of power system stability. Small-signal angle stability is highlighted in this figure for the reason that it lies on the major scope of the present work.

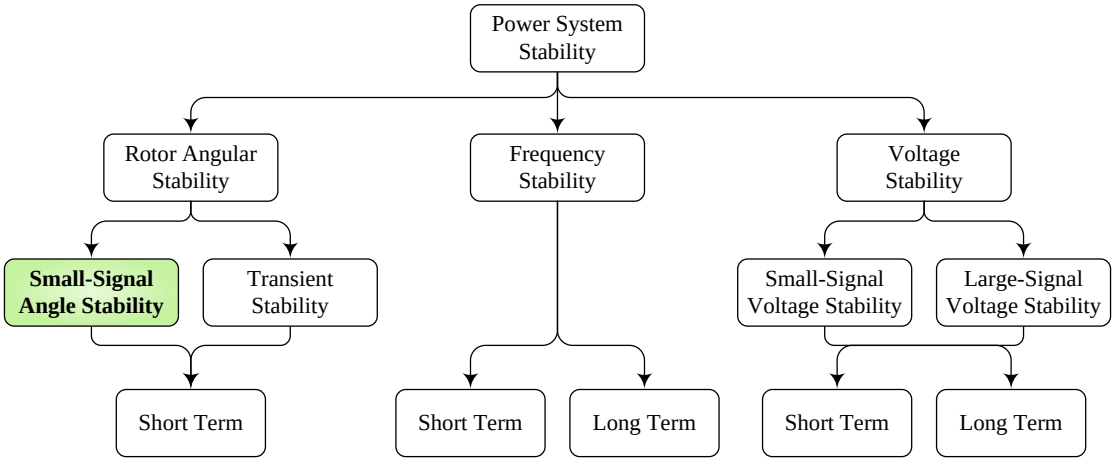

Figure 1.4: Classification of power system stability [52].

1.3.3 Interactions Between Hydroelectric Machinery and the Power Grid

Besides the stability issues described in section 1.3.2, other types of disturbances may be introduced in the power grid coming from interactions with the dynamic behavior of the energy source subsystems.

Specifically in the case of hydropower plants when used to compensate for constant variations of power generation and consumption, instabilities or undesirable disturbances may arise. This may affect the dynamic behavior of the power plant and lead to troublesome interactions with the grid, as mentioned in section 1.2. The prediction of these probable interactions, however, depends on the appropriate modeling of both electrical and hydraulic elements. Results obtained in this way give more precise information about the stability of the system, from hydraulic and electrical viewpoints [60, 71].

The Francis turbine is the most employed type of hydraulic machine due to its wide application range. Francis turbine installations are characterized by complex water flow patterns that develop in the hydraulic machine, which are three-dimensional, rotational and unsteady. As a result, pressure fluctuations may arise from such a water flow behavior [69].

Indeed, the water flow entering the turbine runner presents a swirly characteristic that is induced by its passage through the spiral case, stay vanes and guide vanes. The flow leaving the turbine is nonetheless almost purely axial at the best efficiency point, *i.e.*, the water flow entering the draft tube presents hardly no swirl at rated operating condition. This is not the

case, however, when the turbine operates at off-design conditions. At part load operation, when the flow rate ranges from 50% to 85% of the flow rate at the best efficiency point, there exists a swirly pattern in the water flow leaving the turbine due to a circumferential component on its velocity. Consequently, a helical vortex rope is induced in the draft tube, which has a precession frequency most commonly between 0.2 and 0.4 times the turbine rotational speed n [1, 22].

Thus, the vortex rope precession characterizes periodic pressure pulsations in the draft tube that act as an excitation source for the whole system. Chances exist that the system response to this excitation may be amplified, possibly resulting in intense pressure surges and mechanical power fluctuations. Such fluctuations in their turn may interact with the power network, eventually resulting in considerable electrical power swings.

Indeed, the frequency of part load vortex rope pulsations may coincide with electro-mechanical modes frequency, which ranges from 0.7 to 2.0 Hz. Depending on the stiffness of the power network, the electrical power swings resulting from the resonance of these modes of oscillation may be detrimental to the dynamic behavior of the generating unit and to the stability of the local network. This is particularly the case for hydropower plants operating in islanded and isolated networks.

Figure 1.5 illustrates the part load vortex rope in the draft tube and gives a comparison between the electro-mechanical modes range and the part load vortex rope pulsation range for machines with several distinct rotational speeds n. Considering a network rated frequency of 50 Hz, the corresponding number of pole-pairs of the generator is given in parentheses.

The upper turbine rotational speed value for which vortex rope pulsations may interact with electro-mechanical modes under a network frequency of 50 Hz is $n = 500$ rpm (6 pairs of poles generator). For this rotational speed, which corresponds to a frequency $f_{turb} = 8.3\overline{3}$ Hz, the lower value of the vortex rope frequency range is $f_{VRlow} = 1.6\overline{6}$ Hz ($0.2 \cdot f_{turb}$), falling into the

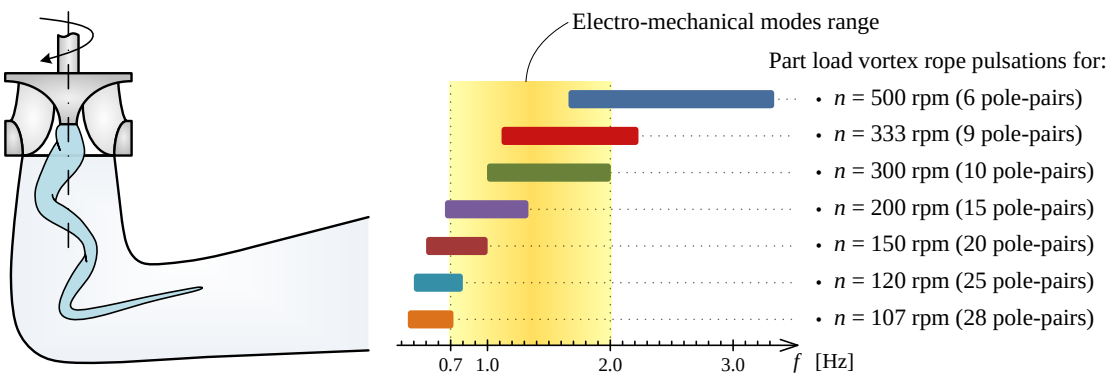

Figure 1.5: Part load vortex rope in the draft tube and its pulsation frequency range.

electro-mechanical frequency range.

Indeed, a generating unit with five pairs of poles in a network with frequency of 50 Hz, which means a rotational speed $n = 600$ rpm, has the lower value of the vortex rope frequency range at $f_{VRlow} = 2.0$ Hz. This corresponds to the maximum possible value of electro-mechanical modes frequency. It is very unlikely that both vortex rope pulsations and electro-mechanical modes happen exactly at this boundary point. For this reason, interactions between vortex rope pulsations and electro-mechanical modes are impropable in this case.

Conversely, the lower turbine rotational speed value for which vortex rope pulsations may interact with electro-mechanical modes under a network frequency of 50 Hz is $n = 107.14$ rpm (28 pairs of poles generator). In this case, the turbine rotational frequency is $f_{turb} = 1.786$ Hz and the upper value of the vortex rope frequency range is consequently $f_{VRupp} = 0.714$ Hz ($0.4 \cdot f_{turb}$). This value lies inside the electro-mechanical frequency range.

The same reasoning can be applied considering an electrical network frequency of 60 Hz. In this case, the upper and lower turbine rotational speed values for which vortex rope pulsations may interact with electro-mechanical modes are, respectively, $n = 514.3$ rpm (7 pairs of poles generator) and $n = 105.9$ rpm (34 pairs of poles generator).

Several other types of excitation sources may arise from the hydraulic circuit due to water flow disturbances in Francis turbines. However, part load vortex rope excitation is the single one described here for the only reason that under its occurrence, due to the frequency range in which it happens, important resonance phenomena may occur between hydraulic and electrical systems (for more information regarding excitation sources in Francis turbines, see [69], chapter 8). Thus, a precise prediction of the natural modes of a hydroelectric unit permits both: (i) to avoid dangerous power swings, when detected during design phase [83]; and (ii) to attenuate undesirable oscillations only detected on site, after commissioning the generating unit.

1.4 Description of the Present Work

1.4.1 Purpose

Considering the facts presented in section 1.1, it is clear that the constant evolution of the power sector, and the challenges originated by a bigger penetration of modern renewable energy sources create the need for analysis tools, which are appropriate for planning new installations and better exploiting the existing ones. Such tools must be capable of both: (i) predicting the dynamic behavior of electrical power networks due to topology changes and inclusions of new power plants and other elements; and (ii) simulating undesired behaviors

in order to give enough information for the solution of problems detected during operation. Moreover, it is important that these tools be at the same time user-friendly, robust and reliable for coping with power networks with high complexity levels.

In this regard, a powerful simulation software for complex energy systems, called SIMSEN, has been developed at EPFL. This is a fully modular, user-friendly simulation software first developed for the analysis of electrical power networks and adjustable speed drives under transient phenomena [89]. Models for electrical machines, transmission lines, loads, power electronic devices, mechanical inertias, and control and regulation functions were accordingly established. Later on, an extension to SIMSEN was proposed (SIMSEN-Hydro), comprising models of hydraulic elements such as turbines, valves and pipes [69]. Besides providing time-domain simulation capabilities for complete hydroelectric installations, there exists the possibility of performing the calculation of eigenvalues and eigenvectors for hydraulic systems with Francis turbines using linearized models.

Thus, the main purpose of the present work is to develop a new tool for small-signal stability analysis of electrical systems to be implemented in SIMSEN, taking advantage of its main features, which are:

- Treatment of systems with any given topology;
- Easy construction of the topology through the connection and parametrization of all elements in an user-friendly graphical user interface (GUI);
- Automatic generation of the full set of differential equations of the global system.

The focus is to be put on the small-signal stability analysis of hydropower plants. Therefore, another goal is to connect the models developed in the framework of the present work to the existing hydraulic linearized models of SIMSEN, so that all interactions of hydraulic, mechanical, electrical and control elements can be determined and analyzed.

Given that the method of small-disturbance stability analysis yields information concerning the stability of the whole system around any operating point (as attested in section 1.3.2), the results of this work shall be a powerful tool for the detection of instability problems in hydropower plants, their interaction with the power network and possible solutions for undesired dynamic behaviors. Moreover, with some treatment of the results, it shall be possible not only to detect the presence of potential instability modes, but also to identify the elements of the system that cause the instability and those that are more affected by it.

It is important to observe that small-signal stability analysis taking into account the hydraulic systems becomes also a long-term problem. Indeed, hydraulic time constants are considerably

higher than electrical ones. Consequently, hydraulic oscillations may develop in a time frame of many seconds up to some minutes.

1.4.2 Methodology

Small-signal stability analysis relies on linear (or linearized) models for calculating eigenvalues and eigenvectors, which give information about the stability of the system under study. Therefore, in order to fulfill the proposed goals of this work and considering the special interest in studying the small-signal stability of hydropower plants and the interaction with the grid, linearized models for several electrical elements comprised in a hydropower plant and in a network have to be developed.

Figure 1.6 gives a schematic representation of the elements that are necessary in order to obtain a complete representation, which are: (1) synchronous machine; (2) power transformers; (3) transmission line models; (4) loads (consumers); (5) induction machine (either as motor or generator); (6) infinite grid representation; (7) automatic voltage regulator (AVR) models; (8) power system stabilizer (PSS); and (9) mechanical inertia system. The link between electrical and hydraulic system, which shall establish their interaction, is made through the mechanical system. Finally, the hydraulic system comprises: (10) reservoirs; (11) surge tanks; (12) penstock (piping elements); (13) Francis turbine with the corresponding characteristic curves; and (14) turbine governing system.

Moreover, these models must keep the modularity concept existing in SIMSEN, *i.e.*, any

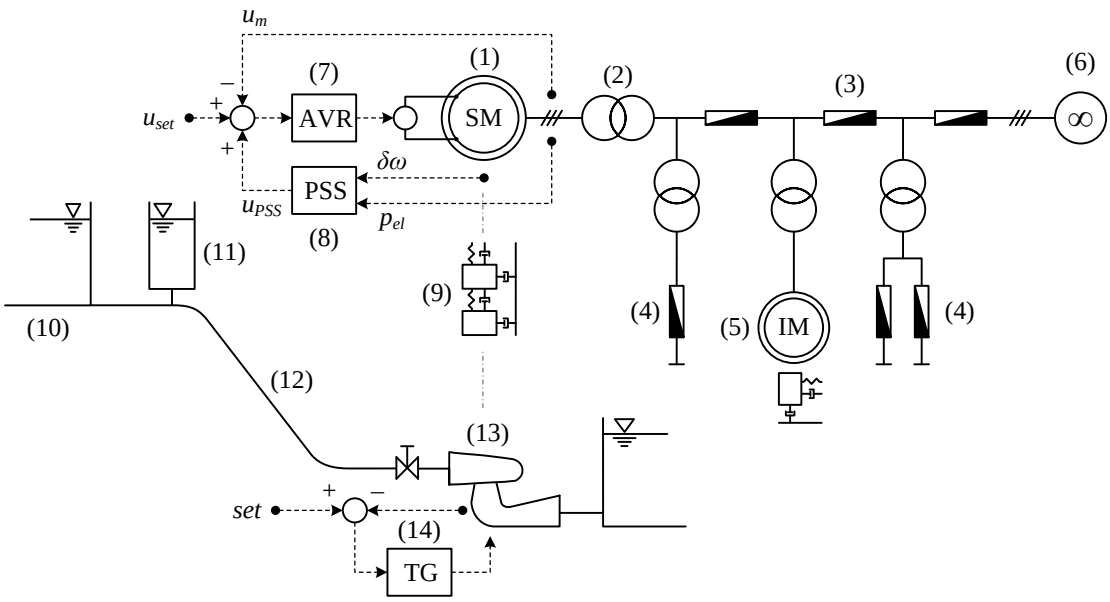

Figure 1.6: Elements for the representation of a hydropower plant and the grid.

topology to be defined by the user comprising these elements must be easy to build in the GUI, the connection of the elements must be treated automatically and the generation of the full set of linearized differential equations must be performed with no additional work to the user.

Therefore, the approach adopted to achieve the proposed goals while respecting these requirements is the analytical linearization of the mathematical models of the elements presented in figure 1.6. These analytical linearized models are then implemented in SIMSEN, yielding a new small-signal stability tool in this software.

Nevertheless, it is important to observe that all the time-domain electrical models in SIMSEN are based on *a,b,c*-phase variables [89]. This differs from traditional models which are based on the well-known *d,q,o*-axis representation (Park's representation). Consequently, in order to take profit of the modularity of SIMSEN, this characteristic has to be respected also for the small-signal models. Therefore, a novel approach is presented in the present work for the analytical development of small-signal models of electrical elements. This approach is based on *a,b,c*-phase variables.

1.4.3 Structure of the Document

Following this introductory chapter, this document is organized as follows:

Chapter 2. A description of traditional techniques of eigenvalue calculation and small-signal stability analysis is presented. Additionally, the most recent publications of eigenanalysis applied to systems described by multi-physics models are discussed. Special attention is paid to eigenanalysis of systems containing renewable energy sources.

Chapter 3. Concepts related to eigenanalysis and small-signal stability are explained in detail. Small-signal stability is associated with the Lyapunov stability concept. Then, an intuitive example of eigenanalysis is presented, which illustrates clearly how eigenvalues and eigenvectors of a system describe its dynamic behavior. Furthermore, the general eigensolution of a system is given and its eigenproperties are explained.

Chapter 4. The time-variant (nonautonomous) nature of the time-domain models of SIMSEN is explained. Considering this characteristic, an extension of eigenanalysis concepts to nonautonomous systems is proposed, founded upon the Floquet Theory. Therewith, a procedure is developed so as to derive small-signal models based on *a,b,c*-phase coordinates. This maintains compatibility with SIMSEN, thus taking advantage of its main benefits. Subsequently, the use of this procedure is illustrated by its application to the salient-pole synchronous machine.

Chapter 5. All small-signal models derived through the procedure proposed in the previous

chapter are introduced and validated. Several illustrative test cases are presented in order to validate the models. Frequencies and time constants related to the calculated eigenvalues are validated either through analytical expressions, or through graphical analysis of results obtained from small-disturbance time-domain simulations. A very good agreement is obtained in all test cases. Thereupon, the small-signal electrical models developed for SIMSEN are proven to be valid and accurate.

Chapter 6. The hydraulic models existing in SIMSEN are introduced. Modeling principles applied to piping systems, Francis turbine, surge tanks and turbine governors are explained. Additionally, the linearization of time-domain hydraulic models is described, highlighting the peculiarities related to each element.

Chapter 7. A case study of an islanded 75 MW hydropower plant is presented. At first, three different scenarios are considered for the electrical system. The most critical one is found to be unstable, due to the very weak connection to the grid. The contribution of a power system stabilizer (IEEE PSS2B) on damping the unstable eigenmode is analyzed.

Then, eigenanalyses of the hydraulic system without and with turbine governor are performed, considering a high-order model. The main hydraulic eigenmodes are highlighted and the influence of the turbine governor over these modes is identified.

Subsequently, the electrical system (considering the most critical scenario without PSS) is coupled to the hydraulic system with turbine governor, yielding a complete high-order representation of the hydropower plant. The interactions between hydraulic and electrical systems are identified, showing that the speed governor is capable of damping the unstable eigenmode of the electrical system. The instability is eliminated with an enhanced set of parameters for the frequency control loop, but it remains badly damped. The PSS is then added to the system in order to guarantee a better dynamic behavior. Nonetheless, results obtained for the complete system (with PSS and with the enhanced tuning of the turbine governor) reveal that hydraulic eigenmodes become far poorly damped, due to adverse interactions between the turbine governor and the PSS. Finally, a solution is proposed in order to avoid such detrimental interactions, achieving a good dynamic behavior for the hydropower plant.

Chapter 8. A case study is performed for an existing 1 GW hydropower plant (4×250 MW generating units). Part load operation is considered, so that disturbances due to vortex rope precession in the draft tube are studied. Initially, the electrical model is validated by comparing time-domain simulation and eigenanalysis results with on-site measurements.

Therewith, eigenanalyses considering a part load operating point are carried out for the system with 1 up to 4 generators synchronized to the grid. The influence of the number of synchronized units on the electro-mechanical (local and intermachine) modes is assessed. Mode shapes of local and intermachine modes are presented in order to illustrate how these

eigenmodes act on the system. Furthermore, the effects of the installation of a power system stabilizer (IEEE PSS2B) are studied. The intermachine eigenmodes are found to have a frequency very close to the frequency of electrical power swings measured on site.

Subsequently, an eigenanalysis of the high-order model of the hydraulic system is performed, and the main eigenvalues are presented. Special attention is given to eigenmodes of the draft tube, since they are likely to interact with vortex rope pulsations. The frequency of the 2nd elastic mode of the draft tube is also found to be very close to the pulsations measured on site. Moreover, this eigenmode has a weak damping ratio. Therefore, the risks of interaction between vortex rope pulsations, draft tube 2nd elastic mode and intermachine modes are strong.

Thereupon, a complete hydroelectric model for the whole installation is established. The eigenanalysis of the complete system confirms the proximity of draft tube and intermachine eigenmodes. Time-domain simulations are then carried out to confirm the interactions. An excitation source located in the draft tube of generating unit 1 simulates pressure pulsations due to vortex rope precession. When happening at the frequency of the 2nd mode of the draft tube, it is verified that these pulsations are amplified and result in significant electrical power swings. Nevertheless, the amplitudes are considerably reduced if the PSS is active, since it strongly damps the intermachine eigenmodes.

Chapter 9. The final summary and conclusions are presented in this chapter. Also, the contributions of the present work are summarized in a specific section. Finally, perspectives of future developments are outlined.

Appendix A. The linearized equations of the small-signal electrical models developed in the scope of the present work are presented in this appendix.

2 State of the Art

2.1 Eigenvalues Computation Methods for Small-Signal Stability

Eigenvalue-based analysis is a classic method applied in the study of dynamic systems and it is the foundation of power system small-signal stability analysis. Based on the state-space representation of the system, its eigenproperties can be extracted.

The most common alternative to obtain the eigenvalues of the system is the application of the QR factorization algorithm. This factorization was first proposed by Francis, in 1961 [26], and it is a very robust algorithm. For the most general cases (unsymmetrical matrices), given a matrix $\mathbf{A} \in \mathbb{R}^{n \times n}$, the algorithm computes its real Schur canonical form $\mathbf{Q}^T\mathbf{A}\mathbf{Q} = \mathbf{T}$, where $\mathbf{Q}$ is an orthogonal matrix ($\mathbf{Q}^T\mathbf{Q} = \mathbf{I}$)[a]. Thus, $\mathbf{T}$ is similar to $\mathbf{A}$ and is also an upper-triangular matrix. Consequently, the eigenvalues of $\mathbf{A}$ are the diagonal entries of $\mathbf{T}$. Once the eigenvalues have been found, the eigenvectors can be computed through partitioning and specific algorithms [30]. The advantages of the QR algorithm are that it has good stability and considerably fast convergence. Moreover, it achieves the calculation of all eigenvalues of the system, allowing a full eigenanalysis.

On the other hand, the QR algorithm is incapable of incorporating sparsity techniques. For a system of order n, the number of floating points operations required is approximately $10n^3$ and the use of memory is proportional to n^2 [30]. Consequently, the QR algorithm is computationally unattractive for systems of very high order, such as large interconnected power systems. Therefore, its application is frequently limited to systems with several hundred

[a] In this work, bold-faced type is used to denote vector quantities. Uppercase letters are used to denote general matrices, whereas lowercase letters denote vectors.

up to a few thousand state variables.

Semlyen and Wang (1988 [93] and 1990 [105]) presented developments in order to incorporate sparse techniques into the algorithm. Also, Henry *et al.* proposed in 2002 an improvement by parallelizing the computation of the QR algorithm, increasing its scalabilty [33].

Geist *et al.* presented in 1999 the BR eigenvalue algorithm, which is better adapted to computing eigenvalues of large-scale systems represented by sparse matrices, reducing computation time and memory requirements [28]. This technique can be preceded by a reduction of the matrix to a similar small-band Hessenberg form (BHESS), as proposed by Howell and Diaa in 2005, decreasing the computation time to about one-fifth of the time required by the QR algorithm to perform the same operation [34].

Ma *et al.* presented in 2006 the first efforts for the application of the BR algorithm in the context of small-signal stability [61]. Recently, Zhao *et al.* (2015) presented further improvements to the BHESS-BR method in order to overcome numerical instabilities that happened in case of matrices of very high order [108]. Although these efforts made this method more suitable to small-signal stability analysis, few applications have been published until the present time. In fact, even though the BHESS-BR method is more efficient than the QR algorithm in terms of computation time and memory consumption, it also represents a considerably high computational cost for large-scale systems. This happens because the number of floating points operations required is quadratically proportional to the order of the matrix [61].

The computational limitations introduced by the algorithms capable of giving the full eigensolution (QR and BR algorithms) led to several developments in the field of eigenvalues computation for small-signal stability. Indeed, large interconnected power networks may be represented by several thousands of state variables. Thus, most of the achievements were based on the interest in reducing computation times, memory requirements and simplifying the interpretation of results.

Byerly *et al.* presented in 1982 the AESOPS algorithm (*Analysis of Essentially Spontaneous Oscillations in Power Systems*) [11]. It is based on a frequency response analysis to obtain the eigenvalues associated with the generator rotor oscillations. Consequently, it provided limited analysis capability. Sauer *et al.* (1991) proposed later a generalization of this algorithm so that the computation of various modes, either separately or simultaneously, became possible [91]. Later on, Lam *et al.* (1994) provided a convergence improvement of the AESOPS algorithm by using a Newton-Raphson iteration scheme [54].

Another technique developed for the simplification of the eigenanalysis of large power systems is the *Selective Modal Analysis* (SMA), proposed by Pérez-Arriaga in 1981 [79]. SMA allows to compute eigenvalues and eigenvectors of the natural modes of interest and also determine

reduced order models related to and containing these modes [80, 81, 102]. Barquin *et al.* (2002) proposed a more general formulation of the algorithms for reduced order eigenanalysis [7]. In this formulation, the reduced order subspaces are updated in each iteration step, improving the convergence of the algorithm.

The *Modified Arnoldi Method* (MAM), proposed by Saad in 1981, was another achievement for the simplication of the eigenvalue problem of large-scale power systems [88]. This algorithm is an improvement of the method proposed by Arnoldi, in 1951, for the solution of large unsymmetrical eigenproblems [6]. MAM is based on a reduction technique in which the matrix whose eigenvalues are to be computed is reduced to an upper Hessenberg matrix [53]. This allows the computation of some eigenvalues of the system around a specified region of the complex plane, avoiding arithmetic steps involved in the QR transformation. In 1996, Lehoucq and Sorensen presented the *Implicitly Restarted Arnoldi Method* (IRAM), with improved convergence [58, 59]. And the efforts of Dookhitram *et al.* (2009) led to a new method for accelerating the convergence of the IRAM [21].

Rommes and Martins proposed two new techniques dedicated to the computation of dominant eigenvalues of large-scale power systems. The *Sensitive Pole Algorithm* (SPA), presented in 2008, computes the eigenvalues most sensitive to parameter changes [84]. In 2010, an algorithm based on the *Subspace Accelerated Rayleigh Quotient Iteration* (SARQI) was developed for the automatic computation of rightmost eigenvalues of large-scale matrices [85].

2.2 Small-Signal Multi-Physics Models for Stability Assessment

In addition to its long-established use in the framework of large-scale power systems, eigenanalysis is a very powerful tool for stability assessment of multi-physics systems, as well as for tuning and design of controllers and stabilizers. Many recent publications present such applications on stability assessment of systems that are much less extensive than large electrical grids.

Kawkabani (2001) derived small-signal expressions for the electromagnetic torque of synchronous generators for the calculation of complex torque coefficients [47]. This method was used for studying the effects of the variation of voltage regulators gain on the stability of power plants. The analysis of the influence of supplementary damping added by power system stabilizers was also performed through this technique. Comparisons with eigenanalysis results were performed in order to confirm the effectiveness of the proposed approach. This work was an extension of the method presented by Canay for the study of torsional interactions between electrical and mechanical systems [12, 13]. Kamwa *et al.* (2005) applied small-signal assessment techniques in order to perform the tuning of IEEE PSS2B and PSS4B for single-machine

infinite-bus and four-machine two-area systems [45]. Martins and Sanches Bossa (2014) performed eigenvalues calculation for the design of a new modal stabilizer [64]. Since the purpose of a modal controller is to act on specific eigenmodes of a system without affecting the other, the knowledge of the eigenvalues is clearly essential. Beza and Bongiorno (2015) derived a small-signal model for a two-machine system with static synchronous compensator with energy storage [8]. This model was applied in the design of an adaptive power oscillation damping controller.

The interactions of power electronic devices with the electrical network has also been studied through small-signal analysis. Sun (2009) reviewed different small-signal models and methods for power electronic devices used in AC distributed power systems, coping with their time-varying nature [100]. Alonso *et al.* (2013) performed small-signal analysis of high power factor AC-DC converters [3]. The small-signal model was derived from the averaged large-signal representation. Kahrobaeian and Mohamed (2014) assessed the small-signal stability of medium-voltage converter-based microgrids when impacted by dynamic loads such as induction motors [44]. A complete small-signal model was proposed and low-, medium- and high-frequency eigenmodes were identified. Chamorro *et al.* (2014) performed small-signal analysis of the Nordic electrical grid in order to analyze the impact of the increasing penetration of renewable energy interfaced by back-to-back voltage source inverters [15]. The influence of such non-synchronous power sources on the damping of electro-mechanical modes was assessed for different levels of penetration. Issa *et al.* (2015) presented a small-signal model of an islanded microgrid with two inverters for the design of a droop control under islanding conditions [39]. Wang *et al.* (2015) applied knowledge from Alonso *et al.* (reference [3]) to derive small-signal models for line-side converters of electric locomotives [103]. These models were used to assess underdamped low-frequency oscillations due to the interaction between the grid and the locomotive converters.

Several recent publications presented efforts on modeling renewable energy sources together with electrical elements, allowing for the analysis of interactions between electrical grids and hydraulic, wind and solar subsystems.

Geng *et al.* (2011) applied small-signal models on the study of speed and torque oscillations of permanent magnet synchronous generators when connected to wind turbines without any damping devices [29]. The small-signal analysis was used on the design of a generator torque controller in order to damp these oscillations. Huang *et al.* (2012) presented a complete model for wind turbines with direct drive permanent magnet (DDPM) synchronous generators, including converters and control scheme [35]. The influence of the controllers' parameters was then analyzed for a single-machine system. De Oliveira *et al.* (2012), concerned with the improvement of small-signal stability margin of wind farms, studied a supplementary control loop for wind turbine generators based on doubly-fed induction generator (DFIG) [19]. Bu

et al. (2012) proposed an analytical method for probabilistic analysis of small-signal stability of power systems when subjected to high penetration of wind power, considering a stochastic variation of wind generation [10]. He *et al.* (2013) provided a small-signal stability comparison between three different concepts of wind turbine generators: DFIG, DDPM generator and squirrel-cage induction generator (SCIG) [32]. The stability of power systems with high penetration of wind power was also the main interest of this study. Arani and Mohamed (2015) demonstrated the positive influence of power- and torque-droop controls applied to DFIG-based wind turbines on the stability of microgrids and weak grids [5]. Jamehbozorg and Radman (2015) studied the small-signal behavior of a power system containing synchronous generators, SCIG-based wind power and energy capacitor units, demonstrating the positive effect of the latter [42].

Small-signal models have also been applied to microgrids containing solar power generation, more specifically PV installations. Guan *et al.* (2014) derived a small-signal model of a hybrid microgrid consisted of a PV station, a small hydropower plant (with simplified representation) and a battery storage system [31]. Based on this model, the performance of the power sharing control was analyzed and the influence of the tuning of controller parameters was demonstrated. Mishra and Ramasubramanian (2015) presented a small-signal model for a microgrid based on PV generation and diesel engine system, taking into account the presence of induction motors as a dynamic load [67]. It was demonstrated that the electro-mechanical oscillation mode of the diesel engine generator tends to become unstable if the power share of the PV installation is increased. A supplementary controller was then introduced in the PV control loop in order to overcome this problem.

Regarding eigenanalysis applied to hydropower systems, Kamwa *et al.* (2002) derived a small-signal model from a transient stability program (large-disturbance model) of the open-loop system seen by a hydro-turbine governor [46]. The model was employed to assess the performance of three different types of hydro-turbine governors installed in distinct hydropower plants of the Canadian electrical network. Liu and Liu (2007) presented a comprehensive small-signal model of a single-machine hydropower plant, including hydraulic elements, taking into account water compressibility and conduit elasticity [60]. This model was applied to an existing small hydropower plant located in China, which experienced oscillatory instabilities since its installation. Different types of interaction were identified and typical oscillation modes were distinguished. Besides electro-mechanical and control oscillation modes, the water elasticity mode and the mechanic-water mode were classified. The first one happened due to the conduit elasticity, whereas the second one was due to the interaction between the conduit and the mechanical system. The eigenanalysis pointed out a way to overcome oscillatory instabilities encountered on site by changing the PSS and voltage regulator parameters. Furthermore, Liu and Liu demonstrated the importance of multi-physics

models for the analysis of small-signal behavior of hydropower plants. Zhou and Wang (2008) performed eigenanalysis to study the effect of pipe elasticity on the stability of low frequency oscillation modes [109]. The importance of adopting high-order elastic models for the hydraulic system was stressed out in order to correctly predict interactions between hydraulic and electro-mechanical oscillation modes. Chompoobutrgool *et al.* (2012) presented a rather accurate, although simplified, model for hydro turbines and governor and demonstrated the importance of careful modeling by performing eigenanalysis of the Nordic power grid [17]. Silva *et al.* presented in 2012 a complete small-signal model of a hydropower plant to analyze speed governor contributions under load rejection conditions [96]. The small signal modeling of electrical elements was based on *a,b,c*-phase variables. Later, Silva *et al.* proposed in 2014 a generalization of the modeling presented in the work of 2012 and applied it to derive fully modular models to the small-signal stability analysis of an islanded hydropower plant [95]. The same modeling concept was applied by Alligné *et al.* further in 2014 for the forced response analysis of hydroelectric systems [2]. Sarmadi and Venkatasubramanian (2015) presented in a recent publication the effects of resonance of inter-area oscillation modes with forced oscillations coming from the hydraulic circuit, particularly from vortex rope pulsations [90]. The interactions of such pulsations with local and inter-area mode are studied through a two-area system in which a forced oscillation simulating a vortex rope pulsation is introduced. Small-signal stability analysis is carried out in order to identify eigenmode frequencies and shapes. Poorly damped oscillation modes likely to interact with vortex rope pulsations were identified, indicating risks of resonance.

It is important to point out that even though all these efforts are of great value, they present an important limitation. In general, they are solutions designed for a specific problem or task. This means that any change in the topology of the systems, such as inclusion of new generating units or addition of loads, cannot be done in a modular way. In other words, every modification requires further efforts in order to adapt the mathematical description of the system, which may be a time-consuming task.

2.3 Power Systems Softwares with Eigenanalysis Capabilities

A number of power system simulation toolboxes and professional softwares incorporate eigenanalysis capabilities at the present time, namely: PacDyn [14]; DIgSILENT PowerFactory [20]; ETAP small-signal stability module [23]; PST (a toolbox based on MATLAB m-files) combined with MatNetFlow and MatNetEig [18, 50]; PSAT (also a MATLAB/Simulink-based toolbox) [65, 66]; NEPLAN® with a small-signal stability module [68]; DSATools™ with SSAT (small-signal analysis tool) [78, 104]; Mudpack [92]; PSS®E with the eigenvalue and modal analysis (NEVA) module [94]; Simpow® [97]; and EUROSTAG® (only eigenvalues computation) with the HERCULES add-on, which incorporates small-signal analysis functions [101].

Persson *et al.* (2003) analyzed the linearization methods used in PSS®E and Simpow® [77]. Eigenvalue calculations were performed for two distinct cases and the results were compared. Whereas Simpow® uses an analytical linearization method, PSS®E uses a numerical linearization routine, which is based on disturbing the state vector to obtain the linearized state matrix. The size of this disturbance was proven to play an important role on the precision of the results. The extraction of eigenvalues in both programs was performed with the QR algorithm.

Kaberere *et al.* (2005) provided a comparison between four industrial-grade power system simulation tools: DIgSILENT PowerFactory, PST, PSS®E and EUROSTAG® [43]. Besides the linearization (analytical or numerical) and eigenvalues calculation methods (QR algorithm in all cases), components modeling and software flexibility were also compared. This comparison was based on the small-signal stability analysis of a classic two-area power system.

It is noteworthy that most of these computer programs are designed to the analysis of large-scale power systems. The components modeling in all of these tools neglect the transients of the network and of the rotating machines' stator, since the focus is put on electro-mechanical oscillation modes. Additionally, the modeling of the whole system is based on the *d,q,o*-axis representation (Park's representation).

2.4 Eigenanalysis Capabilities in SIMSEN

At the time of the proposal of the present work, the advanced version of SIMSEN incorporated eigenanalysis capabilities only for hydraulic circuits including reservoirs, pipes, Francis turbines with rotating inertia and PID turbine governors. The linearized models were developed and validated by Alligné (2011) [1], based on hydroacoustic models presented by Nicolet (2007) [69]. The analytical linearization method was employed.

The calculation of eigenvalues and eigenvectors is performed through the QR algorithm, which is perfectly suitable to SIMSEN purposes. Additionally, SIMSEN includes an eigenmodes visualization tool, which processes the results in order to provide static and dynamic plots the mode shapes.

Part II

Theoretical Approach

3

Small-Signal Stability

3.1 Lyapunov Stability

As mentioned in chapter 1, section 1.3.1, the physically-based definition of power system stability proposed by the *IEEE/CIGRÉ Joint Task Force on Stability Terms and Definitions*[a] is closely related to stability in the sense of Lyapunov. The following theorem combines the definitions of stability in the sense of Lyapunov for nonautonomous, autonomous and linear time-invariant systems.

Theorem (Lyapunov stability [48]). Consider the *nonautonomous* dynamical system defined as $\dot{x} = f(t,x)$. Let $x(t_0) = x_0$ be an equilibrium point for this system, and $D \subset \mathbb{R}^n$ a domain containing x_0. Let $V(t,x) : [0,\infty) \times D \to \mathbb{R}$ be a continuously differentiable function such that

$$W_1(x) \leq V(t,x) \leq W_2(x)$$
$$\frac{\partial V(t,x)}{\partial t} + \nabla V(t,x) \cdot f(t,x) \leq 0$$

for all $t \geq 0$ and $x \in D$, where $W_1(x)$ and $W_2(x)$ are continuous positive definite functions on D. Then, x_0 is *uniformly stable*, that is, the equilibrium point is stable for any time t_0.

Moreover, if

$$\frac{\partial V(t,x)}{\partial t} + \nabla V(t,x) \cdot f(t,x) \leq -W_3(x)$$

[a] "Power system stability is the ability of an electric power system, for a given initial operating condition, to regain a state of operating equilibrium after being subjected to a physical disturbance, with most system variables bounded so that practically the entire system remains intact" [52].

for all $t \geq 0$ and $x \in D$, where $W_3(x)$ is a continuous positive definite function on D. Then, x_0 is *uniformly asymptotically stable*.

In other words, it is possible to say that the equilibrium $x_0 = x(t_0)$ of $\dot{x} = f(t, x)$ is

- *Stable* if, for each $\varepsilon > 0$, there is $\delta = \delta(\varepsilon, t_0) > 0$ such that $\|x_0\| < \delta \Rightarrow \|x(t)\| < \varepsilon$;
- *Uniformly stable* if, for each $\varepsilon > 0$, there is $\delta = \delta(\varepsilon) > 0$ such that $\|x_0\| < \delta \Rightarrow \|x(t)\| < \varepsilon$;
- *Unstable* if it is not stable;
- *Asymptotically stable* if it is stable and there is a positive constant $c = c(t_0)$ such that $x(t) \to x_0$ as $t \to \infty$, for all $\|x_0\| < c$;
- *Uniformly asymptotically stable* if it is uniformly stable, asymptotically stable and c is independent of t_0.

Figure 3.1 gives a geometric interpretation of Lyapunov stability and asymptotic stability for a two-dimensional system.

Now, consider the *autonomous* (time-invariant) dynamical system $\dot{x} = f(x)$. Let x_0 be an equilibrium point and $D \subset \mathbb{R}^n$ be a domain containing x_0. Let $V(x) : D \to \mathbb{R}$ be a continuously differentiable function such that $V(x_0) = 0$ and $V(x) > 0$.

- If $\dot{V}(x) = \nabla V(x) \cdot f(x) \leq 0$, then x_0 is a *stable* equilibrium point;
- If $\dot{V}(x) < 0$, then x_0 is *asymptotically stable*.

Finally, consider the *linear time-invariant* (LTI) dynamical system $\dot{\mathbf{x}}(t) = \mathbf{A} \cdot \mathbf{x}(t)$. The equilibrium point $x(t_0) = x_0$ is

- *Stable* if all eigenvalues (λ_i) of $\mathbf{A}$ satisfy $\Re\{\lambda_i\} \leq 0$;
- *Unstable* if it is not stable;
- *Asymptotically stable* if all eigenvalues of $\mathbf{A}$ satisfy $\Re\{\lambda_i\} < 0$.

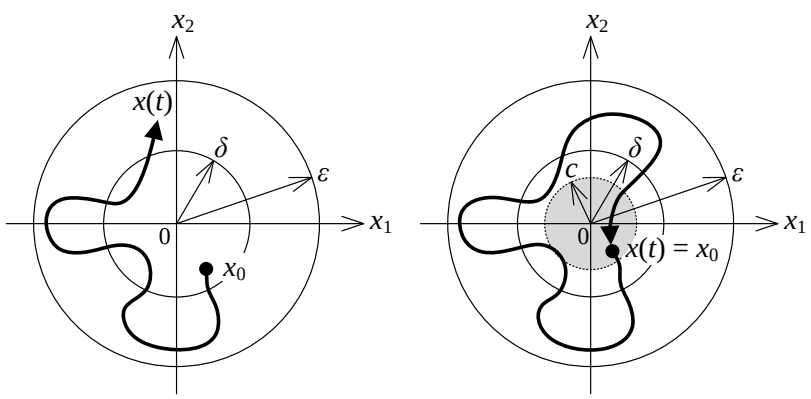

Figure 3.1: Interpretation of Lyapunov stability (left) and asymptotic stability (right) [56].

This last definition, related to LTI systems, is the one traditionally applied in small-signal stability analysis. In the next section, an intuitive example is presented to demonstrate how eigenvalues and eigenvectors relate to the dynamic behavior of a LTI system.

3.2 Eigenanalysis: An Intuitive Example

In order to illustrate how the eigenvalues and eigenvectors of a system can describe its dynamic behavior, it is useful to present a practical, intuitive, simple example[b]. It consists in a real model describing the survival of spotted owls living in the North-American forests in the Pacific Northwest region.

In 1990, environmentalists realized that the spotted owl was threatened with extinction if the old-growth forests were not preserved. Logging activities had been happening for years, slowly reducing the area of the owl's habitat. In order to better understand the issue, mathematical ecologists studied the life cycle of the species, dividing the life cycle of the spotted owl into three stages: juvenile (up to 1 year old), subadult (1 to 2 years) and adult (over 2 years). The owls begin to breed as adults, live for up to 20 years and each owl pair requires 1000 hectares for its exclusive home territory.

Demographic studies demonstrated that in the year $t+1$, the number of new juvenile owls (α_{nj}) is equal to 33% of the number of adults in year t. Although 60% of the juvenile owls lived long enough to become subadults (β_{js}), only 30% of these survive the search for a new home territory (β_{st}). Thus, only 18% of the juvenile owls of year t become subadults in year $t+1$. Finally, 71% of the subadults (γ_{sa}) and 94% of the adults (γ_{aa}) of year t survive to be counted as adults in year $t+1$.

Accordingly, the following mathematical model, using the matrix form $\dot{\mathbf{x}}(t) = \mathbf{A}\cdot\mathbf{x}(t)$, can be used to describe the life cycle of the spotted owls:

$$\begin{bmatrix} \dot{x}_j(t) \\ \dot{x}_s(t) \\ \dot{x}_a(t) \end{bmatrix} = \begin{bmatrix} -1 & 0 & \alpha_{nj} \\ \beta_{js}\cdot\beta_{st} & -1 & 0 \\ 0 & \gamma_{sa} & -1+\gamma_{aa} \end{bmatrix} \begin{bmatrix} x_j(t) \\ x_s(t) \\ x_a(t) \end{bmatrix} \quad , \quad \forall t \in \mathbb{N} \tag{3.1}$$

where $x_j(t)$, $x_s(t)$ and $x_a(t)$ are, respectively, the number of juvenile, subadult and adult owls, and

$$\mathbf{A} = \begin{bmatrix} -1 & 0 & 0.33 \\ 0.18 & -1 & 0 \\ 0 & 0.71 & -0.06 \end{bmatrix}$$

[b] Adapted from D. C. Lay, *Linear Algebra and its Applications*, 4th ed., chap. 5, pp. 265–266,307–309 [57].

The eigenvalues (λ_i) and right eigenvectors ($\mathbf{v}_i$) of the matrix $\mathbf{A}$ are approximately:

$$\lambda_1 = -1.02 + j0.21 \;; \qquad \mathbf{v}_1^T = [\,0.68 \quad -0.06 - j0.59 \quad -0.05 + j0.43\,]$$
$$\lambda_2 = -1.02 - j0.21 \;; \qquad \mathbf{v}_2^T = [\,0.68 \quad -0.06 + j0.59 \quad -0.05 - j0.43\,]$$
$$\lambda_3 = -0.02 \;; \qquad \mathbf{v}_3^T = [\,0.32 \quad 0.06 \quad 0.95\,]$$

The general solution of $\dot{\mathbf{x}}(t) = \mathbf{A} \cdot \mathbf{x}(t)$ has the form:

$$\mathbf{x}(t) = c_1 e^{\lambda_1 t}\mathbf{v}_1 + c_2 e^{\lambda_2 t}\mathbf{v}_2 + c_3 e^{\lambda_3 t}\mathbf{v}_3 \tag{3.2}$$

where $c_i = \mathbf{w}_i \cdot \mathbf{x}(t_0)$ depends on the initial conditions $\mathbf{x}(t_0)$ and the (row) left eigenvectors $\mathbf{w}_i$.

Given that all eigenvalues have negative real parts, the mathematical ecologists could conclude that, based on this model, the spotted owls were faded to extinction. The only hope for them would be the reduction of logging activity.

Indeed, if old-growth forests were preserved so that 50% of the new subadult owls could survive the search for a new home territory, the (2,1)-entry of matrix $\mathbf{A}$ in equation (3.1) would be 0.3 instead of 0.18. In this case, the resulting eigenvalues and right eigenvectors are approximately:

$$\lambda_1 = -1.03 + j0.26 \;; \qquad \mathbf{v}_1^T = [\,-0.08 + j0.58 \quad 0.66 \quad -0.45 - j0.12\,]$$
$$\lambda_2 = -1.03 - j0.26 \;; \qquad \mathbf{v}_2^T = [\,-0.08 - j0.58 \quad 0.66 \quad -0.45 + j0.12\,]$$
$$\lambda_3 = \;\; 0.09 \;; \qquad \mathbf{v}_3^T = [\,0.31 \quad 0.09 \quad 0.95\,]$$

From equation (3.2), one can easily conclude that there is a chance for the spotted owls. As $t \to \infty$, the first two terms tend to zero, whereas the last one increases. Thus, the owl population has a long-term exponential growth rate determined by λ_3. Moreover, $\mathbf{v}_3$ describes the final distribution of the owls by life stage, when the population comes to a balance: for each 95 adults (70%), there will be 31 juveniles (23%) and 9 subadults (7%).

In brief, it is possible to deduce that the real part of the eigenvalues describes the exponential growth/decay, whereas the imaginary part determines the frequency of oscillation. The right eigenvectors define the proportional distribution of the quantities that will be reached in the long term, and the left eigenvectors determine the share of the initial conditions influencing each eigenmode.

3.3 Concepts on Small-Signal Stability

In small-signal stability analysis, disturbances are considered to be sufficiently small so that the system can be linearized around an operating point defining its initial conditions. Moreover,

given that the electrical components are modeled based on the *d,q,o*-axis representation (Park's representation), all the models are time-invariant. Thus, after linearization, the definition of Lyapunov stability for LTI systems, given on page 30, can be applied. The eigenproperties are obtained from the linearized state-space representation of the system.

3.3.1 Linearized State-Space Representation

Any autonomous dynamical system can be described by a set of n nonlinear first-order ordinary differential equations, known as the state equations. The time derivative of each state variable is expressed as a function of the n state variables $x_1(t), ..., x_n(t)$ (contained in the state vector $\mathbf{x}(t) \in \mathbb{R}^n$) and the p system inputs $u_1(t), ..., u_p(t)$ (contained in the input vector $\mathbf{u}(t) \in \mathbb{R}^p$). In the general case, the form of the state equations is:

$$\begin{cases} \dot{x}_1(t) = f_1[\mathbf{x}(t), \mathbf{u}(t)] \\ \dot{x}_2(t) = f_2[\mathbf{x}(t), \mathbf{u}(t)] \\ \qquad \vdots \\ \dot{x}_n(t) = f_n[\mathbf{x}(t), \mathbf{u}(t)] \end{cases} \tag{3.3}$$

Moreover, the outputs of the system are described by a set of q equations also expressed as a function of the state variables and the system inputs:

$$\begin{cases} y_1(t) = g_1[\mathbf{x}(t), \mathbf{u}(t)] \\ y_2(t) = g_2[\mathbf{x}(t), \mathbf{u}(t)] \\ \qquad \vdots \\ y_q(t) = g_q[\mathbf{x}(t), \mathbf{u}(t)] \end{cases} \tag{3.4}$$

The system model may as well be summarized in vector notation as:

$$\begin{cases} \dot{\mathbf{x}}(t) = \mathbf{f}[\mathbf{x}(t), \mathbf{u}(t)] \\ \mathbf{y}(t) = \mathbf{g}[\mathbf{x}(t), \mathbf{u}(t)] \end{cases} \tag{3.5}$$

The linearization of the system of equations (3.5) is performed through first-order Taylor expansions (neglecting the terms of higher order) applied to all the n state equations and q output equations [62], as follows:

$$\begin{cases} \Delta\dot{x}_i = \left.\dfrac{\partial f_i}{\partial x_1}\right|_0 \Delta x_1 + \cdots + \left.\dfrac{\partial f_i}{\partial x_n}\right|_0 \Delta x_n + \left.\dfrac{\partial f_i}{\partial u_1}\right|_0 \Delta u_1 + \cdots + \left.\dfrac{\partial f_i}{\partial u_p}\right|_0 \Delta u_p \\ \Delta y_j = \left.\dfrac{\partial g_j}{\partial x_1}\right|_0 \Delta x_1 + \cdots + \left.\dfrac{\partial g_j}{\partial x_n}\right|_0 \Delta x_n + \left.\dfrac{\partial g_j}{\partial u_1}\right|_0 \Delta u_1 + \cdots + \left.\dfrac{\partial g_j}{\partial u_p}\right|_0 \Delta u_p \end{cases} \tag{3.6}$$

for all $i = 1, 2, \ldots, n$ and $j = 1, 2, \ldots, q$.

The partial derivatives of $f_i[\mathbf{x}(t), \mathbf{u}(t)]$ and $g_i[\mathbf{x}(t), \mathbf{u}(t)]$ are evaluated at the equilibrium point, yielding a system of equations with constant linear coefficients that can be expressed in vector notation as:

$$\begin{cases} \Delta\dot{\mathbf{x}}(t) = \mathbf{A}_\ell \cdot \Delta\mathbf{x}(t) + \mathbf{B}_\ell \cdot \Delta\mathbf{u}(t) \\ \Delta\mathbf{y}(t) = \mathbf{C}_\ell \cdot \Delta\mathbf{x}(t) + \mathbf{D}_\ell \cdot \Delta\mathbf{u}(t) \end{cases} \tag{3.7}$$

The system of equations (3.7) gives the *linearized state-space representation* of a dynamical system, where:

$$\mathbf{A}_\ell = \begin{bmatrix} \left.\frac{\partial f_1}{\partial x_1}\right|_0 & \cdots & \left.\frac{\partial f_1}{\partial x_n}\right|_0 \\ \vdots & \ddots & \vdots \\ \left.\frac{\partial f_n}{\partial x_1}\right|_0 & \cdots & \left.\frac{\partial f_n}{\partial x_n}\right|_0 \end{bmatrix}, \mathbf{A}_\ell \in \mathbb{R}^{n\times n} \quad ; \quad \mathbf{B}_\ell = \begin{bmatrix} \left.\frac{\partial f_1}{\partial u_1}\right|_0 & \cdots & \left.\frac{\partial f_1}{\partial u_p}\right|_0 \\ \vdots & \ddots & \vdots \\ \left.\frac{\partial f_n}{\partial u_1}\right|_0 & \cdots & \left.\frac{\partial f_n}{\partial u_p}\right|_0 \end{bmatrix}, \mathbf{B}_\ell \in \mathbb{R}^{n\times p}$$

$$\mathbf{C}_\ell = \begin{bmatrix} \left.\frac{\partial g_1}{\partial x_1}\right|_0 & \cdots & \left.\frac{\partial g_1}{\partial x_n}\right|_0 \\ \vdots & \ddots & \vdots \\ \left.\frac{\partial g_q}{\partial x_1}\right|_0 & \cdots & \left.\frac{\partial g_q}{\partial x_n}\right|_0 \end{bmatrix}, \mathbf{C}_\ell \in \mathbb{R}^{q\times n} \quad ; \quad \mathbf{D}_\ell = \begin{bmatrix} \left.\frac{\partial g_1}{\partial u_1}\right|_0 & \cdots & \left.\frac{\partial g_1}{\partial u_p}\right|_0 \\ \vdots & \ddots & \vdots \\ \left.\frac{\partial g_q}{\partial u_1}\right|_0 & \cdots & \left.\frac{\partial g_q}{\partial u_p}\right|_0 \end{bmatrix}, \mathbf{D}_\ell \in \mathbb{R}^{q\times p}$$

The matrices $\mathbf{A}_\ell$ (state matrix) and $\mathbf{B}_\ell$ (input matrix) are properties of the system and relate to the system structure and elements. The matrices $\mathbf{C}_\ell$ (output matrix) and $\mathbf{D}_\ell$ (feedforward matrix) depend on the particular choice of output variables. For most physical systems, the outputs are not directly dependent on the inputs, reason for which commonly $\mathbf{D}_\ell = \mathbf{0}$.

3.3.2 Eigensolution of the Linearized System

The free motion of the linearized system is described by:

$$\Delta\dot{\mathbf{x}}(t) = \mathbf{A}_\ell \cdot \Delta\mathbf{x}(t) \tag{3.8}$$

The linearized state matrix $\mathbf{A}_\ell$ characterizes the dynamic behavior of the whole system. Therefore, from its eigenvalues it is possible to predict the small-signal stability of the equilibrium point corresponding to the linearized system.

The eigensolution of the system can be obtained as follows [63]. Consider a column vector $\mathbf{v}$ of dimension $n \times 1$. The eigenvalues of $\mathbf{A}_\ell$ are defined as the scalar λ that satisfies the nontrivial solution of the equation:

$$\mathbf{A}_\ell \cdot \mathbf{v} = \lambda\mathbf{v} \quad \rightarrow \quad (\mathbf{A}_\ell - \lambda\mathbf{I}) \cdot \mathbf{v} = \mathbf{0} \tag{3.9}$$

where $\mathbf{I}$ is the n-dimensional identity matrix. For a nontrivial solution ($\mathbf{v} \neq \mathbf{0}$), this means that:

$$\left|\mathbf{A}_\ell - \lambda \mathbf{I}\right| = 0 \tag{3.10}$$

The expansion of the characteristic equation (3.10) yields the characteristic polynomial of $\mathbf{A}_\ell$, whose n roots are also the n eigenvalues $\lambda_1, \lambda_2, \ldots, \lambda_n$ of $\mathbf{A}_\ell$. The eigenvalues may be either purely real or complex. In most of the cases $\mathbf{A}_\ell$ is real, which means that complex eigenvalues appear in conjugate pairs of the form $\sigma \pm j\omega_d$. The pulsation ω_d represents the damped frequency of the eigenmode. The inverse of the attenuation σ defines the time constant of the decay/growth of the response. Two characteristics of the eigenmode can be determined from these coefficients: the frequency of oscillation (f) and the damping ratio (ζ), as follows:

$$f = \frac{\omega_d}{2\pi} \tag{3.11}$$

$$\zeta = -\frac{\sigma}{\sqrt{\sigma^2 + \omega_d^2}} \tag{3.12}$$

The eigenmode is said to be *over-damped* if $\zeta > 1$, *critically damped* if $\zeta = 1$, *under-damped* if $0 < \zeta < 1$, or *undamped* if $\zeta = 0$. However, if $\zeta < 0$, that is, if $\sigma > 0$, the eigenmode is *unstable*. This means that once this mode is excited by any small disturbance, the system cannot recover its equilibrium. This corresponds to the definition of Lyapunov stability for LTI systems, given on page 30, which states that instabilities are characterized by eigenvalues with positive real parts ($\Re\{\lambda_i\} > 0$).

For each eigenvalue λ_i there is a corresponding eigenvector $\mathbf{v}_i$ that satisfies equation (3.9). This is the right eigenvector of $\mathbf{A}_\ell$ associated with λ_i. Furthermore, it is possible to define the corresponding left eigenvector $\mathbf{w}_i$, which is a row vector that must satisfy the relation:

$$\mathbf{w}_i \cdot \mathbf{A}_\ell = \lambda_i \mathbf{w}_i \tag{3.13}$$

In principle, left and right eigenvector are not uniquely defined. Hence, they are usually normalized in such a way that [51, 86]:

$$\mathbf{w}_i \cdot \mathbf{v}_i = 1 \tag{3.14}$$

On the other hand, left and right eigenvectors related to two distinct eigenvalues are orthogonal, that is:

$$\mathbf{w}_i \cdot \mathbf{v}_j = 0 \tag{3.15}$$

It is suitable to express equations (3.9) and (3.13) in matrix notation, as follows:

$$\mathbf{A}_\ell \cdot \mathbf{V} = \mathbf{V} \cdot \Lambda \tag{3.16}$$

$$\mathbf{W} \cdot \mathbf{A}_\ell = \Lambda \cdot \mathbf{W} \tag{3.17}$$

where

$$\begin{aligned}
\Lambda &= \mathrm{diag}(\lambda_1, \lambda_2, \ldots, \lambda_n)\ , \ \ \Lambda \in \mathbb{R}^{n \times n} \\
\mathbf{V} &= [\ \mathbf{v}_1\ \ \mathbf{v}_2\ \ \cdots\ \ \mathbf{v}_n\ ]\ , \ \ \mathbf{V} \in \mathbb{R}^{n \times n} \\
\mathbf{W} &= \left[\ \mathbf{w}_1^T\ \ \mathbf{w}_2^T\ \ \cdots\ \ \mathbf{w}_n^T\ \right]^T\ , \ \ \mathbf{W} \in \mathbb{R}^{n \times n}
\end{aligned}$$

From equations (3.16) and (3.17) it is possible to conclude that:

$$\mathbf{W} = \mathbf{V}^{-1} \tag{3.18}$$

This corresponds to what is stated by equations (3.14) and (3.15).

Proof. Right- and left-multiplication of equation (3.16) by the inverse of matrix $\mathbf{V}$, as follows:

$$\mathbf{V}^{-1} \cdot \mathbf{A}_\ell \cdot \mathbf{V} \cdot \mathbf{V}^{-1} = \mathbf{V}^{-1} \cdot \mathbf{V} \cdot \Lambda \cdot \mathbf{V}^{-1}$$

yields:

$$\mathbf{V}^{-1} \cdot \mathbf{A}_\ell = \Lambda \cdot \mathbf{V}^{-1}$$

This relation fulfills the condition expressed in equation (3.17). This means that $\mathbf{V}^{-1}$ is a matrix whose rows are the left eigenvectors of $\mathbf{A}_\ell$, proving that relation (3.18) is true. □

Finally, it is easy to verify that the time-domain solution of the free motion equation (3.8) can be given as a function of the initial conditions, and the eigenvalues and eigenvectors of matrix $\mathbf{A}_\ell$, as follows [51, 86]:

$$\Delta\mathbf{x}(t) = \sum_{i=1}^{n} \underbrace{[\mathbf{w}_i \cdot \Delta\mathbf{x}(t_0)]}_{c_i} \mathbf{v}_i\, e^{\lambda_i t} \tag{3.19}$$

where $\Delta\mathbf{x}(t_0)$ is the disturbance at instant zero. The constants $c_i = \mathbf{w}_i \cdot \Delta\mathbf{x}(t_0)$ represent the magnitude of the excitation of the i-th mode resulting from the initial disturbance $\Delta\mathbf{x}(t_0)$ [51].

Equation (3.19) corresponds to the expression (3.2), presented in section 3.2. Some conclusions can be drawn from equation (3.19) that confirm the statements and inferences of section 3.2:

- The free motion response is a linear combination of n dynamic modes related to the n eigenvalues of matrix $\mathbf{A}_\ell$;
- The left eigenvectors $\mathbf{w}_i$ determine the weight of the initial conditions in each mode, that is, the magnitude of excitation of each mode resulting from the initial conditions;
- The right eigenvectors $\mathbf{v}_i$ determine the activity or the proportional action of the state variables in each mode. In other words, the right eigenvectors represent the mode shape;
- The eigenvalues λ_i determine the exponential decrease/growth of the response. In case of complex eigenvalues, the response is oscillatory with frequency determined by $\Im\{\lambda_i\}$ and amplitude exponential decrease/growth determined by $\Re\{\lambda_i\}$;
- Although a specific eigenmode can be unstable ($\Re\{\lambda_i\} > 0$), it might not be excited by a certain disturbance. Nevertheless, the system is still considered unstable since another combination for the vector $\Delta\mathbf{x}(t_0)$ can excite the unstable mode.

3.3.3 Participation Factors

Although eigenvalues give information on system stability and eigenvectors permit to have an indication of the shape of modes, the analysis of results is not always straightforward, especially when the studied systems are of considerable size and complexity. Another difficulty arises from the fact that eigenvectors depend on the units and on the scaling of the state variables [51].

A clearer notion of the relationship between state variables and eigenmodes can be obtained by the calculation of the participation factors as follows [81, 102]:

$$p_{ji} = w_{ij} v_{ji} \tag{3.20}$$

where v_{ji} (w_{ij}) is the j-th entry of the right (left) eigenvector corresponding to the i-th mode.

The participation factor p_{ji} is a dimensionless quantity which denotes the relative involvement of the j-th state variable in the i-th mode, and vice-versa [81]. Considering the condition expressed by equation (3.14), it is possible to write:

$$\sum_{j=1}^{n} p_{ji} = \sum_{i=1}^{n} p_{ji} = 1 \tag{3.21}$$

Frequently, p_{ji} is a complex number. However, for representation purposes, only its magnitude $|p_{ji}|$ is used.

An interesting property of participation factors is that it is possible to define the global partici-

pation factor of a subsystem S (represented by k states) in one mode i [86]:

$$p_{Si} = \left| \sum_{j=1}^{k} p_{ji} \right| \tag{3.22}$$

The calculation of participation factors can be very useful when the system has poorly damped or unstable modes. It gives an indication of instability sources, since they will point out precisely which are the state variables influencing the mode. This way, it is possible to act directly on the root of the problem, facilitating the definition of stabilizer parameters or locations, for instance. Moreover, participation factors play a major role in Selective Modal Analysis (SMA), as mentioned in chapter 2, section 2.1.

3.3.4 Eigenvalue Sensitivity

Eigenvalue sensitivity corresponds to the rate of change of a given eigenvalue λ_i with respect to a specific system parameter γ. By right-multiplying equation (3.13) by $\mathbf{v}_i$ and taking into account that the normalization given by equation (3.14) is respected, it gives [62]:

$$\lambda_i = \mathbf{w}_i \cdot \mathbf{A}_\ell \cdot \mathbf{v}_i \tag{3.23}$$

Then, the sensitivity of λ_i with respect to a parameter γ is:

$$\frac{\partial \lambda_i}{\partial \gamma} = \mathbf{w}_i \cdot \frac{\partial \mathbf{A}_\ell}{\partial \gamma} \cdot \mathbf{v}_i \tag{3.24}$$

If the sensitivity of interest is relative to an entry a_{jk} of matrix $\mathbf{A}_\ell$, then:

$$\frac{\partial \lambda_i}{\partial a_{jk}} = \mathbf{w}_i \cdot \frac{\partial \mathbf{A}_\ell}{\partial a_{jk}} \cdot \mathbf{v}_i = w_{ij} v_{ki} \tag{3.25}$$

If a diagonal entry a_{jj} is considered, the eigenvalue sensitivity corresponds to the participation factor of the j-th state variable in the i-th eigenvalue [74], as defined in equation (3.20):

$$\frac{\partial \lambda_i}{\partial a_{jj}} = w_{ij} v_{ji} = p_{ji} \tag{3.26}$$

3.3.5 Eigenanalysis and Transfer Functions

Despite the fact that the state-space representation describes the system in terms of its whole internal and external behavior, it is sometimes useful to represent the system in a simpler way, regarding the input/output behavior. For this purpose, it is possible to derive the transfer function of a system from its state-space representation. Considering a single-input single-

output system whose output is not a direct function of the input, the linearized state-space representation given in the system of equations (3.7) can be rewritten as follows:

$$\Delta\dot{\mathbf{x}}(t) = \mathbf{A}_\ell \cdot \Delta\mathbf{x}(t) + \mathbf{b}_\ell \, \Delta u(t) \tag{3.27}$$

$$\Delta y(t) = \mathbf{c}_\ell \cdot \Delta\mathbf{x}(t) \tag{3.28}$$

And in the frequency domain:

$$s\,\Delta\mathbf{X}(s) = \mathbf{A}_\ell \cdot \Delta\mathbf{X}(s) + \mathbf{b}_\ell \, \Delta U(s) \quad \rightarrow \quad \Delta\mathbf{X}(s) = (s\mathbf{I} - \mathbf{A}_\ell)^{-1} \cdot \mathbf{b}_\ell \, \Delta U(s) \tag{3.29}$$

$$\Delta Y(s) = \mathbf{c}_\ell \cdot \Delta\mathbf{X}(s) \tag{3.30}$$

By replacing equation (3.29) in equation (3.30), it is possible to obtain the transfer function $G(s)$, defined as:

$$G(s) = \frac{\Delta Y(s)}{\Delta U(s)} = \mathbf{c}_\ell \cdot (s\mathbf{I} - \mathbf{A}_\ell)^{-1} \cdot \mathbf{b}_\ell \tag{3.31}$$

It can be shown that the expansion of $G(s)$ in partial fractions yields (see [51], pp. 719-721):

$$G(s) = \frac{R_1}{s-\lambda_1} + \frac{R_2}{s-\lambda_2} + \cdots + \frac{R_n}{s-\lambda_n} \tag{3.32}$$

where the residues of $G(s)$ are given as $R_i = \mathbf{c}_\ell \cdot \mathbf{v}_i \cdot \mathbf{w}_i \cdot \mathbf{b}_\ell$. Moreover, equation (3.32) shows that the poles of $G(s)$ are given by the eigenvalues of $\mathbf{A}_\ell$.

Now that the basic concepts of small-signal stability have been presented, the development of models for an eigenanalysis tool in the environment of SIMSEN can be tackled. The next chapter presents the approach developed in order to derive small-signal stability models for electrical elements based on the time-domain models of SIMSEN, whereas chapter 6 describes the already existing hydraulic models.

4

Small-Signal Modeling of Electrical Elements

4.1 Time-Domain Models of Electrical Elements in SIMSEN

In order to develop small-signal models which maintain compatibility with the principles of operation of SIMSEN, they must be derived based on the existing time-domain models. Keeping this compatibility means taking advantage of the benefits of SIMSEN, *i.e.*:

- Treatment of systems with any given topology;
- Easy construction of the topology through the connection and parametrization of all elements in an user-friendly GUI;
- Automatic generation of the full set of differential equations of the global system.

On the other hand, it also means respecting the principles of modeling, the state variables and equations that represent each element.

As mentioned in chapter 1, section 1.4.2, all the time-domain electrical models in SIMSEN are based on *a,b,c*-phase variables. This has an important consequence from the viewpoint of eigenanalysis.

When represented in *a,b,c*-phase coordinates, rotating electrical machines are nonautonomous systems. In other words, this means that the state equations depend not only on the inputs and state variables themselves, but also on the time: $\dot{\mathbf{x}} = \mathbf{f}(t, \mathbf{x}, \mathbf{u})$. Consequently, the free motion of the system (when $\mathbf{u} = \mathbf{0}$) is also a function of time.

Indeed, the mutual inductances between stator and rotor windings of rotating electrical machines depend on the angular position of the rotor θ, which in its turn depends on time.

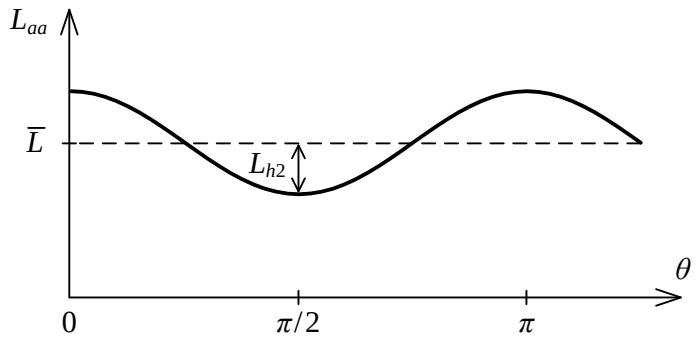

Figure 4.1: Self-inductance for phase a of a salient-pole synchronous machine [16].

Moreover, in the specific case of salient-pole synchronous machines, mutual inductances between stator windings and also their self-inductances depend on θ.

Figure 4.1 represents the variation of the self-inductance L_{aa} of stator phase a as a function of the rotor angular position θ. It can be decomposed in a constant mean value $\overline{L}$, and a periodic oscillating component of amplitude L_{h2} and frequency equal to the double of the angular frequency of the rotor. This periodic variation is due to the anisotropy of the salient-pole synchronous machine rotor, which is illustrated in figure 4.2.

This being said, it is important to bear in mind that the Lyapunov stability criterion based on eigenvalues is applicable exclusively to LTI systems, as it was discussed in chapter 3, section 3.1. Consequently, for small-signal stability analysis purposes, it is not enough to linearize the time-domain models of SIMSEN. This procedure would only produce linear time-variant (LTV)

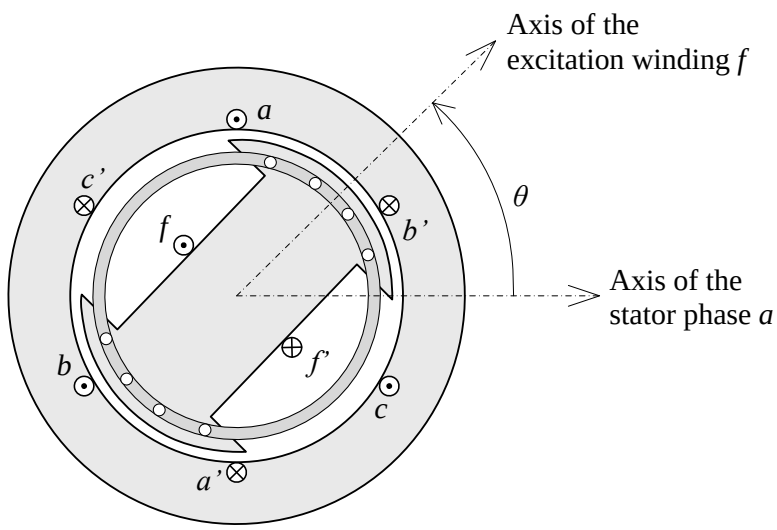

Figure 4.2: Simplified representation of a salient-pole synchronous machine [16].

systems, whose eigenvalues do not straightforwardly define the stability of the system. Indeed, it is possible that LTV are stable when they present positive real part eigenvalues, as well as unstable even though all eigenvalues have negative real parts [73].

Therefore, since the time-domain models of electrical elements available in SIMSEN are nonautonomous systems, they require more treatment than a simple linearization so as to be applied in small-signal stability analysis.

4.2 Extension of Eigenanalysis Concepts to Nonautonomous Systems

The concepts of stability of nonautonomous systems given by the Lyapunov's stability theorem, as presented in chapter 3, section 3.1, are based on the definition of boundary functions $W_{1,2,3}(x)$ and the energetic function $V(t,x)$.

Such way of defining the stability of a system has significant conceptual value. However, it has little computational significance, as Lyapunov's theorem does not give any information on how to define $V(t,x)$. In practice, it is impossible to derive an expression for $V(t,x)$, especially for complex systems such as power systems.

Considering LTV systems, which have the form $\dot{\mathbf{x}}(t) = \mathbf{A}(t) \cdot \mathbf{x}(t)$, a number of concepts have been proposed to inspect the stability, such as dynamic eigenvalues, specific decomposition methods and Ricatti equation taking the role of the characteristic equation [73]. However, the interpretation of the results requires more mathematical efforts and digress from the traditional eigenanalysis. This is not the objective of this work, since it aims at developing an eigenanalysis tool for SIMSEN which is uncomplicated and user-firendly.

Finally, considering linear periodic (LP) systems, for which $\mathbf{A}(t+T) = \mathbf{A}(t)$, it is possible to determine the stability using the Floquet Theory [87]. This theory states that every LP system can be reduced to a LTI system of the form:

$$\dot{\mathbf{z}}(t) = \mathbf{R} \cdot \mathbf{z}(t) \tag{4.1}$$

by way of a stability preserving variable change defined as:

$$\mathbf{x}(t) = \mathbf{L}(t) \cdot \mathbf{z}(t) \tag{4.2}$$

where $\mathbf{L}(t)$ is a continuously differentiable, uniformly bounded, invertible, periodic matrix [110]. By respecting these criteria, $\mathbf{L}(t)$ can be defined as a *Lyapunov transformation*, which is a coordinate transformation (or variable change) that preserves stability.

The transformed state matrix **R** is given by:

$$\mathbf{R} = \mathbf{L}^{-1}(t) \cdot \left[\mathbf{A}(t) \cdot \mathbf{L}(t) - \dot{\mathbf{L}}(t)\right] \tag{4.3}$$

According to the Floquet Theory, stability properties of the original T-periodic state equation are equivalent to stability properties of the LTI system represented by equation 4.1 [87]. This means that the eigenvalues of **R**, known as the *Floquet characteristic exponents*, can be used to determine system stability according to the following theorem.

Theorem (Floquet Theory [87, 110]). A LP system is exponentially asymptotically stable if, and only if, all Floquet characteristic exponents have negative real parts.

Consequently, the eigenanalysis concepts presented in chapter 3 can be extended to nonautonomous, linear periodic systems by applying the Floquet Theory.

4.3 Small-Signal Electrical Models for SIMSEN based on *a,b,c*-Phase Coordinates

As mentioned in section 4.1, the nonautonomous characteristic of the electrical models available in SIMSEN is due to the time-variant behavior of rotating machines parameters. Nevertheless, the varying components have a periodic characteristic, as illustrated in figure 4.1.

Therefore, the Floquet Theory can be applied to these models in order to derive small-signal models which are compatible with SIMSEN characteristics. This means that the state variables of the small-signal models must correspond to those of the already existing time-domain models, *i.e.*, the physical *a,b,c*-phase variables coordinates. This is a crucial criterion to be respected, since it will allow for the determination of the linearized matrices automatically from the circuits built in the SIMSEN GUI. In other words, this means taking advantage of the benefits of SIMSEN, previously listed in section 4.1.

In this regard, a procedure must be followed so as to derive the small-signal models based on *a,b,c*-phase coordinates. This procedure is illustrated in figure 4.3.

The inputs are the time-domain electrical models available in SIMSEN that are to be linearized. The outputs are the corresponding small-signal models based on *a,b,c*-phase coordinates. All small-signal models must be derived following the same procedure in order to guarantee a compatible connection between all elements.

This procedure is divided into three steps, which are explained in the following. Its application is illustrated further, in section 4.4.

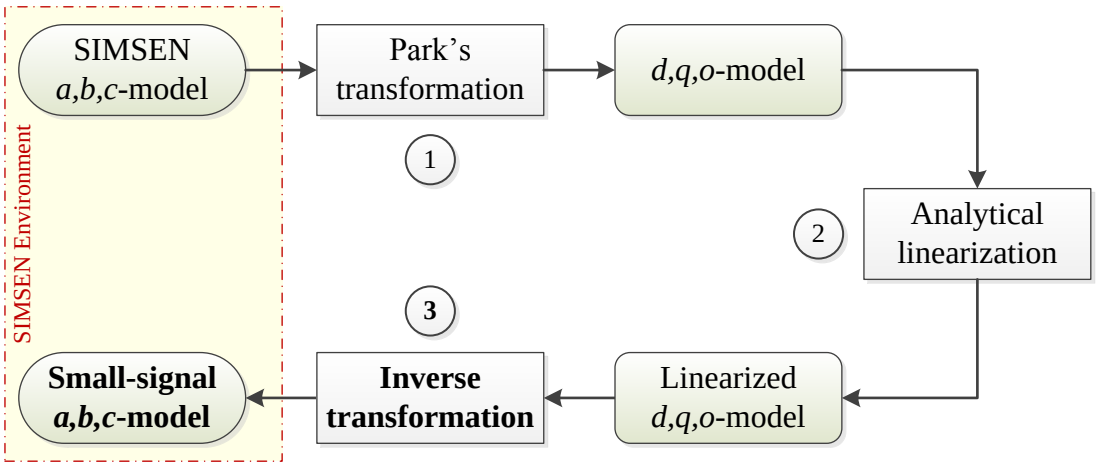

Figure 4.3: Procedure flowchart for determination of small-signal models for SIMSEN.

Step 1: Transformation of SIMSEN nonautonomous models in time-invariant models

The first step is to transform the *a,b,c*-phase coordinates time-domain models in time invariant models. This can be achieved through the well-known Park's transformation, which preserves the steady-state phase quantities and can be applied to voltages, currents and flux linkages. It is defined as:

$$\mathbf{P} = \frac{2}{3}\begin{bmatrix} \cos\theta & \cos\left(\theta - \frac{2\pi}{3}\right) & \cos\left(\theta + \frac{2\pi}{3}\right) \\ -\sin\theta & -\sin\left(\theta - \frac{2\pi}{3}\right) & -\sin\left(\theta + \frac{2\pi}{3}\right) \\ \frac{1}{2} & \frac{1}{2} & \frac{1}{2} \end{bmatrix} \tag{4.4}$$

where θ is the angular position of the rotor.

The relation between *d,q,o*-coordinates and *a,b,c*-coordinates state variables is:

$$\mathbf{x}_{dqo} = \mathbf{P} \cdot \mathbf{x}_{abc} \tag{4.5}$$

Matrix **P** is continuously differentiable, uniformly bounded, invertible and periodic. Therefore, it can be classified as a Lyapunov transformation. Indeed, it is well-known that the Park's transformation preserves the stability of the system, that is, the system is equally stable either if it is seen from the *a,b,c*-phase coordinates or from the Park's representation (*d,q,o*-axis representation).

It is important to note that the matrix representation used in SIMSEN differs from the traditional state-space representation presented in chapter 3. Each element in SIMSEN corresponds to an independent subsystem that is fully represented by a system of first-order differential equations, which can be described under matrix form as [89]:

$$\mathbf{A} \cdot \dot{\mathbf{x}}_{abc} = \mathbf{B} \cdot \mathbf{x}_{abc} + \mathbf{C} \tag{4.6}$$

It is worth pointing out that the matrices **A**, **B** and **C** presented here are not the same as those used in the state-space representation. From this point on any refences to **A**, **B** or **C** are related to the matrices of the formulation used in SIMSEN. The linearized matrices are followed by the "ℓ" subscript.

The formulation presented in equation (4.6) is kept even after the Park's transformation. Considering the inverse of relation (4.5) and substituting it in equation (4.6) yields:

$$\mathbf{A}_{dqo} \cdot \dot{\mathbf{x}}_{dqo} = \mathbf{B}_{dqo} \cdot \mathbf{x}_{dqo} + \mathbf{C}_{dqo} \tag{4.7}$$

with

$$\begin{aligned}
\mathbf{A}_{dqo} &= \mathbf{A} \cdot \mathbf{P}^{-1} \\
\mathbf{B}_{dqo} &= \mathbf{B} \cdot \mathbf{P}^{-1} - \mathbf{A} \cdot \dot{\mathbf{P}}^{-1} \\
\mathbf{C}_{dqo} &= \mathbf{C}
\end{aligned}$$

Step 2: Analytical linearization of the time-invariant models

The models based on *d,q,o*-axis representation are time-invariant models. Once they are linearized, the eigenanalysis concepts presented in chapter 3, section 3.3 can be applied.

The analytical linearization is achieved through first-order Taylor expansions applied to the state equations of the system, as described in section 3.3.1, equation (3.6). This procedure yields a system of the following form:

$$\mathbf{A}_{\ell_{dqo}} \cdot \Delta\dot{\mathbf{x}}_{dqo} = \mathbf{B}_{\ell_{dqo}} \cdot \Delta\mathbf{x}_{dqo} + \mathbf{C}_{\ell} \tag{4.8}$$

At this stage, the eigenvalues could be extracted from the *d,q,o*-state matrix, given by:

$$\mathbf{A}_{\ell_{dqo}}^{-1} \cdot \mathbf{B}_{\ell_{dqo}}$$

Nevertheless, another step is needed in order to adapt the state variables to those used in SIMSEN.

Step 3: Coordinates inverse transformation of the linearized time-invariant models

Even though the first two steps of this procedure are classical operations in the field of electrical systems and rotating machines, they are not enough to yield small-signal models which are suitable for SIMSEN.

Consequently, an inverse transformation is necessary and must be judiciously determined. This transformation ought to be a Lyapunov transformation in the sense that it must preserve the stability of the system. Moreover, it has to perform a state variable transformation to adapt the models back to SIMSEN so that the connection of the elements remain modular, independently of the topology of the system.

At first glance, the inverse Park's transformation $\mathbf{P}^{-1}$ would seemingly be an elementary choice capable of conforming to the needed criteria. But if this transformation is applied as such, a problem remains. Although it preserves system stability and transforms the state variables back to those used in SIMSEN, modularity is not guaranteed. This happens because the inverse Park's transformation when applied to linearized *d,q,o*-models produce inappropriate crossed terms between different elements of the system.

In order for modularity to be kept, crossed terms may exist specifically on the interfaces of the electrical, mechanical, hydraulic and regulation subsystems. These interfaces are either the regulation blocks or the rotating inertias.

In the first case, the crossed terms are related to the inputs coming from the electrical subsystem (for voltage regulator and stabilizers) or from the mechanical and hydraulic subsystems (for turbine governors). Also, the regulators outputs introduce crossed terms with the regulated elements.

In the case of rotating inertias, the crossed terms exist due to the momentum equation that describes the dynamics of the angular speed ω_m of the rotating parts:

$$\frac{J}{P_p}\frac{d\omega_m}{dt} = \sum T = T_{turb} + T_{em} \quad \xrightarrow{linearization} \quad \frac{J}{P_p}\frac{d\Delta\omega_m}{dt} = \Delta T_{turb} + \Delta T_{em} \tag{4.9}$$

where J is the total moment of inertia of the rotating parts, P_p is the number of pairs of poles of the generator, T_{turb} is the turbine torque and T_{em} is the electromagnetic torque of the generator. The cross-influence of the hydraulic and the electrical subsystems on the mechanical one is evidenced by equation (4.9).

Consequently, in order to obtain models which have coherent terms that guarantee modularity, the inverse transformation must be developed based on the inverse Park's transformation, as explained in the following.

From equation (4.5), it is possible to define the inverse Park's transformation as:

$$\mathbf{x}_{abc} = \mathbf{P}^{-1} \cdot \mathbf{x}_{dqo} \tag{4.10}$$

This transformation is only applicable to non-linearized systems. But in order to properly transform the linearized state variables, it is required to linearize equation (4.10) as follows:

$$\Delta\mathbf{x}_{abc} = \left.\frac{\partial \mathbf{x}_{abc}}{\partial \mathbf{x}_{dqo}}\right|_0 \cdot \Delta\mathbf{x}_{dqo} + \left.\left(\frac{\partial \mathbf{x}_{abc}}{\partial \mathbf{P}^{-1}} \cdot \frac{\partial \mathbf{P}^{-1}}{\partial \theta}\right)\right|_0 \Delta\theta$$

Finally, it yields the only inverse transformation capable of consistently producing small-signal electrical models based on *a,b,c*-phase variables:

$$\Delta\mathbf{x}_{abc} = \mathbf{P}^{-1}\big|_0 \cdot \Delta\mathbf{x}_{dqo} + \left.\left(\frac{\partial \mathbf{P}^{-1}}{\partial \theta} \cdot \mathbf{x}_{dqo}\right)\right|_0 \Delta\theta \tag{4.11}$$

Or, under matrix form:

$$\begin{bmatrix} \Delta x_a \\ \Delta x_b \\ \Delta x_c \end{bmatrix} = \begin{bmatrix} \cos\theta_0 & -\sin\theta_0 & 1 \\ \cos\left(\theta_0 - \frac{2\pi}{3}\right) & -\sin\left(\theta_0 - \frac{2\pi}{3}\right) & 1 \\ \cos\left(\theta_0 + \frac{2\pi}{3}\right) & -\sin\left(\theta_0 + \frac{2\pi}{3}\right) & 1 \end{bmatrix} \cdot \begin{bmatrix} \Delta x_d \\ \Delta x_q \\ \Delta x_o \end{bmatrix}$$

$$- \begin{bmatrix} \sin\theta_0 & \cos\theta_0 & 0 \\ \sin\left(\theta_0 - \frac{2\pi}{3}\right) & \cos\left(\theta_0 - \frac{2\pi}{3}\right) & 0 \\ \sin\left(\theta_0 + \frac{2\pi}{3}\right) & \cos\left(\theta_0 + \frac{2\pi}{3}\right) & 0 \end{bmatrix} \cdot \begin{bmatrix} x_{d0} \\ x_{q0} \\ x_{o0} \end{bmatrix} \Delta\theta \tag{4.12}$$

Only the application of this transformation to the linearized *d,q,o*-coordinates models converts them into *a,b,c*-phase coordinates small-signal models adapted to SIMSEN, while preserving system stability and respecting the modularity requirement.

4.4 Proposed Modeling Procedure Applied to the Salient-Pole Synchronous Machine

For the purpose of illustrating step by step the procedure described in section 4.3, an example is presented in this section. The linearization and inverse transformation of the synchronous

machine is performed.

For the sake of clarity and ease of reading, only the development for the equation of the voltage of stator phase a is presented. The full set of equations of the SIMSEN small-signal model for the salient-pole synchronous machine is presented in appendix A, section A.1.

Step 1: Transformation of *a,b,c*-phase coordinates model in *d,q,o*-coordinates model

Applying the Park's transformation to the a,b,c-phase coordinates model of the synchronous machine[a] yields the well-known Park's model:

$$u_d = R_s\, i_d + L_d \frac{d i_d}{d t} + L_{fa} \frac{d i_f}{d t} + L_{Da} \frac{d i_D}{d t} - \omega_m \left(L_q\, i_q + L_{Qa}\, i_Q \right) \tag{4.13}$$

$$u_q = R_s\, i_q + L_q \frac{d i_q}{d t} + L_{Qa} \frac{d i_Q}{d t} + \omega_m \left(L_d\, i_d + L_{fa}\, i_f + L_{Da}\, i_D \right) \tag{4.14}$$

$$u_o = R_s\, i_o + L_o \frac{d i_o}{d t} \tag{4.15}$$

$$u_f = R_f\, i_f + \frac{3}{2} L_{fa} \frac{d i_d}{d t} + L_f \frac{d i_f}{d t} + L_{Df} \frac{d i_D}{d t} \tag{4.16}$$

$$0 = R_D\, i_D + \frac{3}{2} L_{Da} \frac{d i_d}{d t} + L_{Df} \frac{d i_f}{d t} + L_D \frac{d i_D}{d t} \tag{4.17}$$

$$0 = R_Q\, i_Q + \frac{3}{2} L_{Qa} \frac{d i_q}{d t} + L_Q \frac{d i_Q}{d t} \tag{4.18}$$

where quantities with the subscripts d are related to the direct axis (d-axis), q to the quadrature axis (q-axis) and o to the zero phase-sequence axis. The subscript s refers to stator winding parameters, f to the excitation (field) winding, D to the equivalent damper winding in the d-axis and Q to the equivalent damper winding in the q-axis.

Step 2: Analytical linearization of the *d,q,o*-coordinates model

As the second step, the procedure presented in chapter 3, section 3.3 is applied to equations (4.13)–(4.18). It yields:

[a] For the detailed a,b,c-phase coordinates model, please see J. Chatelain, *Machines Electriques*, chap. 7, pp. 340-341 [16].

$$\Delta u_d = R_s \Delta i_d + L_d \frac{d\Delta i_d}{dt} + L_{fa} \frac{d\Delta i_f}{dt} + L_{Da} \frac{d\Delta i_D}{dt} - \omega_{m0} L_q \Delta i_q - \omega_{m0} L_{Qa} \Delta i_Q \\ - \left(L_q i_{q0} + L_{Qa} i_{Q0}\right) \Delta\omega_m \tag{4.19}$$

$$\Delta u_q = R_s \Delta i_q + L_q \frac{d\Delta i_q}{dt} + L_{Qa} \frac{d\Delta i_Q}{dt} + \omega_{m0} L_d \Delta i_d + \omega_{m0} L_{fa} \Delta i_f + \omega_{m0} L_{Da} \Delta i_D \\ - \left(L_d i_{d0} + L_{fa} i_{f0} + L_{Da} i_{D0}\right) \Delta\omega_m \tag{4.20}$$

$$\Delta u_o = R_s \Delta i_o + L_o \frac{d\Delta i_o}{dt} \tag{4.21}$$

$$\Delta u_f = R_f \Delta i_f + \frac{3}{2} L_{fa} \frac{d\Delta i_d}{dt} + L_f \frac{d\Delta i_f}{dt} + L_{Df} \frac{d\Delta i_D}{dt} \tag{4.22}$$

$$0 = R_D \Delta i_D + \frac{3}{2} L_{Da} \frac{d\Delta i_d}{dt} + L_{Df} \frac{d\Delta i_f}{dt} + L_D \frac{d\Delta i_D}{dt} \tag{4.23}$$

$$0 = R_Q \Delta i_Q + \frac{3}{2} L_{Qa} \frac{d\Delta i_q}{dt} + L_Q \frac{d\Delta i_Q}{dt} \tag{4.24}$$

Considering steady-state initial conditions: $i_{D0} = 0$ and $i_{Q0} = 0$.

Step 3: Inverse transformation to *a,b,c*-phase coordinates applied to the stator phase a

From the inverse transformation defined in the previous section, described by equation (4.12), it is possible to write:

$$\Delta u_a = \Delta u_d \cos\theta_0 - \Delta u_q \sin\theta_0 + \Delta u_o - \left(u_{d0} \sin\theta_0 + u_{q0} \cos\theta_0\right) \Delta\theta \tag{4.25}$$

By introducing equations (4.19)–(4.24) in equation (4.25), and considering the following linearized relations:

$$\Delta i_d = \frac{2}{3}\left[\Delta i_a \cos\theta_0 + \Delta i_b \cos\left(\theta_0 - \frac{2\pi}{3}\right) + \Delta i_c \cos\left(\theta_0 + \frac{2\pi}{3}\right)\right] + i_{q0}\Delta\theta$$

$$\Delta i_q = -\frac{2}{3}\left[\Delta i_a \sin\theta_0 + \Delta i_b \sin\left(\theta_0 - \frac{2\pi}{3}\right) + \Delta i_c \sin\left(\theta_0 + \frac{2\pi}{3}\right)\right] - i_{d0}\Delta\theta$$

$$\Delta i_o = \frac{1}{3}\left(\Delta i_a + \Delta i_b + \Delta i_c\right)$$

After some analytical manipulations:

$$
\begin{aligned}
\Delta u_a = & \left\{\frac{2}{3}\left[L_d\cos^2\theta_0 + L_q\sin^2\theta_0\right] + \frac{L_o}{3}\right\}\frac{d\Delta i_a}{dt} \\
& + \left\{\frac{2}{3}\left[L_d\cos\theta_0\cos\left(\theta_0 - \frac{2\pi}{3}\right) + L_q\sin\theta_0\sin\left(\theta_0 - \frac{2\pi}{3}\right)\right] + \frac{L_o}{3}\right\}\frac{d\Delta i_b}{dt} \\
& + \left\{\frac{2}{3}\left[L_d\cos\theta_0\cos\left(\theta_0 + \frac{2\pi}{3}\right) + L_q\sin\theta_0\sin\left(\theta_0 + \frac{2\pi}{3}\right)\right] + \frac{L_o}{3}\right\}\frac{d\Delta i_c}{dt} \\
& + L_{fa}\cos\theta_0\frac{d\Delta i_f}{dt} + L_{Da}\cos\theta_0\frac{d\Delta i_D}{dt} + L_{Qa}\sin\theta_0\frac{d\Delta i_Q}{dt} \\
& + \left[R_s - \frac{\omega_{m0}}{3}\left(L_d - L_q\right)\sin\left(2\theta_0\right)\right]\Delta i_a \\
& - \frac{\omega_{m0}}{3}\left[\left(L_d - L_q\right)\sin\left(2\theta_0 - \frac{2\pi}{3}\right) + \frac{\sqrt{3}}{2}\left(L_d + L_q\right)\right]\Delta i_b \\
& - \frac{\omega_{m0}}{3}\left[\left(L_d - L_q\right)\sin\left(2\theta_0 + \frac{2\pi}{3}\right) - \frac{\sqrt{3}}{2}\left(L_d + L_q\right)\right]\Delta i_c \\
& - \omega_{m0}L_{fa}\sin\theta_0\Delta i_f - \omega_{m0}L_{Da}\sin\theta_0\Delta i_D - \omega_{m0}L_{Qa}\cos\theta_0\Delta i_Q \\
& + \left[\left(L_d - L_q\right)\left(i_{q0}\cos\theta_0 - i_{d0}\sin\theta_0\right) - L_{fa}\,i_{f0}\sin\theta_0\right]\Delta\omega_m \\
& + \left[\left(R_s\,i_{q0} + \omega_{m0}L_q\,i_{d0} - u_{q0}\right)\cos\theta_0 + \left(R_s\,i_{d0} - \omega_{m0}L_d\,i_{q0} - u_{d0}\right)\sin\theta_0\right]\Delta\theta
\end{aligned}
\tag{4.26}
$$

Now, it is possible to adapt the initial conditions and simplify the last two terms of equation (4.26) considering that:

$$
\begin{aligned}
i_{d0} = & \ \frac{2}{3}\left[i_{a0}\cos\theta_0 + i_{b0}\cos\left(\theta_0 - \frac{2\pi}{3}\right) + i_{c0}\cos\left(\theta_0 + \frac{2\pi}{3}\right)\right] \\
i_{q0} = & -\frac{2}{3}\left[i_{a0}\sin\theta_0 + i_{b0}\sin\left(\theta_0 - \frac{2\pi}{3}\right) + i_{c0}\sin\left(\theta_0 + \frac{2\pi}{3}\right)\right]
\end{aligned}
$$

and

$$
\begin{aligned}
u_{d0} &= R_s\,i_{d0} + L_d\frac{di_{d0}}{dt} - \omega_{m0}L_q\,i_{q0} \quad ; \quad \text{with} \quad \frac{di_{d0}}{dt} = 0 \\
&\Longrightarrow \quad R_s\,i_{d0} - u_{d0} = \omega_{m0}L_q\,i_{q0} \\
u_{q0} &= R_s\,i_{q0} + L_d\frac{di_{q0}}{dt} + \omega_{m0}L_d\,i_{d0} + \omega_{m0}L_{fa}\,i_{f0} \quad ; \quad \text{with} \quad \frac{di_{q0}}{dt} = 0 \\
&\Longrightarrow \quad R_s\,i_{q0} - u_{q0} = -\omega_{m0}L_d\,i_{d0} - \omega_{m0}L_{fa}\,i_{f0}
\end{aligned}
$$

Finally, it yields for the phase a:

$$
\begin{aligned}
\Delta u_a = & \left\{\frac{2}{3}\left[L_d \cos^2\theta_0 + L_q \sin^2\theta_0\right] + \frac{L_o}{3}\right\}\frac{d\Delta i_a}{dt} \\
& + \left\{\frac{2}{3}\left[L_d \cos\theta_0 \cos\left(\theta_0 - \frac{2\pi}{3}\right) + L_q \sin\theta_0 \sin\left(\theta_0 - \frac{2\pi}{3}\right)\right] + \frac{L_o}{3}\right\}\frac{d\Delta i_b}{dt} \\
& + \left\{\frac{2}{3}\left[L_d \cos\theta_0 \cos\left(\theta_0 + \frac{2\pi}{3}\right) + L_q \sin\theta_0 \sin\left(\theta_0 + \frac{2\pi}{3}\right)\right] + \frac{L_o}{3}\right\}\frac{d\Delta i_c}{dt} \\
& + L_{fa}\cos\theta_0 \frac{d\Delta i_f}{dt} + L_{Da}\cos\theta_0 \frac{d\Delta i_D}{dt} - L_{Qa}\sin\theta_0 \frac{d\Delta i_Q}{dt} \\
& + \left[R_s - \frac{\omega_{m0}}{3}\left(L_d - L_q\right)\sin\left(2\theta_0\right)\right]\Delta i_a \\
& - \frac{\omega_{m0}}{3}\left[\left(L_d - L_q\right)\sin\left(2\theta_0 - \frac{2\pi}{3}\right) + \frac{\sqrt{3}}{2}\left(L_d + L_q\right)\right]\Delta i_b \\
& - \frac{\omega_{m0}}{3}\left[\left(L_d - L_q\right)\sin\left(2\theta_0 + \frac{2\pi}{3}\right) - \frac{\sqrt{3}}{2}\left(L_d + L_q\right)\right]\Delta i_c \\
& - \omega_{m0} L_{fa}\sin\theta_0 \Delta i_f - \omega_{m0} L_{Da}\sin\theta_0 \Delta i_D - \omega_{m0} L_{Qa}\cos\theta_0 \Delta i_Q \\
& - \left\{\frac{2}{3}\left(L_d - L_q\right)\left[i_{a0}\sin\left(2\theta_0\right) + i_{b0}\sin\left(2\theta_0 - \frac{2\pi}{3}\right) + i_{c0}\sin\left(2\theta_0 + \frac{2\pi}{3}\right)\right]\right. \\
& \qquad \left. + L_{fa} i_{f0}\sin\theta_0\right\}\Delta\omega_m \\
& - \omega_{m0}\left\{\frac{2}{3}\left(L_d - L_q\right)\left[i_{a0}\cos\left(2\theta_0\right) + i_{b0}\cos\left(2\theta_0 - \frac{2\pi}{3}\right) + i_{c0}\cos\left(2\theta_0 + \frac{2\pi}{3}\right)\right]\right. \\
& \qquad \left. + L_{fa} i_{f0}\cos\theta_0\right\}\Delta\theta
\end{aligned}
\tag{4.27}
$$

The complete small-signal model of the salient-pole synchronous machine based on a,b,c-phase coordinates is composed of three stator equations, three rotor equations (for the excitation and the two equivalent damper windings), plus two mechanical equations related to angular speed and angular position of the rotor. The full set of equations can be found in appendix A, section A.1.

The same procedure is applied to all elements for which a small-signal stability model is to be developed. The detailed equations corresponding to each element are presented in appendix A. In chapter 5, these models are introduced and validated.

5 Validation of the Small-Signal Models

5.1 Small-signal Electrical Models Based on *a,b,c*-Phase Coordinates

In this chapter, all the small-signal models based on *a,b,c*-phase coordinates are introduced and validated. All these models were developed through the analytical method presented in chapter 4.

Besides presenting the calculation of the eigenvalues, a validation is performed based either on comparisons with time-domain simulation results or on analytical demonstrations of the origin of the eigenmodes.

As previously stated, the detailed equations of each model are presented in appendix A.

5.2 Construction of System Matrices in SIMSEN

Before presenting any results, it is important to briefly understand how the procedures of SIMSEN perform the construction of the system matrices. In SIMSEN, three-phase elements are subsystems described by three individual differential equations, one for each phase. When such elements are interconnected to form a global system, the generation of the matrices describing the full set of differential equations is accomplished through a specific algorithm which reuses the models of each element to translate the topology of the circuit, based on a connection list[a].

[a]For further details, please see A. Sapin, *Logiciel Modulaire pour la Simulation et l'Etude des Systèmes d'Entraînements et des Réseaux Electriques*, chap. 2, pp. 8,16–19 [89].

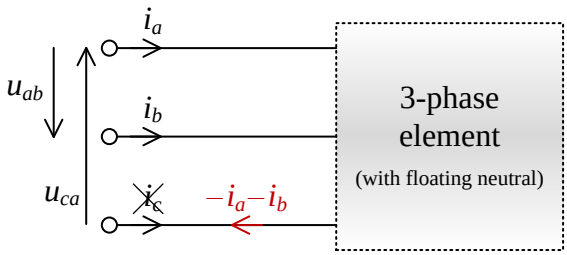

Figure 5.1: Current loops construction in SIMSEN.

If the three-phase elements have floating neutral points, this algorithm performs a simplification. Indeed, in this case one of the currents is linearly dependent on the others: $i_c = -i_a - i_b$. Consequently, this state variable can be eliminated and phase-to-phase voltage equations are used, as illustrated in figure 5.1. The order of the matrices describing the global system is then reduced.

From the viewpoint of eigenanalysis, this has no major consequence on the results. The elimination of the redundant variable only leads to the elimination of one equally redundant eigenmode. It was verified that the eliminated eigenmode is always purely real, negative, and corresponds to the time constant related to the leakage inductances of the corresponding elements. This eigenmode gives no relevant information about the global system small-signal stability.

5.3 Salient-Pole Synchronous Machine

In order to exemplify and validate the small-signal model derived for the salient-pole synchronous machine, an example is presented and the results are discussed. In this example, the synchronous machine (with constant excitation voltage) is connected to an infinite bus, as illustrated in figure 5.2. The machine ratings are presented in table 5.1

The parameters of the machine are those from its equivalent circuit based on the d,q-axis representation, depicted in figure 5.3. For this example, the parameters are presented in table 5.2.

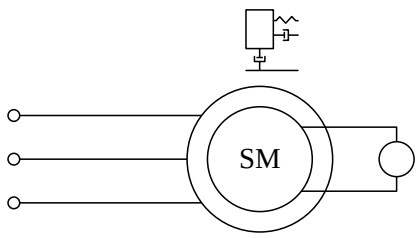

Figure 5.2: Synchronous machine connected to an infinite bus.

Table 5.1: Synchronous machine ratings.

Rated apparent power	S_N	83.0	(MVA)
Rated voltage	U_N	17.5	(kV)
Rated frequency	f_N	50	(Hz)
Number of pairs of poles	P_p	5	(–)
No-load excitation current	$I_{f\delta 0}$	578.3	(A)

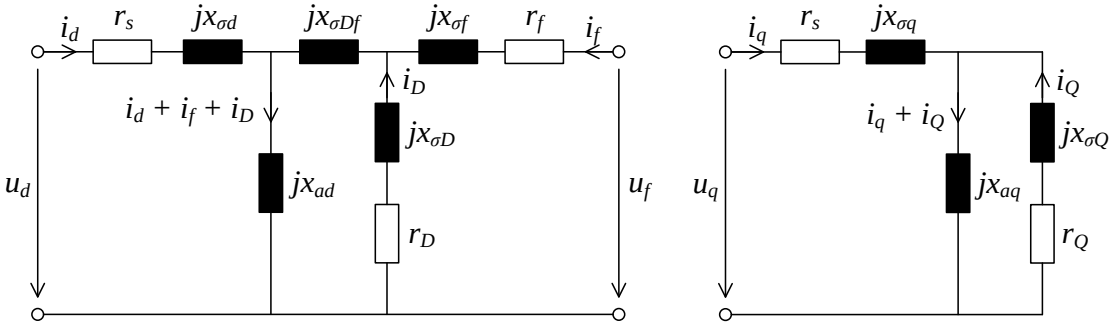

Figure 5.3: Direct- (left) and quadrature-axis (right) equivalent circuit for the synchronous machine.

Table 5.2: Parameters of the synchronous machine.

Resistance of stator winding	r_s	$1.81 \cdot 10^{-3}$	(p.u.)
Leakage reactance of stator winding	$x_{\sigma s}$	0.112	(p.u.)
Magnetizing reactance in the d–axis	x_{ad}	1.027	(p.u.)
Mutual reactance between excitation and damper D	$x_{\sigma Df}$	−0.021	(p.u.)
Resistance of excitation winding	r_f	$4.97 \cdot 10^{-4}$	(p.u.)
Leakage reactance of the excitation winding	$x_{\sigma f}$	0.1968	(p.u.)
Resistance of the equivalent damper winding D	r_D	0.0101	(p.u.)
Leakage reactance of the damper winding D	$x_{\sigma D}$	0.0829	(p.u.)
Magnetizing reactance in the q–axis	x_{aq}	0.6020	(p.u.)
Resistance of the equivalent damper winding Q	r_Q	0.0161	(p.u.)
Leakage reactance of the damper winding Q	$x_{\sigma Q}$	0.0779	(p.u.)
Inertia of rotating parts	J_g	$168.3 \cdot 10^3$	($\mathrm{kg \cdot m^2}$)

The mechanical part is represented by one rotating mass. The inertia J_g is also given in table 5.2. This subsystem is described by two differential equations, related to the angular speed $\Delta\omega_m$ and angular position $\Delta\theta$:

$$\frac{J_g}{P_p}\frac{d\Delta\omega_m}{dt} = \Delta T_{turb} + \Delta T_{em} \tag{5.1}$$

$$\frac{d\Delta\theta}{dt} = \Delta\omega_m \tag{5.2}$$

Consequently, the synchronous machine – infinite bus system is represented by eight differential equations. Nevertheless, as explained in section 5.2, the equation and state variable related to the stator phase c are eliminated.

The eigensolution of the system at rated operating conditions yields seven eigenvalues of the form $\lambda_i = \sigma \pm j\omega_d$. More precisely, two pairs of complex conjugate and three purely real eigenvalues are obtained. The results are given in table 5.3.

Real and imaginary parts are presented separately. In addition, the damping time constant τ ($\tau = 1/|\sigma|$), the damping ratio ζ and the frequency f are calculated based on equations (3.11) and (3.12), given on page 35. Furthermore, the dominant state variables are indicated. They were identified using participation factors calculated according to the concept presented in section 3.3.3. However, the numerical values are not given here in order to simplify the interpretation of the results. The dominant states indicated in table 5.3 are those that presented higher values of participation factor related to each eigenvalue.

The first pair of eigenvalues can be identified as the local mode. It has a frequency that lies in the range of electro-mechanical mode oscillations (0.7 to 2 Hz). Moreover, the dominant states are the stator currents and the mechanical variables. This corresponds to the effect of the local mode which is related to rotor angle oscillations of the generator against the network. It is important to note that the frequency of this mode depends strongly on the operating

Table 5.3: Eigenproperties of the synchronous machine – infinite bus system.

Eigenvalue number i	$\sigma = \Re(\lambda_i)$ (Np/s)	$\omega_d = \Im(\lambda_i)$ (rad/s)	τ (s)	ζ (%)	f (Hz)	Dominant states
1,2	−2.942	10.34	0.340	27.4	1.646	$\Delta\omega_m, \Delta\theta, \Delta i_{abc}$
3,4	−3.484	314.0	0.287	1.11	49.97	Δi_{abc}
5	−25.83	–	0.039	100	–	$\Delta i_Q, \Delta i_{abc}$
6	−20.59	–	0.049	100	–	$\Delta i_D, \Delta i_{abc}$
7	−0.418	–	2.392	100	–	$\Delta i_f, \Delta i_{abc}$

point of the machine.

Furthermore, it is also interesting to observe that the damping time constant of this eigenmode ($\tau = 0.340$ s) is related to the equivalent damper winding D. Indeed, this value of τ is very close to the *short-circuit time constant of the equivalent damper winding* D (T_D), which is equal to 0.344 seconds[b].

The effect of this eigenmode can be observed through a time-domain simulation once the system is disturbed. Figure 5.4 presents the electrical power fluctuation following a +5% step on the external torque applied to the rotor[c]. In the oscillating behavior it is possible to graphically identify a frequency $f = 1.654$ Hz, which confirms the result presented in table 5.3 with a very strong agreement. Additionally, it is possible to determine a decaying envelope calculated from two peaks of the oscillating power. The determination of this envelope yields an attenuation $\sigma = -2.91$. This means $\tau = 0.344$ s which is equal to the short-circuit time constant of the equivalent damper winding D (T_D), thus in good agreement with the eigenanalysis result.

The second pair of eigenvalues (pair 3,4) is clearly related to the frequency of the network. Consequently, the dominant states are the stator currents. Additionally, for these eigenvalues $\tau = 0.287$ s, which is very close to the *armature short-circuit time constant* $T_a = 0.289$ s.

The eigenvalue number 5 is a purely real eigenvalue which is closely related to the equivalent damper winding Q, but also to the stator windings. Its corresponding time constant ($\tau = 0.039$ s) is relatively close to the *subtransient short-circuit time constant in the q-axis* $T''_q = 0.034$ s.

The eigenvalue number 6 is of similar nature. It is strongly related to the equivalent damper winding D and to the stator windings to a less extent. In this case, $\tau = 0.049$ s is relatively close to the *subtransient short-circuit time constant in the d-axis* $T''_d = 0.044$ s.

The last eigenvalue is strongly related both to the field winding and to the stator windings. Its damping has a time constant $\tau = 2.392$ s which cannot be directly compared to any individual time constant of the machine. Nevertheless, it can be clearly observed through time-domain simulation results. This eigenmode appears on the exponential decrease of the aperiodic component happening on the excitation current after the disturbance, as it can be seen in figure 5.5. Besides the oscillation caused by the local mode, which is quickly damped, it is easy to observe the exponential decrease of the excitation current. From two reference points

[b] For details on how the time constants of the synchronous machine can be determined, please see J. Chatelain, *Machines Electriques*, chap. 7, pp. 389-391 [16].

[c] According to the sign convention used in SIMSEN, negative power means generated (delivered) power. In order to better visualize the local mode and its envelope, the curves of electrical power are presented in this chapter with a negative sign ($-p_{el}$).

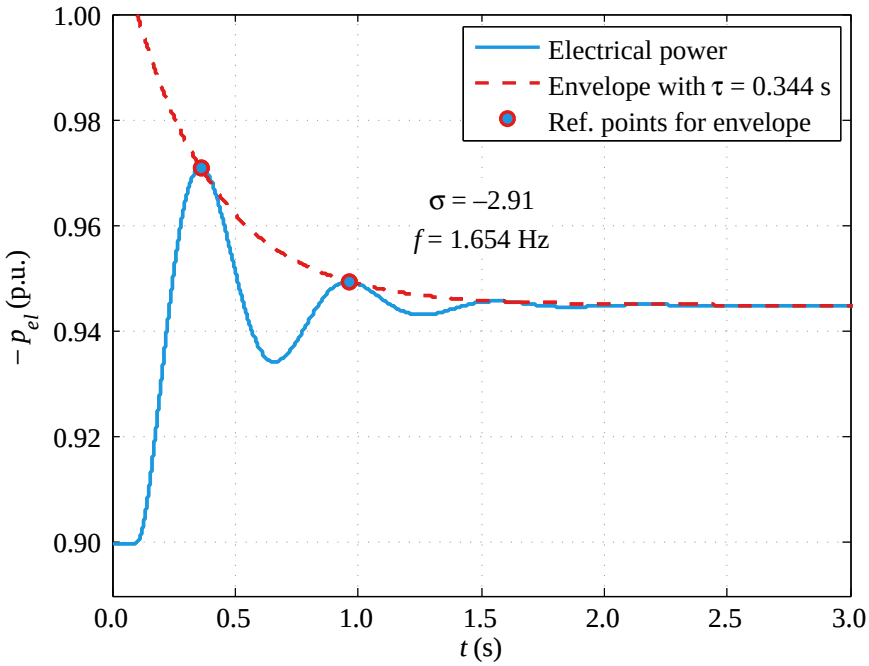

Figure 5.4: Power fluctuation due to the local mode oscillation.

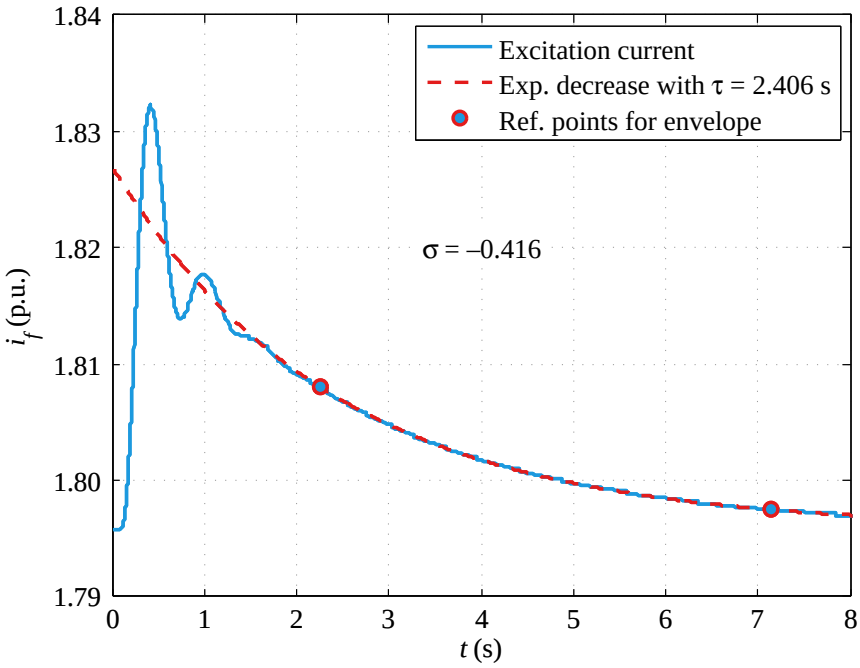

Figure 5.5: Damping of the excitation current related to the corresponding eigenvalue.

taken from the curve, a time constant $\tau = 2.404$ s ($\sigma = 0.416$), confirming the last eigenmode.

5.4 Wound-Rotor Induction Machine

The small-signal model of the wound-rotor induction machine is composed of eight differential equations: three for the *a,b,c*-phases of the stator, three for the *A,B,C*-phases of the rotor and the two mechanical equations, related to the angular speed and position previously described.

In this example, an induction generator with a star-star (*Y*-*Y*) connection and short-circuited rotor windings is considered connected to an infinite bus, as depicted in figure 5.6. The ratings of the machine are presented in table 5.4.

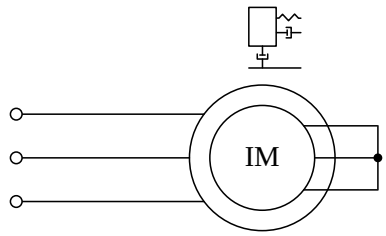

Figure 5.6: Induction machine connected to an infinite bus.

Table 5.4: Induction machine ratings.

Rated apparent power	S_N	83.0	(MVA)
Rated voltage	U_N	18.0	(kV)
Rated frequency	f_N	60	(Hz)
Number of pairs of poles	P_p	8	(–)
Stator-rotor turns ratio	μ	0.598	(–)

The parameters of the machine are those from its equivalent circuit, illustrated in figure 5.7. For this example, the parameters are presented in table 5.5 (obtained from [75]).

The eigensolution of the system at rated voltage and 40% load operating condition yields five eigenvalues, 2 pairs of complex conjugate and 1 purely real eigenvalue. The results are given in table 5.6.

The first pair of eigenvalues correspond to the local mode. It is mostly related to the rotor oscillations against the network, but it also relates to the stator and rotor quantities. It can be observed through a time-domain simulation in which the external torque applied to the rotor is disturbed by a +5% step. The mechanical power fluctuations correspond to the action of the

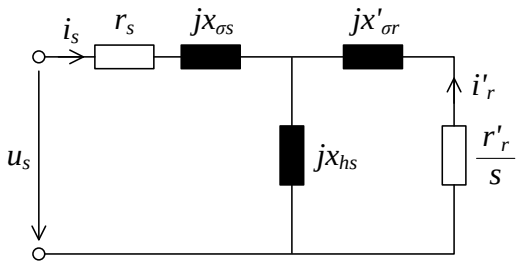

Figure 5.7: Equivalent circuit of the induction machine.

Table 5.5: Parameters of the induction machine.

Resistance of stator windings	r_s	$1.744 \cdot 10^{-3}$	(p.u.)
Leakage reactance of stator windings	$x_{\sigma s}$	0.2604	(p.u.)
Magnetizing reactance	x_{hs}	4.198	(p.u.)
Resistance of the rotor windings	r'_r	$2.015 \cdot 10^{-3}$	(p.u.)
Leakage reactance of rotor windings	$x'_{\sigma r}$	0.2721	(p.u.)
Inertia of rotating parts	J_g	$279.4 \cdot 10^3$	$(\mathrm{kg} \cdot \mathrm{m}^2)$

local mode and are depicted in figure 5.8. It is possible to identify a frequency of oscillation $f = 0.963$ Hz and an envelope that decreases exponentially with a time constant $\tau = 1.270$ s ($\sigma = -0.787$). This is in very good agreement with the properties of the local mode calculated through the small-signal model.

The second pair of eigenvalues correspond to the frequency of the network (60 Hz), and is directly related to the stator currents. The time constant related to these eigenvalues ($\tau = 0.785$ s) is the *transient short-circuit time constant of the stator windings* $T'_s = 0.785$ s[d].

Finally, the eigenvalue number 5 describes a non-oscillatory exponential decrease with $\tau = 0.728$ s. The effect of this eigenvalue can be observed in the behavior of the consumed reactive power, presented in figure 5.9. Besides the oscillating effect of the local mode, it is possible

[d] For details on how the time constants of the induction machine can be determined, please see J. Chatelain, *Machines Electriques*, chap. 6, pp. 300-305 [16].

Table 5.6: Eigenproperties of the induction generator machine – infinite bus system.

Eigenvalue number i	$\sigma = \Re(\lambda_i)$ (Np/s)	$\omega_d = \Im(\lambda_i)$ (rad/s)	τ (s)	ζ (%)	f (Hz)	Dominant states
1,2	−0.781	6.073	1.280	12.76	0.967	$\Delta i_{abc,ABC}, \Delta\omega_m, \Delta\theta$
3,4	−1.274	377.0	0.785	0.338	60.0	Δi_{abc}
5	−1.374	–	0.728	100	–	$\Delta i_{abc,ABC}$

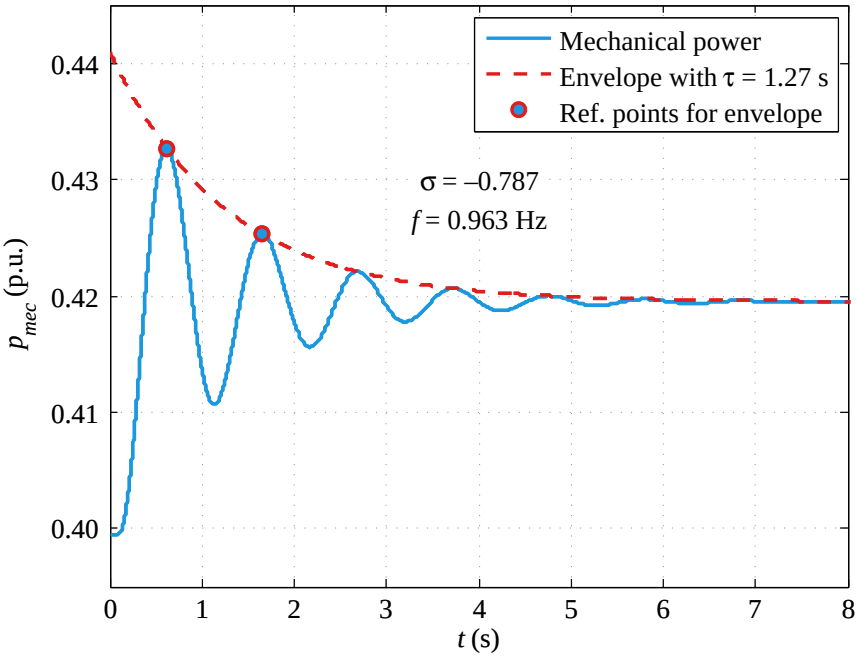

Figure 5.8: Power fluctuation on induction generator due to the local mode oscillation.

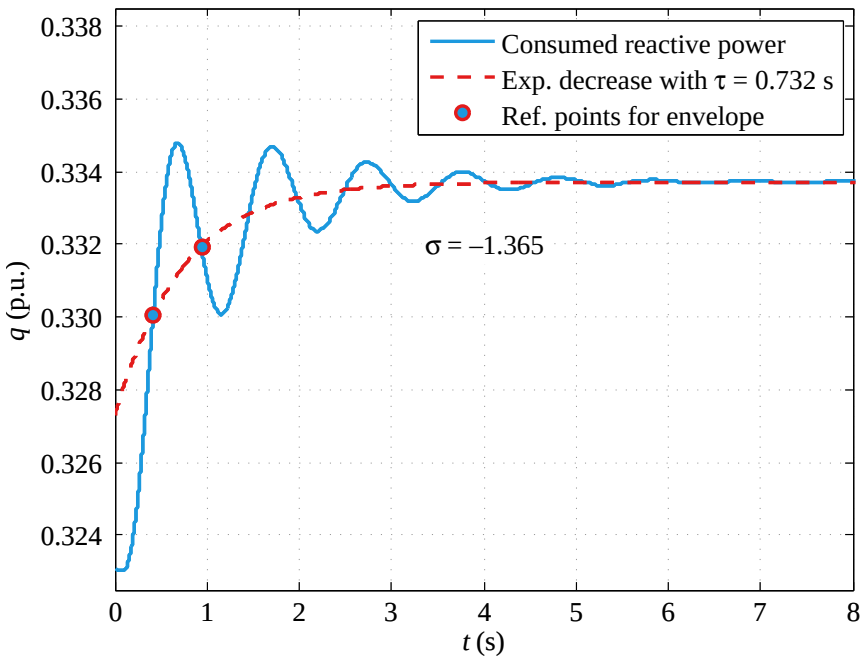

Figure 5.9: Exponential damping of the aperiodic component in the reactive power.

to see that there is an aperiodic component which fades away exponentially. The points describing this component are obtained by taking the mean value between the upper and lower envelopes of the curve. This exponential behavior has a time constant $\tau = 0.732$ s ($\sigma = -1.365$), validating the calculated eigenvalue.

5.5 Power Transformers

The small-signal model for power transformers are basically composed of six equations, one for each phase (state variables Δi_{abc1} and Δi_{abc2}, respectively for primary and secondary sides). If there is a delta connection, then a supplementary equation is added, related to the circulating current in the delta (Δi_{Δ}). The transformer connections available are the vector groups *Yy0*, *Yd5* and *Yd11*.

In order to illustrate and validate the small-signal model of the transformer, an example is presented. Basically, the example of section 5.3 is modified to introduce a transformer of vector group *Yd5* between the synchronous machine and the infinite bus, as presented in figure 5.10. The ratings of the transformer are given in table 5.7.

The parameters required for the transformer are those from its equivalent circuit, depicted in figure 5.11. The parameters used in this example are presented in table 5.8.

Before performing the eigenvalues calculation of the system presented in figure 5.10, it's interesting to calculate the eigenvalues of the transformer alone, so that they can be better identified. The results of this calculation are presented in table 5.9. Differently from the rotating machines, the eigenvalues of the transformer alone are independent of any initial conditions.

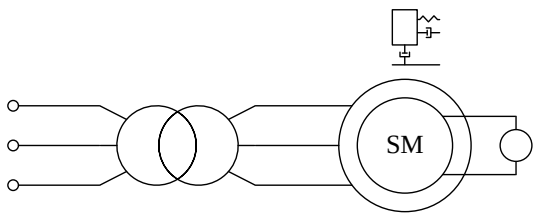

Figure 5.10: *Yd5*-transformer – generator – infinite bus system.

Table 5.7: Power transformer ratings.

Rated apparent power	S_N	84.0	(MVA)
Rated primary voltage	U_{N1}	220.0	(kV)
Rated secondary voltage	U_{N2}	17.5	(kV)
Rated frequency	f_N	50	(Hz)

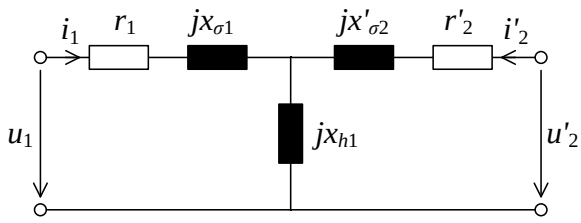

Figure 5.11: Equivalent circuit of a power transformer.

Table 5.8: Parameters of the *Yd5* power transformer.

Short-circuit resistance $(r_1 + r_2)$	r_{cc}	$3.0 \cdot 10^{-3}$	(p.u.)
Short-circuit reactance $(x_{\sigma 1} + x_{\sigma 2})$	x_{cc}	0.14	(p.u.)
Three-phase magnetizing reactance	x_{h1}	5.0	(p.u.)

The first two pairs present a frequency of exactly 50 Hz. It is important to note that this frequency does not have a physical meaning in the case of the transformer alone. It appears as a consequence of the linearization procedure. Indeed, the linearization is applied on the models at a stage where they are represented in the *d,q,o*-axis system (Park's representation). In order to maintain compatibility with the models of rotating machines, the *d,q,o*-axis system is a rotating reference frame for all elements (including transformers, lines, loads, etc.). The frequency of 50 Hz that appears in eigenvalues 1 to 4 is the rotational frequency of the reference frame in which the models were linearized. On the other hand, the real part of all eigenvalues are directly related to the parameters of the transformer.

The first pair has a time constant $\tau = 21.37$ s. This is equal to the time constant related to the magnetizing inductance of the transformer. This time constant can be obtained when the equivalent circuit is seen from the magnetizing branch with both terminals short-circuited, as illustrated in figure 5.12. The *magnetizing time constant* T_{h1} of the transformer can be calculated as:

Table 5.9: Eigenproperties of the power transformer.

Eigenvalue number i	$\sigma = \Re(\lambda_i)$ (Np/s)	$\omega_d = \Im(\lambda_i)$ (rad/s)	τ (s)	ζ (%)	f (Hz)	Dominant states
1,2	−0.0468	314.16	21.37	0.015	50.0	$\Delta i_{abc1,abc2}$
3,4	−6.732	314.16	0.149	2.14	50.0	$\Delta i_{abc1,abc2}$
5	−6.732	–	0.149	100	–	Δi_{Δ}

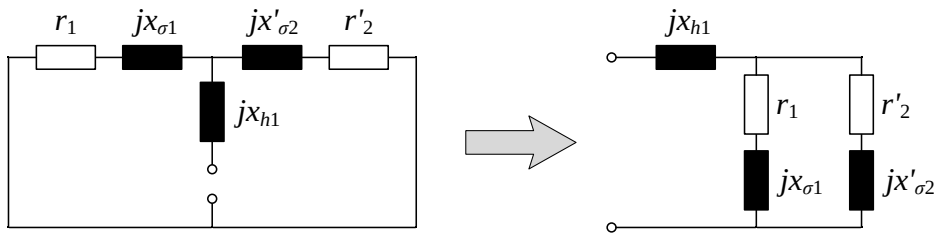

Figure 5.12: Equivalent circuit of the transformer seen from the magnetizing branch.

Table 5.10: Eigenproperties of the transformer – generator – infinite bus system.

Eigenvalue number i	$\sigma = \Re(\lambda_i)$ (Np/s)	$\omega_d = \Im(\lambda_i)$ (rad/s)	τ (s)	ζ (%)	f (Hz)	Dominant states
1,2	−1.423	8.738	0.703	16.0	1.391	$\Delta\omega_m, \Delta\theta, \Delta i_{abc2}$
3,4	−4.967	314.02	0.201	2.14	49.98	Δi_{abc2}
5,6	−0.0643	314.16	15.55	0.020	50.0	$\Delta i_{abc1,abc2}$
7	−18.74	–	0.053	100	–	$\Delta i_Q, \Delta i_{abc2}$
8	−16.58	–	0.060	100	–	$\Delta i_D, \Delta i_{abc2}$
9	−6.732	–	0.149	100	–	Δi_Δ
10	−0.292	–	3.425	100	–	$\Delta i_f, \Delta i_{abc2}$

$$T_{h1} = \frac{x_{h1} + \dfrac{x_{\sigma 1}\, x_{\sigma 2}}{x_{\sigma 1} + x_{\sigma 2}}}{\omega_N \dfrac{r_1\, r_2}{r_1 + r_2}} = 21.37 \text{ s} \tag{5.3}$$

The second pair and the last eigenvalue have the same time constant $\tau = 0.149$ s. The difference between them is that the second pair is related to the primary and secondary currents, whereas the last eigenvalue is related to the circulating current in the delta. This value of τ is equal to the *short-circuit time constant of the transformer* T_{cc}, which can be analytically determined as:

$$T_{cc} = \frac{x_{cc}}{\omega_N\, r_{cc}} = \frac{x_{\sigma 1} + x_{\sigma 2}}{\omega_N\, (r_1 + r_2)} = 0.149 \text{ s} \tag{5.4}$$

Now that the eigenvalues of the transformer are validated, it can be applied to the example illustrated in figure 5.10. The same operating conditions of the case presented in section 5.3 are considered here. The results are presented in table 5.10.

It is possible to notice that the introduction of the transformer adds three eigenvalues (numbers 5, 6 and 9) compared to the example of section 5.3 (see table 5.3). This is due to the windings of the primary side of the transformer and to the delta connection of the secondary

side.

Most remarkably, the inclusion of the transformer shifts the eigenvalues already present in the first example (see table 5.3). This shift makes the system less stiff (damping ratios are reduced). This is indeed logical since the stiffness of this system is due to the infinite bus. The transformer increases the electrical distance between the bus and the generator, which makes it slightly less stable. Without the presence of any regulator, the inclusion of other series elements between the infinite bus and the machine would make it increasingly less stable, tending to make the local mode (pair 1,2) unstable in an extreme case. The other eigenvalues are also shifted indicating that the time constants of the synchronous machine and of the transformer combine together when these two elements are connected.

It is possible to confirm the eigenmodes calculated for this case as it was done in the first example. However, since these modes keep the same nature, the validation procedure is not duplicated here in order to avoid repetition.

5.6 RL and RLC Loads

Electrical loads are modeled by RL and RLC elements. The parameters of the load (values of R_L, L_L and C_L) can be given either directly or indirectly through the specification of an operating point of active and reactive power. In this case, the parameters are calculated by the initialization procedure.

The RL model is composed of three state equations, one for each phase, the last one being eliminated as explained in section 5.2. Thus, it yields two eigenvalues which are the inverse of the time constant $\tau = L_L/R_L$ of a RL circuit. It is relevant to note that these values present also the frequency of the reference frame, as it was the case for the power transformers (this specific frequency has no physical meaning).

The RLC model is represented by six state equations: three related to the phase currents (Δi_{abc}) and three to the capacitor voltages (Δu_{Cabc}). After the elimination of the third phase current, five eigenvalues are obtained.

As a simple illustration, a three phase RLC load connected to a voltage source is considered, as depicted in figure 5.13. The parameters of the load are given in table 5.11. The results of the eigensolution of this elementary system are given in table 5.12. Even though it is a simple example, the interpretation of the results is nonetheless important.

The first two pairs correspond to the two RLC loops formed in SIMSEN. These are oscillatory modes due to the resonance between the inductive and capacitive elements. However, the frequency of these modes is somewhat masked due to the reference frame. The values ob-

Table 5.11: Parameters of the RLC load.

Resistance	R_L	0.90	(Ω)
Inductance	L_L	320.0	(mH)
Capacitance	C_L	18.0	(mF)
Voltage	U	17.5	(kV)
Frequency	f_N	50	(Hz)

Table 5.12: Eigenproperties of the RLC load.

Eigenvalue number i	$\sigma = \Re(\lambda_i)$ (Np/s)	$\omega_d = \Im(\lambda_i)$ (rad/s)	τ (s)	ζ (%)	f (Hz)	Dominant states
1,2	−1.406	301.06 = 314.16 − **13.1**	0.711	0.810	2.085	$\Delta i_{abc}, \Delta u_{Cabc}$
3,4	−1.406	327.26 = 314.16 + **13.1**	0.711	0.810	2.085	$\Delta i_{abc}, \Delta u_{Cabc}$
5	0	–	–	–	–	Δu_{Cc}

tained (301.06 and 327.26 rad/s) are a combination of the real damped frequency ω_d with the frequency of the reference frame ω_a. The actual damped frequency is obtained as follows:

$$\omega_{d_{1,2}} = -\omega_{\lambda_{1,2}} + \omega_a$$
$$\omega_{d_{3,4}} = +\omega_{\lambda_{3,4}} - \omega_a$$

This results in $\omega_d = 13.1$ rad/s, reason for which this value is highlighted in boldface type in table 5.12. Additionally, the values of ζ and f are calculated based on this value of ω_d.

Both values of σ and ω_d can be confirmed analytically. For a RLC circuit, the attenuation σ and the natural (resonance) frequency ω_0 can be calculated based on the parameters of the system, yielding the following results:

$$\sigma = \frac{R_L}{2L_L} = 1.406 \text{ Np/s}$$
$$\omega_0 = \frac{1}{\sqrt{L_L C_L}} = 13.176 \text{ rad/s}$$

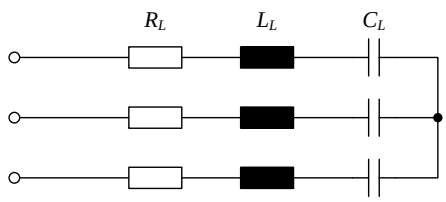

Figure 5.13: RLC load.

Consequently, the damped frequency is:

$$\omega_d = \sqrt{\omega_0^2 - \sigma^2} = 13.101 \text{ rad/s}$$

This is an analytical confirmation of the results presented in table 5.12.

It is also possible to observe the effect of the resonance frequency and its damping through a time-domain simulation which allows for validating the results. A step increase of 5% on the voltage feeding the load makes the amplitude of the currents oscillate.

Figure 5.14 presents the phase a current for which an oscillating envelope can be determined. This envelope has an oscillation frequency equal to the resonance frequency. Moreover, it is possible to identify the damping and the time constant of the mode as it was done in the previous examples. A very good agreement is found between the eigenvalue results , the analytical calculation and the time-domain simulation.

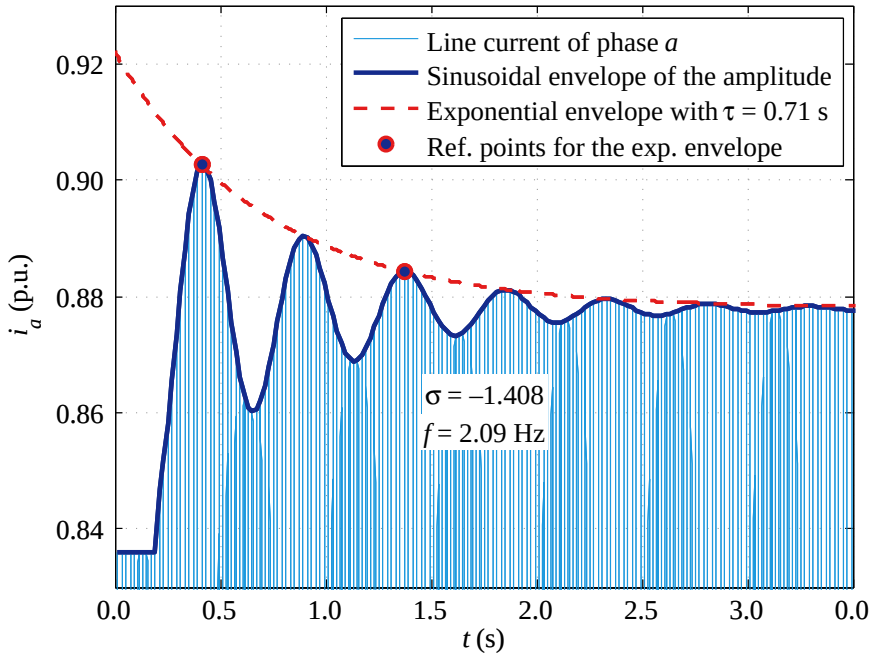

Figure 5.14: Sinusoidal envelope and its exponential damping for a RLC load.

Finally, the last eigenvalue is zero. This happens due to the fact that the state variable Δi_c is eliminated in the construction of the matrices. The state equation related to the capacitor voltage is:

$$C_L \frac{d\Delta u_{Cc}}{dt} = i_c$$

Since $i_c = -i_a - i_b$, there is a linear dependency between this equation and the other capacitor voltage equations. This causes the pure zero eigenvalue, which has no physical meaning and does not indicate any unstable condition.

5.7 Transmission Lines

Two models of transmission lines are developed for small-signal stability: (i) a resistive-inductive (RL) model, convenient for the representation of short transmission lines (with lengths up to 80 km); and (ii) the π-section model, suitable for the representation of medium transmission lines (with lengths between 80 km and 160 km).

The RL model corresponds to a three-phase resistive-inductive element as depicted in figure 5.15. This element is represented by three state variables(Δi_{abc}) and three corresponding state equations which describe the voltage drop between the two terminals of each phase. When applied in a circuit, this element introduces a time constant $\tau = L_{tl}/R_{tl}$ which combines with the time constants of other elements in the same current loop, thus influencing the damping of some eigenmodes. This model will be applied in the example presented in the next section (see section 5.8). Moreover, for the purpose of studying the small-signal stability of hydroelectric power plants, the RL model is sufficient to conveniently represent the connection of the generator (or its step-up transformer) to the power grid.

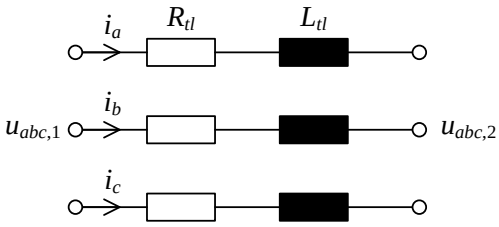

Figure 5.15: Resistive-inductive transmission line.

For specific cases when the representation of network parts with longer lines requires more precision, it is possible to apply the π-section transmission line element. In SIMSEN, this element takes into account the RL elements (R_{tl}, L_{tl}), including mutual inductances (L_{tlm}), single-phase and phase-to-phase capacitances ($C_{\phi n}$ and $C_{\phi\phi}$, respectively), as depicted in figure 5.16.

An important point to observe regarding this model is that in order to keep the formulation presented in equation (4.6), on page 46, residual inductances (L_{res}) are added in series with the capacitive elements. This increases the order of the model to 27. The value of these inductances is determined based on the value of the capacitances as well as on the integration

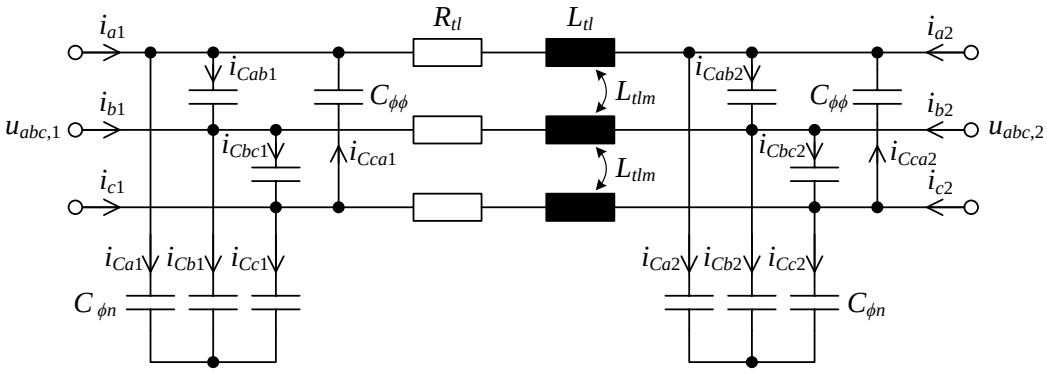

Figure 5.16: Three-phase scheme of a π-section transmission line element.

time step T_{step} configured for time-domain simulations, as follows:

$$L_{res} = \frac{\left(0.5\, T_{step}\right)^2}{C} \tag{5.5}$$

Consequently, if the eigenvalues of the π-section model alone are calculated, the LC branches yield resonance frequencies without any physical meaning, which are equal to:

$$\omega_0 = \frac{1}{\sqrt{L_{res}\, C}} \qquad \longrightarrow \qquad \omega_0 = \frac{2}{T_{step}} \tag{5.6}$$

This value is the same, regardless of the line parameters. Thus, it has no relation with the physical representation of transmission lines.

Nonetheless, the value of these residual inductances is small enough to be generally negligible when the π-section model is combined with other circuit elements that are essentially inductive. This means that when the π-section small-signal model is connected together with other elements, the interaction between the true inductive parts with the capactive characteristic of the line will be correctly represented (still, it is necessary to compensate for the reference frame frequency, as explained in section 5.6).

A simple way to validate the small-signal model of the π-section transmission line is to connect it to a basic RL load and extract the eigenvalues. The validation of the results can be achieved as it was done for the RLC load in section 5.6. The validation procedure must be applied repeatedly for each LC or RLC loop. However, this is not presented here in order to avoid repetition.

5.8 Voltage Regulators

The small-signal models developed for automatic voltage regulators are available under two different configurations (implemented in two distinct modules): (i) the IEEE ST1A voltage regulator, as proposed by the standard IEEE Std 421-5 [38]; and (ii) a model based on the Unitrol® regulator, a commercial AVR broadly known and used worldwide.

The block diagram of the ST1A voltage regulator is presented in figure 5.17. Besides the standard structure proposed by IEEE, a filter is added to the input V_C so that it corresponds to the filtered value of the measured voltage u_m of the regulated machine. In the context of small-signal stability, limitations and discrete elements cannot be taken into account. For this reason, they are represented in gray. After neglecting such elements, the small-signal model of the ST1A regulator is described by five time-domain state equations. Moreover, the linearized expression of the input (Δu_m) is given as a function of the state variable of the regulated machine. These expressions are given in appendix A, section A.6.

The other possible configuration corresponds to the model of the commercial voltage regulator Unitrol®, which has been used in several power plants around the world. Its block diagram is presented in figure 5.18. Once again, the elements not taken into account in the small-signal model are represented in gray. The small-signal model of this regulator is described by four time-domain state equations. The analytical description of the input (Δu_m) is the same as for the ST1A regulator.

In order to illustrate the use of a voltage regulator model, an example is presented based on the test case carried out in section 5.3. A short transmission line (represented by the RL model) is added and the synchronous generator is regulated by the second configuration of AVR. This system is presented in figure 5.19. The parameters and operating point of the generator are kept unchanged, whereas the parameters of the line and the voltage regulator are given in table 5.13.

The results obtained from the eigensolution of this system are presented in table 5.14.

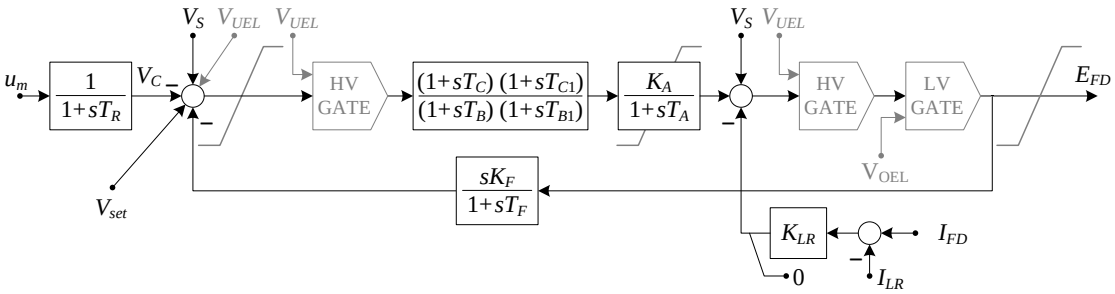

Figure 5.17: IEEE ST1A voltage regulator.

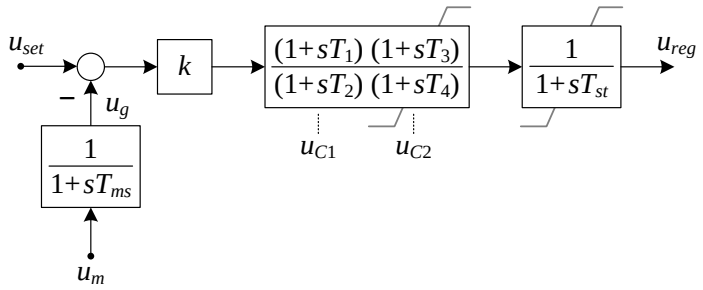

Figure 5.18: Block diagram of the Unitrol® voltage regulator.

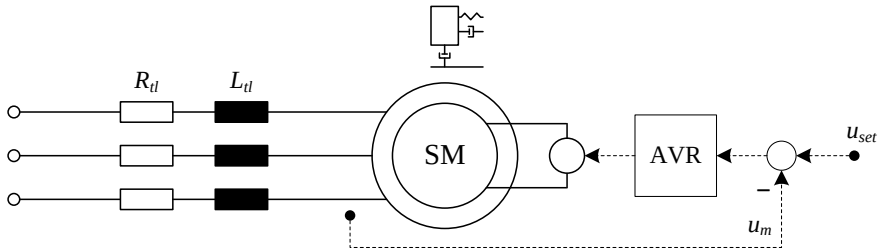

Figure 5.19: Example of synchronous generator with automatic voltage regulator.

Table 5.13: Parameters of RL transmission line and voltage regulator.

Element	Parameters		
Transmission line	R'_{tl}	0.03	(Ω/km)
	L'_{tl}	0.70	(mH/km)
	l	5.0	(km)
Voltage Regulator	k	250	(–)
	T_1	0.10	(s)
	T_2	0.02	(s)
	T_3	1.0	(s)
	T_4	5.0	(s)
	T_{ms}	0.04	(s)
	T_{st}	0.005	(s)

Table 5.14: Eigenproperties of the system with AVR and short transmission line.

Eigenvalue number i	$\sigma = \Re(\lambda_i)$ (Np/s)	$\omega_d = \Im(\lambda_i)$ (rad/s)	τ (s)	ζ (%)	f (Hz)	Dominant states
1,2	−19.74	6.678	0.051	94.7	1.063	$\Delta i_D, \Delta i_f, \Delta u_g, \Delta u_{C1}$
3,4	−0.790	7.748	1.266	10.1	1.233	$\Delta\omega_m, \Delta\theta, \Delta i_{abc}$
5,6	−28.92	313.64	0.035	9.18	49.92	Δi_{abc}
7	−200.77	–	0.005	100	–	Δu_{reg}
8	−47.82	–	0.021	100	–	$\Delta i_f, \Delta i_D, \Delta u_{C1}$
9	−14.21	–	0.070	100	–	$\Delta i_Q, \Delta i_{abc}$
10	−2.152	–	0.465	100	–	$\Delta i_{abc}, \Delta i_f, \Delta u_{C2}$
11	−1.516	–	0.660	100	–	$\Delta i_{abc}, \Delta i_f, \Delta u_{C1}$

It is possible to see that the presence of the AVR not only introduces new eigenvalues, but also generates interactions that give origin to a different oscillatory eigenmode (pair 1,2). It corresponds to the control mode oscillations which are strongly damped. Due to such a high damping ratio, it is not possible to observe the effects of this eigenmode through time-domain simulations. Such a strong damping indicates that the tuning of the AVR parameters is satisfactory, even though this is not an issue in question here. Nevertheless, it is interesting to observe that control modes can become less stable if the regulator is not well tuned.

The presence of the short line also influences the stability of the system. Whereas the damping of the 50 Hz component increases, the local mode (pair 3,4) gets less damped. This is a consequence of the fact that the line decouples the generator from the infinite grid, increasing the electrical distance between both. Moreover, the local mode frequency is also shifted. This indicates that both damping and frequency of the local mode depend on the topology of the system, on whether regulating elements are present or not and on how they are tuned.

The action of the local mode can once again be observed through a time-domain simulation in which a +5% disturbance is applied to the external torque. Figure 5.20 presents the behavior of the electrical power as well as the frequency of oscillation and the damping time constant obtained graphically. Once again it is possible to conclude that a good agreement is obtained between the properties extracted through the eigenvalues calculation and those from the time-domain simulation of a small disturbance.

Finally, the purely real eigenvalues correspond to combinations of time constants of the elements, indicating other forms of interaction that do not represent any risk of instability. The eigenvalue number 7 can be particularly identified as the inverse of the time constant T_{st} from the voltage regulator. The others cannot be directly related to specific parameters of the system.

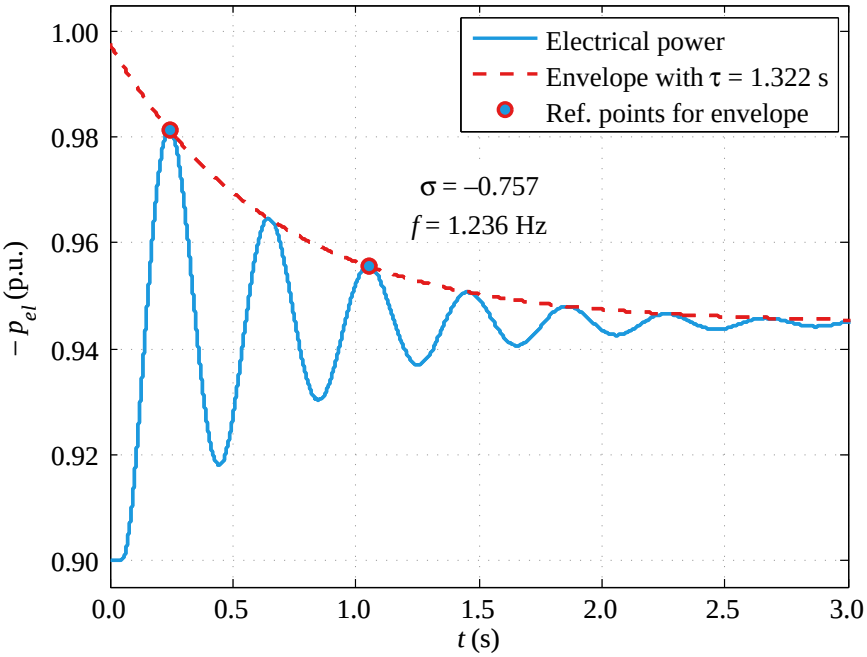

Figure 5.20: Electrical power pulsation of the system with AVR and short transmission line.

5.9 Power System Stabilizer

A small-signal model was developed for the power system stabilizer IEEE PSS2B, proposed by the standard IEEE Std 421-5 [38]. Besides the standard structure, the implementation of this model in SIMSEN includes a filter for each input, as it can be seen in figure 5.21. This model is described either by fourteen or fifteen time-domain state equations, depending on the values of the parameters M and N. In SIMSEN, these parameters can assume either the values $M = 4, N = 1$; or $M = 5, N = 1$; or $M = 2, N = 2$.

Based on the example presented in section 5.5, page 62, a new example is proposed which includes the PSS2B and the same AVR model presented in the previous section, as depicted in figure 5.22. The parameters and operating point previously used are kept unchanged. The

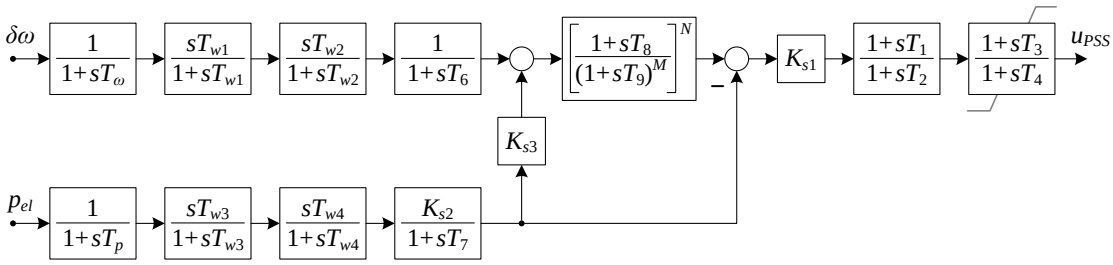

Figure 5.21: IEEE PSS2B power system stabilizer with filtered inputs.

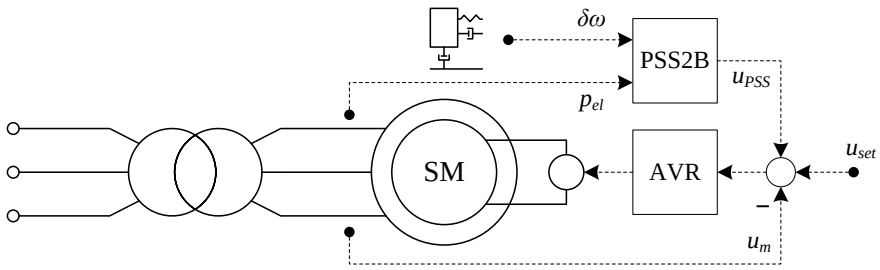

Figure 5.22: Example of synchronous generator with AVR and PSS2B.

Table 5.15: Parameters of the PSS2B.

K_{s1}	1.00	(–)
K_{s2}	1.02	(–)
K_{s3}	1.00	(–)
T_{ω}	$1.00 \cdot 10^{-4}$	(s)
T_p	$1.25 \cdot 10^{-2}$	(s)
$T_{w1...4}$	4.965	(s)
T_1	0.180	(s)
T_2	0.025	(s)
T_3	0.330	(s)
T_4	0.180	(s)
T_6	$1.00 \cdot 10^{-4}$	(s)
T_7	5.00	(s)
T_8	0.500	(s)
T_9	0.100	(s)
M	5	(–)
N	1	(–)

parameters used for the PSS2B are presented in table 5.15.

It is important to mention that in this illustrative case, the gain of the PSS (K_{s1}) is intentionally set to a low value. In this way, it will still be possible to observe at least the local mode oscillations through a disturbed time domain simulation, so that it can validate the eigenvalues results.

The results obtained from the eigensolution of this system are extensively presented in table 5.16. Where the dominant states are identified as "PSS", it means that internal variables of the PSS are dominant. The specific variable Δu_{PSS} corresponds to the output of the stabilizer.

The PSS introduces fifteen state variables in the system. The interpretation of the complete

Table 5.16: Eigenproperties of the system with PSS, AVR and step-up transformer.

Eigenvalue number i	$\sigma = \Re(\lambda_i)$ (Np/s)	$\omega_d = \Im(\lambda_i)$ (rad/s)	τ (s)	ζ (%)	f (Hz)	Dominant states
1,2	−0.206	0.0015	4.854	100	$2.4 \cdot 10^{-6}$	PSS
3,4	−42.34	0.250	0.024	100	0.040	$\Delta i_f, \Delta i_D$, PSS
5,6	−1.270	0.692	0.787	87.8	0.110	$\Delta i_f, \Delta\omega_m, \Delta u_{C1,2}$
7,8	−18.83	2.341	0.053	99.2	0.373	PSS
9,10	−7.221	6.061	0.138	76.6	0.965	PSS, $\Delta i_Q, \Delta\omega_m$
11,12	−20.72	7.587	0.048	93.9	1.208	PSS, $\Delta i_f, \Delta i_D, \Delta\omega_m$
13,14	−1.961	8.357	0.510	22.8	1.330	PSS, $\Delta\omega_m, \Delta\theta, \Delta i_{abc2}$
15,16	−4.897	314.03	0.204	1.56	49.98	Δi_{abc2}
17,18	−0.065	314.16	15.38	0.021	50.00	$\Delta i_{abc1,abc2}$
19	−10000	–	10^{-4}	100	–	PSS
20	−10000	–	10^{-4}	100	–	PSS
21	−200.3	–	0.005	100	–	Δu_{reg}
22	−82.74	–	0.012	100	–	PSS, $\Delta i_f, \Delta i_D$
23	−10.00	–	0.100	100	–	$\Delta u_{PSS}, \Delta u_{C1}$
24	−6.732	–	0.149	100	–	Δi_Δ
25	−5.676	–	0.176	100	–	PSS, $\Delta\omega_m$
26	−5.505	–	0.182	100	–	PSS, $\Delta\omega_m$
27	−0.2014	–	4.965	100	–	PSS
28	−0.2014	–	4.965	100	–	PSS
29	−0.1924	–	5.198	100	–	PSS

list of eigenvalues may become an intricate task. Nonetheless, the indication of the dominant states through the computation of participation factors proves to be very useful.

Indeed, it is possible to see that several of the new eigenvalues are almost exclusively related to internal variables of the PSS and have no significant interaction with the rest of the system. Furthermore, they are either purely real or at least very well damped with a very low frequency.

On the other hand, the presence of the PSS causes the rise of new control modes. Since the PSS gain has a low value in this example, these modes do not represent any risk to the stability of the system. However, in real cases the gain is usually set to high values with the aim to damp inter-area and local oscillations. This decreases the damping of control modes and, in extreme cases, they might become unstable.

Finally, it is interesting to verify the local mode (pair 13,14). When confronted to the value

obtained in the case without AVR and PSS, in table 5.10, page 64 ($\lambda = -1.423 \pm j8.738$, with $\zeta = 16\%$), it is easy to see that even with a low gain the PSS acts positively, increasing the damping ratio. Additionally, the frequency undergoes a slight shift.

A time-domain simulation similar to those performed previously allows for the confirmation of these values. The results from the eigenvalues calculation with the model of the PSS are compliant with the properties extracted from the time-domain results, presented in figure 5.23.

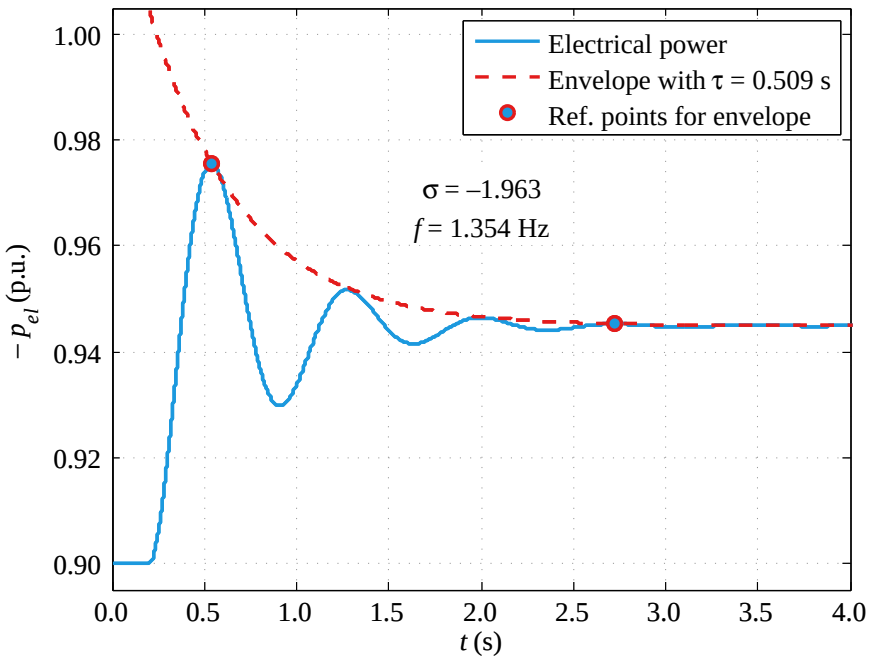

Figure 5.23: Electrical power pulsation with AVR and PSS.

The implementation of these small-signal stability models in SIMSEN allow for the eigen-analysis of systems of much higher complexity. The coupling of the models described in this chapter with small-signal models of hydraulic elements in the same tool is a powerful asset for coherent and comprehensive analyses of hydropower plants and systems.

6 Modeling of Hydraulic Elements

6.1 General

This chapter introduces the principle of modeling of the main hydraulic elements available in SIMSEN. The development of the time-domain models was in reference [69], whereas the linearized models derived from them were proposed in reference [1]. Only the main aspects and models that were used in the present work are presented here in a compact form. For further details, please refer to references [1, 69].

6.2 Hydroacoustic Model of a Pipe

Hydroacoustic modeling is the base of the hydraulic models of SIMSEN. The principle of mass and momentum conservation is applied to describe the dynamic behavior of a pipe filled with water. The water flow is considered to be one-dimensional, given that transversal lengths can be neglected when compared to longitudinal lengths of hydraulic installations. Moreover, it is assumed that the flow is normal to the cross section of the pipe, and the pressure, the density and the flow velocity are uniform in a given cross section [69].

Considering an elementary pipe of length dx (see figure 6.1), the two equations describing its dynamic behavior, based on the conservation of mass and momentum, are [107]:

$$\begin{cases} \dfrac{\partial h}{\partial x} + \dfrac{1}{gA}\dfrac{\partial Q}{\partial t} + \dfrac{\lambda |Q|}{2gDA^2} Q = 0 \\ \dfrac{\partial h}{\partial t} + \dfrac{a^2}{gA}\dfrac{\partial Q}{\partial x} = 0 \end{cases} \tag{6.1}$$

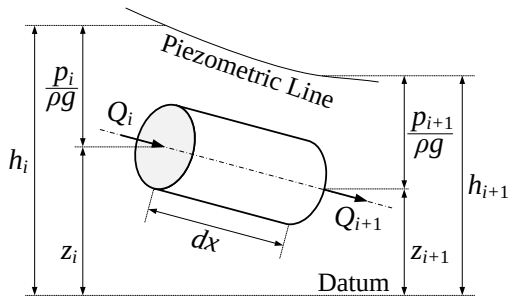

Figure 6.1: Model of a pipe of length dx [69].

where h is the piezometric head (given in meters of water column above a given datum), g is the gravitational acceleration, A is the cross section of the pipe, Q is the water discharge, λ is the local loss coefficient, D is the pipe diameter, and a is the wave speed of the water in the pipe. For the determination of the system of hyperbolic partial differential equations (6.1), it must be considered that there are no vertical displacements of the pipe and that the convective terms related to the transport phenomena can be neglected with respect to propagative terms [69]. This is true due to the fact that hydroacoustic phenomena are caracterized by high wave speeds a and low flow velocities c ($c = Q/A$).

The solution of equations (6.1) is obtained through an analogy with the telegraphist's equations, used in the study of electromagnetic wave propagation in conductors and transmission lines [41, 76, 98]. These equations are given below:

$$\begin{cases} \dfrac{\partial u}{\partial x} + L'_e \dfrac{\partial i}{\partial t} + R'_e i = 0 \\ \dfrac{\partial u}{\partial t} + \dfrac{1}{C'_e}\dfrac{\partial i}{\partial x} = 0 \end{cases} \tag{6.2}$$

where L'_e, R'_e and C'_e are, respectively, the lineic inductance, resistance and capacitance.

The analogy between the equation sets (6.1) and (6.2) is related to the fact that both systems are characterized by a potential state variable (h and u) and a flow rate state variable (Q and i). Thus, it is possible to identify the lineic hydroacoustic resistance R'_h , inductance L'_h and capacitance C'_h, which are defined as follows:

$$R'_h = \frac{\lambda |Q|}{2gDA^2} \tag{6.3}$$

$$L'_h = \frac{1}{gA} \tag{6.4}$$

$$C'_h = \frac{gA}{a^2} \tag{6.5}$$

The hydroacoustic resistance R'_h is related to the head losses through the pipe, the inductance L'_h is related to inertia effects of the water and the capacitance C'_h is related to storage effects due to pressure [69].

The hydroacoustic model represented by the system of equations (6.1) can then be rewritten as:

$$\begin{cases} \dfrac{\partial h}{\partial x} + L'_h \dfrac{\partial Q}{\partial t} + R'_h(Q)\, Q = 0 \\ \dfrac{\partial h}{\partial t} + \dfrac{1}{C'_h} \dfrac{\partial Q}{\partial x} = 0 \end{cases} \tag{6.6}$$

Furthermore, it is important to consider the viscoelastic behavior of the pipe due to energy dissipation during the deflection of the wall, in order to estimate pressure fluctuations and system stability with more accuracy. This additional dissipation is represented by a resistance in series with the capacitance C'_h. This viscoelastic resistance R_{ve} accounts for both fluid and pipe viscoelasticity and is calculated as [1]:

$$R_{ve} = \frac{\mu_{eq}}{A \rho\, g\, dx} \tag{6.7}$$

where μ_{eq} is the equivalent viscoelastic damping of the fluid and the pipe wall and ρ is the density of the fluid.

It can be shown that for a pipe segment of length dx, this model may be represented by an equivalent T-shaped electric circuit (see [69], pp. 42–43) as presented in figure 6.2, where:

$$R_h = R'_h\, dx \quad ; \quad L_h = L'_h\, dx \quad ; \quad C_h = C'_h\, dx$$

Finally, the equivalent circuit of figure 6.2 is described by the following set of three ordinary differential equations:

$$\begin{cases} C_h \dfrac{dh_{i+1/2}}{dt} = Q_i - Q_{i+1} \\ \dfrac{L_h}{2} \dfrac{dQ_i}{dt} = -h_{i+1/2} - \left(\dfrac{R_h}{2} + R_{ve} \right) Q_i + R_{ve}\, Q_{i+1} + h_i \\ \dfrac{L_h}{2} \dfrac{dQ_{i+1}}{dt} = h_{i+1/2} + R_{ve}\, Q_i - \left(\dfrac{R_h}{2} + R_{ve} \right) Q_{i+1} - h_{i+1} \end{cases} \tag{6.8}$$

For a pipe of length l, the modeling is done by considering a series of n pipes of length dx. The number of elements n in which the pipe is discretized influences directly the results. Increasing n improves the accuracy of calculation of the natural frequencies of the pipe [1, 69]. Spatial and temporal discretisation are linked through the so-called Courant-Friedrichs-Lewy

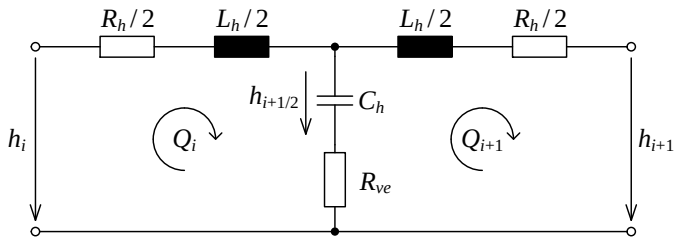

Figure 6.2: Equivalent scheme of a pipe of length dx [69].

condition (CFL condition) and based on Courant number C_r [107]:

$$C_r = \frac{a \cdot dt}{dx} \leq 1$$

where dt is the integration time step.

6.3 Francis Turbine Model

Francis turbines are able of converting both potential and kinetic energy of water into mechanical work (reaction turbines). Structurally, the rotor of a Francis turbine has fixed blades and the water flow is controlled by the guide vanes.

As flow developing in hydraulic machines is very complex, no analytical model is available to represent its dynamic behavior over the four possible quadrants of operation. Therefore, reduced scale model test data are used to model hydraulic machines through a quasi-static approach.

From the viewpoint of an equivalent electric model, the turbine is represented by a pressure source, which converts hydraulic energy into mechanical work. A series equivalent inductance L_t is used to represent water inertia effects. It is calculated as:

$$L_t = \frac{l_{eq}}{g\,\bar{A}} \tag{6.9}$$

where l_{eq} is the turbine equivalent length and $\bar{A}$ is the turbine mean cross section. In addition, a series resistance R_t is used to ensure zero discharge when the guide vanes are fully closed. The equivalent pressure source of the turbine $H_t = H_t(y, \Omega, Q_i)$ is driven by the turbine characteristic, which is a function of the guide vanes opening (GVO) y, the angular rotational speed Ω $\left(\Omega = \frac{2\pi}{60} n\right)$ and the discharge Q_i [69].

Figure 6.3 presents an example of Francis turbine characteristic curves. These curves are determined in terms of the speed factor N_{11}, discharge factor Q_{11} and torque factor T_{11}, which

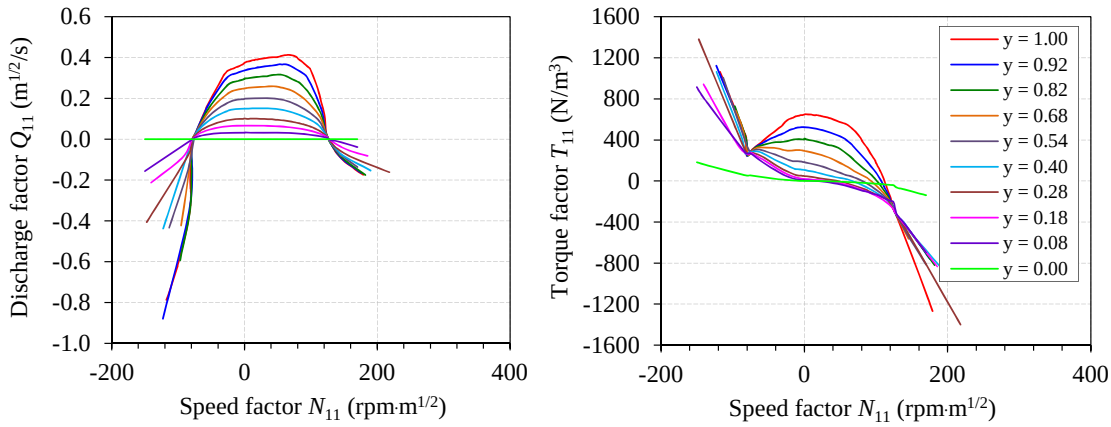

Figure 6.3: Turbine characteristics for different guide vane opening values.

are defined as:

$$N_{11} = \frac{n D_{ref}}{H_{turb}} \quad ; \quad Q_{11} = \frac{Q_i}{D_{ref}^2 \sqrt{H_{turb}}} \quad ; \quad T_{11} = \frac{T_{turb}}{D_{ref}^3 H_{turb}}$$

where n is the rotational speed, D_{ref} is the reference diameter of the turbine, H_{turb} is the net head, Q_i is the discharge and T_{turb} is the turbine torque.

Figure 6.4 presents the model and the equivalent electric circuit representing the Francis turbine. This circuit is described by the following differential equation:

$$L_t \frac{dQ_i}{dt} = -R_t Q_i - H_t(y, \Omega, Q_i) + H_I - H_{\bar{I}} \tag{6.10}$$

The full description of the Francis turbine is achieved with the momentum equation, which describes the dynamics of the angular rotational speed Ω of the rotating parts:

$$J \frac{d\Omega}{dt} = \sum T = T_{turb} + T_{em} \tag{6.11}$$

where J is the moment of inertia of the rotating parts, $T_{turb} = T_{turb}(y, \Omega, Q_i)$ is the turbine

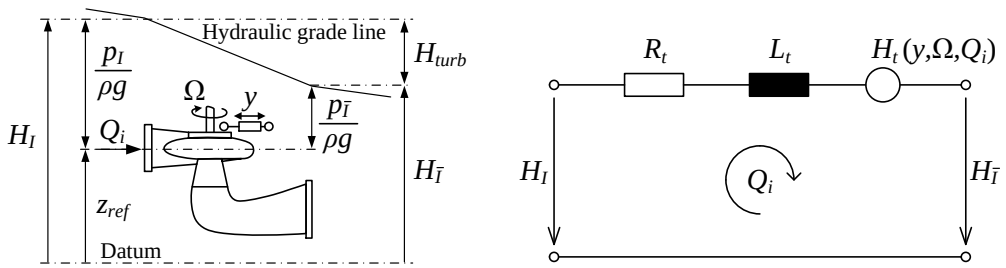

Figure 6.4: Francis turbine model (left) and equivalent scheme (right) [69].

torque, as previously defined, and T_{em} is the electromagnetic torque of the generator, as defined in chapter 4. As it can be seen in figure 6.3, the turbine torque also depends on the guide vanes opening (GVO) y, the angular rotational speed Ω and the discharge Q_i.

6.4 Model of a Surge Tank

The surge tank is a structure used to protect the hydraulic circuit against waterhammer effect. It functions as a free surface for wave reflection, whose water level depends on the discharge time history [69]. The variations of piezometric head h_c are related to the stored discharge Q_c, which evidences a capacitive behavior. Thus, the equivalent capacitance of a surge tank C_{ST} is directly its cross section which is a function of the elevation. Also, the stored discharge is the difference between the upstream Q_{ST_i} and downstream $Q_{ST_{i+1}}$ discharges. In addition, the flow Q_c of the surge tank undergoes head losses due to cross section changes and to a diaphragm commonly placed at the surge tank inlet, which is used to increase damping. These head losses h_d are represented by a resistance $R_d(Q_c)$ which is a function of the discharge [69].

Figure 6.5 depicts the electric equivalent circuit that represents the resistive-capacitive behavior of a surge tank. Equation (6.12), obtained as follows, describes this behavior.

$$h_{ST} = h_c + h_d$$

$$h_d = R_d\, Q_c$$

$$Q_c = Q_{ST_i} - Q_{ST_{i+1}} = C_{ST}\,\frac{dh_c}{dt}$$

Finally:

$$R_d\, C_{ST}\,\frac{dh_c}{dt} = h_{ST} - h_c \tag{6.12}$$

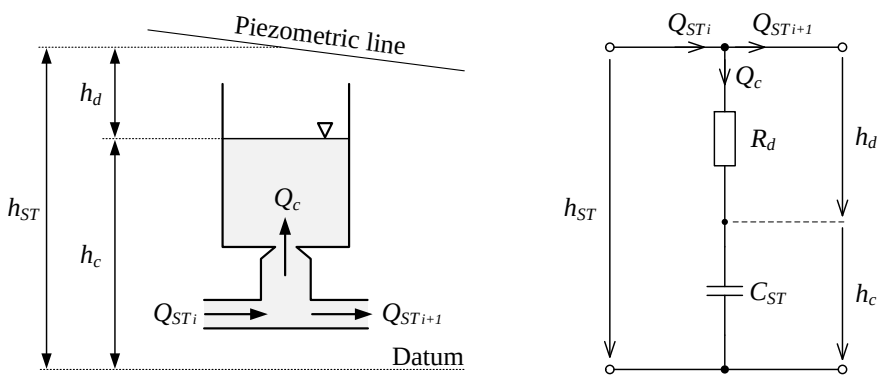

Figure 6.5: Surge tank model (left) and equivalent scheme (right) [69].

6.5 Model of the Turbine Governor

The turbine governor is a regulation device that acts on the guide vanes in order to control either rotational speed, output power, water discharge or, in some cases, reservoir water level. Consequently, the turbine governor input varies according to the regulated quantity.

From the modeling point of view, it can be characterized by the series representation of a PID regulator with filtered input, whose transfer function $G_{tg}(s)$ is as follows:

$$G_{tg}(s) = \frac{Y(s)}{X(s)} = K_p \cdot \frac{1 + s\,T_i}{s\,T_i} \cdot \frac{1 + s\,T_d}{1 + s\,T_f} \tag{6.13}$$

where $X(s)$ is the frequency domain input, $Y(s)$ is the frequency domain output that acts on the guide vanes, K_p is the proportional gain, T_i is the integral time constant, T_d is the derivative time constant and T_f is the filter time constant. The block diagram for this transfer function is represented in figure 6.6.

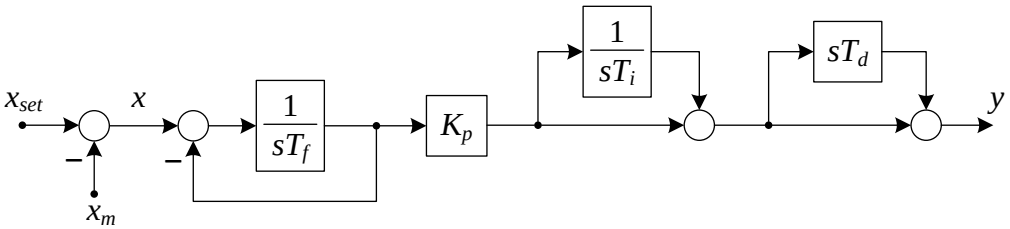

Figure 6.6: Turbine governor block diagram.

In SIMSEN, the time-domain behavior of this block diagram is described by the following set of equations, where x is the input, y_1 and y_2 are implicit state variables of the regulator, and y is the output:

$$\begin{cases} T_f \dfrac{dy_1}{dt} = x - y_1 \\[2ex] T_i \dfrac{dy_2}{dt} = y - y_2 \\[2ex] y = K_p \left(1 + \dfrac{T_d - T_f}{T_f}\right) x - K_p \dfrac{T_d - T_f}{T_f} y_1 + y_2 \end{cases} \tag{6.14}$$

6.6 Linearization of the Hydraulic Models

The linearization of the time-domain hydraulic models is done through first-order Taylor expansions, as described in section 3.3.1, equation (3.6). Considering the equivalent models presented in the previous sections, the mathematical representation of hydraulic elements

presents less nonlinearities than electrical machines. These nonlinearities are mostly related to the proportionality of hydraulic resistances to the discharge Q_i. Other nonlinearities are related to the characteristic curves of the Francis turbine.

Considering the model of the pipe represented by the set of equations (6.8), the nonlinearity is due to the square exponent of the flow rate in the following term [1]:

$$\Delta H_r = \frac{R_h}{2} Q_i = \frac{1}{2} \frac{\lambda dx}{2gDA^2} |Q_i| Q_i$$

Under small disturbances, it is possible to consider that the direction of the water flow does not change ($Q_i > 0$). Thus, the multiplication $|Q_i| Q_i$ becomes Q_i^2 [60]. So:

$$\Delta H_r = \frac{R_h^*}{2} Q_i^2$$

with

$$R_h^* = \frac{\lambda dx}{2gDA^2} = \frac{R_h}{|Q_i|}$$

Finally, the linearized set of equations for a viscoelastic pipe of length dx is:

$$\begin{cases} C_h \dfrac{d\Delta h_{i+1/2}}{dt} = \Delta Q_i - \Delta Q_{i+1} \\ \dfrac{L_h}{2} \dfrac{d\Delta Q_i}{dt} = -\Delta h_{i+1/2} - \left(R_h^* \left|Q_i\right|_0 + R_{ve}\right) \Delta Q_i + R_{ve} \Delta Q_{i+1} + h_i\big|_0 \\ \dfrac{L_h}{2} \dfrac{d\Delta Q_{i+1}}{dt} = \Delta h_{i+1/2} + R_{ve} \Delta Q_i - \left(R_h^* \left|Q_{i+1}\right|_0 + R_{ve}\right) \Delta Q_{i+1} - h_{i+1}\big|_0 \end{cases} \tag{6.15}$$

Regarding the Francis turbine, the equivalent hydraulic resistance introduces a nonlinearity related to the square of the discharge Q_i, in the same way as for the viscoelastic pipe. Furthermore, there are nonlinearities related to the pressure source $H_t(y, \Omega, Q_i)$ and to the torque $T_t(y, \Omega, Q_i)$ [1]. The linearization of these quantities is given by:

$$\Delta H_t = \left.\frac{\partial H_t}{\partial Q_i}\right|_0 \Delta Q_i + \left.\frac{\partial H_t}{\partial \Omega}\right|_0 \Delta \Omega + \left.\frac{\partial H_t}{\partial y}\right|_0 \Delta y$$

$$\Delta T_t = \left.\frac{\partial T_t}{\partial Q_i}\right|_0 \Delta Q_i + \left.\frac{\partial T_t}{\partial \Omega}\right|_0 \Delta \Omega + \left.\frac{\partial T_t}{\partial y}\right|_0 \Delta y$$

Thus, the linearized set of equations for the Francis turbine is:

$$\begin{cases} L_t \dfrac{d\Delta Q_i}{dt} = \left(-2R_t^* Q_i\big|_0 - \dfrac{\partial H_t}{\partial Q_i}\bigg|_0\right)\Delta Q_i - \dfrac{\partial H_t}{\partial \Omega}\bigg|_0 \Delta\Omega - \dfrac{\partial H_t}{\partial y}\bigg|_0 \Delta y + h_I\big|_0 - h_{\bar{I}}\big|_0 \\ J\dfrac{d\Delta\Omega}{dt} = \dfrac{\partial T_t}{\partial Q_i}\bigg|_0 \Delta Q_i + \dfrac{\partial T_t}{\partial \Omega}\bigg|_0 \Delta\Omega + \dfrac{\partial T_t}{\partial y}\bigg|_0 \Delta y + \Delta T_{em} \end{cases} \tag{6.16}$$

with

$$R_t^* = \frac{R_t}{|Q_i|}$$

Therefore, the Francis turbine presents nonlinearities not only related to the resistance term, but also to the turbine characteristics. For this reason, the calculation of the six gradients of system of equations (6.16) is a fundamental task.

In the case of unregulated turbines, the guide vanes opening remain constant and are not a state variable of the system. Therefore, the gradients related to it are not included in the linearized matrix. Moreover, the linearized electromagnetic torque ΔT_{em} is obtained from the electrical machine model. If only the hydraulic circuit is represented, the electromagnetic torque is considered to be a constant value $T_{em}\big|_0$.

Finally, concerning the surge tank model, the only nonlinearity is also related to the resistance term which introduces a quadratic proportionality relative to the discharge. Consequently, the linearization of this term is identical to the resistance term related to the pipe model. By applying the same principle to the equations presented in section 6.4, the resulting linearized model of the surge tank is:

$$\left(2R_d^* Q_c\big|_0\right) C_{ST} \frac{d\Delta h_c}{dt} = h_{ST}\big|_0 - \Delta h_c \tag{6.17}$$

with

$$R_d^* = \frac{R_d}{|Q_c|}$$

The use of hydraulic models for a complete representation of hydropower plants allows for a better determination of the eigenmodes of the system. This is very important in cases where the interactions between the subsystems must be studied, such as output power fluctuations due to the influence of hydraulic phenomena.

Part III

Case Studies

7

Stability Issues and Solutions for an Islanded Hydropower Plant

7.1 Introduction

In a number of countries, the lack of essential electricity infrastructure weakens social and economic development. Plus, reliability and availability are a major issue for the minority that has electricity supply. In many cases, however, such countries have sufficient energy potential to be exploited so that the electricity needs can be met. In sub-Saharan Africa, for example, hydropower accounts for one-fifth of today's power supply, but less then 10% of the estimated technical potential have been exploited [36].

Most frequently, using such hydroelectric potential requires the installation of power plants in remote areas, where the connection with large-scale power grids is nonexistent or at least, very weak. Therefore, hydropower plants installed in such conditions must be capable of withstanding isolated or islanded operation modes. As mentioned in chapter 1, section 1.2, islanded operation is the condition when the power plant and its surrounding network have a weak connection (low short-circuit power) with the power grid, and with no tie-line connections to neighboring systems. Isolated operation happens when the power plant is responsible for feeding a local network without any connection with a large power grid.

The aim of this chapter is to present a case study that illustrates stability issues for islanded hydropower plants, and how regulation systems such as turbine governors and power system stabilizers may contribute to better performance and dynamic behavior. Moreover, this chapter demonstrates how electrical, hydraulic, mechanical and control subsystems may interact sometimes in a positive sense, sometimes in an adverse way.

For this purpose, a hypothetical system is proposed in which a hydropower plant runs under

islanded operation mode, due to weak connections with the electrical network. Different scenarios are possible and the most critical one is analyzed. This system is described hereafter.

7.2 Case Study Description

The system studied in this chapter is a 75 MW hydropower plant which operates under islanded condition. Figure 7.1 presents the layout of this system. The electrical and hydraulic parts, with corresponding control elements, are described in the following subsections.

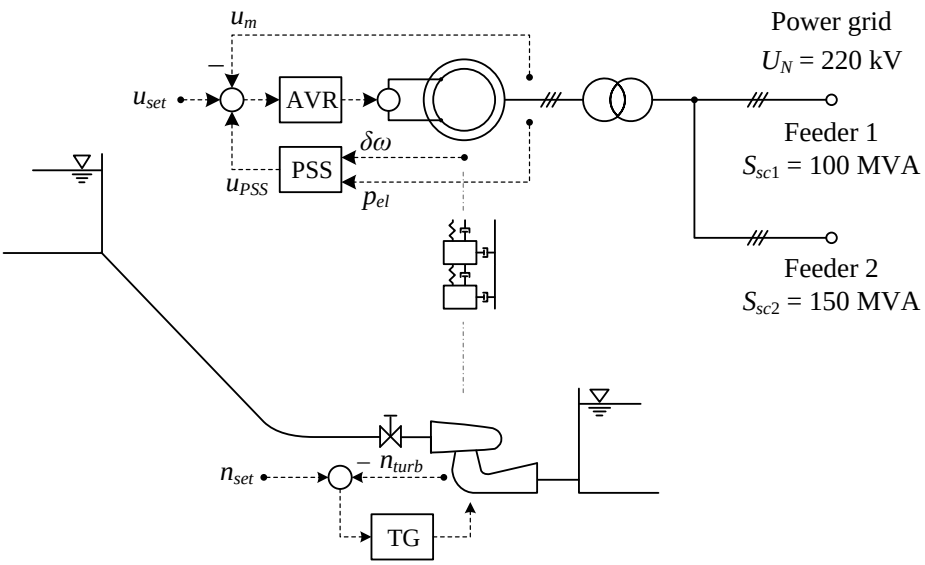

Figure 7.1: Layout of the islanded hydroelectric power plant.

7.2.1 Electrical Subsystem

The electrical part of the power plant is constituted of an 83 MVA salient-pole synchronous generator connected to a 220 kV/17.5 kV *Yd5* step-up transformer. The generator is equipped with the ABB Unitrol® excitation system as voltage regulator (see figure 5.18), and there is the possibility of putting into service a power system stabilizer of type IEEE PSS2B (see figure 5.21).

This power plant is connected to the grid by two parallel feeders but this connection is weak. Feeder 1 has a short-circuit power S_{sc1} = 100 MVA, whereas the feeder 2 has S_{sc2} = 150 MVA. Therefore, the short-circuit power on the point of connection is 250 MVA in the best case, *i.e.*, as long as both feeders are energized. Such a low value of short-circuit power can result in poorly damped electro-mechanical mode oscillations.

Table 7.1 presents the main parameters of the electrical elements of this installation. The parameters of voltage regulator and PSS are given further, in table 7.3.

Table 7.1: Main parameters of the electrical installation.

Element	Ratings / Parameters
Generator	$S_N = 83$ MVA $U_N = 17.5$ kV $f_N = 50$ Hz $P_p = 5$ (number of pairs of poles) $I_{f\delta 0} = 578.3$ A $J_g = 160.3 \cdot 10^3$ kg $\cdot$ m^2 Stator windings connection: Y
Step-up transformer	$S_N = 84$ MVA $U_{N1} = 220$ kV $U_{N2} = 17.5$ kV Vector group: *Yd5*
Power grid	$S_{sc} = 250$ MVA (total short-circuit power) $U_N = 220$ kV $f_N = 50$ Hz

7.2.2 Hydraulic Subsystem

The hydraulic installation is composed of an upstream reservoir, an 1100 meter long penstock feeding a 75 MW Francis turbine, followed by an 100 meter long tailrace tunnel and a lower reservoir. The main parameters of this system are presented in table 7.2.

The penstock is discretized in twenty elements, whereas the tailrace tunnel is represented by five pipe elements. The discretization of the piping system follows the CFL condition, explained in chapter 6, section 6.2. Additionally, the turbine characteristic curves are taken into account.

Consequently, this high order model takes into account effects of water hammer, mass oscillation, and transient behavior of the turbine in the four quadrants, linked to the corresponding rotating inertia.

Furthermore, the hydraulic system is equipped with a turbine governor. Since the connection to the grid is weak, it can run as a speed/frequency regulator, thus contributing to the frequency stability of the system. The frequency regulator used is a PID regulator such as presented in figure 6.6. The corresponding parameters are given in table 7.3.

Table 7.2: Main parameters of the hydraulic installation.

Element	Dimensions
Reservoir	$H_o = 330$ m (gross head)
Penstock	$L = 1100$ m $D = 3.0$ m $a = 1100$ m/s
Francis turbine	$P_N = 75$ MW $n_N = 600$ rpm $H_N = 314.2$ m $\nu = 0.298$ (specific speed) $J_t = 8.0 \cdot 10^3$ kg $\cdot$ m^2
Tailrace tunnel	$L = 100$ m $D = 3.5$ m $a = 1000$ m/s
Coupling shaft	$K_{sh} = 1.26 \cdot 10^8$ Nm/rad (torsional stiffness) $\mu_{sh} = 5.0 \cdot 10^3$ Nms/rad (viscous damping)

Table 7.3: Parameters of the control and regulation elements.

Element	Parameters		
Turbine governor	$K_p = 1.0$		
	$T_f = 0.5$ s	$T_i = 3.7$ s	$T_d = 1.0$ s
Voltage regulator	$k = 150$		
	$T_1 = 0.1$ s	$T_2 = 0.02$ s	$T_3 = 1.22$ s
	$T_4 = 5.0$ s	$T_{ms} = 0.04$ s	$T_{st} = 0.005$ s
Stabilizer (PSS)	$M = 5$	$N = 1$	
	$K_{s1} = 20$	$K_{s2} = 0.625$	$K_{s3} = 1.0$
	$T_\omega = 0.1$ ms	$T_p = 12.5$ ms	$T_{w1...4} = 4.96$ s
	$T_1 = 0.15$ s	$T_2 = 0.09$ s	$T_3 = 0.15$ s
	$T_4 = 0.09$ s	$T_6 = 0.1$ ms	$T_7 = 5.0$ s
	$T_8 = 1.05$ s	$T_9 = 0.21$ s	

7.2.3 Possible Scenarios

Considering possible outages of the feeders and the unreliability of weak power grids, three scenarios are proposed:

1. Regular scenario – both feeders are operational and the short-circuit power is, consequently, 250 MVA;
2. Intermediate scenario – connection with feeder 1 is lost. The power plant remains synchronized only to feeder 2, with 150 MVA of short-circuit power. Thus, the system is less rigid;
3. Critical scenario – feeder 2 is out of service and the connection with feeder 1 only guarantees 100 MVA of short-circuit power. This is the most demanding condition for the operation of this power plant.

Due to the low short-circuit power, in all these scenarios the power plant is considered to run under islanded operation condition. Eigenanalyses performed in the following section for the three cases indicate if these scenarios are stable or not. Instabilities are amended through the introduction of stabilizing signal from a power system stabilizer.

Further, in section 7.4, the main hydraulic eigenmodes are presented. And finally, in section 7.5, eigenanalysis of the most critical scenario is performed considering the complete representation of the hydroelectric system. Interactions between hydraulic, electrical and control parts are pointed out.

7.3 Eigenanalysis of the Electrical System

The eigenanalysis of the electrical system is carried out considering an over-excited, full load operation of the power plant, with power factor equal to 0.90. This means: $u = 1.04$ p.u., $p_{el} = -0.90$ p.u. and $q = -0.436$ p.u [a]. The system is considered first without PSS, which will be applied later in order to enhance the small-signal stability of the power plant.

7.3.1 The Regular Scenario

As stated previously, the regular scenario corresponds to the condition when the power plant is connected to the grid through both feeders, meaning a 250 MVA short-circuit power. The results of the eigensolution of the system under this configuration are given in table 7.4.

[a] As stated in chapter 5, section 5.3, according to the sign convention used in SIMSEN, negative power means generated (delivered) power. In order to keep consistency with the other parts of this document, the curves of electrical power are presented in this chapter with a negative sign ($-p_{el}$).

Table 7.4: Eigenvalues of the electrical system considering the regular scenario.

Nature of the eigenmode	λ	ζ (%)	f (Hz)
Control mode	$-19.5 \pm j5.21$	96.6	0.829
Electro-mechanical local mode	$-0.37 \pm j6.75$	5.47	1.074
Stator windings	$-9.55 \pm j314.04$	3.04	49.98
Transformer magnetizing branch	$-0.17 \pm j314.16$	0.05	50.0
Voltage regulator	-200.6	100	–
Voltage regulator and rotor windings	-48.2	100	–
Damper windings	-13.0	100	–
Generator windings and regulator	-2.39	100	–
Generator windings and regulator	-1.02	100	–

The characteristics of all eigenvalues were described in a detailed way in chapter 5, and will not be individually analyzed anew.

It is particularly important to observe that the electro-mechanical local mode is relatively poorly damped. This is due to the weak network. Nonetheless, this represents the best case. With lower short-circuit powers in the other scenarios, this eigenmode tends to be even less damped.

7.3.2 The Intermediate Scenario

If the connection with feeder 1 is lost, the short-circuit power drops to 150 MVA. Table 7.5 presents the results of the eigensolution of the system under this condition.

Whereas most of the eigenvalues undergo slight modifications, the local mode clearly approaches the limit of stability, with a very weak damping ratio (ζ). This indicates that the critical scenario, the most severe one, shall present instabilities. This is confirmed in the following subsection.

7.3.3 The Critical Scenario

Considering now a 100 MVA short-circuit power, the results presented in table 7.6 confirm the expectation that this condition would result in instabilities. The local mode becomes unstable which means that any small disturbance is sufficient to break the balance of the system.

A time-domain simulation permits to confirm these findings. Figure 7.2 shows that by applying

Table 7.5: Eigenvalues of the electrical system considering the intermediate scenario.

Nature of the eigenmode	λ	ζ (%)	f (Hz)
Control mode	$-19.1 \pm j5.27$	96.4	0.839
Electro-mechanical local mode	$-0.06 \pm j5.78$	1.04	0.920
Stator windings	$-10.6 \pm j314.06$	3.37	49.98
Transformer magnetizing branch	$-0.17 \pm j314.16$	0.05	50.0
Voltage regulator	-200.6	100	–
Voltage regulator and rotor windings	-48.2	100	–
Damper windings	-12.0	100	–
Generator windings and regulator	-2.91	100	–
Generator windings and regulator	-0.98	100	–

Table 7.6: Eigenvalues of the electrical system considering the critical scenario.

Nature of the eigenmode	λ	ζ (%)	f (Hz)
Control mode	$-18.8 \pm j5.29$	96.3	0.841
Electro-mechanical local mode	$0.16 \pm j4.90$	-3.26	0.780
Stator windings	$-11.4 \pm j314.08$	3.63	49.99
Transformer magnetizing branch	$-0.18 \pm j314.16$	0.06	50.0
Voltage regulator	-200.7	100	–
Voltage regulator and rotor windings	-48.1	100	–
Damper windings	-11.2	100	–
Generator windings and regulator	-3.37	100	–
Generator windings and regulator	-0.95	100	–

a positive 5% step on the external torque of the rotating inertia representing the generator rotor, the oscillations are slowly damped in the regular scenario. In the intermediate one, the damping is imperceptible; the system is at the limit of stability. And in the critical scenario, the system is not capable of damping the oscillations of the rotor, resulting in power fluctuations that grow continually. For the three cases, the frequency of oscillation corresponds to the frequencies of the local modes identified through the eigenanalysis.

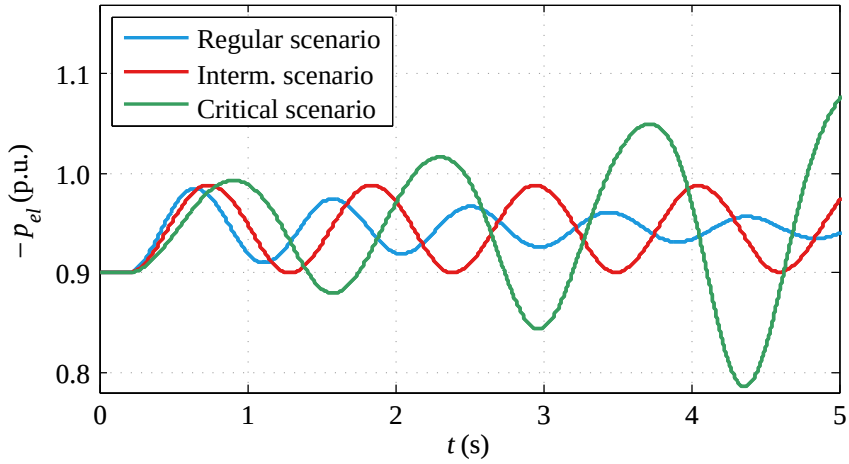

Figure 7.2: Electrical power behavior for different values of short-circuit power.

In general, it is possible to conclude that besides the local mode, the other eigenvalues are not significantly affected by reduction of short-circuit power.

7.3.4 Contribution of the PSS to the Stability of the Local Mode

In order to cope with unstable or badly damped electro-mechanical modes and enhance the stability of the power plant, power system stabilizers are a suitable solution. In order to illustrate the effects of the PSS, the critical scenario is considered, since it is unstable. Enhancing the stability of the power plant for the worst condition will also make it more stable, for the cases with a higher level of short-circuit power.

A power system stabilizer of type IEEE PSS2B is thus added to the system. The set of parameters used for the stabilizer, presented in table 7.3, was established based on the parameters given in reference [45]. They were, nevertheless, adapted for this specific case.

The eigenvalues of the system are recalculated for different values of gain K_{s1}, ranging from 0 to 50. As shown in chapter 5, section 5.9, new control modes appear when the PSS is added. Nevertheless, in this case they are not significant, since they have high damping ratios (ζ).

Table 7.7 summarizes the results for the local mode with different values of K_{s1}. Figure 7.3 depicts a root locus representation of these results. It is possible to see that with $K_{s1} = 2.775$ the limit of stability is reached. A gain $K_{s1} = 20$ adds sufficient damping to the local mode and is the value chosen for the setting of the PSS. Although higher values could be adopted, this is not necessary. Moreover, stabilizers with excessively high gains are more likely to induce harmful undesired interactions. Therefore, $K_{s1} = 20$ seems a good compromise.

Table 7.7: Evolution of the local mode with the PSS gain, considering the critical scenario.

Value of K_{s1}	Local mode	ζ (%)	f (Hz)
0.0	$0.16 \pm j4.90$	-3.26	0.780
1.0	$0.10 \pm j4.92$	-2.03	0.783
2.775	$0.0 \pm j4.95$	0.0	0.788
5.0	$-0.13 \pm j5.00$	2.60	0.796
10.0	$-0.44 \pm j5.10$	8.60	0.812
20.0	$-1.10 \pm j5.32$	20.2	0.847
30.0	$-1.80 \pm j5.56$	30.8	0.885
40.0	$-2.51 \pm j5.79$	39.8	0.922
50.0	$-3.21 \pm j5.91$	47.7	0.941

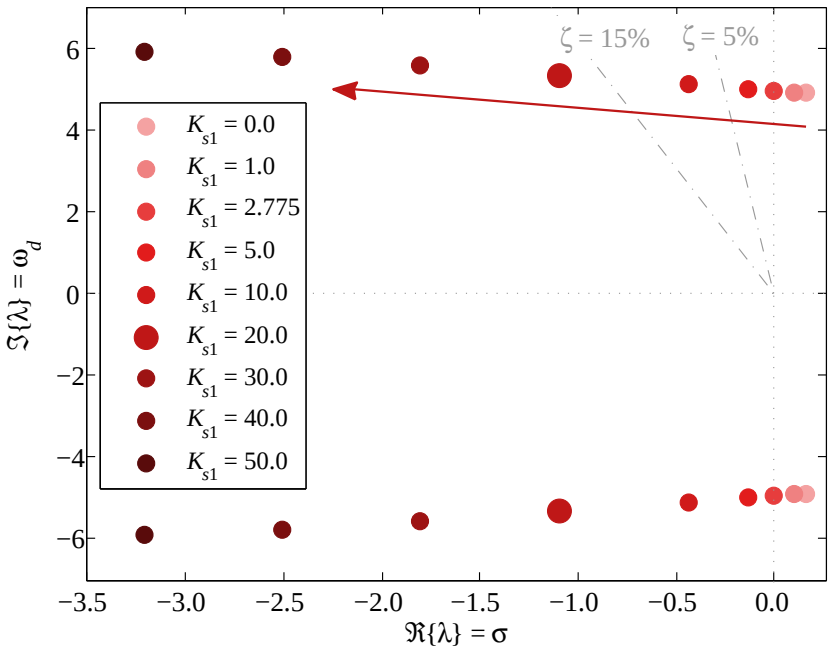

Figure 7.3: Evolution of local mode with the PSS gain K_{s1}, considering the critical scenario.

The complete list of eigenvalues of the electrical system (considering the critical scenario), after the final setting of the PSS, is given in table 7.8.

Besides, it is possible to confirm the better small-signal stability of the system once again through a time-domain simulation of the same nature as the previous one. Figure 7.4 illustrates the effect of the PSS over the local mode. The previously unstable system is now capable of operating under the most critical condition with a good performance in terms of small-signal stability.

Table 7.8: Eigenvalues of the electrical system considering the critical scenario, with PSS ($K_{s1} = 20$).

Nature of the eigenmode	λ	ζ (%)	f (Hz)
Control mode (PSS)	$-6.50 \pm j1.55$	97.3	0.247
Control mode (PSS)	$-2.87 \pm j2.01$	81.9	0.320
Control mode (AVR and PSS)	$-14.4 \pm j4.58$	95.3	0.729
Electro-mechanical local mode	$-1.10 \pm j5.32$	20.2	0.847
Stator windings	$-11.4 \pm j314.08$	3.63	49.99
Tansformer magnetizing branch	$-0.18 \pm j314.16$	0.06	50.0
Power system stabilizer	-10000	100	–
Power system stabilizer	-10000	100	–
Voltage regulator	-200.7	100	–
Power system stabilizer	-81.4	100	–
Voltage regulator and rotor windings	-47.2	100	–
PSS, excitation and damper windings	-17.5	100	–
Damper windings	-11.4	100	–
Power system stabilizer	-10.5	100	–
Power system stabilizer	-6.20	100	–
Power system stabilizer	-1.97	100	–
Generator windings and AVR	-1.00	100	–
PSS and rotating mass	-0.24	100	–
Power system stabilizer	-0.20	100	–
Power system stabilizer	-0.20	100	–
Power system stabilizer	-0.19	100	–
PSS and rotating mass	-0.18	100	–

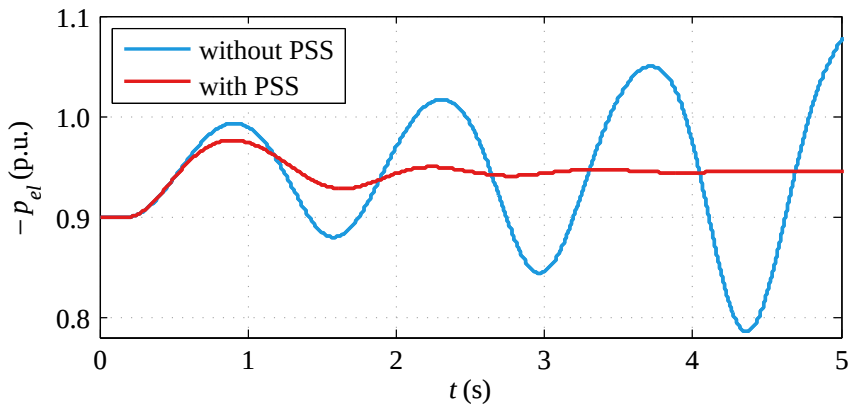

Figure 7.4: Electrical power response without and with PSS ($K_{s1} = 20$), in the critical scenario.

7.4 Eigenanalysis of the Hydraulic System

The eigenvalues calculation of the hydraulic system permits to identify the eigenmodes that are more relevant to this analysis, *i.e.*, those that are most likely to interact with the generator and with the grid. Therefore, the eigenanalysis performed in this section takes into account the hydraulic subsystem as described in section 7.2.2. The operating point considered here matches the one for which the calculations of the previous section were performed. This means that the Francis turbine runs under full load condition.

A reduced list of eigenvalues of the hydraulic system is presented in table 7.9. Since the representation of this system has a relatively high order (due to the spatial discretization of the piping system), the extensive list of eigenvalues is not given here. Only the most relevant modes are presented.

The results are presented for the system without and with active turbine governor in order to

Table 7.9: Most relevant eigenvalues of the hydraulic system.

Nature of the eigenmode	without turbine governor			with turbine governor		
	λ	ζ (%)	f (Hz)	λ	ζ (%)	f (Hz)
Hydromechanical	-0.207	100	–	$-0.48 \pm j0.79$	51.9	0.125
Penstock 1st elastic	$-1.10 \pm j2.68$	38.0	0.427	$-1.14 \pm j3.43$	31.5	0.546
Penstock 2nd elastic	$-0.77 \pm j5.52$	13.8	0.879	$-0.98 \pm j5.71$	16.9	0.909
Penstock 3rd elastic	$-0.49 \pm j8.46$	5.78	1.346	$-0.56 \pm j8.50$	6.57	1.353
Penstock 4th elastic	$-0.25 \pm j11.33$	2.21	1.803	$-0.26 \pm j11.35$	2.29	1.806

ease the identification of the hydraulic eigenmodes. As it can be seen, the activation of the frequency control loop alters the eigenvalues, especially those with lower frequency values.

The hydromechanical mode corresponds to the interaction between the rotating inertia of the turbine and the inertia of the water flow through the penstock. The other four modes indicated in table 7.9 are related to the elastic characteristic of the penstock.

The spatial discretization of the piping system allows for the representation of the hydraulic mode shapes also in a spatial form. From such representation, it is possible to observe how the effect of each mode is distributed along the elements of the hydraulic installation. Figure 7.5 depicts the mode shapes of all eigenvalues given in table 7.9 (for detailed information on the characteristics and behavior of these eigemodes, please see reference [70]).

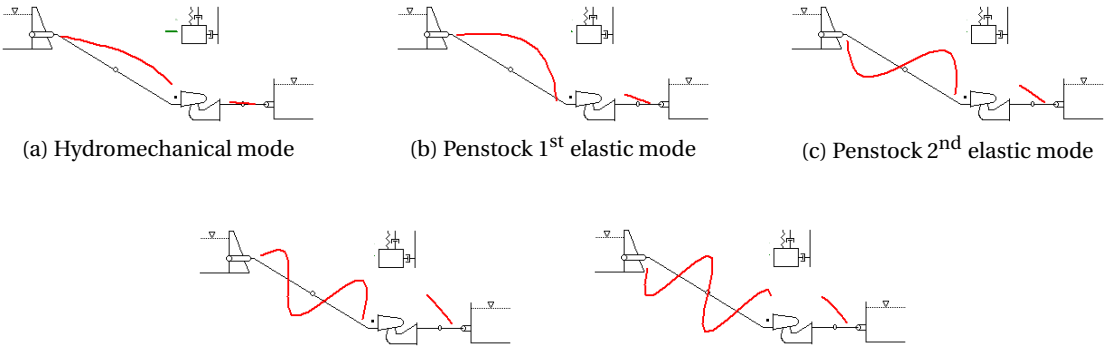

(a) Hydromechanical mode (b) Penstock 1st elastic mode (c) Penstock 2nd elastic mode

(d) Penstock 3rd elastic mode (e) Penstock 4th elastic mode

Figure 7.5: Most relevant hydraulic mode shapes.

In order to guarantee that hydraulic modes do not affect the dynamic behavior of the electrical system, and vice-versa, it is important to go further on the analysis. A complete hydroelectric model is necessary for this purpose.

7.5 Eigenanalysis of the Complete Hydroelectric System

The construction of the complete hydroelectric model is achieved by combining the electrical and hydraulic models studied in the previous sections. The electrical system is considered to be in the critical scenario (S_{sc} = 100 MVA). At first, the PSS is not taken into account so that the contribution of the hydraulic system to damping the unstable local mode can be assessed. The PSS is added further to the system and its interaction with other elements is then evaluated.

The interface between hydraulic and electrical subsystems lies in the mechanical coupling between turbine and generator inertias, through coupling shaft. Consequently, interactions between hydraulic and electrical subsystems are related to interactions between the mechan-

ical and the electromagnetic torques. It is known that the mechanical system behaves as a low-pass filter because of the high value of inertia of the generator [71, 95]. Consequently, interactions between the hydraulic and electrical elements are expected to happen at a low frequency range.

7.5.1 Interactions between the Hydraulic and the Electrical Subsystems

Table 7.10 presents the results of the eigensolution of the hydroelectric system with turbine governor but without PSS. Only the most relevant eigenvalues are given. Hydraulic and electrical subsystems interact in such a way that the main eigenvalues of the global system are all modified. As expected, this interaction happens in the low frequency range. For eigenvalues with frequencies higher than 2 Hz, no significant change occurs.

Table 7.10: Most relevant eigenvalues of the hydroelectric system with turbine governor, without PSS.

Nature of the eigenmode	λ	ζ (%)	f (Hz)
Hydromechanical mode	-1.69	100	–
Penstock 1st elastic mode	$-0.80 \pm j2.62$	29.2	0.417
Penstock 2nd elastic mode	$-0.84 \pm j6.13$	13.6	0.976
Penstock 3rd elastic mode	$-0.60 \pm j8.54$	7.00	1.359
Penstock 4th elastic mode	$-0.27 \pm j11.35$	2.38	1.806
Electro-mechanical local mode	$0.056 \pm j4.82$	-1.16	0.767
Mechanical torsional mode	$-2.58 \pm j131.93$	1.96	21.00

The hydromechanical eigenmode experiences an important change. In the global representation, it is no longer an oscillatory mode, differently from the expected behavior estimated from the purely hydraulic model with turbine governor (see table 7.9).

The inclusion of the electrical model also shows that the first two elastic modes of the penstock are actually slightly less damped. Moreover, the frequency of the 1st elastic mode is considerably modified. In the case of the 2nd elastic mode, the frequency shift is smaller. On the other hand, the changes experienced by the 3rd and 4th elastic modes are considerably less significant. Although their damping ratio (ζ) is increased, the increment is minor. The frequency shift is also weak. Indeed, as the frequency of the eigenvalue approaches 2 Hz, less significant are the modifications caused by interactions with the electrical subsystem.

It is also possible to see that the local mode remains unstable. Nonetheless, the inclusion of the hydraulic model in the global representation shows that the hydraulic subsystem gives

a contribution in the sense of damping this eigenmode. The damping ratio, which was −3.26% with the purely electrical representation (see table 7.6), is actually equal to −1.16%. This indicates that the hydraulic system is capable of adding some damping to the local mode. Moreover, it is probable that this contribution is stronger if the tuning of the frequency regulator is better adapted to the islanded condition of the power plant. This is done in the next subsection, with a new set of parameters for the turbine governor.

The instability of the local mode affects not only the electrical subsystem, but also the hydraulic installation. This can be confirmed through a time-domain simulation in which a step increase of 5% is applied on the external torque of the turbine rotating inertia. Figure 7.6 illustrates the dynamic behavior of both the purely hydraulic and the complete hydroelectric models. Whereas the hydraulic model suggests that the system is stable, the complete representation of the system shows that, in reality, the instability of the local mode propagates throughout the whole system. It can be verified that turbine net head and torque present unstable oscillations at the frequency of the local mode.

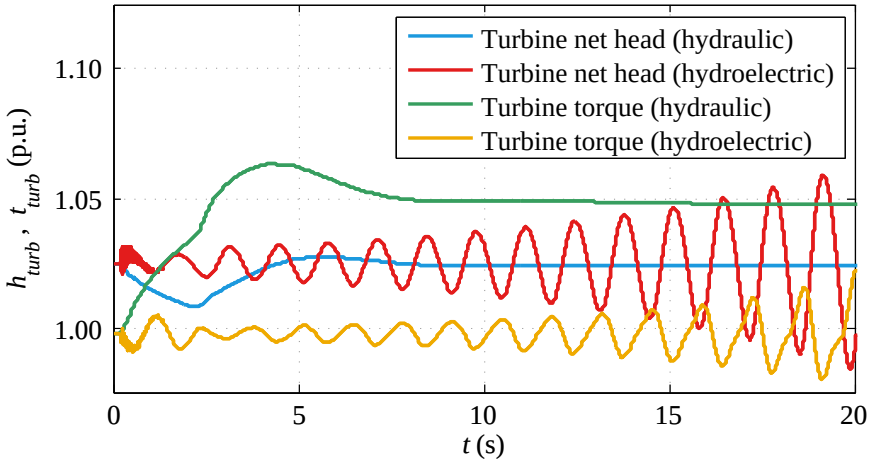

Figure 7.6: Turbine net head and torque for the hydraulic and hydroelectric models.

Finally, since the rotors of turbine and generator are represented by individual rotating masses, a new eigenmode appears in the results. It corresponds to the torsional mode between the two rotating inertias. This eigenvalue depends on the characteristics of the coupling shaft as well as on the values of inertia of both rotating masses.

7.5.2 Contribution of the Turbine Governor to the Stability of the Local Mode

As mentioned in the previous subsection, the results of the global model indicate that the hydraulic elements contribute to damp the local mode oscillations, at least for the operating point considered in this analysis. Moreover, if the tuning of the turbine governor is better

adapted for a more stable behavior under islanded operation, the contribution of the hydraulic subsystem can be enhanced.

Generally, increasing the integration time constant of the PID controller yields a more stable dynamic behavior. On the other hand, this has the effect of deteriorating the performance of the controller. In other words, although the stability is increased, the peak values of the first cycles of oscillation are bigger. Therefore, a good compromise between stability and performance must be found. For a stable islanded operation, the increase of the integration time constant must be particularly substantial.

Furthermore, for stabilizing the local mode in this case, it is also necessary to increase the derivative time constant. The derivative term of the PID controller tends to rapidly counter-weight speed deviations. Thus, the controller can better contribute to damp the deviations caused by local mode oscillations with a higher derivative time constant. The proportional gain is also increased in order to boost the contribution of the turbine governor to the small-signal stability of the global system. Further details on tuning of hydraulic turbine regulators can be found in references [51, 106].

For the case of the hydropower plant studied in this chapter, the following *enhanced tuning* for the turbine governor is sufficient to make the local mode stable. Even though the *initial tuning* of the turbine governor is considerably modified (see table 7.3), the parameters of the enhanced tuning stay in a reasonable, realistic range considering islanded operation:

$$K_p = 2.3 \; ; \; T_f = 0.35 \text{ s} \; ; \; T_i = 25 \text{ s} \; ; \; T_d = 2.95 \text{ s}.$$

Table 7.11 presents the results of the most relevant eigenmodes when calculated with the enhanced tuning of turbine governor.

Table 7.11: Most relevant eigenvalues of the hydroelectric system with enhanced tuning of turbine governor, without PSS.

Nature of the eigenmode	λ	ζ (%)	f (Hz)
Hydromechanical mode	$-1.11 \pm j0.63$	87.0	0.100
Penstock 1st elastic mode	$-0.10 \pm j2.44$	4.09	0.388
Penstock 2nd elastic mode	$-0.31 \pm j7.50$	4.13	1.194
Penstock 3rd elastic mode	$-0.97 \pm j10.10$	9.56	1.608
Penstock 4th elastic mode	$-0.66 \pm j11.58$	5.69	1.843
Electro-mechanical local mode	$-0.026 \pm j4.72$	0.55	0.751
Mechanical torsional mode	$-13.42 \pm j156.1$	8.56	24.84

These results confirm the expectation of damping the local mode through the turbine governor. Indeed, the enhancement proposed for the frequency control loop tuning makes the local mode stable, despite the low value of damping ratio. Nonetheless, besides eliminating the instability, the action of the turbine governor has some negative effects. This new tuning considerably decreases the damping ratio of the 1st and 2nd elastic modes of the penstock.

On the other hand, the 3rd and 4th elastic modes become slightly better damped. It is also interesting to observe that especially the 2nd and 3rd penstock eigenmodes undergo considerable frequency shifts, suffering strong distortions in their shapes. This renders the interpretation of the eigenmodes more intricate.

Additionally, the hydromechanical mode turns into an oscillatory eigenmode again, with a strong damping ratio. Finally, the action of the turbine governor over the torsional mode is remarkable. The increase of both damping ratio and frequency is considerable.

In order to verify the interactions between hydraulic and electrical subsystems, a calculation of participation factors is performed. Given the relatively high order of this system, a novel didactic form to present the participation matrix is proposed here, by using a graphical representation through a color map.

Figure 7.7 gives such representation in which the participation factors are normalized by column so that the highest value in each column is 1. The eigenmodes are distributed along the horizontal axis and identified by numbers, according to their nature indicated in the legend of the figure. The state variables are distributed along the vertical axis and are separated by groups identified by distinct letters, also described in the legend of the figure.

It can be seen that the low-order penstock elastic eigenmodes (numbers 02 and 05 to 07) have a considerable degree of interaction with the mechanical variables (group H). This is also the case for the hydromechanical mode (number 01). It is interesting to observe these eigenmodes interact also with the electrical system (variables of groups D and E). On the other hand, the influence of higher-order modes of the penstock (number 08) stays confined in the hydraulic installation (variables of groups A, B and F).

It is also possible to observe that, in this case, the eigenmodes related to the tailrace (number 09) have their influence limited to the lower part of the hydraulic installation, *i.e.*, turbine and lower reservoir – group A – and tailrace tunnel – groups C and G.

Additionally, the interaction of the local mode (number 03) with all the system is clearly demonstrated in figure 7.7, since it participates in almost all groups of state variables. Conversely, the control mode (number 04), which is due to the voltage regulator and is highly damped, influences only the rotor currents (group E) and the regulator variables (group I).

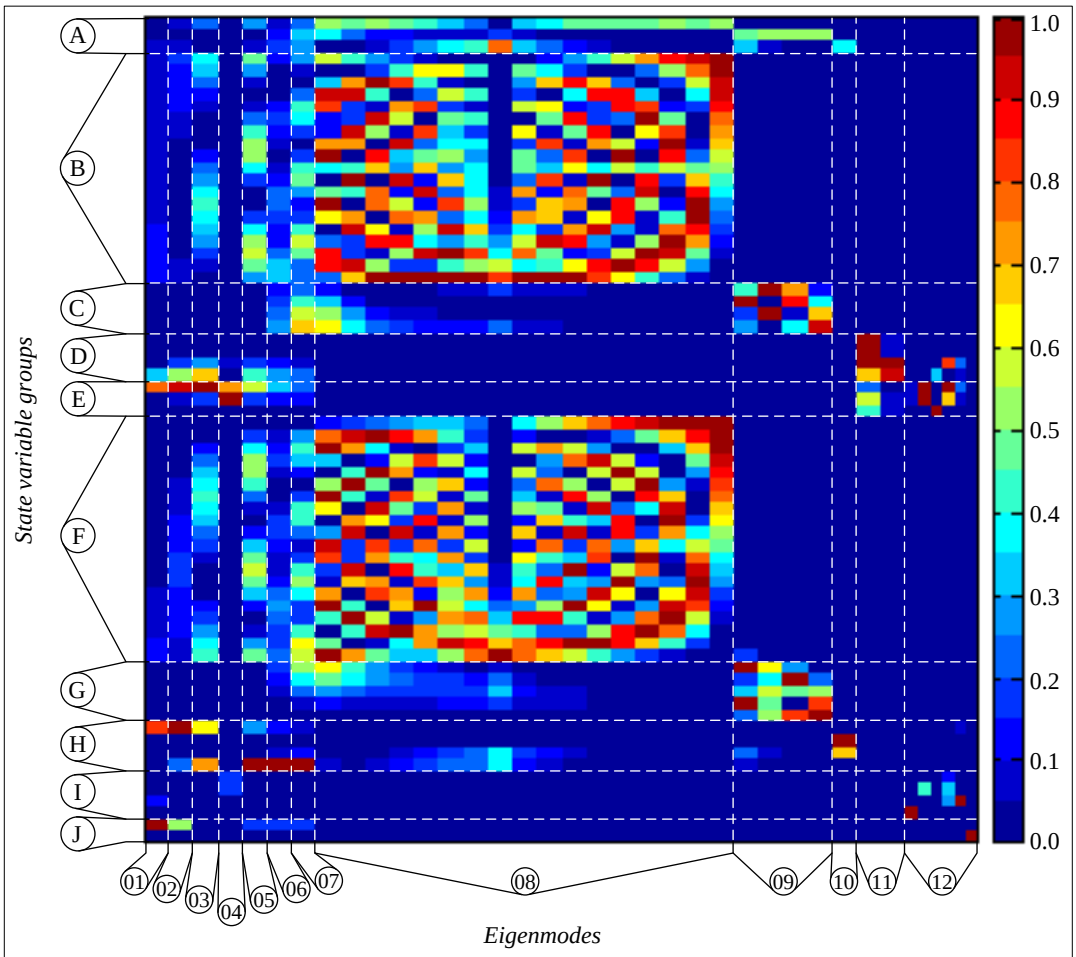

Meaning of the state variables groups:

A	Turbine and reservoirs discharges
B	Penstock discharges
C	Tailrace tunnel discharges
D	Generator stator and grid currents
E	Generator rotor currents
F	Penstock heads
G	Tailrace tunnel heads
H	Mechanical masses speed and angle
I	Voltage regulator state variables
J	Turbine governor state variables

Nature of eigenmodes:

01	Hydromechanical mode
02	Penstock 1st elastic mode
03	Electro-mechanical local mode
04	Control mode
05	Penstock 2nd elastic mode
06	Penstock 3rd elastic mode
07	Penstock 4th elastic mode
08	Penstock higher-order elastic modes
09	Tailrace tunnel elastic modes
10	Mechanical torsional mode
11	Stator and grid modes (50 Hz)
12	Purely real eigenvalues

Figure 7.7: Participation factors color map plot for the hydroelectric system, with enhanced tuning of turbine governor, without PSS.

As an illustration, figures 7.8 and 7.9 show the effect of the new tuning of the turbine governor over the dynamic behavior of the system. Once again, a 5% step is applied to the external torque of the turbine rotating inertia.

It is possible to confirm that the instability of the local mode is eliminated, but it remains badly damped. Therefore, the use of a PSS is still necessary to enhance the small-signal stability of the power plant.

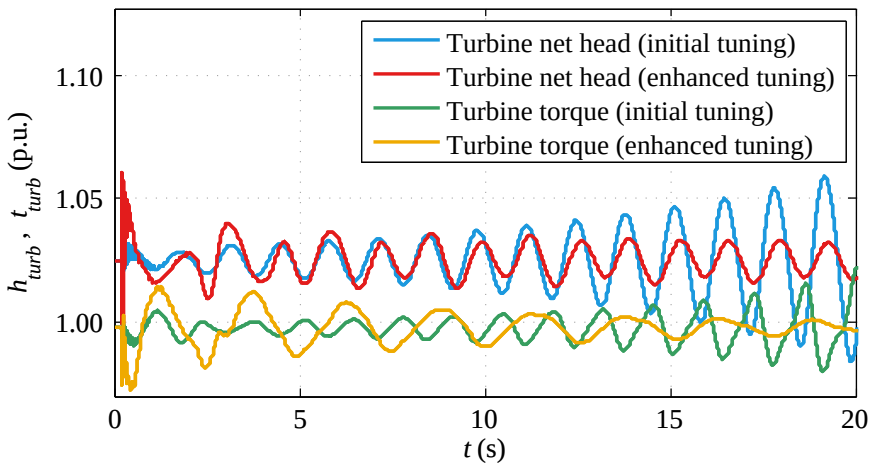

Figure 7.8: Turbine net head and torque with initial and enhanced tuning of the governor.

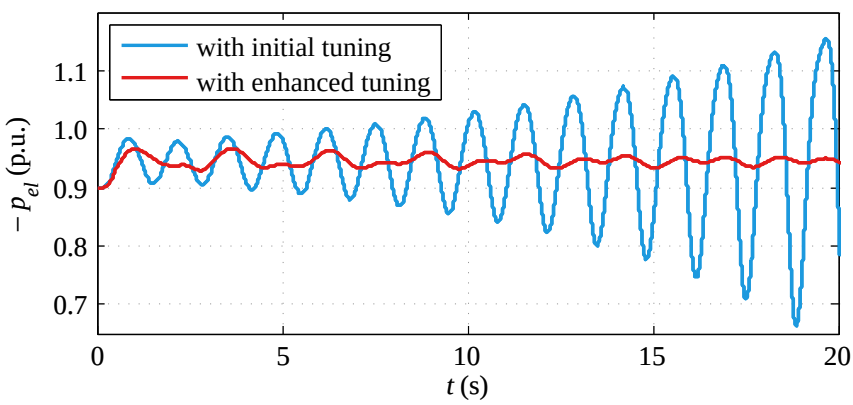

Figure 7.9: Electrical power response with initial and enhanced tuning of the governor.

7.5.3 Interaction between the Turbine Governor and the PSS

Considering the last results, the PSS is added back to the system in order to finally guarantee a better dynamic behavior. The parameters for the PSS are the same as used previously, and the enhanced tuning of the turbine governor is maintained.

Table 7.12 presents the results of the most relevant eigenmodes calculated for this case. Clearly, the interaction between the turbine governor and the PSS results in some conflicting effects that are detrimental to the dynamic behavior of the system.

Whereas the damping ratio of the local mode is greatly increased, the penstock 1st elastic mode experiences a drastic reduction of damping, approaching the limit of stability. Besides the damping ratio decrease already caused by the enhanced tuning of the governor in the previous case, the PSS adds some destabilizing effects to this eigenmode. This is a precarious, undesirable condition, since disturbances could result in significant pressure oscillations, causing substantial mechanical torque pulsations, finally resulting in electrical power swings that could be harmful both to the hydropower plant and to the weak power grid.

Table 7.12: Most relevant eigenvalues of the hydroelectric system with enhanced tuning of turbine governor, with PSS ($K_{s1} = 20$).

Nature of the eigenmode	λ	ζ (%)	f (Hz)
Hydromechanical mode	$-0.58 \pm j0.96$	51.7	0.153
Penstock 1st elastic mode	$-0.025 \pm j2.07$	1.21	0.329
Penstock 2nd elastic mode	$-0.18 \pm j4.74$	3.79	0.754
Penstock 3rd elastic mode	$-0.33 \pm j7.54$	4.37	1.200
Penstock 4th elastic mode	$-0.69 \pm j11.55$	5.96	1.838
Electro-mechanical local mode	$-2.77 \pm j5.78$	43.2	0.920
Mechanical torsional mode	$-13.42 \pm j156.1$	8.56	24.84

Consequently, the problem must be solved by adopting a different set of parameters either for the turbine governor or for the PSS. A plausible solution is to decrease the contribution of the governor so that the penstock eigenmodes are less affected, while ensuring sufficient damping of the local mode oscillations and a satisfactory dynamic behavior of the whole installation. One possibility to achieve this goal is to set the turbine governor back to its initial tuning, recalled hereafter:

$$K_p = 1.0 \; ; \; T_f = 0.5 \text{ s} \; ; \; T_i = 3.7 \text{ s} \; ; \; T_d = 1.0 \text{ s}.$$

Since under this set up the effect of the turbine governor over the whole system was more conservative, the tendency is that the hydraulic modes regain a more stable condition, with the PSS playing the major role of damping the local mode.

Table 7.13 presents the most relevant eigenvalues of the global system, considering this new set up of regulators. These results show that a more cautious tuning of the turbine governor reduces the adverse interactions with the PSS, leading to an overall more stable system.

Table 7.13: Most relevant eigenvalues of the hydroelectric system with initial tuning of turbine governor ($K_p = 1.0$; $T_f = 0.5$ s ; $T_i = 3.7$ s ; $T_d = 1.0$ s), with PSS ($K_{s1} = 20$).

Nature of the eigenmode	λ	ζ (%)	f (Hz)
Hydromechanical mode	$-1.01 \pm j0.78$	79.1	0.124
Penstock 1st elastic mode	$-0.55 \pm j2.29$	23.4	0.364
Penstock 2nd elastic mode	$-0.55 \pm j4.82$	11.3	0.767
Penstock 3rd elastic mode	$-0.61 \pm j8.53$	7.13	1.358
Penstock 4th elastic mode	$-0.27 \pm j11.35$	2.38	1.806
Electro-mechanical local mode	$-3.41 \pm j4.81$	57.8	0.766
Mechanical torsional mode	$-2.58 \pm j131.93$	1.96	21.00

Time-domain simulations of the same nature as the previous ones are carried out, in order to illustrate the better dynamic behavior of the system under this last configuration. It is clear in figures 7.10 and 7.11 that the system has a better dynamic behavior if the turbine governor has a more conservative tuning, when the PSS is active.

Furthermore, it is easy to see the consequences of the badly damped 1st elastic mode of the penstock. Indeed, pressure pulsations are converted into undesirable electrical power swings.

The solution presented here in order to solve the problem originated by detrimental interactions between regulators, hydraulic and electrical elements is one among several other possibilities. Certainly, other plausible solutions exist with different parameters tuning for the turbine governor, PSS and also the voltage regulator, which was not modified along this study.

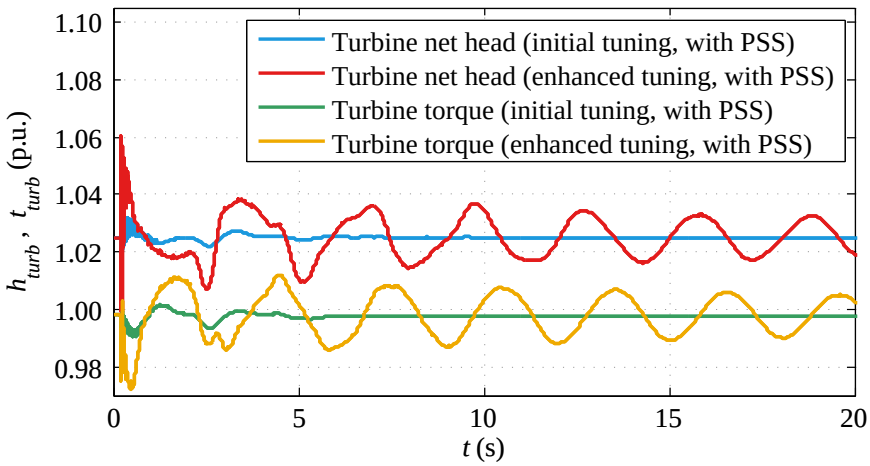

Figure 7.10: Turbine net head and torque with initial and enhanced tuning of the governor, with PSS.

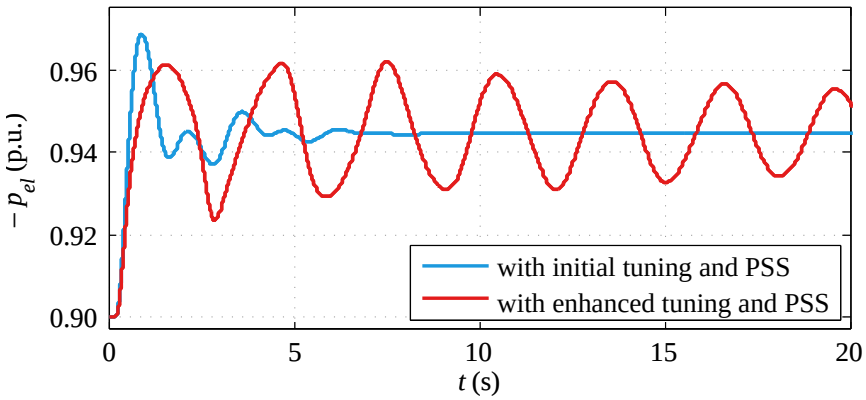

Figure 7.11: Electrical power response with initial and enhanced tuning of the governor, with PSS.

7.6 Concluding Remarks

This case study allowed to apply the small-signal models developed in the present work to the study of the dynamic behavior of hydropower plants subjected to islanded operation condition, due to weak connections with the network.

For the electrical model, three problematic scenarios were considered in which electromechanical local mode oscillations were badly damped. In the most critical case, the power grid was not stiff enough to withstand the oscillations, resulting in an unstable system.

A power system stabilizer of type IEEE PSS2B was then employed in order to overcome the unstable condition of the most critical scenario. The influence of the PSS gain over the local mode was studied in order to obtain a stable condition, with the most convenient setting.

Then, an eigenanalysis of the hydraulic system was carried out in order to identify the most relevant hydraulic eigenmodes. It was also possible to observe how the frequency control loop of the turbine governor modifies the low-frequency modes of the penstock.

Thereupon, it was possible to combine electrical and hydraulic models in order to build the complete high-order model of the hydropower plant. Results obtained from this global model, first without PSS, demonstrated that the system remained unstable, even though the eigensolution of the purely hydraulic system did not indicate any instability. Nevertheless, it was shown that the effects of the unstable local mode propagate to the hydraulic installation, resulting in undamped pressure fluctuations.

On the other hand, the complete representation of the power plant showed that the hydraulic installation had a positive influence on the damping of the local mode. This observation led to a modification of the turbine governor tuning to an enhanced set of parameters, more

appropriate for islanded operation. It was also observed that this new set of parameters made the 1st elastic eigenmode of the penstock less damped. But it also permitted the stabilization of the unstable local mode.

Although stable, the local mode remained badly damped, reason for which the PSS was added to the complete hydroelectric model. Nevertheless, the effect was adverse. Whereas the local mode became well damped, interactions between turbine governor and PSS led to a drastic destabilization of the 1st mode of the penstock. Badly damped oscillations due to this mode appeared to influence not only the hydraulic circuit, but also the electrical system, since pressure fluctuations resulted in mechanical torque oscillation, which induced considerable power swings.

Therefore, it is possible to conclude that significant interactions may happen between hydraulic, electrical and control elements that may induce undesirable dynamic behavior of the system, such as badly damped or even undamped modes of oscillation. These adverse interactions cannot be anticipated with partial models, like purely hydraulic or purely electrical representations. Consequently, comprehensive, multi-physics small-signal models are necessary for a complete assessment of the real small-signal stability of a hydropower plant.

8

Power Fluctuations in an Existing Hydropower Plant

8.1 Introduction

As mentioned in chapter 1, section 1.3.3, part load operation of Francis turbines is a condition likely to cause periodic pressure pulsations due to vortex rope precession in the draft tube. The frequency of this pulsating behavior is most commonly between 0.2 and 0.4 times the turbine rotational speed. Such phenomenon may also induce torque fluctuations in the mechanical system that may interact with the generator and the power system, possibly leading to significant electrical power swings [49, 83]. This is particularly true if the frequency of the vortex rope precession coincides with the frequency of the electro-mechanical modes related to the power plant [22, 69]. Furthermore, if the hydropower plant operates in islanded or isolated networks these power swings may be very detrimental to the dynamic behavior of the power plant and of the local network.

The purpose of this chapter is to present a case study that illustrates the effects of pressure pulsations due to vortex rope precession on the draft tube of Francis turbines. The investigated system is an existing 1 GW hydropower plant (4 × 250 MW Francis turbines) which was previously analyzed in references [69] and [72].

Whereas these works proposed a methodology for the assessment of part load resonance risk based on time-domain simulation, the eigenanalysis approach is used here. Furthermore, the electro-mechanical modes are identified not only for one single generator, but also for cases where a different number of generators are connected to the grid. Another important difference is that the grid is not considered here as an infinite bus. This allows for a more precise representation of the dynamic behavior of the electrical system.

Moreover, a specific value is calibrated for the draft tube wave speed a to match simulations and calculations to on-site measurements. In practice, the determination of the wave speed is a challenging task that requires specific knowledge which is out of the scope of the present work [55]. Therefore, the wave speed is considered to be a constant parameter.

8.2 Case Study Description

The hydropower plant studied in this chapter is composed of 4 × 250 MW generating units. The layout of the power plant is presented in figure 8.1. The electrical and hydraulic subsystems are described in the following subsections.

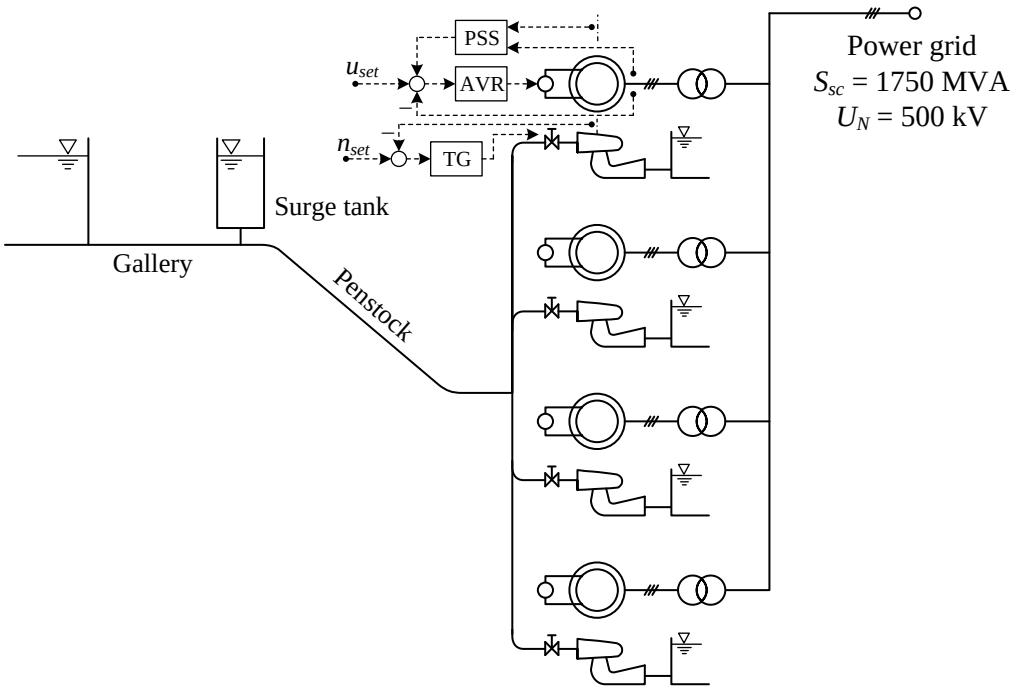

Figure 8.1: Layout of the hydroelectric powerplant [72].

8.2.1 Electrical Model

The electrical subsystem of the power plant is constituted of 4 × 281.5 MVA synchronous generators connected to four corresponding 500 kV/18 kV *Yd5* step-up transformers. The ABB Unitrol® excitation system (see figure 5.18) is applied as voltage regulator and a power system stabilizer of type IEEE PSS2B (see figure 5.21) is available. The four machines are connected to the power grid through two parallel transmission lines. The model used to represent these lines is the RL model. The main parameters of the electrical elements are given in table 8.1.

Table 8.1: Main parameters of the electrical installation.

Element	Ratings / Parameters
Generator	$S_N = 281.5$ MVA $U_N = 18$ kV $f_N = 50$ Hz $P_p = 9$ (number of pairs of poles) $I_{f\delta 0} = 777$ A $J_g = 2.25 \cdot 10^6$ kg$\cdot$m^2 Stator windings connection: Y
Step-up transformer	$S_N = 281.5$ MVA $U_{N1} = 500$ kV $U_{N2} = 18$ kV Vector group: *Yd5*
Transmission line	$R_{tl} = 2.8\ \Omega$ $L_{tl} = 120$ mH
Power grid	$S_{sc} = 1750$ MVA (short-circuit power) $U_N = 500$ kV $f_N = 50$ Hz

The short-circuit power of the grid (S_{sc}) is actually an unknown parameter in this study. The value presented in table 8.1 was deduced from comparison between measurements and simulation results and is validated further, in section 8.3.

8.2.2 Hydraulic Model

The hydraulic installation comprises an 1485 meter long gallery, a surge tank with variable cross section, an 1396.5 meter long penstock and a manifold feeding 4 × 250 MW Francis turbines. The main parameters of the system are presented in table 8.2.

The penstock is discretized in 116 elements, whereas the draft tube is represented by two pipe elements. The discretization of the penstock and piping system respects the CFL condition, explained in chapter 6, section 6.2. Moreover, the turbine characteristic curves are taken into account. Therefore, this high order model takes into account effects of water hammer, mass oscillation, and transient behavior of the turbine in the four quadrants, linked to the corresponding rotating inertia.

In order to simplify the identification of the hydroelectric interactions in the eigenanalysis, the turbine governor is not taken into account in the model.

Table 8.2: Main parameters of the hydraulic installation.

Element	Dimensions
Gallery	$L = 1485$ m $D = 9.2$ m $a = 1200$ m/s
Surge tank	$A_{ST} = 133$ m^2 (mid tank section)
Penstock	$L = 1396.5$ m $D = 8.8 / 7.15$ m $a = 1200$ m/s
Draft tube	$L = 25$ m $a = 56$ m/s (with vortex rope)
Francis turbine	$P_N = 250$ MW $n_N = 333.\overline{3}$ rpm $H_N = 352$ m $\nu = 0.22$ (specific speed) $J_t = 1.71 \cdot 10^5$ kg$\cdot$m^2
Coupling shaft	$K_{sh} = 3.61 \cdot 10^8$ Nm/rad (torsional stiffness) $\mu_{sh} = 6.7 \cdot 10^3$ Nms/rad (viscous damping)

8.2.3 Problems Encountered During Operation

During the operation of the power plant at part load condition, undesirable electrical power swings were detected. It was assumed that such oscillations were due to interactions of the electrical system with draft tube vortex rope. For this turbine (which has a rotation speed $n = 333.\overline{3}$ rpm), the frequency range of part load vortex rope pulsation is 1.11 to 2.22 Hz. This matches the typical range of electro-mechanical modes (0.7 to 2.0 Hz). Therefore, such interaction is likely to occur. It depends, however, on the operating point of the generators and on the topology of the electrical system, since these two factors influence the frequency and damping of the electro-mechanical modes.

On-site measurements during part load operation ($p_{el} = -0.426$ p.u.) allowed to record the pulsating behavior. Figure 8.2 gives an example of it during the operation of one single unit with active PSS, under part load condition. The low peak-to-peak amplitude can be associated to the damping contribution of the stabilizer. Although the frequency of oscillation is not constant, it is possible to graphically estimate that it varies around the value of 1.34 Hz, approximately. Through eigenvalues calculation of the hydraulic system, it shall be possible to confirm this value. This is done in section 8.5.

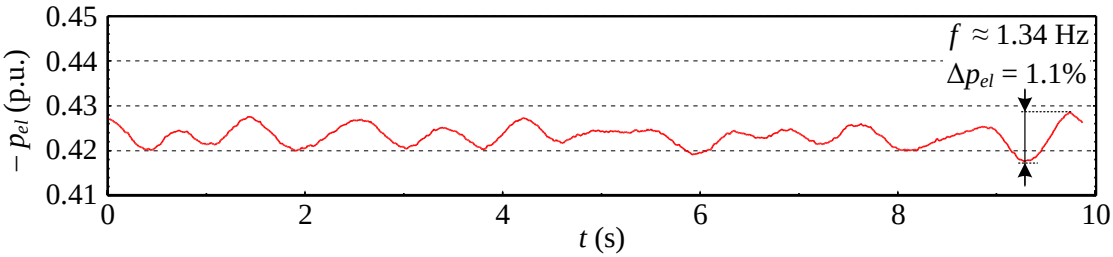

Figure 8.2: Electrical power swing recorded on-site with active PSS.

Before doing so, however, the parameters of the electrical model are validated in section 8.3 through comparison with on-site measurements. Then, eigenanalyses are performed to determine the electro-mechanical eigenmodes of the electrical system under different topologies (1, 2, 3 or 4 generators synchronized to the grid, with and without PSS).

8.3 Validation of the Electrical Model

In order to validate the parameters of the electrical model, time-domain simulations are compared to on-site measurements, which were performed in order to validate the tuning of both voltage regulator and PSS. During these tests, only one machine was synchronized to the grid. The disturbance applied to the system is a ±2% step on the set-point of the voltage regulator. The reaction of the system is observed on the active (P_{el}) and reactive (Q) powers[a], compensated frequency (f_{comp} – derived from the rotational speed of the generator), excitation voltage (u_f) and PSS output (u_{PSS}), in case it is active.

At first, the system is tested with inactive PSS. Figure 8.3 presents measurement and time-domain simulation results. The very good agreement that can be observed in this comparison validates the model, including the proposed short-circuit power of the network (S_{sc} = 1750 MVA). It is easy to observe the action of the local mode oscillations. Due to the relatively low short-circuit power of the grid, these oscillations take some time to be damped.

To verify the characteristics of the local mode, it is possible to perform the calculation of eigenvalues for this system considering the same operating point of measurements: $u = 0.969$ p.u., $p_{el} = -0.85$ p.u. and $q = -0.02$ p.u.

The extensive list of eigenvalues is presented in table 8.3. Real and imaginary parts are presented separately. In addition, the damping time constant τ ($\tau = 1/|\sigma|$), the damping

[a]As stated in chapter 5, section 5.3, according to the sign convention used in SIMSEN, negative power means generated (delivered) power. In order to adapt simulation to measurement results, the curves of electrical power are presented in this chapter with a negative sign ($-P_{el}$,$-Q$).

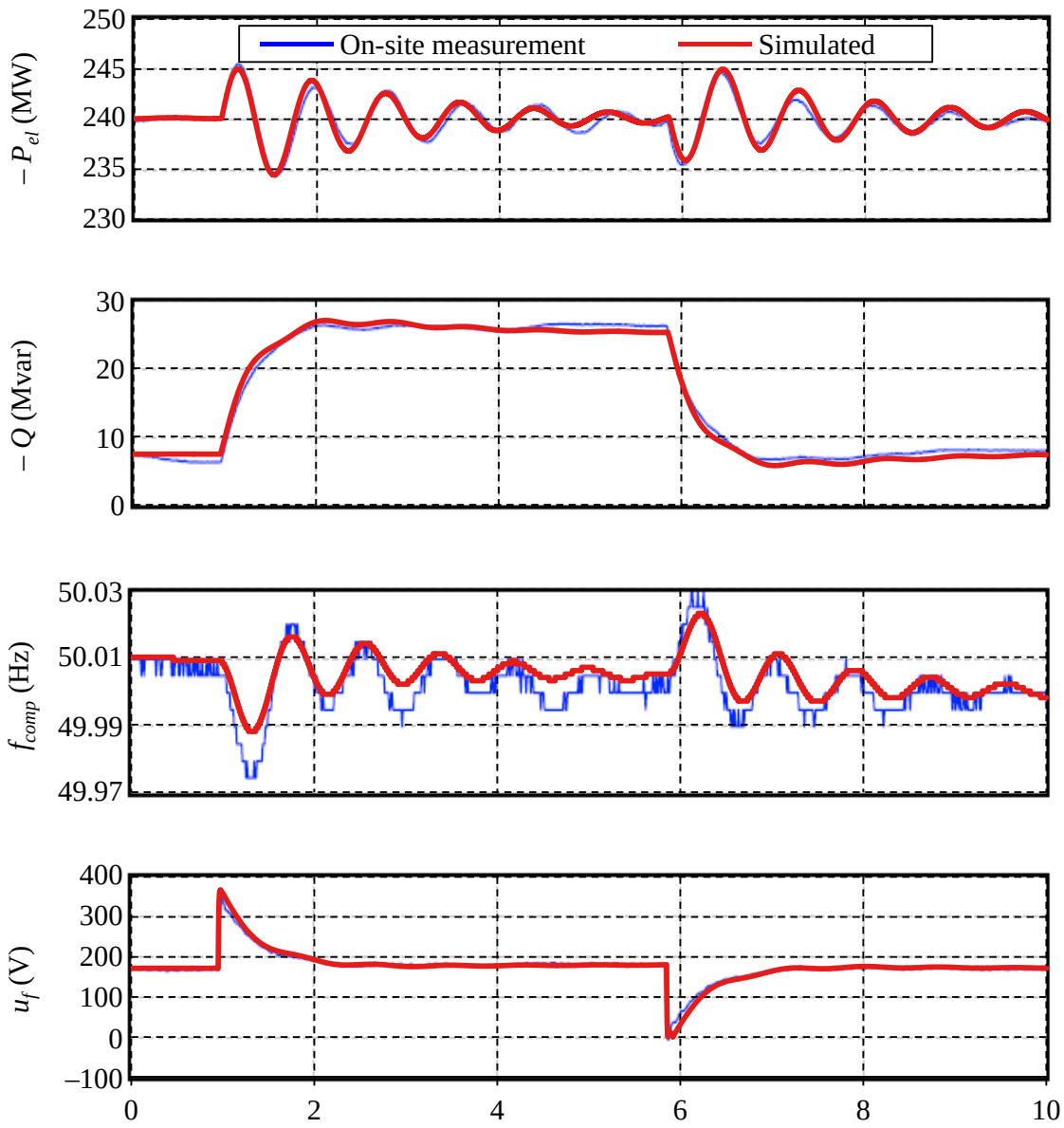

Figure 8.3: On-site measurement versus time-domain simulation, without PSS.

ratio ζ and the frequency f are calculated based on equations (3.11) and (3.12). Furthermore, the dominant state variables are indicated. They were identified using participation factors calculated according to the concept presented in section 3.3.3. For more information on the meaning of the state variables, please refer to chapter 5, sections 5.3, 5.5 and 5.8.

The characteristics of all eigenmodes are not discussed here, since the nature of each one was already explained in chapter 5. It is however important to mention that the pair of eigenvalues 5, 6 is related to the presence of the power transformer. Its low real part is due to the fact that the magnetizing reactance of the transformer is approximated by a high relative value, which

Table 8.3: Eigenproperties of the system with a single machine, without PSS.

Eigenvalue number i	$\sigma = \Re(\lambda_i)$ (Np/s)	$\omega_d = \Im(\lambda_i)$ (rad/s)	τ (s)	ζ (%)	f (Hz)	Dominant states
1,2	−0.524	7.687	1.908	6.80	1.223	$\Delta\omega_m, \Delta\theta, \Delta i_{abc2}, \Delta i_f$
3,4	−23.01	314.02	0.043	7.31	49.98	Δi_{abc2}
5,6	−0.003	314.16	$333.\overline{3}$	0.001	50.0	$\Delta i_{abc1,abc2}$
7	−218.6	–	0.0046	100	–	$\Delta u_g, \Delta u_{reg}, \Delta i_f$
8	−178.3	–	0.0056	100	–	$\Delta u_g, \Delta u_{reg}, \Delta i_f$
9	−92.40	–	0.011	100	–	Δi_Δ
10	−40.00	–	0.025	100	–	Δu_{C2}
11	−14.08	–	0.071	100	–	Δi_D
12	−5.562	–	0.180	100	–	$\Delta i_{abc}, \Delta i_f, \Delta i_Q$
13	−2.225	–	0.449	100	–	$\Delta i_f, \Delta\theta, \Delta u_{C1}$
14	−1.105	–	0.905	100	–	$\Delta i_f, \Delta u_{C1}$

does not have any considerable influence on the dynamical behavior of the system.

It is interesting to focus on the local mode (pair 1,2) which is the dominant one, as it was observed in figure 8.3. From the time-domain behavior, it is possible to validate the properties of this eigenmode. Figure 8.4 presents the behavior of the active power after the first disturbance.

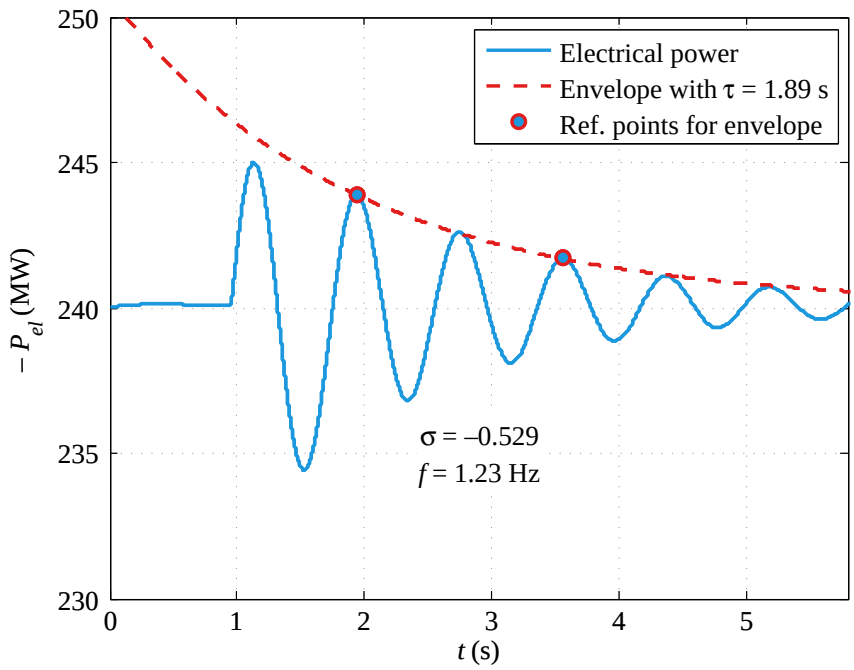

Figure 8.4: Frequency and attenuation time constant from time-domain results, without PSS.

It is possible to graphically extract from it the oscillating frequency f, the attenuation σ and the damping time constant τ. The good match with the eigenvalues result permits to affirm that a very good agreement exists between measurements, time-domain and small-signal models.

It is also relevant to validate the electrical model including the power system stabilizer. In order to perform the same type of validation as in the case without PSS, field data is used from a test of the same nature, including also the stabilizer with reduced gain.

Figure 8.5 presents measurement and time-domain simulation results for this case. Once again, the very good agreement that can be observed in this comparison validates the model with the PSS. The action of the local mode oscillations remains considerable due to the low setting of the PSS gain in this case.

As in the previous case, the calculation of the eigenvalues of the system containing the PSS is performed considering the same operating point of measurements: $u = 0.987$ p.u., $p_{el} = -0.85$ p.u., $q = -0.07$ p.u.

The exhaustive list of eigenvalues is presented in table 8.4. Indications of dominant states identified as "PSS" means that internal variables of the PSS are dominant. The specific variable u_{PSS} corresponds to the output of the stabilizer. For more information on the meaning of the state variables, please refer to chapter 5, sections 5.3, 5.5 and 5.8.

For a detailed discussion on the nature of these eigenvalues, please refer to chapter 5. Nonetheless, it is important to observe that the zero eigenvalue presented in table 8.4 (eigenvalue number 29) only happens due to the fact that one of the wash-out blocks of the PSS is not taken into account in the real system, and has to be artificially eliminated in the mathematical model.

At this point, it is interesting to focus on the local mode, since it is the dominant one also in this case. From the time-domain behavior, it is possible to validate the properties of the local mode, given by the pair 1,2 of table 8.4.

The active power behavior after the first disturbance is presented in figure 8.6. The fact that the first peak does not respect the exponential decay indicates that the first period of the transient is also influenced by another eigenmode, which is rapidly damped.

Nonetheless, once this influence is damped, the global transient behavior is satisfactorily described by the oscillating frequency f, the attenuation σ and the damping time constant τ extracted from this graph. Moreover, they present a good agreement with the eigenvalues result.

Therefore, the electrical model including the PSS also gives a good representation of the real system.

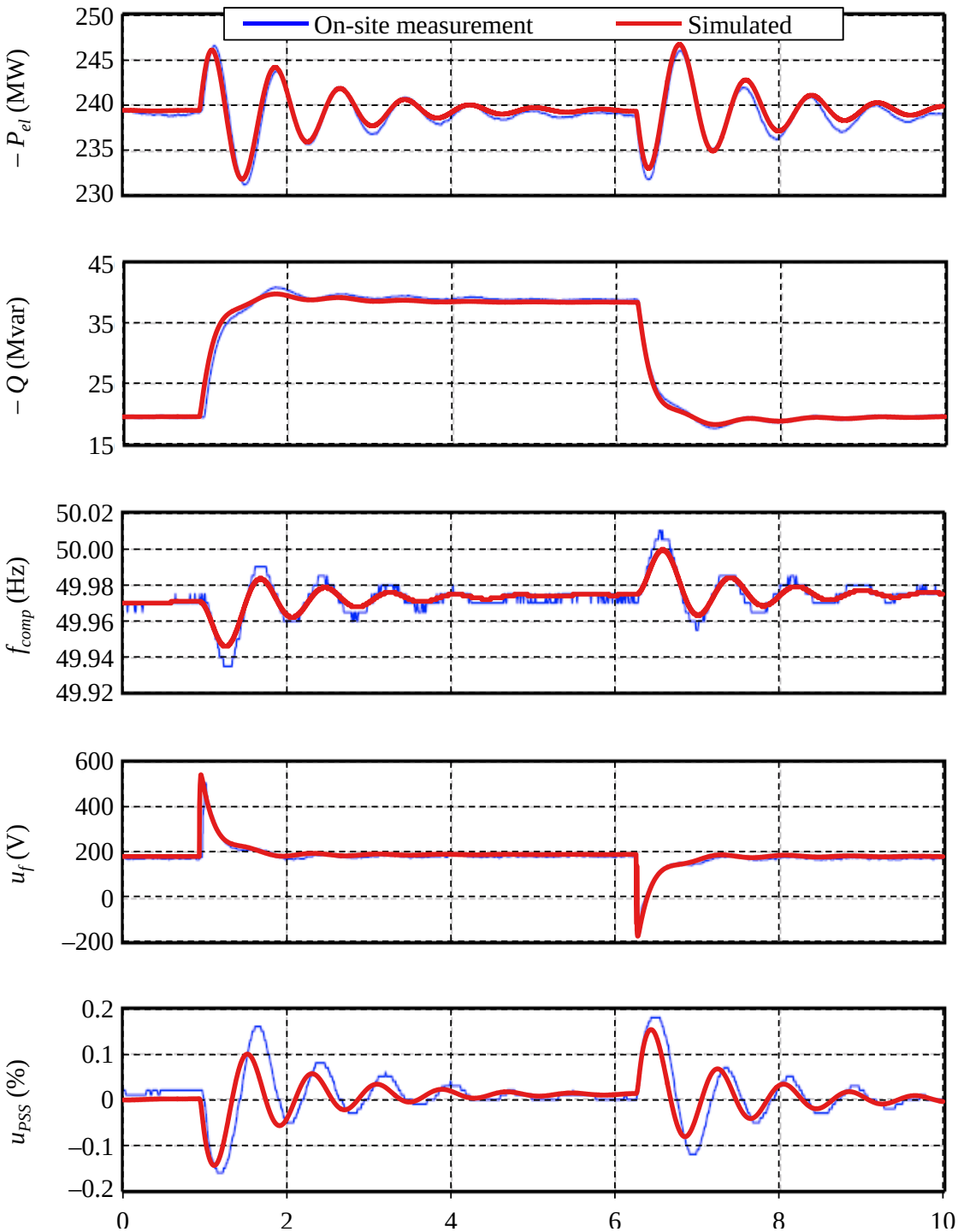

Figure 8.5: On-site measurement versus time-domain simulation, PSS with reduced gain.

Table 8.4: Eigenproperties of the system with a single machine, PSS with reduced gain.

Eigenvalue number i	$\sigma = \Re(\lambda_i)$ (Np/s)	$\omega_d = \Im(\lambda_i)$ (rad/s)	τ (s)	ζ (%)	f (Hz)	Dominant states
1,2	−0.896	7.955	1.116	11.2	1.266	$\Delta\omega_m, \Delta\theta, \Delta i_{abc2}, \Delta i_f$
3,4	−9.112	0.078	0.110	100	0.012	PSS
5,6	−8.146	1.776	0.123	97.7	0.283	$\Delta\omega_m, \Delta\theta$, PSS
7,8	−11.74	3.245	0.085	96.4	0.516	$\Delta i_f \Delta i_D, \Delta\omega_m, \Delta\theta$
9,10	−49.14	10.09	0.020	97.9	1.606	$\Delta i_f \Delta i_D, u_{PSS}$, PSS
11,12	−23.02	313.95	0.043	7.31	49.98	Δi_{abc2}
13,14	−0.003	314.16	$333.\overline{3}$	0.001	50.0	$\Delta i_{abc1,abc2}$
15	−10000	–	10^{-4}	100	–	PSS
16	−10000	–	10^{-4}	100	–	PSS
17	−10000	–	10^{-4}	100	–	PSS
18	−225.8	–	0.004	100	–	$\Delta u_g, \Delta u_{reg}, \Delta i_f$
19	−169.1	–	0.006	100	–	$\Delta u_g, \Delta u_{reg}, \Delta i_f$
20	−92.34	–	0.011	100	–	Δi_Δ
21	−40.00	–	0.025	100	–	Δu_{C2}
22	−13.75	–	0.073	100	–	$\Delta\omega_m, \Delta i_D, \Delta i_f$, PSS
23	−3.231	–	0.310	100	–	Δi_Q
24	−1.119	–	0.894	100	–	PSS
25	−0.104	–	9.615	100	–	PSS
26	−0.100	–	10.0	100	–	PSS
27	−0.100	–	10.0	100	–	PSS
28	−0.097	–	10.31	100	–	PSS
29	0	–	–	–	–	PSS

8.4 Eigenanalysis of the Electrical System at Part Load Condition

In order to perform an analysis focused on the understanding of the interactions between the vortex rope phenomenon and the electrical system, the four units are considered in the operating point corresponding to the conditions of the measurement presented in figure 8.2. This means an under-excited, part load condition with: $u = 0.97$ p.u., $p_{el} = -0.426$ p.u. and $q = +0.345$ p.u.

Although such an operating point may sound implausible most of the time, it should not be disconsidered. The high flexibility of hydropower plants creates the possibility for them to be requested to run under many different operating conditions. In some cases, it might be more advantageous to divide the demand of power among all the machines rather than

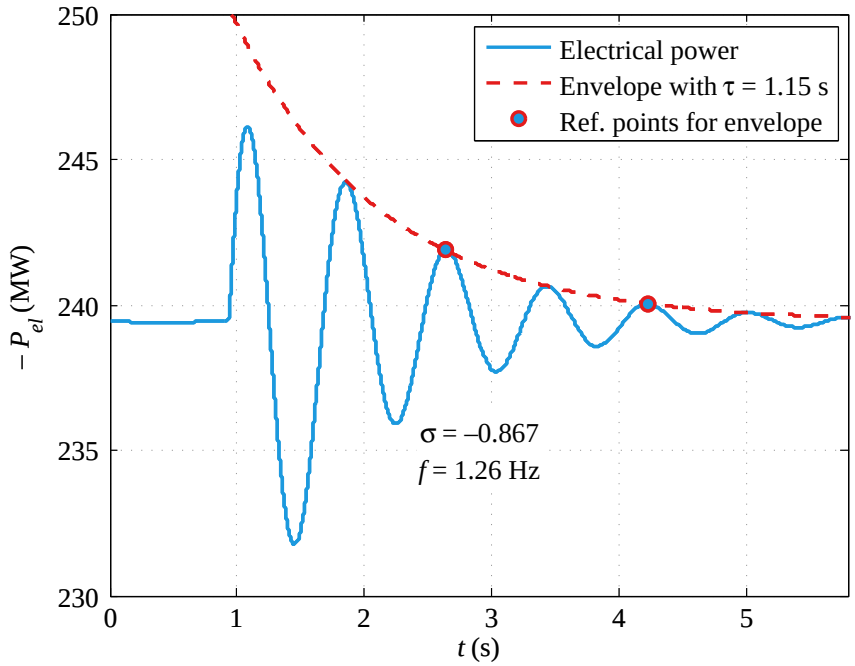

Figure 8.6: Frequency and attenuation time constant from time-domain results, with PSS.

concentrating it all in some of them, while desynchronizing others.

The eigenanalysis performed here aims at revealing the electro-mechanical modes of the system, since they are those likely to interact with vortex rope pulsations. Consequently, only the results regarding electro-mechanical modes are presented in this section.

The number of generating units connected to the power grid is considered a variable parameter, which is gradually increased in such a way that the eigenvalues are calculated for four different configurations with one up to four generating units on operation. The calculations are performed for the cases without and with PSS (with gain implemented on site).

Considering the case with only one generating unit synchronized to the grid, the results of the eigensolution of the system are given in table 8.5. It can be seen that even without PSS the system has a rather good damping ratio (approximately 15%). Nonetheless, the activation of the stabilizer increases the attenuation while shifting down the damped frequency, as it should be expected.

Additionally, the PSS introduces a new control mode whose frequency is close to the local mode one. It is, however, very well damped with a damping ratio over 80%. Consequently, it is less relevant for the dynamic behavior of the system than the local mode. This is the case for all the control modes introduced by the PSS in the case studied in this section. They all have damping ratios higher than 80% and are therefore not discussed here.

Table 8.5: Local mode of one generating unit, with and without PSS.

Nature of the eigenmode	without PSS			with PSS		
	λ	ζ (%)	f (Hz)	λ	ζ (%)	f (Hz)
Local	$-1.06 \pm j7.00$	15.0	1.114	$-3.35 \pm j5.46$	52.3	0.869

Table 8.6: Electro-mechanical modes for two generating units, with and without PSS.

Nature of the eigenmode	without PSS			with PSS		
	λ	ζ (%)	f (Hz)	λ	ζ (%)	f (Hz)
Local	$-0.71 \pm j6.17$	11.4	0.982	$-2.33 \pm j5.17$	41.1	0.823
Intermachine	$-1.88 \pm j8.34$	22.0	1.327	$-7.28 \pm j8.53$	64.9	1.358

The results for the case with two generating units connected to the grid are presented in table 8.6. For this case, the local mode is less damped and its frequency is also changed. As explained previously, this mode represents the oscillations of the whole power plant against the grid. This means that the rotors of all machines oscillate with the same frequency and same phase. Therefore, from the point of view of the network, these oscillations can be seen as the oscillations of one equivalent machine, with larger power and inertia. As the ratio between the power of this "equivalent machine" and the short-circuit power of the network increases, the damping ratio of the local mode decreases. Furthermore, the value of the frequency of the local mode reduces, since the equivalent inertia increases.

A new electro-mechanical eigenmode appears in the system. It corresponds to an intermachine mode. The oscillations related to this mode happen mainly inside the power plant, with one machine swinging against the other. This can be verified with a graphical representation of the mode shapes. It is important to notice that the PSS considerably increases the damping of this mode, while slightly shifting its frequency.

Figure 8.7 gives the representation of the shapes of local and intermachine modes on the rotational speed of both generators. The size of the arrows is normalized to the biggest one in the representation, while their positions indicate the phase of the modes. Figure 8.7a reveals clearly that the local mode has the same phase on both machines (G1 and G2), whereas figure 8.7b shows the phase opposition of the intermachine mode.

Table 8.7 presents the result of the electro-mechanical modes for the case with three machines connected to the grid. The increase of the total power of the plant leads to a decrease of damping ratio and frequency of the local mode. On the other hand, the intermachine mode identified in the case with two machines does not undergo significant changes. However, a new intermachine mode appears which has very similar eigenproperties to the first one.

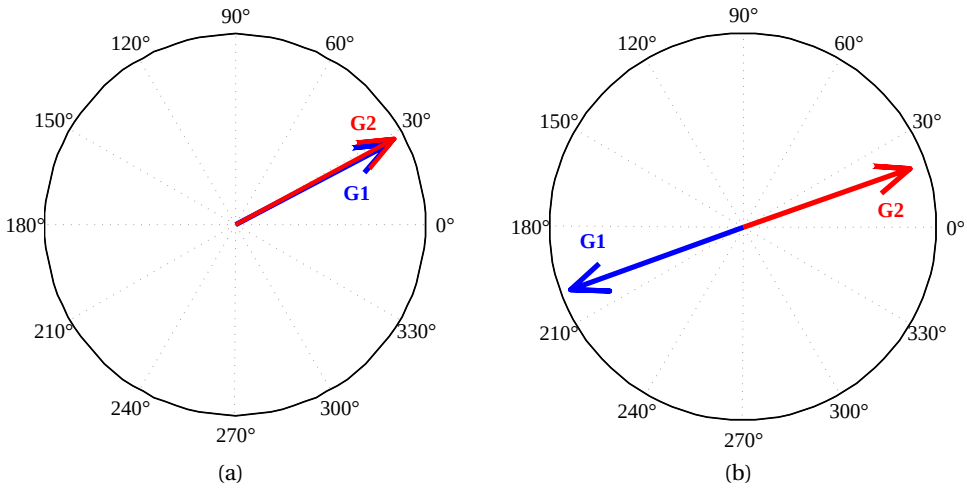

Figure 8.7: Mode shapes of the local mode (a) and the intermachine mode (b), with two generating units.

Table 8.7: Electro-mechanical modes for three generating units, with and without PSS.

Nature of the eigenmode	without PSS			with PSS		
	λ	ζ (%)	f (Hz)	λ	ζ (%)	f (Hz)
Local	$-0.52 \pm j5.66$	9.15	0.901	$-1.85 \pm j4.87$	35.5	0.775
Intermachine 1	$-1.88 \pm j8.36$	21.9	1.330	$-7.29 \pm j8.48$	65.2	1.350
Intermachine 2	$-1.87 \pm j8.27$	22.0	1.316	$-7.27 \pm j8.54$	64.8	1.359

Nevertheless, they do not act in the same manner.

Figure 8.8 presents the shapes of the local and intermachine modes. Figure 8.8a depicts the in-phase characteristic of the local mode. Figure 8.8b shows that the first intermachine mode corresponds to oscillations of the first unit (G1) against the other two (G2 and G3). On the other hand, figure 8.8c reveals that the second intermachine mode is related to oscillations of units two and three in phase opposition.

Finally, the results of the eigenvalue calculation for the electro-mechanical modes after the introduction of the fourth unit are given in table 8.8. Once again, the local mode undergoes a reduction of both damping ratio and frequency, as it should be expected.

The intermachine modes, on the other hand, do not suffer any considerable modification with the introduction of another generator. Nevertheless, a new mode of the same nature appears. Now, all three intermachine modes are equal in value. Nevertheless, each one of them acts differently.

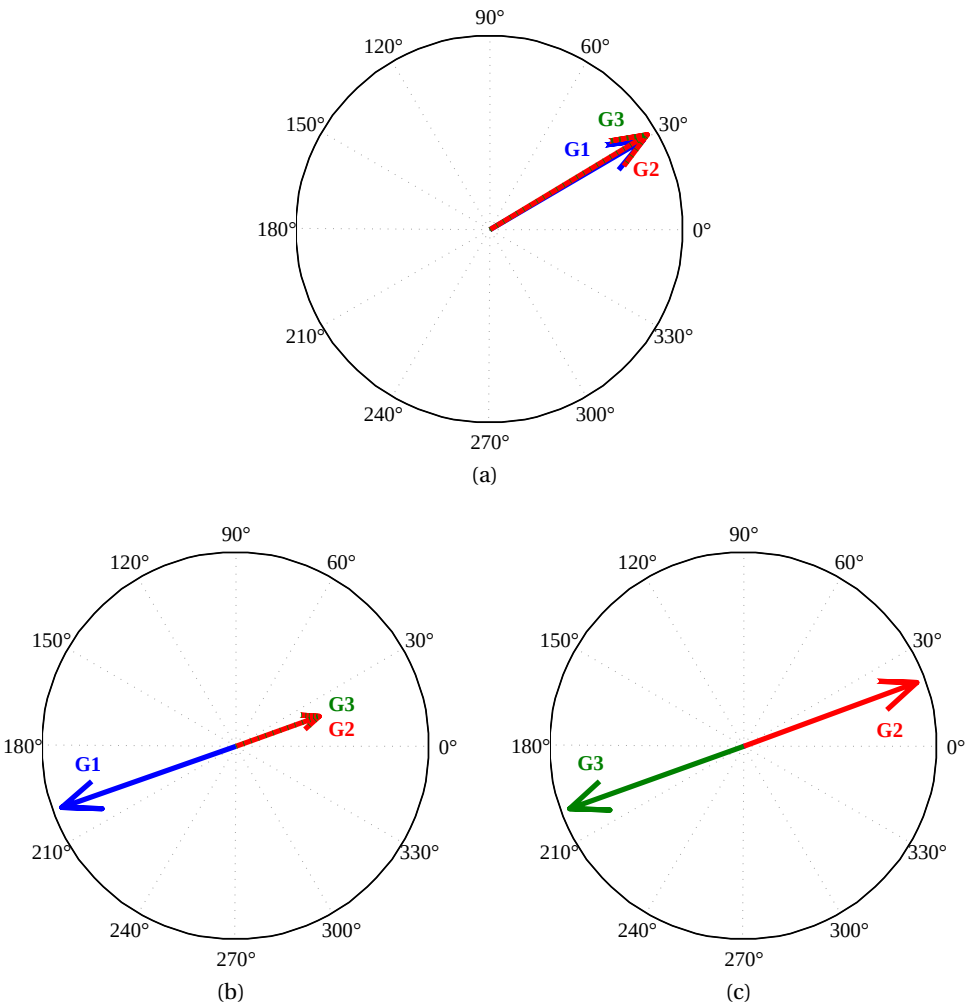

Figure 8.8: Mode shapes of the local mode (a), the first intermachine mode (b) and the second intermachine mode (c), with three generating units.

Figure 8.9 presents the shapes of the local and the intermachine modes for the case with four generating units. Figure 8.9a illustrates once again the in-phase characteristic of the local mode for all four generators. Figure 8.9b shows that the first intermachine mode corresponds

Table 8.8: Electro-mechanical modes for four generating units, with and without PSS.

Nature of the eigenmode	without PSS			with PSS		
	λ	ζ (%)	f (Hz)	λ	ζ (%)	f (Hz)
Local	$-0.41 \pm j5.35$	7.64	0.851	$-1.57 \pm j4.67$	31.9	0.743
Intermachine 1	$-1.88 \pm j8.41$	21.8	1.338	$-7.26 \pm j8.57$	64.6	1.364
Intermachine 2	$-1.88 \pm j8.41$	21.8	1.338	$-7.26 \pm j8.57$	64.6	1.364
Intermachine 3	$-1.88 \pm j8.41$	21.8	1.338	$-7.26 \pm j8.57$	64.6	1.364

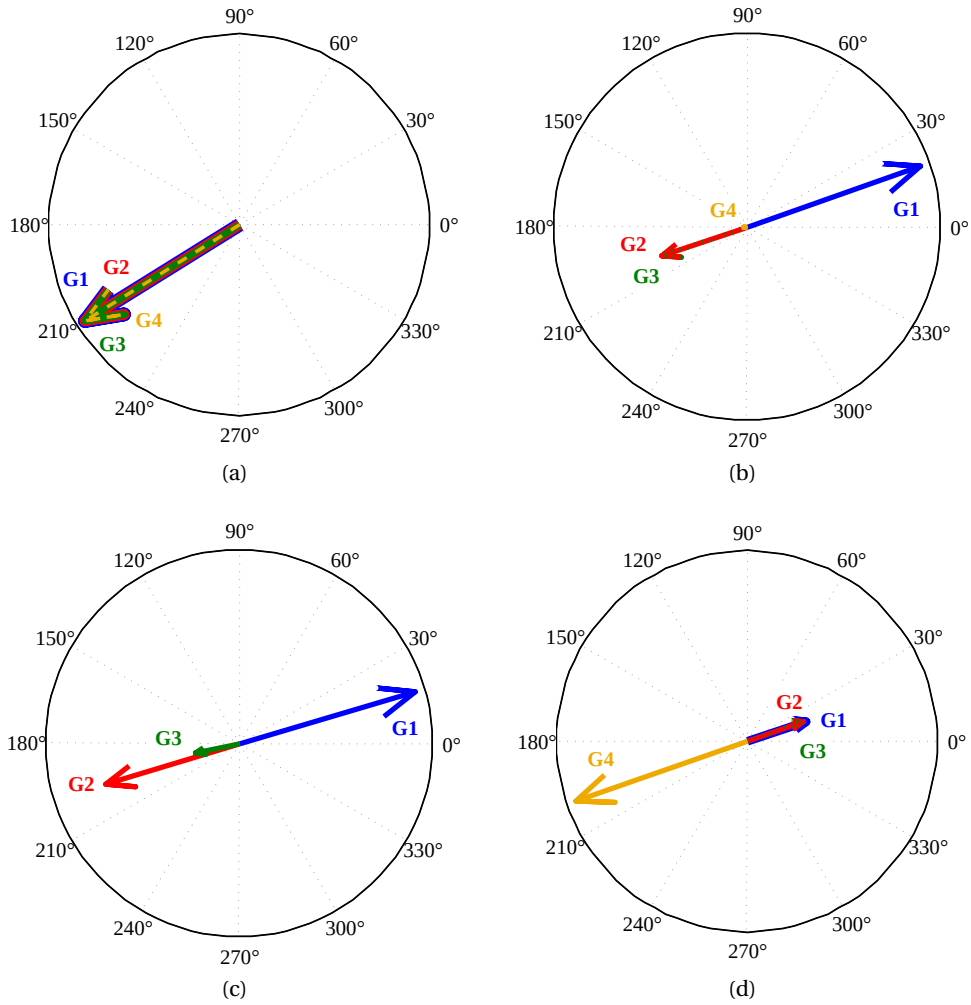

Figure 8.9: Mode shapes of the local mode (a), the first intermachine mode (b), the second intermachine mode (c) and the third intermachine mode (d), with four generating units.

to oscillations of the generator one (G1) against the other three generators (G2, G3 and G4 – the participation of generator four is very weak). The second intermachine mode is related to oscillations of generator one against mostly generator two and, in a less extent, generator three (see figure 8.9c). Finally, the third and last intermachine mode (represented in figure 8.9d) is involved in oscillations of the generator four against the other three generators.

In all four cases, the effect of the PSS is very clear. Besides considerably increasing the damping ratio of the local mode, the PSS contributes even more to the damping of the intermachine modes. Moreover, whereas the local mode frequency is shifted by the PSS, the changes caused by the PSS in the frequency of the intermachine modes are very small.

It is interesting to observe that the frequency of the intermachine modes, with or without PSS,

is close to the frequency estimated to the pulsation identified by the on-site measurements, presented in figure 8.2. This means that some interactions are likely to occur between the electrical and the hydraulic system around this value of frequency (~ 1.34 Hz).

Figure 8.10 illustrates the evolution of the local mode on the complex plane (with and without PSS) with the number of generators connected to the network. The arrows in this figure indicate an increasing number of generating units synchronized to the grid. Moreover, two slopes are given (for $\zeta = 5\%$ and $\zeta = 15\%$) as reference values of damping ratio. The reduction of the damping ratio with the growth of total generated power (more generators synchronized to the grid) is clear.

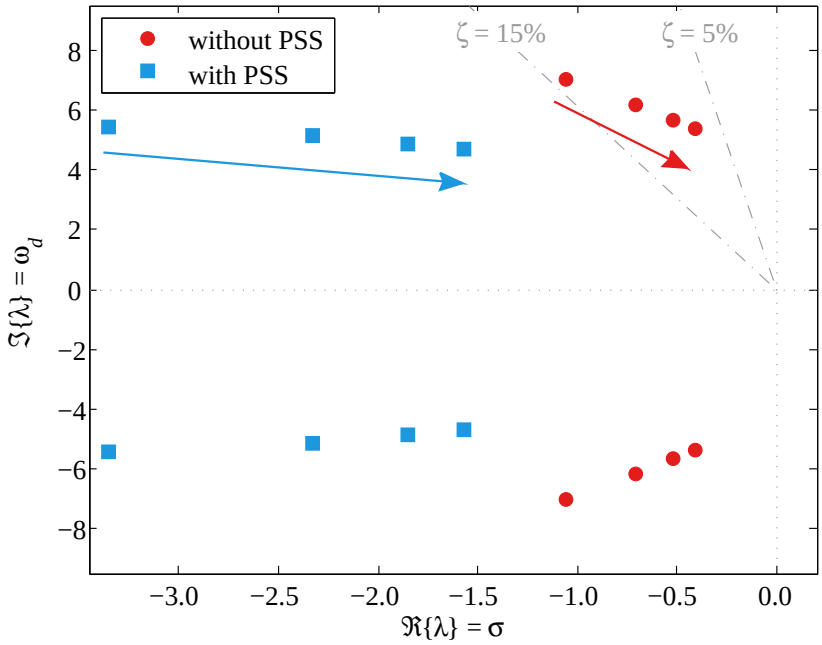

Figure 8.10: Evolution of local mode with the number of generating units.

8.5 Eigenanalysis of the Hydraulic System at Part Load Condition

Following the study of the electrical subsystem, the analysis of the hydraulic one is an important step to identify the eigenmodes that are most likely to interact with the generators and the power grid. Therefore, the eigenanalysis performed in this section takes into account the hydraulic subsystem as described in section 8.2.2, also including the inertia of the generator rotor (given in table 8.1). The operating point considered here is the part load condition used in the previous section ($P_{turb} = 120$ MW).

A reduced list of eigenvalues of the hydraulic system is presented in table 8.9. Given the high

Table 8.9: Most relevant eigenvalues of the hydraulic system.

Nature of the eigenmode	λ	ζ (%)	f (Hz)
Mass flow oscillation mode	$-0.002 \pm j0.052$	3.84	0.008
Gallery 1st elastic mode	$-0.02 \pm j2.40$	0.83	0.382
Penstock 1st elastic mode	$-1.02 \pm j2.16$	42.7	0.344
Penstock 2nd elastic mode	$-0.68 \pm j4.41$	15.2	0.702
Draft tube 1st elastic common mode	$-0.02 \pm j3.50$	0.57	0.557
Draft tube 1st elastic intermach. modes	$-0.07 \pm j3.50$	2.00	0.557
Draft tube 2nd elastic common mode	$-0.005 \pm j8.38$	0.06	1.333
Draft tube 2nd elastic intermach. modes	$-0.01 \pm j8.39$	0.12	1.335

order of the system due to the spatial discretization of the piping system, the extensive list of eigenvalues is not given here. Only the most relevant modes are presented. On the other hand, the spatial discretization of the piping system allows for the representation of the hydraulic mode shapes also in a spatial form. Such representation permits to observe how the influence of each mode is distributed along the elements of the hydraulic installation.

The mass flow oscillation mode corresponds to interactions between the upstream reservoir and the surge tank [71]. The pressure mode shape for this eigenmode is presented in figure 8.11a. The gallery 1st elastic mode is mostly related to the characteristics of the piping of the gallery and its mode shape is represented figure 8.11b. The mode shapes of the 1st and 2nd elastic eigenmodes of the penstock are represented in figures 8.12a and 8.12b, respectively. For detailed information on the characteristics and behavior of these eigemodes, please refer to reference [70].

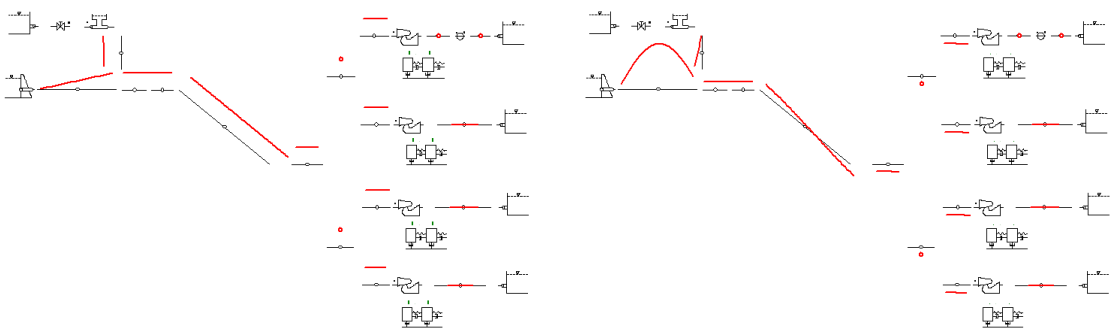

(a) (b)

Figure 8.11: Mass flow oscillation (a) and gallery 1st elastic (b) pressure mode shapes.

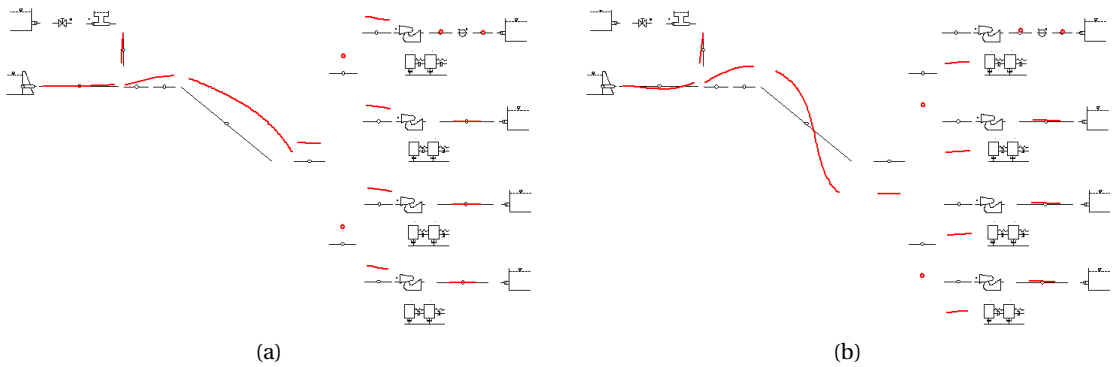

(a) (b)

Figure 8.12: Pressure mode shapes of the penstock 1st (a) and 2nd (b) elastic modes.

The two draft tube elastic eigenmodes are also relevant. The mode shapes for the 1st and 2nd elastic modes of the draft tube are depicted in figures 8.13 and 8.14, respectively. The eigenvalues related to both the 1st and 2nd modes appear four times in the results. For each of them, in one occurrence the eigenvalue has a weaker damping ratio. These less damped modes have the same phases in all four generating units. Oscillations due to such modes add up and their influences go upstream through the penstock, surge tank and gallery. This is the case of the eigenmode shapes represented in figures 8.13a and 8.14a for the 1st and 2nd draft tube elastic modes, respectively. Due to their common nature for all four units of the system, these modes are called here draft tube 1st and 2nd elastic *common* modes.

Conversely, the other three occurrences of each of the two draft tube elastic modes have a distinct characteristic. They indicate intermachine oscillations, since their actions in the four machines happen in phase opposition. Therefore, the superposed contributions of the four machines cancel each other in the penstock. Consequently, they do not have an upstream influence. This can be seen in the representation of the eigenmode shapes given in

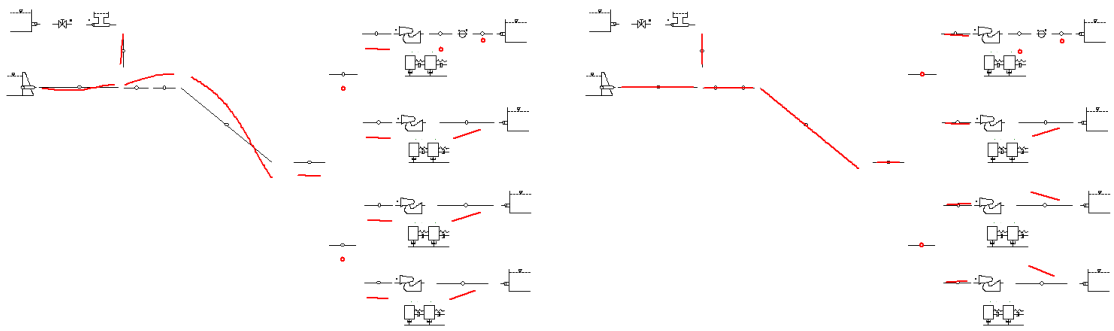

(a) (b)

Figure 8.13: Pressure mode shapes of the draft tube 1st elastic common (a) and intermachine (b) modes.

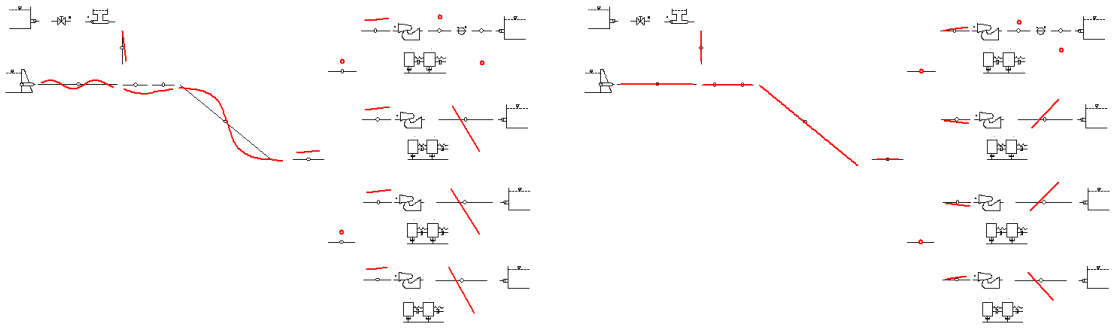

(a) (b)

Figure 8.14: Pressure mode shapes of the draft tube 2nd elastic common (a) and intermachine (b) modes.

figures 8.13b and 8.14b for the 1st and 2nd draft tube elastic modes, respectively. Taking into account the phase opposition of these oscillations, these modes are called here draft tube 1st and 2nd elastic *intermachine* modes.

The influence of these two modes on the whole hydraulic system can be confirmed through a forced response analysis, which is performed using the linearized matrices of the model. Figure 8.15 depicts the forced response of the hydraulic system to an excitation source located in the draft tube of generating unit 1. The pressures of the penstock, turbine 1 inlet and turbine 1 draft tube are represented, together with the rotational speed of the mechanical masses representing the turbine and the generator of unit 1.

Even though the frequency response of the penstock pressure shows the presence of several resonance frequencies (the elastic modes of the penstock), it is easy to observe that for all the hydraulic quantities represented in figure 8.15, the strongest resonances happen at the frequencies of the draft tube elastic modes. Furthermore, the influence of these resonance frequencies is not restricted to the hydraulic system, since they also happen in the rotational speeds. Therefore, oscillations at such frequencies are likely to spread to the electrical system through the mechanical torque behavior.

Finally, it is important to stress that the frequency of the 2nd draft tube elastic mode lies in the range of 0.2 to 0.4 times the rotational frequency of the turbine in which vortex rope pulsations are likely to occur ($1.\overline{1}$ to $2.\overline{2}$ Hz, since $f_{turb} = n_N/60 = 5.\overline{5}$ Hz). Therefore, a risk of resonance exists. Moreover, the frequency of this eigenmode corresponds to the frequency of the power fluctuations recorded on-site, which are depicted in figure 8.2. Furthermore, it is very close to the frequency of the electrical intermachine eigenmodes presented in the previous section. This indicates that significant interactions may happen between hydraulic, mechanical and electrical subsystem at least around this frequency value.

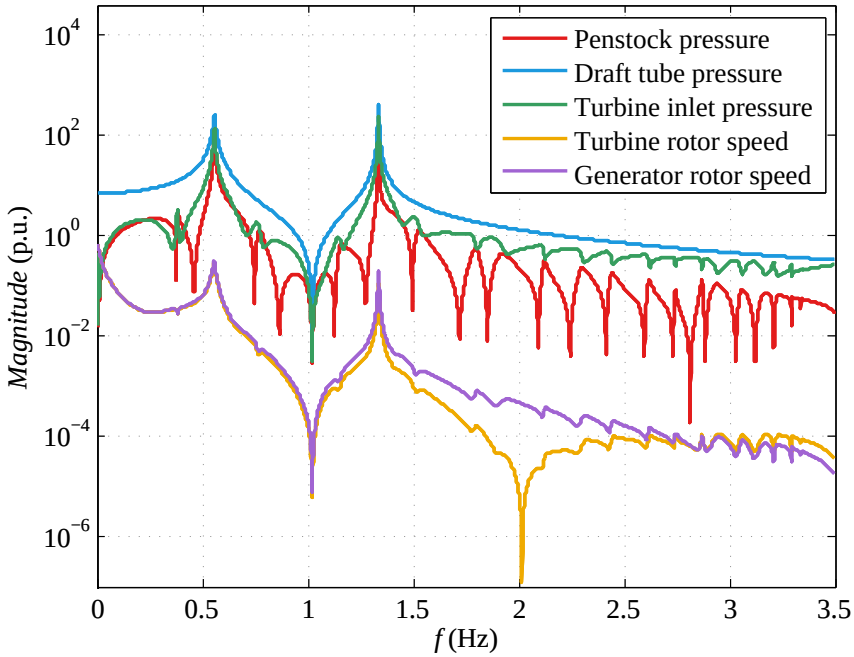

Figure 8.15: Forced response of the hydraulic system.

8.6 Hydroelectric System Eigenanalysis at Part Load Condition

The composition of the complete hydroelectric model is obtained by combining the electrical and hydraulic models studied in the previous sections. The interface between these two systems lies in the mechanical coupling between turbine and generator inertias, through coupling shaft. Consequently, interactions between hydraulic and electrical subsystems are related to interactions between the mechanical and the electromagnetic torques. Moreover, because of the high value of inertia of the generator, the mechanical system behaves as a low-pass filter [71, 95]. Therefore, interactions between the hydraulic and electrical elements are expected to happen at a low frequency range.

The calculation of eigenvalues is performed for the system both without and with PSS. In the first case, the order of the complete system is 433, whereas in the latter the order is 493. Thus, the extensive list of eigenvalues is not given here. The reduced list containing the most relevant eigenvalues for this case is presented in table 8.10. The letters that identify the nature of the eigenmodes are specified in the legend below the table.

By comparing these results with those obtained for the purely electrical and hydraulic systems (see tables 8.8 and 8.9, respectively), it is possible to see that the influence of one system over the other does not affect all the relevant eigemodes.

The mass flow oscillation (A) and the gallery elastic (B) eigenmodes are not subjected to any

Table 8.10: Most relevant eigenvalues of the hydroelectric system, with and without PSS.

Nature of the eigenmode	without PSS			with PSS		
	λ	ζ (%)	f (Hz)	λ	ζ (%)	f (Hz)
A	$-0.002 \pm j0.052$	3.84	0.008	$-0.002 \pm j0.052$	3.84	0.008
B	$-0.02 \pm j2.40$	0.83	0.382	$-0.02 \pm j2.40$	0.83	0.382
C	$-0.98 \pm j2.09$	42.5	0.333	$-0.97 \pm j2.10$	41.9	0.334
D	$-0.63 \pm j4.39$	14.2	0.699	$-0.66 \pm j4.33$	15.1	0.689
E	$-0.02 \pm j3.50$	0.57	0.557	$-0.02 \pm j3.50$	0.57	0.557
F	$-0.07 \pm j3.50$	2.00	0.557	$-0.07 \pm j3.50$	2.00	0.557
G	$-0.005 \pm j8.38$	0.06	1.333	$-0.005 \pm j8.38$	0.06	1.333
H	$-0.01 \pm j8.39$	0.12	1.335	$-0.01 \pm j8.39$	0.12	1.335
I	$-0.43 \pm j5.44$	7.88	0.866	$-1.59 \pm j4.83$	31.3	0.769
J	$-1.92 \pm j8.53$	22.0	1.358	$-7.20 \pm j8.34$	65.3	1.327
K	$-0.20 \pm j47.9$	0.42	7.624	$-0.22 \pm j47.9$	0.46	7.624
L	$-0.07 \pm j47.5$	0.15	7.560	$-0.07 \pm j47.5$	0.15	7.560

Legend (nature of the eigenmode):

A Mass flow oscillation eigenmode
B Gallery 1st elastic eigenmode
C Penstock 1st elastic eigenmode
D Penstock 2nd elastic eigenmode
E Draft tube 1st elastic common eigenmode
F Draft tube 1st elastic intermachine eigenmodes 1, 2 and 3
G Draft tube 2nd elastic common eigenmode
H Draft tube 2nd elastic intermachine eigenmodes 1, 2 and 3
I Electro-mechanical local eigenmode
J Electro-mechanical intermachine eigenmodes 1, 2 and 3
K Torsional eigenmodes
L High-order penstock elastic eigenmode with strong interaction with torsional modes

modification. The elastic eigenmodes of the penstock (C and D), on the other hand, undergo slight changes. Both damping ratio and frequency of the 1st penstock mode are decreased. The modification is more significant in terms of frequency, whereas the reduction of the damping ratio is weak. For the 2nd penstock mode, the frequency is slightly decreased, whereas the

damping ratio only drops if the PSS is deactivated. The eigenmodes of the draft tubes of the four turbines (E, F, G and H) are not modified by the introduction of the electrical system.

Considering the electro-mechanical eigenmodes (I and J), the influence of the introduction of the model of the hydraulic system has distinct effects if the electrical system is either without or with PSS. For the local mode (I), in the absence of PSS both frequency and damping ratio are subjected to a minor increase. If the PSS is activated, the inclusion of the hydraulic model shows that the damping ratio is slightly weaker (yet high) than the value obtained with the purely electrical model, whereas the frequency shift is weak. Considering the intermachine eigenmodes (J), the frequency is increased for the system without PSS, whereas it suffers a light decrease for the system with PSS. In both cases, the damping ratio has a very subtle increase.

It is interesting to observe that the representation of the rotors of turbines and generators by independent mechanical masses introduces torsional eigenmodes (K) in the system, which are related to oscillations of the turbine rotor against the generator rotor. These modes have a strong interaction with a high-order mode from the penstock (L) which lies in the same frequency range.

Reference [71] demonstrated that a stiff network introduces a stabilization effect in the low frequency range (especially below 1 Hz). In the present case, however, the power grid is not stiff (it has a limited short-circuit power). Therefore, the effect of the electrical network over the low-frequency modes is either weak or even imperceptible in some cases. Moreover, it does not contribute to enhance the damping ratio of the draft tube eigenmodes. Consequently, hydraulic resonances due to part load vortex rope precession in the draft tube are likely to affect also the electrical system through torque oscillations.

Indeed, the 2nd draft tube mode has a frequency (1.333 Hz) very close to the electro-mechanical intermachine mode (1.327 Hz in the case with PSS). This mode is very well damped (ζ = 65.3%) but if resonances in the draft tube are amplified by turbine head fluctuations, and consequently, by mechanical torque oscillations, the electromagnetic torque will also pulsate, resulting in significant electrical power swing. The high damping ratio of the intermachine eigenmode is nevertheless important to limit the amplitude of these oscillations.

It is convenient to perform also time-domain simulations in order to confirm that the interactions predicted by the eigenvalues results are indeed a risk to the power plant. To this end, time-domain simulations are performed with a pressure excitation source placed in the draft tube of generating unit 1. The pressure source has a frequency equal to 1.33 Hz and amplitude equal to 2% (4% peak-to-peak) of the rated turbine head (H_N).

Figure 8.16 shows that such pressure fluctuations, which could be caused by vortex rope

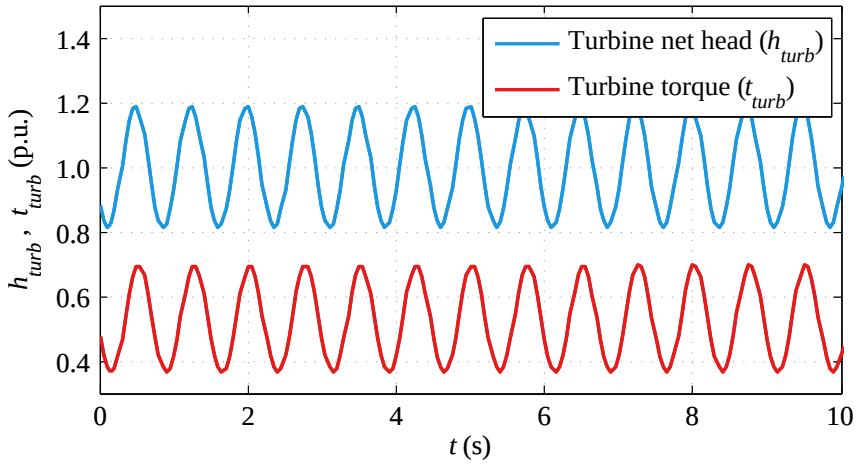

Figure 8.16: Turbine net head and torque response to vortex rope pulsation of 2% H_N.

precession in the draft tube, lead to turbine head peak-to-peak oscillations equal to 38% of the nominal head, and to mechanical torque peak-to-peak oscillations equal to 34% of the rated torque of the turbine.

These torque fluctuations are reflected in the electrical system as power swings of high amplitude. Figure 8.17 illustrates the oscillatory behavior for the cases without and with PSS. If the PSS is out of service, electrical power fluctuations reach 62% of the rated power of the generator (peak-to-peak value). When the PSS is active, the peak-to-peak value drops to 31%. This reduction is due to the fact that the interactions around 1.33 Hz are better damped by the high damping ratio of the intermachine mode. Nonetheless, such a level of power swing is not acceptable and can be very detrimental not only to the power plant, but also to the local network.

Therefore, it is clear that vortex rope precession must be avoided in order to spare the instal-

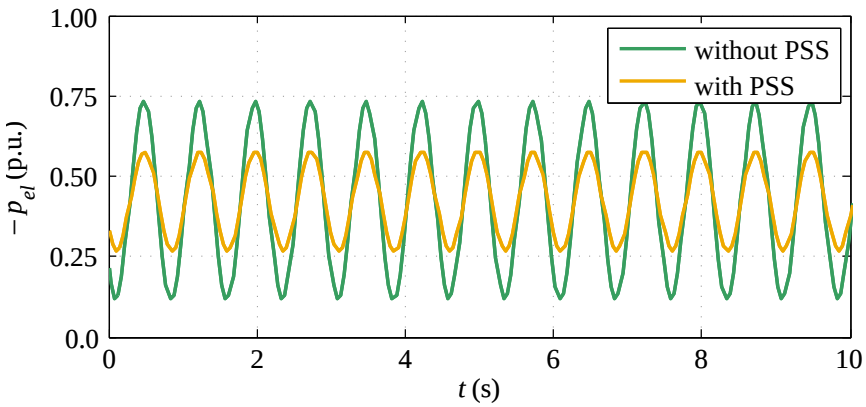

Figure 8.17: Electrical power swing due to vortex rope pulsation of 2% H_N.

lation serious consequences that could result from this resonant behavior. Avoiding vortex rope precession can be achieved through measures such as compressed air injection in the draft tube or installation of fins [40]. Compressed air injection modifies the wave speed in the draft tube, which results in changing the characteristics of the draft tube eigenmodes [27]. Fins installed in the cone of the turbine outlet introduce changes of geometry that shift the precession frequency of the vortex rope. Another possibility is to tune the PSS parameters or to condition the PSS power input signal with a filtered draft tube pressure signal in order to avoid the disturbances [9].

Finally, it is interesting to calibrate the amplitude of the excitation source in order to reproduce the power fluctuations measured on-site, presented in figure 8.2. Investigations revealed that the measured 1.1% peak-to-peak electrical power swing can be caused by a very weak excitation on the draft tube. For the system with the PSS, the amplitude of the excitation was equal to 0.021% (0.042% peak-to-peak) of the rated turbine head (H_N).

Figure 8.18 presents the electrical power fluctuations caused by such an excitation source. The unit 1 (where the excitation is placed) oscillates with a peak-to-peak amplitude equal to 1.11% of the rated power of the generator. The other three units have a peak-to-peak oscillation equal to 0.4%. Moreover, they oscillate in phase opposition with respect to unit 1 (intermachine mode 1, illustrated in figure 8.9b).

Such a low value of excitation indicates that very few energy is necessary to cause electrical power swings in this hydropower plant. This means that the broadband excitation spectrum in the draft tube is sufficient to cause undesired behavior with considerable power fluctuation under part load operating condition.

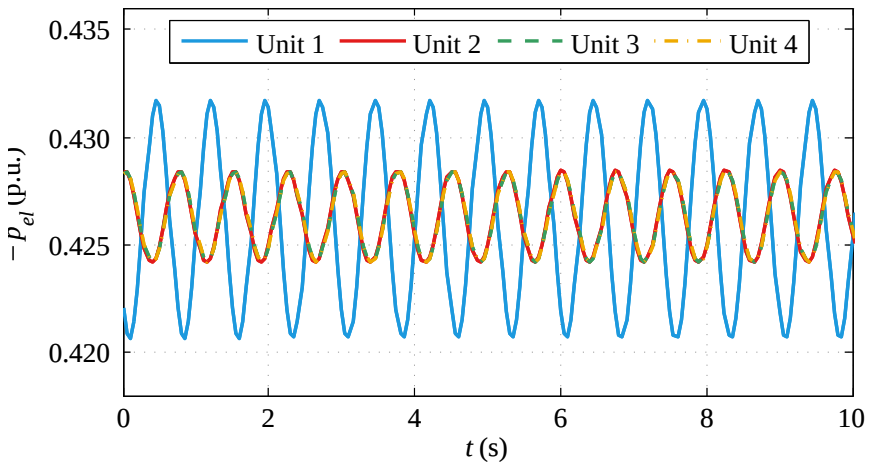

Figure 8.18: Electrical power swing due to vortex rope pulsation of 0.021% H_N.

8.7 Concluding Remarks

This case study permitted to apply the small-signal models developed in the present work in the study of a real situation, likely to occur in several existing hydropower plants. Due to its flexibility, such power plants may be required to repeatedly operate under part load condition and must keep stability during this mode of operation.

First, the validation of the electrical system was performed through comparison between on-site measurements, time-domain simulations and eigenvalue calculations. Then, eigen-analyses of the electrical system at part load were performed in order to identify the electro-mechanical modes likely to interact with vortex rope pulsations in the draft tube. These analyses also showed the evolution of the local mode as a function of the number of generating units synchronized to the grid. Additionally, the intermachine eigenmodes were identified and representations of the mode shapes showed that each intermachine mode has a distinct action over the generators, even though their damping ratios and frequencies were equal.

Subsequently, the hydraulic system was studied. The main eigenmodes were presented and their mode shapes were illustrated. The 2nd draft tube elastic eigenmode was identified as a possible source of problem, since its frequency is in the range of both draft tube vortex rope precession and electro-mechanical eigenmodes. Thus, resonant interactions are likely to occur.

Finally, the complete hydroelectric system was also studied through eigenanalysis. It was verified that only slight modifications happen to eigenmodes of both hydraulic and electrical nature. Therefore, the complete system confirmed that the 2nd draft tube mode and the intermachine mode were very close and likely to interact. Time-domain simulations were then performed to confirm such interaction and demonstrated that pulsations originated in the draft tube are largely amplified and result in high power swings, which have harmful consequences to the power plant and to the local grid. Moreover, very low excitation values corresponding to the broadband oscillation spectrum were found to be sufficient to cause the electrical power fluctuations measured on-site.

Therefore, vortex rope precession must absolutely be avoided at this hydropower plant in order to avoid damages and malfunctioning both in the power plant and in the local grid. Solutions such as compressed air injection in the draft tube or installation of fins in the cone of the turbine outlet can be helpful to avoid or to change the characteristics of vortex load precession, thus reducing pressure fluctuations in the draft tube during part load operation.

Part IV

Conclusions

9 Summary, Conclusions and Perspectives

9.1 Summary

As mentioned in chapter 1, section 1.4.1, the main purpose of the present work was to develop a new tool for small-signal stability analysis of electrical systems to be implemented in SIMSEN, so that it would be possible not only to build comprehensive small-signal electrical models, but also to combine them with hydraulic ones.

For this purpose, and in order to take advantage of the main assets of SIMSEN, it was necessary to respect the modeling principles already existing in this software. This means electrical models based on *a,b,c*-phase variables which differ from classical models, based on Park's representation (*d,q,o*-axis).

As stated in chapter 1, section 1.3.2, and chapter 3, section 3.1, small-signal stability analysis of a system is based on the calculation of its eigenvalues and eigenvectors. For linear time-invariant (LTI) systems, the characteristics of eigenvalues inform if it is stable around a given equilibrium point or not. On the other hand, if the system is time-variant (non-LTI), eigenanalysis techniques cannot be directly applied.

Electrical machines models based on *a,b,c*-phase variables are time-variant systems. Thus, it would not be coherent to straightforwardly linearize the time-domain models existing in SIMSEN, in order to extract their eigenvalues for small-signal stability analysis purposes. Therefore, a new methodology was developed for the derivation of small-signal models from non-LTI time-domain models. This new methodology, presented in chapter 4, section 4.3, guarantees a coherent linearization of the models (by applying the analytical linearization method), whilst preserving compatibility with the modeling principles of SIMSEN. This means

that by using this methodology, it is possible to obtain small-signal models of electrical elements based on *a,b,c*-phase variables, which are fully compatible with both eigenanalysis techniques and the SIMSEN environment.

All small-signal electrical models obtained through the proposed methodology were applied in test cases presented in chapter 5. These test cases allowed for the validation of the models, since all the results were confirmed either analytically or through comparison with time-domain simulations. Both frequency and damping ratio of the calculated eigenvalues were demonstrated to be coherent.

In chapter 6, the modeling principles of hydraulic elements were explained. Time-domain models for pipes, Francis turbine, surge tank and turbine governor were presented. Then, peculiarities related to the linearization of hydraulic models for the derivation of small-signal models were described.

Subsequently, electrical and hydraulic small-signal models were applied in two case studies, with comprehensive modeling of hydropower plants. In both cases, all the hydraulic, mechanical, electrical and regulation elements were taken into account, so that complete small-signal models were used in order to assess all possible interactions between these subsystems.

The first case study, presented in chapter 7, analyzed the dynamic behavior of an islanded hydropower plant. The contribution of power system stabilizers to damp unstable electro-mechanical eigenmodes was demonstrated. Also, it was shown that in the case of an islanded power plant, the frequency control loop of the turbine governor is also capable of enhancing the stability of the electro-mechanical eigenmodes. Nonetheless, this case study also permitted to reveal adverse interactions that are likely to occur between the turbine governor and the PSS. These interactions, which depend strongly on the tuning of each regulator, had the tendency to drastically destabilize eigenmodes related to the hydraulic installation. Even though these effects are somewhat known and have been observed in practical cases, the use of a complete multi-physics model allowed for the predictive assessment of such risk, whilst giving a clear indication of its origin and possible solution. Therefore, a comprehensive model is important in order to allow a judicious tuning of all regulators, avoiding undesirable on-site problems.

The second case study, presented in chapter 8, focused on the small-signal stability of an existing 1000 MW hydropower plant (4×250 MW generating units) during part load operation. Due to their flexibility, hydropower plants may be frequently required to operate under such condition, which is likely to cause the occurrence of vortex load on the draft tube of the turbine. The complete hydroelectric model used in this case study showed that pressure fluctuations due to vortex rope pulsation may coincide with draft tube modes and also with electro-mechanical modes, leading to considerable power swings on the electrical system. Therefore, it was possible to conclude that vortex rope pulsation must absolutely be avoided

at this hydropower plant, in order to prevent damages and malfunctioning both of the power plant and of the local grid.

9.2 Conclusions

As highlighted in chapter 1, the power sector is in constant evolution. Considering the installation of new power plants and the constant need to study more flexible modes of operation, it is clear that reliable, robust and user-friendly tools are necessary to assess the dynamic behavior of power plants and grid.

Moreover, based on the conclusions withdrawn from the case studies of chapters 7 and 8, presented in sections 7.6 and 8.7 respectively, it is clear that multi-physics models are necessary in order to assess the real small-signal behavior of the global system.

The tool developed in the present work meets these needs. By taking advantage of the assets of SIMSEN, it is a reliable and robust tool, with a user-friendly graphical interface (GUI). By incorporating electrical, mechanical, hydraulic and regulation elements, it is capable of providing comprehensive, precise, multi-physics models of hydroelectric systems.

9.3 Contributions of the Present Work

Applications of small-signal stability analysis techniques on multi-physics systems, such as those presented in chapter 2, section 2.2, are most commonly developed for specific cases or on very particular purposes. Consequently, the extension of these applications to systems with any different topological structure requires time-consuming efforts, in order to establish the new set of differential equations of the new system.

Moreover, the computational tools presented in chapter 2, section 2.3, are dedicated to large-scale power systems. Small-signal models for several electrical elements are available, especially those related to transmission networks, as well as generators and loads. On the other hand, no special attention is paid to the nature of the energy sources. For example, turbines are often represented by constant torques, which do not correspond to the reality. Furthermore, these electrical models are based on Park's representation.

Therefore, one of the contributions of the present work is the new procedure applied to derive small-signal models for electrical elements, presented in chapter 4. The models derived by applying this method are based on *a,b,c*-phase variables, which is a novel approach in small-signal stability analysis. The innovative aspect of this procedure is related to a new inverse transformation, which was defined based on the inverse Park's transformation. This new transformation is the only one capable of converting the linearized models to *a,b,c*-

phase coordinates, whilst correctly taking into account all the supplementary terms due to linearization and keeping the modular structure of the system. Furthermore, by doing so the resulting models were compatible with SIMSEN, and after their implementation it was possible to take profit of the modular characteristic of this software.

Furthermore, once the small-signal electrical models developed in the scope of the present work were combined with the hydraulic ones already existing in SIMSEN, complete and detailed modeling of hydroelectric systems, taking into account electrical and hydraulic subsystems including their control elements was made possible. This means that this is a truly multi-physics small-signal analysis tool. This is an important contribution, in the sense that interactions between hydraulic, mechanical, electrical and regulation elements can be correctly identified, allowing for preventing resonance problems that cannot be detected if turbines are modeled by a constant torque.

The examples presented in chapters 7 and 8 demonstrated that such a detailed modeling allows for the identification not only of the instabilities or adverse interactions, but also of the sources of any undesired phenomena. Once such phenomena and their causes are clearly detected, adequate solutions can be proposed either to a better exploitation of existing installations, or to satisfactory adjustments of projects of new installations.

Additionally, another contribution of this work is a new graphical interface, which was developed in MATLAB in order to treat the calculation and representation of participation factors. It was applied in all validations and test cases presented in this work. This interface gives the possibility for a new didactic and intuitive form of representation of participation factors based on color maps, which facilitates the identification of interactions between subsystems, characterized by their corresponding state variables. An example of this representation was given in chapter 7, figure 7.7.

Finally, with the implementation of the small-signal electrical models, it was possible to take advantage of the main features of SIMSEN in such a way that a novel small-signal stability tool was obtained. It comprises small-signal models of all elements necessary to build a detailed representation of power plants and grids (see figure 1.6). The major advantages of this tool are three of the strongest assets of SIMSEN, namely:

- Treatment of systems with any given topology – *a modular tool*;
- Simple construction of topologies in an user-friendly GUI, through graphical connection and parametrization of all elements – *easy association and configuration of building blocks*;
- Automatic generation of the full set of differential equations of the global system – *rapidly and safely performed*.

In other words, this means that topological changes in the structure of the system do not require much effort from the user. Through a graphical modification (in the GUI) of connections and elements to be changed, the new problem can be solved without any need for the user to adapt the matrices or equations describing the system. This fastidious, burdensome task is automatically treated in SIMSEN. This is a considerable advantage over the models presented in the publications discussed in chapter 2, section 2.2.

9.4 Perspectives

9.4.1 Other Standard Types of Regulators

Considering the large number of standard models for voltage regulators and power system stabilizers proposed by IEEE [38], one interesting perspective is the inclusion of some new models in the small-signal stability tool.

Nowadays, advanced versions of SIMSEN also include models ST4B and ST8C for voltage regulators, and PSS4B for power system stabilizer. Together with the ST1A and PSS2B, these are well-known models used worldwide, which could make the small-signal stability tool even more complete.

The derivation of the small-signal model follows the same principles as for the ST1A and PSS2B, and the linearized expressions for the inputs were already developed.

9.4.2 Parametric Studies through Eigenvalue Sensitivity

High-order models comprising different control and regulation structures may depict several sources of interactions that have to be avoided, as shown in chapters 7 and 8. The tuning of regulators play a major role in this context. It may have either a positive or a negative influence in the dynamic behavior of the system. Consequently, the parameters set of regulators need to be carefully determined.

A convenient and effective tool for the tuning of regulators is the calculation of eigenvalue sensitivity. This concept was presented in chapter 3, section 3.3.4. It corresponds to the rate of change of a given eigenvalue with respect to a specific parameter of the system. Therefore, eigenvalue sensitivity can give valuable information on how parameters of regulators should be adjusted, in order to obtain a better dynamic performance of the global system.

9.4.3 Extension to other Renewable Energy Systems

Considering the growing penetration of new renewable energy sources (other than hydro) in the power generation mix, and bearing in mind their intermittent characteristic, it can also be interesting to develop multi-physics small-signal models for wind, tidal and solar PV power plants.

For this purpose, small-signal models of wind and tidal turbines, photovoltaic panels, pseudo-continuous power converters and permanent magnet synchronous machines need to be developed. Such accomplishment shall yield an even more comprehensive small-signal tool. With such a fully modular, multi-physics, mixed-sources tool, it shall be possible to perform advanced analyses, with very high level of modeling.

Part V

Appendices

A

Small-Signal Models Based on *a,b,c*-Phase Coordinates

The equations describing all small-signal models based on *a,b,c*-phase variables coordinates, derived during the present work, are presented in this appendix. These models were developed according to the procedure presented in chapter 4, section 4.3 and validated all along chapter 5. The actual values of parameters are used instead of *per-unit* values.

The elements whose models are given here are:

- Salient-pole synchronous machine;
- Wound-rotor induction machine;
- Power transformers (vector groups *Yy0*, *Yd5* and *Yd11*);
- RL and RLC loads;
- RL and π-section models of transmission lines;
- Voltage regulators (IEEE ST1A and Unitrol®);
- Power system stabilizer IEEE PSS2B.

A.1 Salient-Pole Synchronous Machine

A.1.1 Stator Equations

$$\begin{aligned}\Delta u_a = {} & \alpha_{11}\frac{d\Delta i_a}{dt} + \alpha_{12}\frac{d\Delta i_b}{dt} + \alpha_{13}\frac{d\Delta i_c}{dt} + \alpha_{14}\frac{d\Delta i_f}{dt} + \alpha_{15}\frac{d\Delta i_D}{dt} + \alpha_{16}\frac{d\Delta i_Q}{dt} \\ & + \beta_{11}\Delta i_a + \beta_{12}\Delta i_b + \beta_{13}\Delta i_c + \beta_{14}\Delta i_f + \beta_{15}\Delta i_D + \beta_{16}\Delta i_Q + \beta_{17}\Delta\omega_m + \beta_{18}\Delta\theta\end{aligned} \tag{A.1}$$

Where

$$\alpha_{11} = \frac{2}{3}\left[L_d \cos^2\theta_0 + L_q \sin^2\theta_0\right] + \frac{L_o}{3}$$

$$\alpha_{12} = \frac{2}{3}\left[L_d \cos\theta_0 \cos\left(\theta_0 - \frac{2\pi}{3}\right) + L_q \sin\theta_0 \sin\left(\theta_0 - \frac{2\pi}{3}\right)\right] + \frac{L_o}{3}$$

$$\alpha_{13} = \frac{2}{3}\left[L_d \cos\theta_0 \cos\left(\theta_0 + \frac{2\pi}{3}\right) + L_q \sin\theta_0 \sin\left(\theta_0 + \frac{2\pi}{3}\right)\right] + \frac{L_o}{3}$$

$$\alpha_{14} = L_{fa} \cos\theta_0$$

$$\alpha_{15} = L_{Da} \cos\theta_0$$

$$\alpha_{16} = -L_{Qa} \sin\theta_0$$

$$\beta_{11} = R_s - \frac{\omega_{m0}}{3}\left(L_d - L_q\right)\sin(2\theta_0)$$

$$\beta_{12} = -\frac{\omega_{m0}}{3}\left[\left(L_d - L_q\right)\sin\left(2\theta_0 - \frac{2\pi}{3}\right) + \frac{\sqrt{3}}{2}\left(L_d + L_q\right)\right]$$

$$\beta_{13} = -\frac{\omega_{m0}}{3}\left[\left(L_d - L_q\right)\sin\left(2\theta_0 + \frac{2\pi}{3}\right) - \frac{\sqrt{3}}{2}\left(L_d + L_q\right)\right]$$

$$\beta_{14} = -\omega_{m0} L_{fa} \sin\theta_0$$

$$\beta_{15} = -\omega_{m0} L_{Da} \sin\theta_0$$

$$\beta_{16} = -\omega_{m0} L_{Qa} \cos\theta_0$$

$$\beta_{17} = -\left\{\frac{2}{3}\left(L_d - L_q\right)\left[i_{a0}\sin(2\theta_0) + i_{b0}\sin\left(2\theta_0 - \frac{2\pi}{3}\right) + i_{c0}\sin\left(2\theta_0 + \frac{2\pi}{3}\right)\right] + L_{fa}\, i_{f0} \sin\theta_0\right\}$$

$$\beta_{18} = -\omega_{m0}\left\{\frac{2}{3}\left(L_d - L_q\right)\left[i_{a0}\cos(2\theta_0) + i_{b0}\cos\left(2\theta_0 - \frac{2\pi}{3}\right) + i_{c0}\cos\left(2\theta_0 + \frac{2\pi}{3}\right)\right] + L_{fa}\, i_{f0} \cos\theta_0\right\}$$

$$\begin{aligned}\Delta u_b = \alpha_{21}\frac{d\Delta i_a}{dt} + \alpha_{22}\frac{d\Delta i_b}{dt} + \alpha_{23}\frac{d\Delta i_c}{dt} + \alpha_{24}\frac{d\Delta i_f}{dt} + \alpha_{25}\frac{d\Delta i_D}{dt} + \alpha_{26}\frac{d\Delta i_Q}{dt} \\ + \beta_{21}\Delta i_a + \beta_{22}\Delta i_b + \beta_{23}\Delta i_c + \beta_{24}\Delta i_f + \beta_{25}\Delta i_D + \beta_{26}\Delta i_Q + \beta_{27}\Delta\omega_m + \beta_{28}\Delta\theta\end{aligned} \tag{A.2}$$

Where

$$\alpha_{21} = \frac{2}{3}\left[L_d\cos\left(\theta_0 - \frac{2\pi}{3}\right)\cos\theta_0 + L_q\sin\left(\theta_0 - \frac{2\pi}{3}\right)\sin\theta_0\right] + \frac{L_o}{3}$$

$$\alpha_{22} = \frac{2}{3}\left[L_d\cos^2\left(\theta_0 - \frac{2\pi}{3}\right) + L_q\sin^2\left(\theta_0 - \frac{2\pi}{3}\right)\right] + \frac{L_o}{3}$$

$$\alpha_{23} = \frac{2}{3}\left[L_d\cos\left(\theta_0 - \frac{2\pi}{3}\right)\cos\left(\theta_0 + \frac{2\pi}{3}\right) + L_q\sin\left(\theta_0 - \frac{2\pi}{3}\right)\sin\left(\theta_0 + \frac{2\pi}{3}\right)\right] + \frac{L_o}{3}$$

$$\alpha_{24} = L_{fa}\cos\left(\theta_0 - \frac{2\pi}{3}\right)$$

$$\alpha_{25} = L_{Da}\cos\left(\theta_0 - \frac{2\pi}{3}\right)$$

$$\alpha_{26} = -L_{Qa}\sin\left(\theta_0 - \frac{2\pi}{3}\right)$$

$$\beta_{21} = -\frac{\omega_{m0}}{3}\left[\left(L_d - L_q\right)\sin\left(2\theta_0 - \frac{2\pi}{3}\right) - \frac{\sqrt{3}}{2}\left(L_d + L_q\right)\right]$$

$$\beta_{22} = R_s - \frac{\omega_{m0}}{3}\left(L_d - L_q\right)\sin\left(2\theta_0 + \frac{2\pi}{3}\right)$$

$$\beta_{23} = -\frac{\omega_{m0}}{3}\left[\left(L_d - L_q\right)\sin\left(2\theta_0\right) + \frac{\sqrt{3}}{2}\left(L_d + L_q\right)\right]$$

$$\beta_{24} = -\omega_{m0}L_{fa}\sin\left(\theta_0 - \frac{2\pi}{3}\right)$$

$$\beta_{25} = -\omega_{m0}L_{Da}\sin\left(\theta_0 - \frac{2\pi}{3}\right)$$

$$\beta_{26} = -\omega_{m0}L_{Qa}\cos\left(\theta_0 - \frac{2\pi}{3}\right)$$

$$\begin{aligned}\beta_{27} = -\Bigg\{\frac{2}{3}\left(L_d - L_q\right)\left[i_{a0}\sin\left(2\theta_0 - \frac{2\pi}{3}\right) + i_{b0}\sin\left(2\theta_0 + \frac{2\pi}{3}\right) + i_{c0}\sin\left(2\theta_0\right)\right] \\ + L_{fa}\,i_{f0}\sin\left(\theta_0 - \frac{2\pi}{3}\right)\Bigg\}\end{aligned}$$

$$\begin{aligned}\beta_{28} = -\omega_{m0}\Bigg\{\frac{2}{3}\left(L_d - L_q\right)\left[i_{a0}\cos\left(2\theta_0 - \frac{2\pi}{3}\right) + i_{b0}\cos\left(2\theta_0 + \frac{2\pi}{3}\right) + i_{c0}\cos\left(2\theta_0\right)\right] \\ + L_{fa}\,i_{f0}\cos\left(\theta_0 - \frac{2\pi}{3}\right)\Bigg\}\end{aligned}$$

$$\begin{aligned}\Delta u_c = {} & \alpha_{31}\frac{d\Delta i_a}{dt} + \alpha_{32}\frac{d\Delta i_b}{dt} + \alpha_{33}\frac{d\Delta i_c}{dt} + \alpha_{34}\frac{d\Delta i_f}{dt} + \alpha_{35}\frac{d\Delta i_D}{dt} + \alpha_{36}\frac{d\Delta i_Q}{dt} \\ & + \beta_{31}\Delta i_a + \beta_{32}\Delta i_b + \beta_{33}\Delta i_c + \beta_{34}\Delta i_f + \beta_{35}\Delta i_D + \beta_{36}\Delta i_Q + \beta_{37}\Delta\omega_m + \beta_{38}\Delta\theta\end{aligned} \tag{A.3}$$

Where

$$\alpha_{31} = \frac{2}{3}\left[L_d\cos\left(\theta_0+\frac{2\pi}{3}\right)\cos\theta_0 + L_q\sin\left(\theta_0+\frac{2\pi}{3}\right)\sin\theta_0\right] + \frac{L_o}{3}$$

$$\alpha_{32} = \frac{2}{3}\left[L_d\cos\left(\theta_0+\frac{2\pi}{3}\right)\cos\left(\theta_0-\frac{2\pi}{3}\right) + L_q\sin\left(\theta_0+\frac{2\pi}{3}\right)\sin\left(\theta_0-\frac{2\pi}{3}\right)\right] + \frac{L_o}{3}$$

$$\alpha_{33} = \frac{2}{3}\left[L_d\cos^2\left(\theta_0+\frac{2\pi}{3}\right) + L_q\sin^2\left(\theta_0+\frac{2\pi}{3}\right)\right] + \frac{L_o}{3}$$

$$\alpha_{34} = L_{fa}\cos\left(\theta_0+\frac{2\pi}{3}\right)$$

$$\alpha_{35} = L_{Da}\cos\left(\theta_0+\frac{2\pi}{3}\right)$$

$$\alpha_{36} = -L_{Qa}\sin\left(\theta_0+\frac{2\pi}{3}\right)$$

$$\beta_{31} = -\frac{\omega_{m0}}{3}\left[\left(L_d-L_q\right)\sin\left(2\theta_0+\frac{2\pi}{3}\right) + \frac{\sqrt{3}}{2}\left(L_d+L_q\right)\right]$$

$$\beta_{32} = -\frac{\omega_{m0}}{3}\left[\left(L_d-L_q\right)\sin\left(2\theta_0\right) - \frac{\sqrt{3}}{2}\left(L_d+L_q\right)\right]$$

$$\beta_{33} = R_s - \frac{\omega_{m0}}{3}\left(L_d-L_q\right)\sin\left(2\theta_0-\frac{2\pi}{3}\right)$$

$$\beta_{34} = -\omega_{m0}L_{fa}\sin\left(\theta_0+\frac{2\pi}{3}\right)$$

$$\beta_{35} = -\omega_{m0}L_{Da}\sin\left(\theta_0+\frac{2\pi}{3}\right)$$

$$\beta_{36} = -\omega_{m0}L_{Qa}\cos\left(\theta_0+\frac{2\pi}{3}\right)$$

$$\begin{aligned}\beta_{37} = -\Bigg\{ & \frac{2}{3}\left(L_d-L_q\right)\left[i_{a0}\sin\left(2\theta_0+\frac{2\pi}{3}\right) + i_{b0}\sin\left(2\theta_0\right) + i_{c0}\sin\left(2\theta_0-\frac{2\pi}{3}\right)\right] \\ & + L_{fa}\,i_{f0}\sin\left(\theta_0+\frac{2\pi}{3}\right)\Bigg\}\end{aligned}$$

$$\begin{aligned}\beta_{38} = -\omega_{m0}\Bigg\{ & \frac{2}{3}\left(L_d-L_q\right)\left[i_{a0}\cos\left(2\theta_0+\frac{2\pi}{3}\right) + i_{b0}\cos\left(2\theta_0\right) + i_{c0}\cos\left(2\theta_0-\frac{2\pi}{3}\right)\right] \\ & + L_{fa}\,i_{f0}\cos\left(\theta_0+\frac{2\pi}{3}\right)\Bigg\}\end{aligned}$$

A.1.2 Rotor Equations

$$\Delta u_f = \alpha_{41}\frac{d\Delta i_a}{dt} + \alpha_{42}\frac{d\Delta i_b}{dt} + \alpha_{43}\frac{d\Delta i_c}{dt} + \alpha_{44}\frac{d\Delta i_f}{dt} + \alpha_{45}\frac{d\Delta i_D}{dt} + \beta_{44}\Delta i_f + \beta_{47}\Delta\omega_m \tag{A.4}$$

Where

$$\alpha_{41} = L_{fa}\cos\theta_0$$

$$\alpha_{42} = L_{fa}\cos\left(\theta_0 - \frac{2\pi}{3}\right)$$

$$\alpha_{43} = L_{fa}\cos\left(\theta_0 + \frac{2\pi}{3}\right)$$

$$\alpha_{44} = L_f$$

$$\alpha_{45} = L_{Df}$$

$$\beta_{44} = R_f$$

$$\beta_{47} = -L_{fa}\left[i_{a0}\sin\theta_0 + i_{b0}\sin\left(\theta_0 - \frac{2\pi}{3}\right) + i_{c0}\sin\left(\theta_0 + \frac{2\pi}{3}\right)\right]$$

$$0 = \alpha_{51}\frac{d\Delta i_a}{dt} + \alpha_{52}\frac{d\Delta i_b}{dt} + \alpha_{53}\frac{d\Delta i_c}{dt} + \alpha_{54}\frac{d\Delta i_f}{dt} + \alpha_{55}\frac{d\Delta i_D}{dt} + \beta_{55}\Delta i_D + \beta_{57}\Delta\omega_m \tag{A.5}$$

Where

$$\alpha_{51} = L_{Da}\cos\theta_0$$

$$\alpha_{52} = L_{Da}\cos\left(\theta_0 - \frac{2\pi}{3}\right)$$

$$\alpha_{53} = L_{Da}\cos\left(\theta_0 + \frac{2\pi}{3}\right)$$

$$\alpha_{54} = L_{Df}$$

$$\alpha_{55} = L_D$$

$$\beta_{55} = R_D$$

$$\beta_{57} = -L_{Da}\left[i_{a0}\sin\theta_0 + i_{b0}\sin\left(\theta_0 - \frac{2\pi}{3}\right) + i_{c0}\sin\left(\theta_0 + \frac{2\pi}{3}\right)\right]$$

$$0 = \alpha_{61}\frac{d\Delta i_a}{dt} + \alpha_{62}\frac{d\Delta i_b}{dt} + \alpha_{63}\frac{d\Delta i_c}{dt} + \alpha_{66}\frac{d\Delta i_Q}{dt} + \beta_{66}\Delta i_Q + \beta_{67}\Delta\omega_m \tag{A.6}$$

Where

$$\alpha_{61} = -L_{Qa}\sin\theta_0$$

$$\alpha_{62} = -L_{Qa}\sin\left(\theta_0 - \frac{2\pi}{3}\right)$$

$$\alpha_{63} = -L_{Qa}\sin\left(\theta_0 + \frac{2\pi}{3}\right)$$

$$\alpha_{66} = L_Q$$

$$\beta_{66} = R_Q$$

$$\beta_{67} = -L_{Qa}\left[i_{a0}\cos\theta_0 + i_{b0}\cos\left(\theta_0 - \frac{2\pi}{3}\right) + i_{c0}\cos\left(\theta_0 + \frac{2\pi}{3}\right)\right]$$

A.1.3 Mechanical Equations

$$\frac{J}{P_p}\frac{d\Delta\omega_m}{dt} = \sum\Delta T = \Delta T_{em} + \sum\Delta T_{mec} \tag{A.7a}$$

With

$$\Delta T_{em} = \beta_{71}\Delta i_a + \beta_{72}\Delta i_b + \beta_{73}\Delta i_c + \beta_{74}\Delta i_f + \beta_{75}\Delta i_D + \beta_{76}\Delta i_Q + \beta_{78}\Delta\theta \tag{A.7b}$$

Where

$$\beta_{71} = -P_p\left\{\frac{2}{3}\left(L_d - L_q\right)\left[i_{a0}\sin(2\theta_0) + i_{b0}\sin\left(2\theta_0 - \frac{2\pi}{3}\right) + i_{c0}\sin\left(2\theta_0 + \frac{2\pi}{3}\right)\right] + L_{fa}\,i_{f0}\sin\theta_0\right\}$$

$$\beta_{72} = -P_p\left\{\frac{2}{3}\left(L_d - L_q\right)\left[i_{a0}\sin\left(2\theta_0 - \frac{2\pi}{3}\right) + i_{b0}\sin\left(2\theta_0 + \frac{2\pi}{3}\right) + i_{c0}\sin(2\theta_0)\right] + L_{fa}\,i_{f0}\sin\left(\theta_0 - \frac{2\pi}{3}\right)\right\}$$

$$\beta_{73} = -P_p\left\{\frac{2}{3}\left(L_d - L_q\right)\left[i_{a0}\sin\left(2\theta_0 + \frac{2\pi}{3}\right) + i_{b0}\sin(2\theta_0) + i_{c0}\sin\left(2\theta_0 - \frac{2\pi}{3}\right)\right] + L_{fa}\,i_{f0}\sin\left(\theta_0 + \frac{2\pi}{3}\right)\right\}$$

$$\beta_{74} = -P_p L_{fa}\left[i_{a0}\sin\theta_0 + i_{b0}\sin\left(\theta_0 - \frac{2\pi}{3}\right) + i_{c0}\sin\left(\theta_0 + \frac{2\pi}{3}\right)\right]$$

$$\beta_{75} = -P_p L_{Da}\left[i_{a0}\sin\theta_0 + i_{b0}\sin\left(\theta_0 - \frac{2\pi}{3}\right) + i_{c0}\sin\left(\theta_0 + \frac{2\pi}{3}\right)\right]$$

$$\beta_{76} = -P_p L_{Qa}\left[i_{a0}\cos\theta_0 + i_{b0}\cos\left(\theta_0 - \frac{2\pi}{3}\right) + i_{c0}\cos\left(\theta_0 + \frac{2\pi}{3}\right)\right]$$

$$\begin{aligned}\beta_{78} = -P_p \Bigg\{ &\frac{2}{3}\left(L_d - L_q\right)\Bigg[i_{a0}^2\cos^2(2\theta_0) + 2i_{a0}i_{b0}\cos\left(2\theta_0 - \frac{2\pi}{3}\right) \\ &+ 2i_{a0}i_{c0}\cos\left(2\theta_0 + \frac{2\pi}{3}\right) + i_{b0}^2\cos^2\left(2\theta_0 + \frac{2\pi}{3}\right) + 2i_{b0}i_{c0}\cos(2\theta_0) \\ &+ i_{c0}^2\cos^2\left(2\theta_0 - \frac{2\pi}{3}\right)\Bigg] \\ &+ \frac{3}{2}L_{fa}i_{f0}\left[i_{a0}\cos\theta_0 + i_{b0}\cos\left(\theta_0 - \frac{2\pi}{3}\right) + i_{c0}\cos\left(\theta_0 + \frac{2\pi}{3}\right)\right]\Bigg\}\end{aligned}$$

$$\frac{d\Delta\theta}{dt} = \Delta\omega_m \tag{A.8}$$

A.2 Wound-Rotor Induction Machine

A.2.1 Stator Equations

$$\begin{aligned}\Delta u_a = &\alpha_{11}\frac{d\Delta i_a}{dt} + \alpha_{12}\frac{d\Delta i_b}{dt} + \alpha_{13}\frac{d\Delta i_c}{dt} + \alpha_{14}\frac{d\Delta i_A}{dt} + \alpha_{15}\frac{d\Delta i_B}{dt} + \alpha_{16}\frac{d\Delta i_C}{dt} \\ &+ \beta_{11}\Delta i_a + \beta_{12}\Delta i_b + \beta_{13}\Delta i_c + \beta_{14}\Delta i_A + \beta_{15}\Delta i_B + \beta_{16}\Delta i_C + \beta_{17}\Delta\omega_m + \beta_{18}\Delta\theta_m\end{aligned} \tag{A.9}$$

Where

$$\alpha_{11} = \frac{2L_s + L_{os}}{3}$$

$$\alpha_{12} = \frac{-L_s + L_{os}}{3}$$

$$\alpha_{13} = \frac{-L_s + L_{os}}{3}$$

$$\alpha_{14} = \frac{2}{3}L_{sr}\cos\theta_{m0}$$

$$\alpha_{15} = \frac{2}{3}L_{sr}\cos\left(\theta_{m0} + \frac{2\pi}{3}\right)$$

$$\alpha_{16} = \frac{2}{3}L_{sr}\cos\left(\theta_{m0} - \frac{2\pi}{3}\right)$$

$$\beta_{11} = R_s$$

$$\beta_{12} = -\frac{\sqrt{3}}{3}\,\omega_{a0}\,L_s$$

$$\beta_{13} = \frac{\sqrt{3}}{3}\,\omega_{a0}\,L_s$$

$$\beta_{14} = -\frac{2}{3}\,\omega_{a0}\,L_{sr}\sin\theta_{m0}$$

$$\beta_{15} = -\frac{2}{3}\,\omega_{a0}\,L_{sr}\sin\left(\theta_{m0} + \frac{2\pi}{3}\right)$$

$$\beta_{16} = -\frac{2}{3}\,\omega_{a0}\,L_{sr}\sin\left(\theta_{m0} - \frac{2\pi}{3}\right)$$

$$\beta_{17} = -\frac{2}{3}\,L_{sr}\left[i_{A0}\sin\theta_{m0} + i_{B0}\sin\left(\theta_{m0} + \frac{2\pi}{3}\right) + i_{C0}\sin\left(\theta_{m0} - \frac{2\pi}{3}\right)\right]$$

$$\beta_{18} = -\frac{2}{3}\,\omega_{a0}\,L_{sr}\left[i_{A0}\cos\theta_{m0} + i_{B0}\cos\left(\theta_{m0} + \frac{2\pi}{3}\right) + i_{C0}\cos\left(\theta_{m0} - \frac{2\pi}{3}\right)\right]$$

$$\begin{aligned}\Delta u_b = {} & \alpha_{21}\frac{d\Delta i_a}{dt} + \alpha_{22}\frac{d\Delta i_b}{dt} + \alpha_{23}\frac{d\Delta i_c}{dt} + \alpha_{24}\frac{d\Delta i_A}{dt} + \alpha_{25}\frac{d\Delta i_B}{dt} + \alpha_{26}\frac{d\Delta i_C}{dt} \\ & + \beta_{21}\Delta i_a + \beta_{22}\Delta i_b + \beta_{23}\Delta i_c + \beta_{24}\Delta i_A + \beta_{25}\Delta i_B + \beta_{26}\Delta i_C + \beta_{27}\Delta\omega_m + \beta_{28}\Delta\theta_m\end{aligned} \tag{A.10}$$

Where

$$\alpha_{21} = \frac{-L_s + L_{os}}{3}$$

$$\alpha_{22} = \frac{2\,L_s + L_{os}}{3}$$

$$\alpha_{23} = \frac{-L_s + L_{os}}{3}$$

$$\alpha_{24} = \frac{2}{3}\,L_{sr}\cos\left(\theta_{m0} - \frac{2\pi}{3}\right)$$

$$\alpha_{25} = \frac{2}{3}\,L_{sr}\cos\theta_{m0}$$

$$\alpha_{26} = \frac{2}{3}\,L_{sr}\cos\left(\theta_{m0} + \frac{2\pi}{3}\right)$$

$$\beta_{21} = \frac{\sqrt{3}}{3}\,\omega_{a0}\,L_s$$

$$\beta_{22} = R_s$$

$$\beta_{23} = -\frac{\sqrt{3}}{3}\,\omega_{a0}\,L_s$$

$$\beta_{24} = -\frac{2}{3}\,\omega_{a0}\,L_{sr}\sin\left(\theta_{m0} - \frac{2\pi}{3}\right)$$

$$\beta_{25} = -\frac{2}{3}\,\omega_{a0}\,L_{sr}\sin\theta_{m0}$$

$$\beta_{26} = -\frac{2}{3}\,\omega_{a0}\,L_{sr}\sin\left(\theta_{m0} + \frac{2\pi}{3}\right)$$

$$\beta_{27} = -\frac{2}{3}\,L_{sr}\left[i_{A0}\sin\left(\theta_{m0} - \frac{2\pi}{3}\right) + i_{B0}\sin\theta_{m0} + i_{C0}\sin\left(\theta_{m0} + \frac{2\pi}{3}\right)\right]$$

$$\beta_{28} = -\frac{2}{3}\,\omega_{a0}\,L_{sr}\left[i_{A0}\cos\left(\theta_{m0} - \frac{2\pi}{3}\right) + i_{B0}\cos\theta_{m0} + i_{C0}\cos\left(\theta_{m0} + \frac{2\pi}{3}\right)\right]$$

$$\begin{aligned}\Delta u_c = {} & \alpha_{31}\frac{d\Delta i_a}{dt} + \alpha_{32}\frac{d\Delta i_b}{dt} + \alpha_{33}\frac{d\Delta i_c}{dt} + \alpha_{34}\frac{d\Delta i_A}{dt} + \alpha_{35}\frac{d\Delta i_B}{dt} + \alpha_{36}\frac{d\Delta i_C}{dt} \\ & + \beta_{31}\Delta i_a + \beta_{32}\Delta i_b + \beta_{33}\Delta i_c + \beta_{34}\Delta i_A + \beta_{35}\Delta i_B + \beta_{36}\Delta i_C + \beta_{37}\Delta\omega_m + \beta_{38}\Delta\theta_m\end{aligned} \tag{A.11}$$

Where

$$\alpha_{31} = \frac{-L_s + L_{os}}{3}$$

$$\alpha_{32} = \frac{-L_s + L_{os}}{3}$$

$$\alpha_{33} = \frac{2\,L_s + L_{os}}{3}$$

$$\alpha_{34} = \frac{2}{3}\,L_{sr}\cos\left(\theta_{m0} + \frac{2\pi}{3}\right)$$

$$\alpha_{35} = \frac{2}{3}\,L_{sr}\cos\left(\theta_{m0} - \frac{2\pi}{3}\right)$$

$$\alpha_{36} = \frac{2}{3}\,L_{sr}\cos\theta_{m0}$$

$$\beta_{31} = -\frac{\sqrt{3}}{3}\,\omega_{a0}\,L_s$$

$$\beta_{32} = \frac{\sqrt{3}}{3}\,\omega_{a0}\,L_s$$

$$\beta_{33} = R_s$$

$$\beta_{34} = -\frac{2}{3}\,\omega_{a0}\,L_{sr}\sin\left(\theta_{m0} + \frac{2\pi}{3}\right)$$

$$\beta_{35} = -\frac{2}{3}\,\omega_{a0}\,L_{sr}\sin\left(\theta_{m0} - \frac{2\pi}{3}\right)$$

$$\beta_{36} = -\frac{2}{3}\,\omega_{a0}\,L_{sr}\sin\theta_{m0}$$

$$\beta_{37} = -\frac{2}{3}\,L_{sr}\left[i_{A0}\sin\left(\theta_{m0} + \frac{2\pi}{3}\right) + i_{B0}\sin\left(\theta_{m0} - \frac{2\pi}{3}\right) + i_{C0}\sin\theta_{m0}\right]$$

$$\beta_{38} = -\frac{2}{3}\,\omega_{a0}\,L_{sr}\left[i_{A0}\cos\left(\theta_{m0} + \frac{2\pi}{3}\right) + i_{B0}\cos\left(\theta_{m0} - \frac{2\pi}{3}\right) + i_{C0}\cos\theta_{m0}\right]$$

A.2.2 Rotor Equations

$$\begin{aligned}\Delta u_A = {} & \alpha_{41}\frac{d\Delta i_a}{dt} + \alpha_{42}\frac{d\Delta i_b}{dt} + \alpha_{43}\frac{d\Delta i_c}{dt} + \alpha_{44}\frac{d\Delta i_A}{dt} + \alpha_{45}\frac{d\Delta i_B}{dt} + \alpha_{46}\frac{d\Delta i_C}{dt} \\ & + \beta_{41}\Delta i_a + \beta_{42}\Delta i_b + \beta_{43}\Delta i_c + \beta_{44}\Delta i_A + \beta_{45}\Delta i_B + \beta_{46}\Delta i_C + \beta_{47}\Delta\omega_m + \beta_{48}\Delta\theta_m\end{aligned} \tag{A.12}$$

Where

$$\alpha_{41} = \frac{2}{3}\,L_{sr}\cos\theta_{m0}$$

$$\alpha_{41} = \frac{2}{3}\,L_{sr}\cos\left(\theta_{m0} - \frac{2\pi}{3}\right)$$

$$\alpha_{43} = \frac{2}{3}\,L_{sr}\cos\left(\theta_{m0} + \frac{2\pi}{3}\right)$$

$$\alpha_{44} = \frac{2\,L_r + L_{or}}{3}$$

$$\alpha_{45} = \frac{-L_r + L_{or}}{3}$$

$$\alpha_{46} = \frac{-L_r + L_{or}}{3}$$

$$\beta_{41} = \frac{2}{3}\,(\omega_{a0} - \omega_{m0})\,L_{sr}\sin\theta_{m0}$$

$$\beta_{42} = \frac{2}{3}\,(\omega_{a0} - \omega_{m0})\,L_{sr}\sin\left(\theta_{m0} - \frac{2\pi}{3}\right)$$

$$\beta_{43} = \frac{2}{3}\,(\omega_{a0} - \omega_{m0})\,L_{sr}\sin\left(\theta_{m0} + \frac{2\pi}{3}\right)$$

$$\beta_{44} = R_r$$

$$\beta_{45} = -\frac{\sqrt{3}}{3}\,(\omega_{a0} - \omega_{m0})\,L_r$$

$$\beta_{46} = \frac{\sqrt{3}}{3}\,(\omega_{a0} - \omega_{m0})\,L_r$$

$$\beta_{47} = -\frac{2}{3} L_{sr} \left[i_{a0} \sin\theta_{m0} + i_{b0} \sin\left(\theta_{m0} - \frac{2\pi}{3}\right) + i_{c0} \sin\left(\theta_{m0} + \frac{2\pi}{3}\right) \right]$$

$$\beta_{48} = \frac{2}{3} (\omega_{a0} - \omega_{m0}) L_{sr} \left[i_{a0} \cos\theta_{m0} + i_{b0} \cos\left(\theta_{m0} - \frac{2\pi}{3}\right) + i_{c0} \cos\left(\theta_{m0} + \frac{2\pi}{3}\right) \right]$$

$$\begin{aligned} \Delta u_B = {} & \alpha_{51} \frac{d\Delta i_a}{dt} + \alpha_{52} \frac{d\Delta i_b}{dt} + \alpha_{53} \frac{d\Delta i_c}{dt} + \alpha_{54} \frac{d\Delta i_A}{dt} + \alpha_{55} \frac{d\Delta i_B}{dt} + \alpha_{56} \frac{d\Delta i_C}{dt} \\ & + \beta_{21} \Delta i_a + \beta_{52} \Delta i_b + \beta_{53} \Delta i_c + \beta_{54} \Delta i_A + \beta_{55} \Delta i_B + \beta_{56} \Delta i_C + \beta_{57} \Delta\omega_m + \beta_{58} \Delta\theta_m \end{aligned} \tag{A.13}$$

Where

$$\alpha_{51} = \frac{2}{3} L_{sr} \cos\left(\theta_{m0} + \frac{2\pi}{3}\right)$$

$$\alpha_{52} = \frac{2}{3} L_{sr} \cos\theta_{m0}$$

$$\alpha_{53} = \frac{2}{3} L_{sr} \cos\left(\theta_{m0} - \frac{2\pi}{3}\right)$$

$$\alpha_{54} = \frac{-L_r + L_{or}}{3}$$

$$\alpha_{55} = \frac{2L_r + L_{or}}{3}$$

$$\alpha_{56} = \frac{-L_r + L_{or}}{3}$$

$$\beta_{51} = \frac{2}{3} (\omega_{a0} - \omega_{m0}) L_{sr} \sin\left(\theta_{m0} + \frac{2\pi}{3}\right)$$

$$\beta_{52} = \frac{2}{3} (\omega_{a0} - \omega_{m0}) L_{sr} \sin\theta_{m0}$$

$$\beta_{53} = \frac{2}{3} (\omega_{a0} - \omega_{m0}) L_{sr} \sin\left(\theta_{m0} - \frac{2\pi}{3}\right)$$

$$\beta_{54} = \frac{\sqrt{3}}{3} (\omega_{a0} - \omega_{m0}) L_r$$

$$\beta_{55} = R_r$$

$$\beta_{56} = -\frac{\sqrt{3}}{3} (\omega_{a0} - \omega_{m0}) L_r$$

$$\beta_{57} = -\frac{2}{3} L_{sr} \left[i_{a0} \sin\left(\theta_{m0} + \frac{2\pi}{3}\right) + i_{b0} \sin\theta_{m0} + i_{c0} \sin\left(\theta_{m0} - \frac{2\pi}{3}\right) \right]$$

$$\beta_{58} = \frac{2}{3} (\omega_{a0} - \omega_{m0}) L_{sr} \left[i_{a0} \cos\left(\theta_{m0} + \frac{2\pi}{3}\right) + i_{b0} \cos\theta_{m0} + i_{c0} \cos\left(\theta_{m0} - \frac{2\pi}{3}\right) \right]$$

$$\begin{aligned}\Delta u_C = \alpha_{61}\frac{d\Delta i_a}{dt} + \alpha_{62}\frac{d\Delta i_b}{dt} + \alpha_{63}\frac{d\Delta i_c}{dt} + \alpha_{64}\frac{d\Delta i_A}{dt} + \alpha_{65}\frac{d\Delta i_B}{dt} + \alpha_{66}\frac{d\Delta i_C}{dt} \\ + \beta_{61}\Delta i_a + \beta_{62}\Delta i_b + \beta_{63}\Delta i_c + \beta_{64}\Delta i_A + \beta_{65}\Delta i_B + \beta_{66}\Delta i_C + \beta_{67}\Delta\omega_m + \beta_{68}\Delta\theta_m\end{aligned} \tag{A.14}$$

Where

$$\alpha_{61} = \frac{2}{3}L_{sr}\cos\left(\theta_{m0} - \frac{2\pi}{3}\right)$$

$$\alpha_{62} = \frac{2}{3}L_{sr}\cos\left(\theta_{m0} + \frac{2\pi}{3}\right)$$

$$\alpha_{63} = \frac{2}{3}L_{sr}\cos\theta_{m0}$$

$$\alpha_{64} = \frac{-L_r + L_{or}}{3}$$

$$\alpha_{65} = \frac{-L_r + L_{or}}{3}$$

$$\alpha_{66} = \frac{2L_r + L_{or}}{3}$$

$$\beta_{61} = \frac{2}{3}(\omega_{a0} - \omega_{m0})L_{sr}\sin\left(\theta_{m0} - \frac{2\pi}{3}\right)$$

$$\beta_{62} = \frac{2}{3}(\omega_{a0} - \omega_{m0})L_{sr}\sin\left(\theta_{m0} + \frac{2\pi}{3}\right)$$

$$\beta_{63} = \frac{2}{3}(\omega_{a0} - \omega_{m0})L_{sr}\sin\theta_{m0}$$

$$\beta_{64} = -\frac{\sqrt{3}}{3}(\omega_{a0} - \omega_{m0})L_r$$

$$\beta_{65} = \frac{\sqrt{3}}{3}(\omega_{a0} - \omega_{m0})L_r$$

$$\beta_{66} = R_r$$

$$\beta_{67} = -\frac{2}{3}L_{sr}\left[i_{a0}\sin\left(\theta_{m0} - \frac{2\pi}{3}\right) + i_{b0}\sin\left(\theta_{m0} + \frac{2\pi}{3}\right) + i_{c0}\sin\theta_{m0}\right]$$

$$\beta_{68} = \frac{2}{3}(\omega_{a0} - \omega_{m0})L_{sr}\left[i_{a0}\cos\left(\theta_{m0} - \frac{2\pi}{3}\right) + i_{b0}\cos\left(\theta_{m0} + \frac{2\pi}{3}\right) + i_{c0}\cos\theta_{m0}\right]$$

A.2.3 Mechanical Equations

$$\frac{J}{P_p}\frac{d\Delta\omega_m}{dt} = \sum\Delta T = \Delta T_{em} + \sum\Delta T_{mec} \tag{A.15a}$$

With

$$\Delta T_{em} = \beta_{71}\Delta i_a + \beta_{72}\Delta i_b + \beta_{73}\Delta i_c + \beta_{74}\Delta i_A + \beta_{75}\Delta i_B + \beta_{76}\Delta i_C + \beta_{78}\Delta\theta_m \tag{A.15b}$$

Where

$$\beta_{71} = -\frac{2}{3}P_p L_{sr}\left[i_{A0}\sin\theta_{m0} + i_{B0}\sin\left(\theta_{m0}+\frac{2\pi}{3}\right) + i_{C0}\sin\left(\theta_{m0}-\frac{2\pi}{3}\right)\right]$$

$$\beta_{72} = -\frac{2}{3}P_p L_{sr}\left[i_{A0}\sin\left(\theta_{m0}-\frac{2\pi}{3}\right) + i_{B0}\sin\theta_{m0} + i_{C0}\sin\left(\theta_{m0}+\frac{2\pi}{3}\right)\right]$$

$$\beta_{73} = -\frac{2}{3}P_p L_{sr}\left[i_{A0}\sin\left(\theta_{m0}+\frac{2\pi}{3}\right) + i_{B0}\sin\left(\theta_{m0}-\frac{2\pi}{3}\right) + i_{C0}\sin\theta_{m0}\right]$$

$$\beta_{74} = -\frac{2}{3}P_p L_{sr}\left[i_{a0}\sin\theta_{m0} + i_{b0}\sin\left(\theta_{m0}-\frac{2\pi}{3}\right) + i_{c0}\sin\left(\theta_{m0}+\frac{2\pi}{3}\right)\right]$$

$$\beta_{75} = -\frac{2}{3}P_p L_{sr}\left[i_{a0}\sin\left(\theta_{m0}+\frac{2\pi}{3}\right) + i_{b0}\sin\theta_{m0} + i_{c0}\sin\left(\theta_{m0}-\frac{2\pi}{3}\right)\right]$$

$$\beta_{76} = -\frac{2}{3}P_p L_{sr}\left[i_{a0}\sin\left(\theta_{m0}-\frac{2\pi}{3}\right) + i_{b0}\sin\left(\theta_{m0}+\frac{2\pi}{3}\right) + i_{c0}\sin\theta_{m0}\right]$$

$$\begin{aligned}\beta_{78} = -\frac{2}{3}P_p L_{sr}\Big[&(i_{a0}\,i_{A0} + i_{b0}\,i_{B0} + i_{c0}\,i_{C0})\cos\theta_{m0}\\ &+ (i_{a0}\,i_{C0} + i_{b0}\,i_{A0} + i_{c0}\,i_{B0})\cos\left(\theta_{m0}-\frac{2\pi}{3}\right)\\ &+ (i_{a0}\,i_{B0} + i_{b0}\,i_{C0} + i_{c0}\,i_{A0})\cos\left(\theta_{m0}+\frac{2\pi}{3}\right)\Big]\end{aligned}$$

$$\frac{d\Delta\theta_m}{dt} = \Delta\omega_m \tag{A.16}$$

A.3 Power Transformers

A.3.1 Vector Group *Yy0*

Primary Side

$$\begin{aligned}\Delta u_{a1} = {} & L_{11}\frac{d\Delta i_{a1}}{dt} - L_{11m}\frac{d\Delta i_{b1}}{dt} - L_{11m}\frac{d\Delta i_{c1}}{dt} + L_{12}\frac{d\Delta i_{a2}}{dt} - L_{12m}\frac{d\Delta i_{b2}}{dt}\\ & - L_{12m}\frac{d\Delta i_{c2}}{dt} + R_1\Delta i_{a1} - \frac{\sqrt{3}}{3}\omega_{a0}\left(L_{11}+L_{11m}\right)\Delta i_{b1}\\ & + \frac{\sqrt{3}}{3}\omega_{a0}\left(L_{11}+L_{11m}\right)\Delta i_{c1} - \frac{\sqrt{3}}{3}\omega_{a0}\left(L_{12}+L_{12m}\right)\Delta i_{b2} + \frac{\sqrt{3}}{3}\omega_{a0}\left(L_{12}+L_{12m}\right)\Delta i_{c2}\end{aligned} \tag{A.17}$$

$$\begin{aligned}\Delta u_{b1} = &-L_{11m}\frac{d\Delta i_{a1}}{dt} + L_{11}\frac{d\Delta i_{b1}}{dt} - L_{11m}\frac{d\Delta i_{c1}}{dt} - L_{12m}\frac{d\Delta i_{a2}}{dt} + L_{12}\frac{d\Delta i_{b2}}{dt}\\ &- L_{12m}\frac{d\Delta i_{c2}}{dt} + \frac{\sqrt{3}}{3}\omega_{a0}\left(L_{11}+L_{11m}\right)\Delta i_{a1} + R_1\Delta i_{b1}\\ &- \frac{\sqrt{3}}{3}\omega_{a0}\left(L_{11}+L_{11m}\right)\Delta i_{c1} + \frac{\sqrt{3}}{3}\omega_{a0}\left(L_{12}+L_{12m}\right)\Delta i_{a2} - \frac{\sqrt{3}}{3}\omega_{a0}\left(L_{12}+L_{12m}\right)\Delta i_{c2}\end{aligned} \tag{A.18}$$

$$\begin{aligned}\Delta u_{c1} = &-L_{11m}\frac{d\Delta i_{a1}}{dt} - L_{11m}\frac{d\Delta i_{b1}}{dt} + L_{11}\frac{d\Delta i_{c1}}{dt} - L_{12m}\frac{d\Delta i_{a2}}{dt} - L_{12m}\frac{d\Delta i_{b2}}{dt}\\ &+ L_{12}\frac{d\Delta i_{c2}}{dt} - \frac{\sqrt{3}}{3}\omega_{a0}\left(L_{11}+L_{11m}\right)\Delta i_{a1} + \frac{\sqrt{3}}{3}\omega_{a0}\left(L_{11}+L_{11m}\right)\Delta i_{b1}\\ &+ R_1\Delta i_{c1} - \frac{\sqrt{3}}{3}\omega_{a0}\left(L_{12}+L_{12m}\right)\Delta i_{a2} + \frac{\sqrt{3}}{3}\omega_{a0}\left(L_{12}+L_{12m}\right)\Delta i_{b2}\end{aligned} \tag{A.19}$$

Secondary Side

$$\begin{aligned}\Delta u_{a2} = &L_{12}\frac{d\Delta i_{a1}}{dt} - L_{12m}\frac{d\Delta i_{b1}}{dt} - L_{12m}\frac{d\Delta i_{c1}}{dt} + L_{22}\frac{d\Delta i_{a2}}{dt} - L_{22m}\frac{d\Delta i_{b2}}{dt}\\ &- L_{22m}\frac{d\Delta i_{c2}}{dt} - \frac{\sqrt{3}}{3}\omega_{a0}\left(L_{12}+L_{12m}\right)\Delta i_{b1} + \frac{\sqrt{3}}{3}\omega_{a0}\left(L_{12}+L_{12m}\right)\Delta i_{c1}\\ &+ R_2\Delta i_{a2} - \frac{\sqrt{3}}{3}\omega_{a0}\left(L_{22}+L_{22m}\right)\Delta i_{b2} + \frac{\sqrt{3}}{3}\omega_{a0}\left(L_{22}+L_{22m}\right)\Delta i_{c2}\end{aligned} \tag{A.20}$$

$$\begin{aligned}\Delta u_{b2} = &-L_{12m}\frac{d\Delta i_{a1}}{dt} + L_{12}\frac{d\Delta i_{b1}}{dt} - L_{12m}\frac{d\Delta i_{c1}}{dt} - L_{22m}\frac{d\Delta i_{a2}}{dt} + L_{22}\frac{d\Delta i_{b2}}{dt}\\ &- L_{22m}\frac{d\Delta i_{c2}}{dt} + \frac{\sqrt{3}}{3}\omega_{a0}\left(L_{12}+L_{12m}\right)\Delta i_{a1} - \frac{\sqrt{3}}{3}\omega_{a0}\left(L_{12}+L_{12m}\right)\Delta i_{c1}\\ &+ \frac{\sqrt{3}}{3}\omega_{a0}\left(L_{22}+L_{22m}\right)\Delta i_{a2} + R_2\Delta i_{b2} - \frac{\sqrt{3}}{3}\omega_{a0}\left(L_{22}+L_{22m}\right)\Delta i_{c2}\end{aligned} \tag{A.21}$$

$$\begin{aligned}\Delta u_{c2} = &-L_{12m}\frac{d\Delta i_{a1}}{dt} - L_{12m}\frac{d\Delta i_{b1}}{dt} + L_{12}\frac{d\Delta i_{c1}}{dt} - L_{22m}\frac{d\Delta i_{a2}}{dt} - L_{22m}\frac{d\Delta i_{b2}}{dt}\\ &+ L_{22}\frac{d\Delta i_{c2}}{dt} - \frac{\sqrt{3}}{3}\omega_{a0}\left(L_{12}+L_{12m}\right)\Delta i_{a1} + \frac{\sqrt{3}}{3}\omega_{a0}\left(L_{12}+L_{12m}\right)\Delta i_{b1}\\ &- \frac{\sqrt{3}}{3}\omega_{a0}\left(L_{22}+L_{22m}\right)\Delta i_{a2} + \frac{\sqrt{3}}{3}\omega_{a0}\left(L_{22}+L_{22m}\right)\Delta i_{b2} + R_2\Delta i_{c2}\end{aligned} \tag{A.22}$$

A.3.2 Vector Group *Yd5*

Primary Side

$$\begin{aligned}\Delta u_{a1} = {} & L_{11}\frac{d\Delta i_{a1}}{dt} - L_{11m}\frac{d\Delta i_{b1}}{dt} - L_{11m}\frac{d\Delta i_{c1}}{dt} + L_{12m}\frac{d\Delta i_{b2}}{dt} + 2L_{12m}\frac{d\Delta i_{c2}}{dt} \\ & - (L_{12} - 2L_{12m})\frac{d\Delta i_{\Delta}}{dt} + R_1\Delta i_{a1} - \frac{\sqrt{3}}{3}\omega_{a0}(L_{11} + L_{11m})\Delta i_{b1} \\ & + \frac{\sqrt{3}}{3}\omega_{a0}(L_{11} + L_{11m})\Delta i_{c1} + \frac{\sqrt{3}}{3}\omega_{a0}(L_{12} + L_{12m})\Delta i_{b2}\end{aligned} \tag{A.23}$$

$$\begin{aligned}\Delta u_{b1} = {} & -L_{11m}\frac{d\Delta i_{a1}}{dt} + L_{11}\frac{d\Delta i_{b1}}{dt} - L_{11m}\frac{d\Delta i_{c1}}{dt} - L_{12}\frac{d\Delta i_{b2}}{dt} - (L_{12} - L_{12m})\frac{d\Delta i_{c2}}{dt} \\ & - (L_{12} - 2L_{12m})\frac{d\Delta i_{\Delta}}{dt} + \frac{\sqrt{3}}{3}\omega_{a0}(L_{11} + L_{11m})\Delta i_{a1} + R_1\Delta i_{b1} \\ & - \frac{\sqrt{3}}{3}\omega_{a0}(L_{11} + L_{11m})\Delta i_{c1} + \frac{\sqrt{3}}{3}\omega_{a0}(L_{12} + L_{12m})\Delta i_{c2}\end{aligned} \tag{A.24}$$

$$\begin{aligned}\Delta u_{c1} = {} & -L_{11m}\frac{d\Delta i_{a1}}{dt} - L_{11m}\frac{d\Delta i_{b1}}{dt} + L_{11}\frac{d\Delta i_{c1}}{dt} + L_{12m}\frac{d\Delta i_{b2}}{dt} - (L_{12} - L_{12m})\frac{d\Delta i_{c2}}{dt} \\ & - (L_{12} - 2L_{12m})\frac{d\Delta i_{\Delta}}{dt} - \frac{\sqrt{3}}{3}\omega_{a0}(L_{11} + L_{11m})\Delta i_{a1} + \frac{\sqrt{3}}{3}\omega_{a0}(L_{11} + L_{11m})\Delta i_{b1} \\ & + R_1\Delta i_{c1} - \frac{\sqrt{3}}{3}\omega_{a0}(L_{12} + L_{12m})\Delta i_{b2} - \frac{\sqrt{3}}{3}\omega_{a0}(L_{12} + L_{12m})\Delta i_{c2}\end{aligned} \tag{A.25}$$

Secondary Side

$$\begin{aligned}\Delta u_{a2} = {} & -\frac{L_{12} + L_{12m}}{3}\frac{d\Delta i_{a1}}{dt} + \frac{L_{12} + L_{12m}}{3}\frac{d\Delta i_{b1}}{dt} - \frac{L_{22} + L_{22m}}{3}\frac{d\Delta i_{b2}}{dt} \\ & - \frac{L_{22} + L_{22m}}{3}\frac{d\Delta i_{c2}}{dt} + \frac{\sqrt{3}}{9}\omega_{a0}(L_{12} + L_{12m})\Delta i_{a1} + \frac{\sqrt{3}}{9}\omega_{a0}(L_{12} + L_{12m})\Delta i_{b1} \\ & - \frac{2\sqrt{3}}{9}\omega_{a0}(L_{12} + L_{12m})\Delta i_{c1} - \left[\frac{R_2}{3} + \frac{\sqrt{3}}{9}\omega_{a0}(L_{22} + L_{22m})\right]\Delta i_{b2} \\ & - \left[\frac{R_2}{3} - \frac{\sqrt{3}}{9}\omega_{a0}(L_{22} + L_{22m})\right]\Delta i_{c2}\end{aligned} \tag{A.26}$$

$$\begin{aligned}\Delta u_{b2} = &-\frac{L_{12}+L_{12m}}{3}\frac{d\Delta i_{b1}}{dt}+\frac{L_{12}+L_{12m}}{3}\frac{d\Delta i_{c1}}{dt}+\frac{L_{22}+L_{22m}}{3}\frac{d\Delta i_{b2}}{dt}\\ &-\frac{2\sqrt{3}}{9}\omega_{a0}\left(L_{12}+L_{12m}\right)\Delta i_{a1}+\frac{\sqrt{3}}{9}\omega_{a0}\left(L_{12}+L_{12m}\right)\Delta i_{b1}\\ &+\frac{\sqrt{3}}{9}\omega_{a0}\left(L_{12}+L_{12m}\right)\Delta i_{c1}+\left[\frac{R_2}{3}-\frac{\sqrt{3}}{9}\omega_{a0}\left(L_{22}+L_{22m}\right)\right]\Delta i_{b2}\\ &-\frac{2\sqrt{3}}{9}\omega_{a0}\left(L_{22}+L_{22m}\right)\Delta i_{c2}\end{aligned} \tag{A.27}$$

$$\begin{aligned}\Delta u_{c2} = &\frac{L_{12}+L_{12m}}{3}\frac{d\Delta i_{a1}}{dt}-\frac{L_{12}+L_{12m}}{3}\frac{d\Delta i_{c1}}{dt}+\frac{L_{22}+L_{22m}}{3}\frac{d\Delta i_{c2}}{dt}\\ &+\frac{\sqrt{3}}{9}\omega_{a0}\left(L_{12}+L_{12m}\right)\Delta i_{a1}-\frac{2\sqrt{3}}{9}\omega_{a0}\left(L_{12}+L_{12m}\right)\Delta i_{b1}\\ &+\frac{\sqrt{3}}{9}\omega_{a0}\left(L_{12}+L_{12m}\right)\Delta i_{c1}+\frac{2\sqrt{3}}{9}\omega_{a0}\left(L_{22}+L_{22m}\right)\Delta i_{b2}\\ &+\left[\frac{R_2}{3}+\frac{\sqrt{3}}{9}\omega_{a0}\left(L_{22}+L_{22m}\right)\right]\Delta i_{c2}\end{aligned} \tag{A.28}$$

Circulating Current of the Δ-Connection

$$\begin{aligned}0 = &-\left(L_{12}-2L_{12m}\right)\frac{d\Delta i_{a1}}{dt}-\left(L_{12}-2L_{12m}\right)\frac{d\Delta i_{b1}}{dt}-\left(L_{12}-2L_{12m}\right)\frac{d\Delta i_{c1}}{dt}\\ &+\left(L_{22}-2L_{22m}\right)\frac{d\Delta i_{b2}}{dt}+2\left(L_{22}-2L_{22m}\right)\frac{d\Delta i_{c2}}{dt}+3\left(L_{22}-2L_{22m}\right)\frac{d\Delta i_{\Delta}}{dt}\\ &+R_2\Delta i_{b2}+2R_2\Delta i_{c2}+3R_2\Delta i_{\Delta}\end{aligned} \tag{A.29}$$

A.3.3 Vector Group *Yd11*

Equations representing power transformers of vector group *Yd11* are the same as those for *Yd5* transformers. Nonetheless, the polarity between primary and secondary sides is inverted, due to the windings connection.

Therefore, the sign of mutual inductances L_{12} and L_{12m} must be inverted, so that this effect is taken into account.

A.4 Electrical Loads

A.4.1 RL Series Load

$$\Delta u_a = L_L \frac{d\Delta i_a}{dt} + R_L \Delta i_a - \frac{\sqrt{3}}{3}\omega_{a0} L_L \Delta i_b + \frac{\sqrt{3}}{3}\omega_{a0} L_L \Delta i_c \tag{A.30}$$

$$\Delta u_b = L_L \frac{d\Delta i_b}{dt} + \frac{\sqrt{3}}{3}\omega_{a0} L_L \Delta i_a + R_L \Delta i_b - \frac{\sqrt{3}}{3}\omega_{a0} L_L \Delta i_c \tag{A.31}$$

$$\Delta u_c = L_L \frac{d\Delta i_c}{dt} - \frac{\sqrt{3}}{3}\omega_{a0} L_L \Delta i_a + \frac{\sqrt{3}}{3}\omega_{a0} L_L \Delta i_b + R_L \Delta i_c \tag{A.32}$$

A.4.2 RLC Series Load

$$\Delta u_a = L_L \frac{d\Delta i_a}{dt} + R_L \Delta i_a - \frac{\sqrt{3}}{3}\omega_{a0} L_L \Delta i_b + \frac{\sqrt{3}}{3}\omega_{a0} L_L \Delta i_c + \Delta u_{Ca} \tag{A.33}$$

$$\Delta u_b = L_L \frac{d\Delta i_b}{dt} + \frac{\sqrt{3}}{3}\omega_{a0} L_L \Delta i_a + R_L \Delta i_b - \frac{\sqrt{3}}{3}\omega_{a0} L_L \Delta i_c + \Delta u_{Cb} \tag{A.34}$$

$$\Delta u_c = L_L \frac{d\Delta i_c}{dt} - \frac{\sqrt{3}}{3}\omega_{a0} L_L \Delta i_a + \frac{\sqrt{3}}{3}\omega_{a0} L_L \Delta i_b + R_L \Delta i_c + \Delta u_{Cc} \tag{A.35}$$

$$\Delta i_a = C_L \frac{d\Delta u_{Ca}}{dt} - \frac{\sqrt{3}}{3}\omega_{a0} C_L \Delta u_{Cb} + \frac{\sqrt{3}}{3}\omega_{a0} C_L \Delta u_{Cc} \tag{A.36}$$

$$\Delta i_b = C_L \frac{d\Delta u_{Cb}}{dt} + \frac{\sqrt{3}}{3}\omega_{a0} C_L \Delta u_{Ca} - \frac{\sqrt{3}}{3}\omega_{a0} C_L \Delta u_{Cc} \tag{A.37}$$

$$\Delta i_c = C_L \frac{d\Delta u_{Cc}}{dt} - \frac{\sqrt{3}}{3}\omega_{a0} C_L \Delta u_{Ca} + \frac{\sqrt{3}}{3}\omega_{a0} C_L \Delta u_{Cb} \tag{A.38}$$

A.5 Transmission Lines

A.5.1 RL Transmission Line

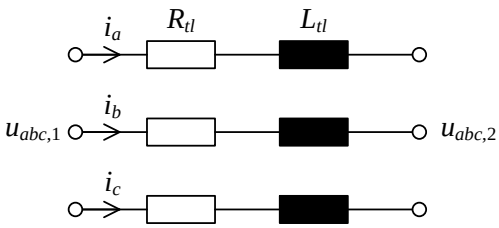

Figure A.1: Resistive-inductive transmission line.

$$\Delta u_{a1} = L_{tl}\frac{d\Delta i_a}{dt} + R_{tl}\,\Delta i_a - \frac{\sqrt{3}}{3}\omega_{a0}\,L_{tl}\,\Delta i_b + \frac{\sqrt{3}}{3}\omega_{a0}\,L_{tl}\,\Delta i_c + \Delta u_{a2} \tag{A.39}$$

$$\Delta u_{b1} = L_{tl}\frac{d\Delta i_b}{dt} + \frac{\sqrt{3}}{3}\omega_{a0}\,L_{tl}\,\Delta i_a + R_{tl}\,\Delta i_b - \frac{\sqrt{3}}{3}\omega_{a0}\,L_{tl}\,\Delta i_c + \Delta u_{b2} \tag{A.40}$$

$$\Delta u_{c1} = L_{tl}\frac{d\Delta i_c}{dt} - \frac{\sqrt{3}}{3}\omega_{a0}\,L_{tl}\,\Delta i_a + \frac{\sqrt{3}}{3}\omega_{a0}\,L_{tl}\,\Delta i_b + R_{tl}\,\Delta i_c + \Delta u_{c2} \tag{A.41}$$

A.5.2 π-Section Model of Transmission Line

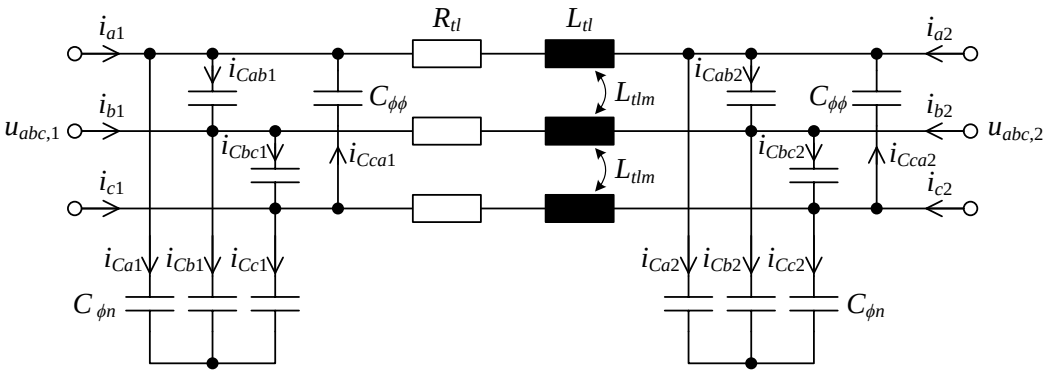

Figure A.2: Three-phase scheme of a π-section transmission line element.

Voltage Drop on RL Series Element

$$\begin{aligned}\Delta u_a = {} & L_{tl}\frac{d\Delta i_a}{dt} + L_{tlm}\frac{d\Delta i_b}{dt} + L_{tlm}\frac{d\Delta i_c}{dt} + R_{tl}\,\Delta i_a \\ & - \frac{\sqrt{3}}{3}\,\omega_{a0}\,(L_{tl} - L_{tlm})\,\Delta i_b + \frac{\sqrt{3}}{3}\,\omega_{a0}\,(L_{tl} - L_{tlm})\,\Delta i_c\end{aligned} \tag{A.42}$$

$$\begin{aligned}\Delta u_b = {} & L_{tlm}\frac{d\Delta i_a}{dt} + L_{tl}\frac{d\Delta i_b}{dt} + L_{tlm}\frac{d\Delta i_c}{dt} + \frac{\sqrt{3}}{3}\,\omega_{a0}\,(L_{tl} - L_{tlm})\,\Delta i_a \\ & + R_{tl}\,\Delta i_b - \frac{\sqrt{3}}{3}\,\omega_{a0}\,(L_{tl} - L_{tlm})\,\Delta i_c\end{aligned} \tag{A.43}$$

$$\begin{aligned}\Delta u_c = {} & L_{tlm}\frac{d\Delta i_a}{dt} + L_{tlm}\frac{d\Delta i_b}{dt} + L_{tl}\frac{d\Delta i_c}{dt} - \frac{\sqrt{3}}{3}\,\omega_{a0}\,(L_{tl} - L_{tlm})\,\Delta i_a \\ & + \frac{\sqrt{3}}{3}\,\omega_{a0}\,(L_{tl} - L_{tlm})\,\Delta i_b + R_{tl}\,\Delta i_c\end{aligned} \tag{A.44}$$

Phase-to-Ground Voltages on First End of the Line

$$\Delta u_{a1} = \Delta u_{Ca1} + L_{res}\frac{d\Delta i_{Ca1}}{dt} - \frac{\sqrt{3}}{3}\,\omega_{a0}\,L_{res}\,\Delta i_{Cb1} + \frac{\sqrt{3}}{3}\,\omega_{a0}\,L_{res}\,\Delta i_{Cc1} \tag{A.45}$$

$$\Delta u_{b1} = \Delta u_{Cb1} + L_{res}\frac{d\Delta i_{Cb1}}{dt} + \frac{\sqrt{3}}{3}\,\omega_{a0}\,L_{res}\,\Delta i_{Ca1} - \frac{\sqrt{3}}{3}\,\omega_{a0}\,L_{res}\,\Delta i_{Cc1} \tag{A.46}$$

$$\Delta u_{c1} = \Delta u_{Cc1} + L_{res}\frac{d\Delta i_{Cc1}}{dt} - \frac{\sqrt{3}}{3}\,\omega_{a0}\,L_{res}\,\Delta i_{Ca1} + \frac{\sqrt{3}}{3}\,\omega_{a0}\,L_{res}\,\Delta i_{Cb1} \tag{A.47}$$

Phase-to-Phase Voltages on First End of the Line

$$\Delta u_{ab1} = \Delta u_{Cab1} + L_{res}\frac{d\Delta i_{Cab1}}{dt} - \frac{\sqrt{3}}{3}\,\omega_{a0}\,L_{res}\,\Delta i_{Cbc1} + \frac{\sqrt{3}}{3}\,\omega_{a0}\,L_{res}\,\Delta i_{Cca1} \tag{A.48}$$

$$\Delta u_{bc1} = \Delta u_{Cbc1} + L_{res}\frac{d\Delta i_{Cbc1}}{dt} + \frac{\sqrt{3}}{3}\omega_{a0}L_{res}\Delta i_{Cab1} - \frac{\sqrt{3}}{3}\omega_{a0}L_{res}\Delta i_{Cca1} \tag{A.49}$$

$$\Delta u_{ca1} = \Delta u_{Cca1} + L_{res}\frac{d\Delta i_{Cca1}}{dt} - \frac{\sqrt{3}}{3}\omega_{a0}L_{res}\Delta i_{Cab1} + \frac{\sqrt{3}}{3}\omega_{a0}L_{res}\Delta i_{Cbc1} \tag{A.50}$$

Phase-to-Phase Voltages on Second End of the Line

$$\Delta u_{ab2} = \Delta u_{Cab2} + L_{res}\frac{d\Delta i_{Cab2}}{dt} - \frac{\sqrt{3}}{3}\omega_{a0}L_{res}\Delta i_{Cbc2} + \frac{\sqrt{3}}{3}\omega_{a0}L_{res}\Delta i_{Cca2} \tag{A.51}$$

$$\Delta u_{bc2} = \Delta u_{Cbc2} + L_{res}\frac{d\Delta i_{Cbc2}}{dt} + \frac{\sqrt{3}}{3}\omega_{a0}L_{res}\Delta i_{Cab2} - \frac{\sqrt{3}}{3}\omega_{a0}L_{res}\Delta i_{Cca2} \tag{A.52}$$

$$\Delta u_{ca2} = \Delta u_{Cca2} + L_{res}\frac{d\Delta i_{Cca2}}{dt} - \frac{\sqrt{3}}{3}\omega_{a0}L_{res}\Delta i_{Cab2} + \frac{\sqrt{3}}{3}\omega_{a0}L_{res}\Delta i_{Cbc2} \tag{A.53}$$

Phase-to-Ground Voltages on Second End of the Line

$$\Delta u_{a2} = \Delta u_{Ca2} + L_{res}\frac{d\Delta i_{Ca2}}{dt} - \frac{\sqrt{3}}{3}\omega_{a0}L_{res}\Delta i_{Cb2} + \frac{\sqrt{3}}{3}\omega_{a0}L_{res}\Delta i_{Cc2} \tag{A.54}$$

$$\Delta u_{b2} = \Delta u_{Cb2} + L_{res}\frac{d\Delta i_{Cb2}}{dt} + \frac{\sqrt{3}}{3}\omega_{a0}L_{res}\Delta i_{Ca2} - \frac{\sqrt{3}}{3}\omega_{a0}L_{res}\Delta i_{Cc2} \tag{A.55}$$

$$\Delta u_{c2} = \Delta u_{Cc2} + L_{res}\frac{d\Delta i_{Cc2}}{dt} - \frac{\sqrt{3}}{3}\omega_{a0}L_{res}\Delta i_{Ca2} + \frac{\sqrt{3}}{3}\omega_{a0}L_{res}\Delta i_{Cb2} \tag{A.56}$$

Phase-to-Ground Currents on First End of the Line

$$\Delta i_{Ca1} = C_{\phi n}\frac{d\Delta u_{Ca1}}{dt} - \frac{\sqrt{3}}{3}\omega_{a0}C_{\phi n}\Delta u_{Cb1} + \frac{\sqrt{3}}{3}\omega_{a0}C_{\phi n}\Delta u_{Cc1} \tag{A.57}$$

$$\Delta i_{Cb1} = C_{\phi n} \frac{d\Delta u_{Cb1}}{dt} + \frac{\sqrt{3}}{3} \omega_{a0} C_{\phi n} \Delta u_{Ca1} - \frac{\sqrt{3}}{3} \omega_{a0} C_{\phi n} \Delta u_{Cc1} \tag{A.58}$$

$$\Delta i_{Cc1} = C_{\phi n} \frac{d\Delta u_{Cc1}}{dt} - \frac{\sqrt{3}}{3} \omega_{a0} C_{\phi n} \Delta u_{Ca1} + \frac{\sqrt{3}}{3} \omega_{a0} C_{\phi n} \Delta u_{Cb1} \tag{A.59}$$

Phase-to-Phase Currents on First End of the Line

$$\Delta i_{Cab1} = C_{\phi\phi} \frac{d\Delta u_{Cab1}}{dt} - \frac{\sqrt{3}}{3} \omega_{a0} C_{\phi\phi} \Delta u_{Cbc1} + \frac{\sqrt{3}}{3} \omega_{a0} C_{\phi\phi} \Delta u_{Cca1} \tag{A.60}$$

$$\Delta i_{Cbc1} = C_{\phi\phi} \frac{d\Delta u_{Cbc1}}{dt} + \frac{\sqrt{3}}{3} \omega_{a0} C_{\phi\phi} \Delta u_{Cab1} - \frac{\sqrt{3}}{3} \omega_{a0} C_{\phi\phi} \Delta u_{Cca1} \tag{A.61}$$

$$\Delta i_{Cca1} = C_{\phi\phi} \frac{d\Delta u_{Cca1}}{dt} - \frac{\sqrt{3}}{3} \omega_{a0} C_{\phi\phi} \Delta u_{Cab1} + \frac{\sqrt{3}}{3} \omega_{a0} C_{\phi\phi} \Delta u_{Cbc1} \tag{A.62}$$

Phase-to-Phase Currents on Second End of the Line

$$\Delta i_{Cab2} = C_{\phi\phi} \frac{d\Delta u_{Cab2}}{dt} - \frac{\sqrt{3}}{3} \omega_{a0} C_{\phi\phi} \Delta u_{Cbc2} + \frac{\sqrt{3}}{3} \omega_{a0} C_{\phi\phi} \Delta u_{Cca2} \tag{A.63}$$

$$\Delta i_{Cbc2} = C_{\phi\phi} \frac{d\Delta u_{Cbc2}}{dt} + \frac{\sqrt{3}}{3} \omega_{a0} C_{\phi\phi} \Delta u_{Cab2} - \frac{\sqrt{3}}{3} \omega_{a0} C_{\phi\phi} \Delta u_{Cca2} \tag{A.64}$$

$$\Delta i_{Cca2} = C_{\phi\phi} \frac{d\Delta u_{Cca2}}{dt} - \frac{\sqrt{3}}{3} \omega_{a0} C_{\phi\phi} \Delta u_{Cab2} + \frac{\sqrt{3}}{3} \omega_{a0} C_{\phi\phi} \Delta u_{Cbc2} \tag{A.65}$$

Phase-to-Ground Currents on Second End of the Line

$$\Delta i_{Ca2} = C_{\phi n} \frac{d\Delta u_{Ca2}}{dt} - \frac{\sqrt{3}}{3} \omega_{a0} C_{\phi n} \Delta u_{Cb2} + \frac{\sqrt{3}}{3} \omega_{a0} C_{\phi n} \Delta u_{Cc2} \tag{A.66}$$

$$\Delta i_{Cb2} = C_{\phi n}\frac{d\Delta u_{Cb2}}{dt} + \frac{\sqrt{3}}{3}\omega_{a0}\,C_{\phi n}\,\Delta u_{Ca2} - \frac{\sqrt{3}}{3}\omega_{a0}\,C_{\phi n}\,\Delta u_{Cc2} \tag{A.67}$$

$$\Delta i_{Cc2} = C_{\phi n}\frac{d\Delta u_{Cc2}}{dt} - \frac{\sqrt{3}}{3}\omega_{a0}\,C_{\phi n}\,\Delta u_{Ca2} + \frac{\sqrt{3}}{3}\omega_{a0}\,C_{\phi n}\,\Delta u_{Cb2} \tag{A.68}$$

A.6 Voltage Regulators

A.6.1 IEEE ST1A

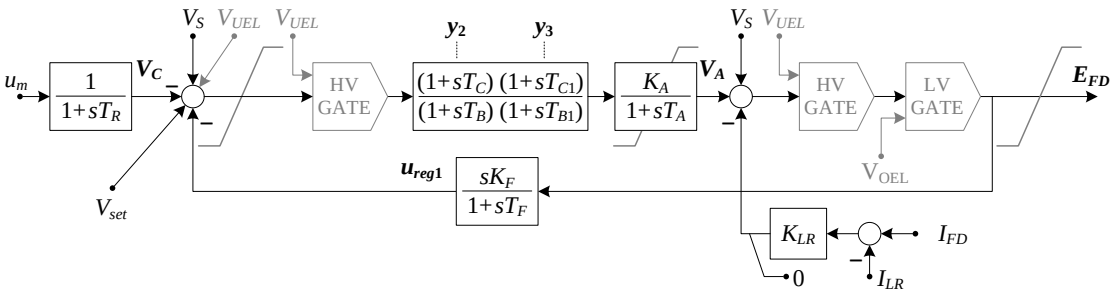

Figure A.3: IEEE ST1A voltage regulator.

$$T_R\frac{d\Delta V_C}{dt} = \Delta u_m - \Delta V_C \tag{A.69}$$

$$\begin{aligned} T_B\frac{d\Delta y_2}{dt} + T_C\frac{d\Delta V_C}{dt} + T_C\frac{d\Delta u_{reg1}}{dt} - k_1\,T_C\frac{d\Delta V_S}{dt} &= -\Delta y_2 - \Delta V_C \\ &\quad - \Delta u_{reg1} + k_1\Delta V_S \end{aligned} \tag{A.70}$$

$$T_{B1}\frac{d\Delta y_3}{dt} - T_{C1}\frac{d\Delta y_2}{dt} = \Delta y_2 - \Delta y_3 \tag{A.71}$$

$$T_A\frac{d\Delta V_A}{dt} = K_A\,\Delta y_3 - \Delta V_A \tag{A.72}$$

$$\begin{aligned} T_F\frac{d\Delta u_{reg1}}{dt} - K_F\frac{d\Delta V_A}{dt} - k_2\,K_F\frac{d\Delta V_S}{dt} + \frac{K_F\,K_{LR}}{I_{f\delta 0}}\frac{d\Delta i_f}{dt} &= -\Delta y_2 - \Delta V_C \\ &\quad - \Delta u_{reg1} + k_1\Delta V_S \end{aligned} \tag{A.73}$$

The linearized output ΔE_{FD} is:

$$\Delta E_{FD} = \Delta V_A + k_2\,\Delta V_S - \frac{K_{LR}}{I_{f\delta 0}}\,\Delta i_f \tag{A.74}$$

Which is applied to the excitation voltage as:

$$\Delta u_f = R_f I_{f\delta 0} \Delta E_{FD} \tag{A.75}$$

The value of k_1 and k_2 vary according to the use of a PSS. If the PSS is inactive, $k_1 = k_2 = 0$. If the PSS is active, k_1 and k_2 are either equal to 0 or 1 according to the following relation: $k_2 = 1 \oplus k_1$.

The analytical expression of the input Δu_m in given in section A.6.3.

A.6.2 Unitrol®

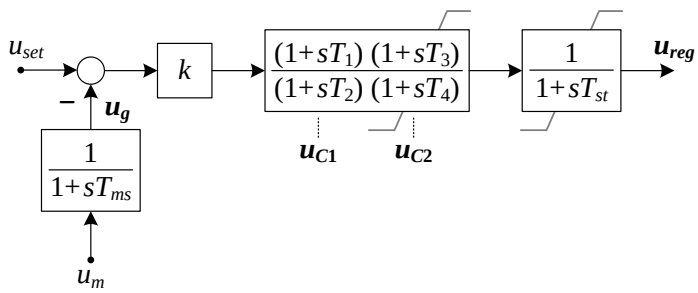

Figure A.4: Block diagram of the Unitrol® voltage regulator.

$$T_{ms} \frac{d\Delta u_g}{dt} = \Delta u_m - \Delta u_g \tag{A.76}$$

$$T_2 \frac{d\Delta u_{C1}}{dt} = \Delta u_{set} - \Delta u_g - \Delta u_{C1} \tag{A.77}$$

$$\begin{aligned} T_3 \frac{d\Delta u_{C2}}{dt} &= k \frac{T_1\,T_3}{T_2\,T_4} \Delta u_{set} - k \frac{T_1\,T_3}{T_2\,T_4} \Delta u_g - k \frac{T_3\,(T_1 - T_2)}{T_2\,T_4} \Delta u_{C1} \\ &\quad + \left(\frac{T_4 - T_3}{T_3\,T_4} - 1 \right) \Delta u_{C2} \end{aligned} \tag{A.78}$$

$$\begin{aligned} T_{st} \frac{d\Delta u_{reg}}{dt} &= k \frac{T_1\,T_3}{T_2\,T_4} \Delta u_{set} - k \frac{T_1\,T_3}{T_2\,T_4} \Delta u_g - k \frac{T_3\,(T_1 - T_2)}{T_2\,T_4} \Delta u_{C1} \\ &\quad + \frac{T_4 - T_3}{T_3\,T_4} \Delta u_{C2} \end{aligned} \tag{A.79}$$

The output Δu_{reg} is applied to the excitation voltage as:

$$\Delta u_f = R_f I_{f\delta 0} \Delta u_{reg} \tag{A.80}$$

If a PSS is active, its output is added to the set-point Δu_{set}.

The analytical expression of the input Δu_m in given in section A.6.3.

A.6.3 Voltage Input (Δu_m)

$$\begin{aligned}\Delta u_m = -\frac{\sqrt{2}}{\sqrt{3}U_N}\Bigg\{&\sin(\delta_o+\theta_0)\,\Delta u_a + \sin\left(\delta_o+\theta_0-\frac{2\pi}{3}\right)\Delta u_b + \sin\left(\delta_o+\theta_0+\frac{2\pi}{3}\right)\Delta u_c \\ &+\left[\sin(\delta_o+\theta_0)\,u_{a0} + \sin\left(\delta_o+\theta_0-\frac{2\pi}{3}\right)u_{v0} + \sin\left(\delta_o+\theta_0+\frac{2\pi}{3}\right)u_{c0}\right]\Delta\theta\Bigg\}\end{aligned} \tag{A.81}$$

The analytical expressions for Δu_a, Δu_b and Δu_c were defined in section A.1.

A.7 Power System Stabilizer IEEE PSS2B

The stabilizer PSS2B is described either by fourteen or fifteen time-domain state equations, depending on the values of the parameters M and N. In SIMSEN, these parameters can assume either the values $M = 4, N = 1$; or $M = 5, N = 1$; or $M = 2, N = 2$. The system of equations presented here correspond to the case with $M = 5, N = 1$ (fifteen equations).

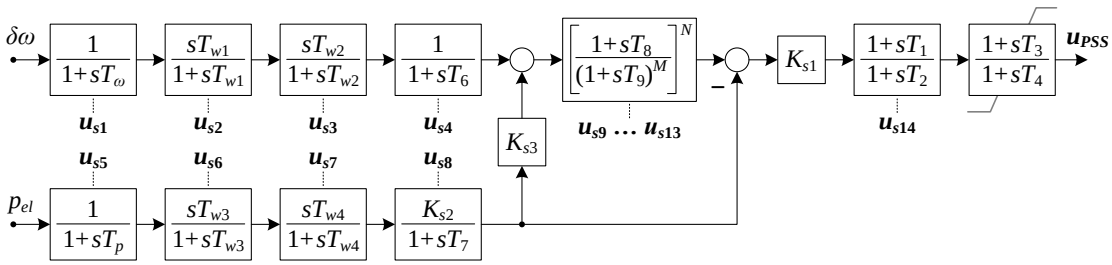

Figure A.5: IEEE PSS2B power system stabilizer with filtered inputs.

$$T_\omega \frac{d\Delta u_{s1}}{dt} = \frac{\Delta\omega_m}{\omega_N} - \Delta u_{s1} \tag{A.82}$$

$$T_{w1}\frac{d\Delta u_{s2}}{dt} - T_{w1}\frac{d\Delta u_{s1}}{dt} = -\Delta u_{s2} \tag{A.83}$$

$$T_{w2}\frac{d\Delta u_{s3}}{dt} - T_{w2}\frac{d\Delta u_{s2}}{dt} = -\Delta u_{s3} \tag{A.84}$$

$$T_6 \frac{d\Delta u_{s4}}{dt} = \Delta u_{s3} - \Delta u_{s4} \tag{A.85}$$

$$T_p \frac{d\Delta u_{s5}}{dt} = \Delta p_{el} - \Delta u_{s5} \tag{A.86}$$

$$T_{w3} \frac{d\Delta u_{s6}}{dt} - T_{w3} \frac{d\Delta u_{s5}}{dt} = -\Delta u_{s6} \tag{A.87}$$

$$T_{w4} \frac{d\Delta u_{s7}}{dt} - T_{w4} \frac{d\Delta u_{s6}}{dt} = -\Delta u_{s7} \tag{A.88}$$

$$T_7 \frac{d\Delta u_{s8}}{dt} = K_{s2}\, \Delta u_{s7} - \Delta u_{s8} \tag{A.89}$$

$$T_9 \frac{d\Delta u_{s9}}{dt} = \Delta u_{s4} + K_{s3}\, \Delta u_{s8} - \Delta u_{s9} \tag{A.90}$$

$$T_9 \frac{d\Delta u_{s10}}{dt} = \Delta u_{s9} - \Delta u_{s10} \tag{A.91}$$

$$T_9 \frac{d\Delta u_{s11}}{dt} = \Delta u_{s10} - \Delta u_{s11} \tag{A.92}$$

$$T_9 \frac{d\Delta u_{s12}}{dt} = \Delta u_{s11} - \Delta u_{s12} \tag{A.93}$$

$$T_9 \frac{d\Delta u_{s13}}{dt} - T_8 \frac{d\Delta u_{s12}}{dt} = \Delta u_{s12} - \Delta u_{s13} \tag{A.94}$$

$$T_2 \frac{d\Delta u_{s14}}{dt} - K_{s1}\, T_1 \frac{d\Delta u_{s13}}{dt} + K_{s1}\, T_1 \frac{d\Delta u_{s8}}{dt} = -K_{s1}\Delta u_{s8} + K_{s1}\Delta u_{s13} - \Delta u_{s14} \tag{A.95}$$

$$T_4 \frac{d\Delta u_{pss}}{dt} - T_3 \frac{d\Delta u_{s14}}{dt} = \Delta u_{s14} - \Delta u_{pss} \tag{A.96}$$

The input Δp_{el} of equation (A.86) is defined as:

$$\Delta p_{el} = -\frac{1}{S_N}\left(i_{a0}\,\Delta u_a + u_{a0}\,\Delta i_a + i_{b0}\,\Delta u_b + u_{b0}\,\Delta i_b + i_{c0}\,\Delta u_c + u_{c0}\,\Delta i_c\right) \tag{A.97}$$

The analytical expressions for Δu_a, Δu_b and Δu_c were defined in section A.1.

Bibliography

[1] ALLIGNÉ, S. *Forced and Self Oscillations of Hydraulic Systems Induced by Cavitation Vortex Rope of Francis Turbines.* Ph.D. dissertation, École Polytechnique Fédérale de Lausanne, Switzerland, 2011.

[2] ALLIGNÉ, S., SILVA, P. C. O., BÉGUIN, A., KAWKABANI, B., ALLENBACH, P., NICOLET, C., AND AVELLAN, F. Forced Response Analysis of Hydroelectric Systems. *IOP Conference Series: Earth and Environmental Science vol. 22*, issue 4 (Dec. 2014), 1–14.

[3] ALONSO, J. M., GACIO, D., SICHIROLLO, F., SEIDEL, A. R., AND DALLA COSTA, M. A. A Straightforward Methodology to Modeling High Power Factor AC-DC Converters. *IEEE Transactions on Power Electronics vol. 28*, issue 10 (Oct. 2013), 4723–4731.

[4] ANDERSON, G. *Modelling and Analysis of Electric Power Systems.* Lecture 227-0526-00. ITET ETHZ, Zürich, Sept. 2008.

[5] ARANI, M. F. M., AND MOHAMED, Y. A.-R. I. Analysis and Impacts of Implementing Droop Control in DFIG-Based Wind Turbines on Microgrid/Weak-Grid Stability. *IEEE Transactions on Power Systems vol. 30*, issue 1 (Jan. 2015), 385–396.

[6] ARNOLDI, W. E. The Principle of Minimized Iterations in the Solution of the Matrix Eigenvalue Problem. *Quarterly of Applied Mathematics vol. 9* (1951), 17–29.

[7] BARQUIN, J., ROUCO, L., AND VARGAS, H. R. Generalized Selective Modal Analysis. In *Proceedings of the IEEE Power Engineering Society Winter Meeting* (New York, USA, Jan. 2002), vol. vol. 2, pp. 1194–1199.

[8] BEZA, M., AND BONGIORNO, M. An Adaptive Power Oscillation Damping Controller by STATCOM With Energy Storage. *IEEE Transactions on Power Systems vol. 30*, issue 1 (Jan. 2015), 484–493.

[9] BOLLINGER, K. E., NETTLETON, L. D., AND GURNEY, J. H. Reducing the Effect of Penstock Pressure Pulsations on Hydro Electric Plant Power System Stabilizer Signals. *IEEE Transactions on Energy Conversion vol. 8*, issue 4 (Dec. 1993), 628–631.

[10] BU, S. Q., DU, W., WANG, H. F., CHEN, Z., XIAO, L. Y., AND LI, H. F. Probabilistic Analysis of Small-Signal Stability of Large-Scale Power Systems as Affected by Penetration of Wind Generation. *IEEE Transactions on Power Systems vol. 27*, issue 2 (May 2012), 762–770.

[11] BYERLY, R. T., BENNON, R. J., AND SHERMAN, D. E. Eigenvalue Analysis of Synchronizing Power Flow Oscillations in Large Electric Power Systems. *IEEE Transactions on Power Apparatus and Systems vol. PAS-101*, issue 1 (Jan. 1982), 235–243.

[12] CANAY, I. M. A Novel Approach to the Torsional Interaction and Electrical Damping of the Synchronous Machine Part I: Theory. *IEEE Transactions on Power Apparatus and Systems vol. PAS-101*, issue 10 (Oct. 1982), 3630–3638.

[13] CANAY, I. M. A Novel Approach to the Torsional Interaction and Electrical Damping of the Synchronous Machine Part II: Application to an arbitrary network. *IEEE Transactions on Power Apparatus and Systems vol. PAS-101*, issue 10 (Oct. 1982), 3639–3647.

[14] CEPEL BRAZIL. PacDyn. Available from: http://www.pacdyn.cepel.br [accessed on 16 May 2015], 2015.

[15] CHAMORRO, H. R., GHANDHARI, M., AND ERIKSSON, R. Influence of the Increasing Non-Synchronous Generation on Small Signal Stability. In *Proceedings of the 2014 IEEE PES General Meeting, Conference Exposition* (National Harbor, USA, July 2014), pp. 1–5.

[16] CHATELAIN, J. *Machines Electriques*, vol. vol. X of *Traité d'Electricité*. Presses Polytechniques Romandes, Lausanne, Switzerland, 1983.

[17] CHOMPOOBUTRGOOL, Y., LI, W., AND VANFRETTI, L. Development and Implementation of a Nordic Grid Model for Power System Small-Signal and Transient Stability Studies in a Free and Open Source Software. In *Proceedings of the 2012 IEEE Power and Energy Society General Meeting* (San Diego, USA, July 2012), pp. 1–8.

[18] CHOW, J., AND CHEUNG, K. A Toolbox for Power System Dynamics and Control Engineering Education and Research. *IEEE Transactions on Power Systems vol. 7*, issue 4 (Nov. 1992), 1559–1564.

[19] DE OLIVEIRA, R. V., ZAMADEI, J. A., CARDOSO, M. A., AND ZAMODZKI, R. Control of Wind Generation Units Based on Doubly-Fed Induction Generator for Small-Signal Stability Enhancement. In *Proceedings of the 2012 IEEE Power and Energy Society General Meeting* (San Diego, USA, July 2012).

[20] DIGSILENT GMBH. DIgSILENT PowerFactory. Available from: http://tinyurl.com/DIgSILENT-PowerFactory [accessed on 16 May 2015], 2015.

[21] DOOKHITRAM, K., BOOJHAWON, R., AND BHURUTH, M. A New Method for Accelerating Arnoldi Algorithms for Large Scale Eigenproblems. *Mathematics and Computers in Simulation vol. 80*, issue 2 (Oct. 2009), 387–401.

[22] DÖRFLER, P., SICK, M., AND COUTU, A. *Flow-Induced Pulsation and Vibration in Hydroelectric Machinery*. Springer-Verlag, London, 2013.

[23] ETAP. ETAP Small Signal Stability Module. Available from: http://etap.com/dynamics-transients/small-signal-stability.htm [accessed on 16 May 2015], 2015.

[24] EVANS, R. D., AND BERGVALL, R. C. Experimental Analysis of Stability and Power Limitations. *AIEE Transactions vol. 43* (Apr. 1924), 329–340.

[25] FISHER, R. K., KOUTNIK, J., MEIER, L., LOOSE, V., ENGELS, K., AND BEYER, T. A Comparison of Advanced Pumped Storage Equipment Drivers in the US and Europe. In *HydroVision International 2012* (Louisville, USA, July 2012), PennWell Corporation.

[26] FRANCIS, J. G. F. The QR Transformation: A Unitary Analogue to the LR Transformation - Part 1. *The Computer Journal vol. 4*, issue 3 (1961), 265–271.

[27] GAUTAM, P., GUMMER, J. H., AND POTT, J. Local Penstock Resonance Resulting from Turbine Operation. In *Proceedings of Hydro 2014* (Cernobbio, Italy, Oct. 2014).

[28] GEIST, G. A., HOWELL, G. W., AND WATKINS, D. S. The BR Eigenvalue Algorithm. *SIAM Journal on Matrix Analysis and Applications vol. 20*, issue 4 (July 1999), 1083–1098.

[29] GENG, H., XU, D., WU, B., AND YANG, G. Active Damping for PMSG-Based WECS With DC-Link Current Estimation. *IEEE Transactions on Industrial Electronics vol. 58*, issue 4 (Apr. 2011), 1110–1119.

[30] GOLUB, G. H., AND VAN LOAN, C. F. *Matrix Computations*, 4th ed. The Johns Hopkins University Press, Baltimore, 2013.

[31] GUAN, Y., VASQUEZ, J. C., GUERRERO, J. M., WU, D., FENG, W., AND WANG, Y. Frequency Stability of Hierarchically Controlled Hybrid Photovoltaic-Battery-Hydropower Microgrids. In *Proceedings of the 2014 IEEE Energy Conversion Congress and Exposition (ECCE)* (Pittsburgh, USA, Sept. 2014), pp. 1573–1580.

[32] HE, P., WEN, F., LEDWICH, G., AND XUE, Y. Small Signal Stability Analysis of Power Systems with High Penetration of Wind Power. *Journal of Modern Power Systems and Clean Energy vol. 1*, issue 3 (Oct. 2013), 241–248.

[33] HENRY, G., WATKINS, D., AND DONGARRA, J. A Parallel Implementation of the Nonsymmetric QR Algorithm for Distributed Memory Architectures. *SIAM Journal on Scientific Computing vol. 24*, issue 1 (2002), 284–311.

[34] HOWELL, G. W., AND DIAA, N. BHESS: Gaussian Reduction to a Similar Banded Hessenberg Form. *ACM Transactions on Mathematical Software vol. 31*, issue 1 (Mar. 2005), 166–185.

[35] HUANG, H., MAO, C., LU, J., AND WANG, D. Small-Signal Modelling and Analysis of Wind Turbine with Direct Drive Permanent Magnet Synchronous Generator Connected to Power Grid. *IET Renewable Power Generation vol. 6*, issue 1 (Jan. 2012), 48–58.

[36] IEA (INTERNATIONAL ENERGY AGENCY). *Africa Energy Outlook 2014*. IEA Publications, Paris, Oct. 2014.

[37] IEA (INTERNATIONAL ENERGY AGENCY). *World Energy Outlook 2014*. IEA Publications, Paris, Nov. 2014.

[38] IEEE POWER ENGINEERING SOCIETY. *IEEE Recommended Practice for Excitation System Models for Power System Stability Studies (IEEE Std 421.5-2005)*. 2006.

[39] ISSA, W. R., ABUSARA, M. A., AND SHARKH, S. M. Control of Transient Power During Unintentional Islanding of Microgrids. *IEEE Transactions on Power Electronics vol. 30*, issue 8 (Aug. 2015), 4573–4584.

[40] JACOB, T. *Evaluation sur Modèle Réduit et Prédiction de la Stabilité de Fonctionnement des Turbines Francis*. Ph.D. dissertation, École Polytechnique Fédérale de Lausanne, Switzerland, 1993.

[41] JAEGER, C. *Fluid Transients in Hydro-Electric Engineering Practice*. Blackie, Glasgow, U.K., 1977.

[42] JAMEHBOZORG, A., AND RADMAN, G. Small Signal Analysis of Power Systems With Wind and Energy Storage Units. *IEEE Transactions on Power Systems vol. 30*, issue 1 (Jan. 2015), 298–305.

[43] KABERERE, K., FOLLY, K., NTOMBELA, M., AND PETROIANU, A. Comparative Analysis and Numerical Validation of Industrial-Grade Power System Simulation Tools: Application to Small-Signal Stability. In *15th Power Systems Computation Conference (PSCC)* (Liège, Belgium, Aug. 2005), pp. 1–7.

[44] KAHROBAEIAN, A., AND MOHAMED, Y. A.-R. I. Analysis and Mitigation of Low-Frequency Instabilities in Autonomous Medium-Voltage Converter-Based Microgrids With Dynamic Loads. *IEEE Transactions on Industrial Electronics vol. 61*, issue 4 (Apr. 2014), 1643–1658.

[45] KAMWA, I., GRONDIN, R., AND TRUDEL, G. IEEE PSS2b versus PSS4b: The Limits of Performance of Modern Power System Stabilizers. *IEEE Transactions on Power Systems vol. 20*, issue 2 (May 2005), 903–915.

[46] KAMWA, I., LEFEBVRE, D., AND LOUD, L. Small Signal Analysis of Hydro-Turbine Governors in Large Interconnected Power Plants. In *Proceedings of the IEEE Power Engineering Society Winter Meeting* (New York, USA, Jan. 2002), vol. vol. 2, pp. 1178–1183.

[47] KAWKABANI, B. Extension of the Complex Torque Coefficient Method for Synchronous Generators to Auxiliary Devices in Electrical Networks. In *EPE'2001, 9th European Conference on Power Electronics and Applications* (Graz, Austria, Aug. 2001).

[48] KHALIL, H. K. *Nonlinear Systems*, 3rd ed. Prentice Hall, Upper Saddle River, NJ, 2002.

[49] KONIDARIS, D. N., AND TEGOPOULOS, J. A. Investigation of Oscillatory Problems of Hydraulic Generating Units Equipped with Francis Turbines. *IEEE Transactions on Energy Conversion vol. 12*, issue 4 (Dec. 1997), 419–425.

[50] KTH ROYAL INSTITUTE OF TECHNOLOGY. PST (Power System Toolbox) and MatNetEig. Available from: http://tinyurl.com/PST-MatNetEig [accessed on 16 May 2015], 2015.

[51] KUNDUR, P. *Power System Stability and Control.* McGraw-Hill, New York, 1994.

[52] KUNDUR, P., PASERBA, J., AJJARAPU, V., ANDERSSON, G., BOSE, A., CANIZARES, C., HATZIARGYRIOU, N., HILL, D., STANKOVIC, A., TAYLOR, C., VAN CUTSEM, T., AND VITTAL, V. Definition and Classification of Power System Stability: IEEE/CIGRE Joint Task Force on Stability Terms and Definitions. *IEEE Transactions on Power Systems vol. 19*, issue 2 (Aug. 2004), 1387–1401.

[53] KUNDUR, P., ROGERS, G. J., WONG, D. Y., WANG, L., AND LAUBY, M. G. A Comprehensive Computer Program Package for Small Signal Stability Analysis of Power Systems. *IEEE Transactions on Power Systems vol. 5*, issue 4 (Nov. 1990), 1076–1083.

[54] LAM, D. M., YEE, H., AND CAMPBELL, B. An Efficient Improvement of the AESOPS Algorithm for Power System Eigenvalue Calculation. *IEEE Transactions on Power Systems vol. 9*, issue 4 (Nov. 1994), 1880–1885.

[55] LANDRY, C., FAVREL, A., MÜLLER, A., NICOLET, C., YAMAMOTO, K., AND AVELLAN, F. Experimental Investigation of the Local Wave Speed in a Draft Tube with Cavitation Vortex Rope. *IOP Conf. Ser.: Earth Environ. Sci. vol. 22*, issue 3 (Mar. 2014), 1–8.

[56] LAVRETSKY, E., AND WISE, K. A. Lyapunov Stability of Motion. In *Robust and Adaptive Control*, Advanced Textbooks in Control and Signal Processing. Springer-Verlag, London, 2013, pp. 225–261.

[57] LAY, D. C. *Linear Algebra and its Applications*, 4th ed. Pearson Education, New York, 2012.

[58] LEHOUCQ, R., AND SORENSEN, D. Deflation Techniques for an Implicitly Restarted Arnoldi Iteration. *SIAM. J. Matrix Anal. & Appl. vol. 17*, issue 4 (Oct. 1996), 789–821.

[59] LEHOUCQ, R., SORENSEN, D., AND YANG, C. The Implicitly Restarted Arnoldi Method. In *ARPACK Users' Guide: Solution of Large-Scale Eigenvalue Problems with Implicitly Restarted Arnoldi Methods*. SIAM (Society for Industrial and Applied Mathematics), USA, 1998, pp. 43–66.

[60] LIU, X., AND LIU, C. Eigenanalysis of Oscillatory Instability of a Hydropower Plant Including Water Conduit Dynamics. *IEEE Transactions on Power Systems vol. 22*, issue 2 (May 2007), 675–681.

[61] MA, J., DONG, Z. Y., AND ZHANG, P. Comparison of BR and QR Eigenvalue Algorithms for Power System Small Signal Stability Analysis. *IEEE Transactions on Power Systems vol. 21*, issue 4 (Nov. 2006), 1848–1855.

[62] MACHOWSKI, J., BIALEK, J. W., AND BUMBY, J. R. *Power System Dynamics: Stability and Control*, 2nd ed. John Wiley & Sons, Inc., Chichester, UK, 2008.

[63] MAKAROV, Y. V., DONG, Z. Y., AND WEBSTER (ED.), J. Eigenvalues and Eigenfunctions. In *Wiley Encyclopedia of Electrical and Electronics Engineering*. John Wiley & Sons, Inc., Chichester, UK, 1999, pp. 208–220.

[64] MARTINS, N., AND SANCHES BOSSA, T. H. A Modal Stabilizer for the Independent Damping Control of Aggregate Generator and Intraplant Modes in Multigenerator Power Plants. *IEEE Transactions on Power Systems vol. 29*, issue 6 (Nov. 2014), 2646–2661.

[65] MILANO, F. An Open Source Power System Analysis Toolbox. *IEEE Transactions on Power Systems vol. 20*, issue 3 (Aug. 2005), 1199–1206.

[66] MILANO, F. PSAT (Power System Analysis Toolbox). Available from: http://faraday1.ucd.ie/psat.html [accessed on 16 May 2015], 2015.

[67] MISHRA, S., AND RAMASUBRAMANIAN, D. Improving the Small Signal Stability of a PV-DE-Dynamic Load-Based Microgrid Using an Auxiliary Signal in the PV Control Loop. *IEEE Transactions on Power Systems vol. 30*, issue 1 (Jan. 2015), 166–176.

[68] NEPLAN AG. NEPLAN® Small Signal Stability Module. Available from: http://www.neplan.ch/description/small-signal-stability-2 [accessed on 16 May 2015], 2015.

[69] NICOLET, C. *Hydroacoustic Modelling and Numerical Simulation of Unsteady Operation of Hydroelectric Systems.* Ph.D. dissertation, École Polytechnique Fédérale de Lausanne, Switzerland, 2007.

[70] NICOLET, C., ALLIGNÉ, S., KAWKABANI, B., KOUTNIK, J., SIMOND, J.-J., AND AVELLAN, F. Stability Study of Francis Pump-Turbine at Runaway. In *3rd IAHR International Meeting of the Workgroup on Cavitation and Dynamic Problems in Hydraulic Machinery and Systems* (Brno, Czech Republic, Oct. 2009), pp. 371–384.

[71] NICOLET, C., GREIVELDINGER, B., HEROU, J.-J., KAWKABANI, B., ALLENBACH, P., SIMOND, J.-J., AND AVELLAN, F. High-Order Modeling of Hydraulic Power Plant in Islanded Power Network. *IEEE Transactions on Power Systems vol. 22*, issue 4 (Nov. 2007), 1870–1880.

[72] NICOLET, C., HEROU, J.-J., GREIVELDINGER, B., ALLENBACH, P., SIMOND, J.-J., AND AVELLAN, F. Methodology for Risk Assessment of Part Load Resonance in Francis Turbine Power Plant. In *IAHR Int. Meeting of WG on Cavitation and Dynamic Problems in Hydraulic Machinery and Systems* (Barcelona, June 2006), pp. 1–16.

[73] OCHS, K. A Note on Stability of Linear Time-Variant Electrical Circuits Having Constant Eigenvalues. *International Journal of Circuit Theory and Applications vol. 41*, issue 9 (Sept. 2013), 960–971.

[74] PAGOLA, F. L., PÉREZ-ARRIAGA, I. J., AND VERGHESE, G. C. On Sensitivities, Residues and Participations: Applications to Oscillatory Stability Analysis and Control. *IEEE Transactions on Power Systems vol. 4*, issue 1 (Feb. 1989), 278–285.

[75] PANNATIER, Y. *Optimisation des Stratégies de Réglage d'une Installation de Pompage-Turbinage à Vitesse Variable.* Ph.D. dissertation, École Polytechnique Fédérale de Lausanne, Switzerland, 2010.

[76] PAYNTER, H. M. Surge and Water Hammer Problems. *Trans. ASCE vol. 146* (1953), 962–1009.

[77] PERSSON, J., SODER, L., SLOOTWEG, J., ROUCO, L., AND KLING, W. A Comparison of Eigenvalues Obtained with Two Dynamic Simulation Software Packages. In *Proceedings of the 2003 IEEE Power Tech Conference* (Bologna, Italy, June 2003), vol. vol. 2, pp. 1–6.

[78] POWERTECH LABS INC. DSATools™ SSAT. Available from: http://www.dsatools.com/html/prod_ssat.php [accessed on 16 May 2015], 2015.

[79] PÉREZ-ARRIAGA, I. J. *Selective Modal Analysis with Applications to Electric Power Systems.* Ph.D. dissertation, Massachussets Institute of Technology, Cambridge, MA, USA, June 1981.

[80] PÉREZ-ARRIAGA, I. J., PAGOLA, F. L., VERGHESE, G. C., AND SCHWEPPE, F. C. Selective Modal Analysis in Power Systems. In *American Control Conference* (San Francisco, CA, USA, June 1983), pp. 650–655.

[81] PÉREZ-ARRIAGA, I. J., VERGHESE, G. C., AND SCHWEPPE, F. C. Selective Modal Analysis with Applications to Electric Power Systems, Part I: Heuristic Introduction. *IEEE Transactions on Power Apparatus and Systems vol. PAS-101*, issue 9 (Sept. 1982), 3117–3125.

[82] REN21. 2014. *Renewables 2014 Global Status Report.* REN21 Secretariat, Paris, 2014.

[83] RHEINGANS, W. J. Power Swings in Hydroelectric Power Plants. *Transactions of the ASME vol. 62* (Apr. 1940), 171–184.

[84] ROMMES, J., AND MARTINS, N. Computing Large-Scale System Eigenvalues Most Sensitive to Parameter Changes, With Applications to Power System Small-Signal Stability. *IEEE Transactions on Power Systems vol. 23*, issue 2 (May 2008), 434–442.

[85] ROMMES, J., MARTINS, N., AND FREITAS, F. D. Computing Rightmost Eigenvalues for Small-Signal Stability Assessment of Large-Scale Power Systems. *IEEE Transactions on Power Systems vol. 25*, issue 2 (May 2010), 929–938.

[86] ROUCO, L. Eigenvalue-based Methods for Analysis and Control of Power System Oscillations. In *IEE Colloquium on Power System Dynamics Stabilisation (Digest No. 1998/196 and 1998/278)* (Coventry, England, Feb. 1998), IET, pp. 3/1–3/6.

[87] RUGH, W. J. *Linear System Theory*, 2nd ed. Prentice Hall, Upper Saddle River, NJ, 1996.

[88] SAAD, Y. Variations on Arnoldi's Method for Computing Eigenelements of Large Unsymmetric Matrices. *Linear Algebra and Its Applications vol. 34*, issue 1 (June 1981), 184–198.

[89] SAPIN, A. *Logiciel Modulaire pour la Simulation et l'Etude des Systèmes d'Entraînement et des Réseaux Electriques.* Ph.D. dissertation, École Polytechnique Fédérale de Lausanne, Switzerland, 1995.

[90] SARMADI, S. A. N., AND VENKATASUBRAMANIAN, V. Inter-Area Resonance in Power Systems From Forced Oscillations. *IEEE Transactions on Power Systems vol. PP (Early Access Articles)*, issue 99 (2015), 1–9.

[91] SAUER, P. W., RAJAGOPALAN, C., AND PAI, M. A. An Explanation and Generalization of the AESOPS and PEALS Algorithms. *IEEE Transactions on Power Systems vol. 6*, issue 1 (Feb. 1991), 293–299.

[92] SCHOOL OF ELECTRICAL AND ELECTRONIC ENGINEERING, THE UNIVERSITY OF ADELAIDE. Mudpack, An Interactive Software Package for Investigating the Small-Signal Dynamic Performance of Multi-Machine Power Systems. Available from: http://tinyurl.com/MudpackSSS [accessed on 16 May 2015], 2015.

[93] SEMLYEN, A., AND WANG, L. Sequential Computation of the Complete Eigensystem for the Study Zone in Small Signal Stability Analysis of Large Power Systems. *IEEE Transactions on Power Systems vol. 3*, issue 2 (May 1988), 715–725.

[94] SIEMENS PTI. PSS®E, Power Transmission System Planning. Available from: http://tinyurl.com/PSSE-NEVA [accessed on 16 May 2015], 2015.

[95] SILVA, P. C. O., ALLIGNE, S., ALLENBACH, P., NICOLET, C., AND KAWKABANI, B. A Fully Modular Tool for Small-Signal Stability Analysis of Hydroelectric Systems. In *2014 International Conference on Electrical Machines (ICEM)* (Sept. 2014), pp. 1697–1703.

[96] SILVA, P. C. O., KAWKABANI, B., ALLIGNÉ, S., NICOLET, C., SIMOND, J.-J., AND AVELLAN, F. Stability Study on Hydroelectric Production Site Using Eigenvalues Analysis Method. *Journal of Energy and Power Engineering vol. 6* (June 2012), 940–948.

[97] SOLVINA AB. Simpow®, Simulation of Power Systems. Available from: http://www.solvina.se/simpow/technical-info [accessed on 16 May 2015], 2015.

[98] SOUZA JR., O. H., BARBIERI, N., AND SANTOS, A. H. M. Study of Hydraulic Transients in Hydropower Plants through Simulation of Nonlinear Model of Penstock and Hydraulic Turbine Model. *IEEE Transactions on Power Systems vol. 14*, issue 4 (Nov. 1999), 1269–1272.

[99] STEINMETZ, C. P. Power Control and Stability of Electric Generating Stations. *AIEE Transactions vol. 39* (July 1920), 1215–1287.

[100] SUN, J. Small-Signal Methods for AC Distributed Power Systems – A Review. *IEEE Transactions on Power Electronics vol. 24*, issue 11 (Nov. 2009), 2545–2554.

[101] TRACTEBEL ENGINEERING. HERCULES, an EUROSTAG® Add-on. Available from: http://www.eurostag.be/en/products/eurostag/functions/small-signal/small-signal-analysis [accessed on 16 May 2015], 2015.

[102] VERGHESE, G. C., PÉREZ-ARRIAGA, I. J., AND SCHWEPPE, F. C. Selective Modal Analysis With Applications to Electric Power Systems, Part II: The Dynamic Stability Problem. *IEEE Transactions on Power Apparatus and Systems vol. PAS-101*, issue 9 (Sept. 1982), 3126–3134.

[103] WANG, H., MINGLI, W., AND SUN, J. Analysis of Low-Frequency Oscillation in Electric Railways Based on Small-Signal Modeling of Vehicle-Grid System in dq Frame. *IEEE Transactions on Power Electronics vol. 30*, issue 9 (Sept. 2015), 5318–5330.

[104] WANG, L., HOWELL, F., KUNDUR, P., CHUNG, C., AND XU, W. A Tool for Small-Signal Security Assessment of Power Systems. In *PICA2001: Proceedings of the 22nd IEEE Power Engineering Society International Conference on Power Industry Computer Applications* (Sydney, Australia, May 2001), pp. 246–252.

[105] WANG, L., AND SEMLYEN, A. Application of Sparse Eigenvalue Techniques to the Small Signal Stability Analysis of Large Power Systems. *IEEE Transactions on Power Systems vol. 5*, issue 2 (May 1990), 635–642.

[106] WORKING GROUP ON PRIME MOVER AND ENERGY SUPPLY MODELS FOR SYSTEM DYNAMIC PERFORMANCE STUDIES. Hydraulic Turbine and Turbine Control Models for System Dynamic Studies. *IEEE Transactions on Power Systems vol. 7*, issue 1 (Feb. 1992), 167–179.

[107] WYLIE, E. B., AND STREETER, V. L. *Fluid Transients in Systems*. Prentice Hall, Englewood Cliffs, NJ, 1993.

[108] ZHAO, W., YAN, Z., AND FANG, X. Application of an Improved BHESS-BR Method to the Small Signal Stability Analysis of Power Systems. *International Transactions on Electrical Energy Systems vol. 25*, issue 4 (Apr. 2015), 661–677.

[109] ZHOU, J., AND WANG, Y. Effect of Water Elasticity in Hydropower's Pressurized Pipeline on Stability of Low Frequency Oscillation. In *DRPT2008: Proceedings of the Third International Conference on Electric Utility Deregulation and Restructuring and Power Technologies* (Nanjing, China, Apr. 2008), pp. 745–750.

[110] ZHU, J. J. A Note on Extension of the Eigenvalue Concept. *IEEE Control Systems vol. 13*, issue 6 (Dec. 1993), 68–70.

List of Symbols

Acronyms

AVR	Automatic voltage regulator
CIGRÉ	International Council on Large Electric Systems (*Conseil International des Grands Réseaux Électriques*)
DDPM	Direct drive permanent magnet synchronous machine
DFIG	Doubly-fed induction generator
EPFL	Ecole Polytechnique Fédérale de Lausanne, in Switzerland
GUI	Graphical user interface
GVO	Guide vanes opening
HVDC	High-voltage direct current
IEA	International Energy Agency
IEEE	Institute of Electrical and Electronics Engineers
IM	Induction machine
LP	Linear periodic system
LTI	Linear time-invariant system
LTV	Linear time-variant system
OECD	Organization for Economic Co-operation and Development
PID	Proportional-integral-derivative

PSS	Power system stabilizer
PV	Photovoltaics
SCIG	Squirrel-cage induction generator
SIMSEN	Simulation Software for Energy Systems (*SIMulateur Modulaire pour Systèmes ENergetiques électriques*)
SM	Synchronous machine
TG	Turbine governor

Greek

$\delta\omega$	Generator speed deviation (PSS input)	[p.u.]
λ	Local loss coefficient	[–]
λ_i	i-th eigenvalue of a matrix	[–]
μ	Induction machine stator-rotor turns ratio	[–]
μ_{eq}	Equivalent viscoelastic damping	[Pa·s]
ν	Specific speed of the turbine	[–]
Ω	Mechanical angular speed	[rad/s]
ω_0	Natural frequency of an eigenmode	[rad/s]
ω_a	Angular frequency of the rotating reference frame	[rad/s]
ω_d	Damped frequency of an eigenmode ($\omega_d = \Im\{\lambda_i\}$)	[rad/s]
ω_m	Angular speed	[rad/s]
ω_N	Nominal angular frequency on the network ($\omega_N = 2\pi f_N$)	[rad/s]
ρ	Density of a fluid	[kg/m^3]
σ	Attenuation of an eigenmode ($\sigma = \Re\{\lambda_i\}$)	[Np/s]
τ	Damping time constant related to an eigenvalue	[s]
θ	Angular position of the rotor of a synchronous machine	[rad]
θ_m	Relative angular position of the rotor of an induction machine	[rad]

ζ	Damping ratio of an eigenmode	[–]

Latin

$\bar{A}$	Turbine mean cross section	[m^2]
A	Cross section of a pipe	[m^2]
a	Wave speed of the water in a pipe	[m/s]
c	Water flow velocity	[m/s]
C'_e	Transmission line lineic capacitance	[F/m]
C'_h	Hydroacoustic lineic capacitance	[m]
C_r	Courant number	[–]
$C_{\phi n}$	Transmission line phase-to-ground capacitance	[F]
$C_{\phi\phi}$	Transmission line phase-to-phase capacitance	[F]
C_{ST}	Surge tank equivalent capacitance	[m^2]
D	Diameter of a pipe	[m]
D_{ref}	Turbine reference diameter	[m]
E_{FD}	Output of the AVR IEEE ST1A	[p.u.]
f_{turb}	Turbine rotational frequency	[Hz]
f_{VRlow}	Lower value of the vortex rope pulsation frequency	[Hz]
f_{VRupp}	Upper value of the vortex rope pulsation frequency	[Hz]
g	Gravitational acceleration ($g \simeq 9.81$ m/s^2)	[m/s^2]
G_{tg}	Transfer function of a turbine governor	[–]
h	Piezometric head	[mWC]
h_c	Surge tank piezometric head	[mWC]
h_d	Surge tank head losses	[mWC]
H_I	Turbine inlet head	[mWC]

H_t	Turbine equivalent pressure source	[mWC]
$H_{\bar{I}}$	Turbine outlet head	[mWC]
h_{ST}	Surge tank total head	[mWC]
H_{turb}	Turbine net head	[mWC]
$I_{f\delta 0}$	Synchronous machine no-load excitation current	[A]
J	Moment of inertia	[kg·m^2]
K_p	Proportional gain	[–]
$\overline{L}$	Mean value of L_{aa}	[H]
L'_e	Transmission line lineic inductance	[H/m]
L'_h	Hydroacoustic lineic inductance	[s^2/m^3]
L_D	Damper D winding self-inductance	[H]
L_d	Self-inductance on the d-axis	[H]
L_f	Excitation winding self-inductance	[H]
L_o	Self-inductance on the Zero phase-sequence axis	[H]
L_Q	Damper Q winding self-inductance	[H]
L_q	Self-inductance on the q-axis	[H]
L_r	Induction machine rotor self-inductance	[H]
L_s	Induction machine stator self-inductance	[H]
L_t	Turbine hydroacoustic inductance	[s^2/m^2]
L_{11m}	Power transformer primary mutual inductance	[H]
L_{11}	Power transformer primary winding self-inductance	[H]
L_{12m}	Power transformer mutual inductance between primary and secondary	[H]
L_{12}	Power transformer mutual inductance between primary and secondary	[H]
L_{22m}	Power transformer secondary mutual inductance	[H]
L_{22}	Power transformer secondary winding self-inductance	[H]

L_{aa}	Self-inductance of synchronous machine stator phase a	[H]
L_{Da}	Mutual inductance between damper D and stator windings	[H]
L_{Df}	Mutual inductance between damper D and excitation windings	[H]
l_{eq}	Turbine equivalent length	[m]
L_{fa}	Mutual inductance between excitation and stator windings	[H]
L_{h2}	Amplitude of the oscillating component of L_{aa}	[H]
L_{or}	Induction machine rotor leakage inductance	[H]
L_{os}	Induction machine stator leakage inductance	[H]
L_{Qa}	Mutual inductance between damper Q and stator windings	[H]
L_{sr}	Induction machine mutual inductance between stator and rotor windings	[H]
L_{tlm}	Transmission line mutual inductance	[H]
L_{tl}	Transmission line self-inductance	[H]
n	Rotational speed	[rpm]
N_{11}	Francis turbine speed factor	[rpm·m$^{1/2}$]
P_p	Number of pairs of poles	[–]
p_{el}	Generator active power	[p.u.]
p_{ji}	Participation factor of the j-th state variable in the i-th mode	[–]
Q	Water discharge	[m^3/s]
Q_c	Surge tank stored discharge	[m^3/s]
Q_{11}	Francis turbine discharge factor	[m$^{1/2}$/s]
$Q_{ST_{i+1}}$	Surge tank downstream discharge	[m^3/s]
Q_{ST_i}	Surge tank upstream discharge	[m^3/s]
r'_2	Power transformer secondary winding resistance	[p.u.]
R'_e	Transmission line lineic resistance	[Ω/m]
R'_h	Hydroacoustic lineic resistance	[s/m^3]

r'_r	Rotor windings resistance	[p.u.]
R_1	Power transformer primary winding resistance	[Ω]
r_1	Power transformer primary winding resistance	[p.u.]
R_2	Power transformer secondary winding resistance	[Ω]
R_D	Equivalent damper D winding resistance	[Ω]
R_d	Surge tank equivalent resistance	[s/m^2]
r_D	Equivalent damper D winding resistance	[p.u.]
R_f	Excitation winding resistance	[Ω]
r_f	Excitation winding resistance	[p.u.]
R_Q	Equivalent damper Q winding resistance	[Ω]
r_Q	Equivalent damper Q winding resistance	[p.u.]
R_r	Induction machine rotor winding resistance	[Ω]
R_s	Stator winding resistance	[Ω]
r_s	Stator winding resistance	[p.u.]
R_t	Turbine equivalent resistance	[s/m^2]
r_{cc}	Power transformer short-circuit resistance	[p.u.]
R_{tl}	Transmission line resistance	[Ω]
R_{ve}	Hydroacoustic viscoelastic resistance	[s/m^2]
s	Induction machine slip	[–]
S_{sc}	Short-circuit power	[MVA]
T''_d	Subtransient short-circuit time constant in the d-axis	[s]
T''_q	Subtransient short-circuit time constant in the q-axis	[s]
T'_s	Transient short-circuit time constant of induction machine stator	[s]
T_a	Armature short-circuit time constant	[s]
T_D	Short-circuit time constant of the equivalent damper winding D	[s]

T_d	Derivative time constant	[s]
T_f	Filter time constant	[s]
T_i	Integral time constant	[s]
T_{11}	Francis turbine torque factor	[N/m^3]
T_{cc}	Power transformer short-circuit time constant	[s]
T_{em}	Electromagnetic torque	[N·m]
T_{h1}	Power transformer magnetizing time constant	[s]
T_{turb}	Turbine torque	[N·m]
u_g	Generator filtered voltage for the Unitrol®	[p.u.]
u_m	Generator terminal voltage	[p.u.]
u_{C1}	Internal variable of the Unitrol®	[p.u.]
u_{C2}	Internal variable of the Unitrol®	[p.u.]
u_{PSS}	PSS output	[p.u.]
u_{reg1}	Internal variable of the AVR IEEE ST1A	[p.u.]
u_{reg}	Output of the Unitrol®	[p.u.]
$u_{s1...14}$	Internal variables of the stabilizer IEEE PSS2B	[p.u.]
u_{set}	AVR voltage set-point	[p.u.]
$V(t,x)$	Energetic function related to Lypaunov stability definition	[–]
V_A	Internal variable of the AVR IEEE ST1A	[p.u.]
V_C	Generator filtered voltage for the AVR IEEE ST1A	[p.u.]
$W_{1...3}(x)$	Boundary functions related to Lypaunov stability definition	[–]
$x'_{\sigma 2}$	Power transformer secondary winding leakage reactance	[p.u.]
$x'_{\sigma r}$	Leakage reactance of rotor windings	[p.u.]
$x_{\sigma 1}$	Power transformer primary winding leakage reactance	[p.u.]
$x_{\sigma Df}$	Mutual reactance between excitation and damper D	[p.u.]

$x_{\sigma D}$	Leakage reactance of damper winding D	[p.u.]
$x_{\sigma f}$	Leakage reactance of excitation winding	[p.u.]
$x_{\sigma Q}$	Leakage reactance of damper winding Q	[p.u.]
$x_{\sigma s}$	Leakage reactance of stator winding	[p.u.]
x_{ad}	Magnetizing reactance in the d–axis	[p.u.]
x_{aq}	Magnetizing reactance in the q–axis	[p.u.]
x_{cc}	Power transformer short-circuit reactance	[p.u.]
x_{h1}	Power transformer three-phase magnetizing reactance	[p.u.]
x_{hs}	Magnetizing reactance	[p.u.]
y	Guide vanes opening	[–]
y_2	Internal variable of the AVR IEEE ST1A	[p.u.]
y_3	Internal variable of the AVR IEEE ST1A	[p.u.]

Matrices and Vectors

$\mathbf{A}_\ell$	Linearized state matrix of a system
$\mathbf{A}$	State matrix
$\mathbf{B}_\ell$	Linearized input matrix of a system
$\mathbf{C}_\ell$	Linearized output matrix of a system
$\mathbf{D}_\ell$	Linearized feedforward matrix of a system
$\mathbf{I}$	Identity matrix
Λ	Matrix containing the eigenvalues of a system ($\Lambda = \mathrm{diag}(\lambda_1, \ldots, \lambda_n)$)
$\mathbf{P}$	Park's transformation
$\mathbf{Q}$	Orthogonal matrix involved in the QR factorization algorithm
$\mathbf{T}$	Upper-triangular matrix involved in the QR factorization algorithm
$\mathbf{u}(t)$	Input vector of a system

$\mathbf{V}$	Matrix containing the right eigenvectors of a system ($\mathbf{V} = [\ \mathbf{v}_1\ \ \mathbf{v}_2\ \ \cdots\ \ \mathbf{v}_n\ ]$)
$\mathbf{v}_i$	Right eigenvector related to the i-th eigenvalue (λ_i) of a matrix
$\mathbf{W}$	Matrix containing the left eigenvectors of a system ($\mathbf{W} = \left[\ \mathbf{w}_1^T\ \ \mathbf{w}_2^T\ \ \cdots\ \ \mathbf{w}_n^T\ \right]^T$)
$\mathbf{w}_i$	Left eigenvector related to the i-th eigenvalue (λ_i) of a matrix
$\mathbf{x}(t)$	State vector of a system ($\mathbf{x} = [\ x_1\ \ x_2\ \ \cdots\ \ x_n\ ]^T$)
$\mathbf{y}(t)$	Output vector of a system

Subscripts

0	Equilibrium point
1	Power transformer primary side
2	Power transformer secondary side
ABC	Induction machine rotor windings
abc	Phase (abc) coordinates
a	Stator phase a
b	Stator phase b
c	Stator phase c
D	Equivalent damper winding in the d-axis
d	Direct axis (d-axis)
dqo	Park's (dqo) coordinates
f	Excitation (field)
ℓ	Linearized
o	Zero phase-sequence axis
Q	Equivalent damper winding in the q-axis
q	Quadrature axis (q-axis)
s	Stator
set	Set-point
tl	Transmission line

List of Figures

1.1 Worldwide electricity generation forecast by source 4

1.2 Share of energy production by source and by region 5

1.3 Intermittency of wind and solar PV in Germany in 2010 6

1.4 Classification of power system stability 10

1.5 Part load vortex rope in the draft tube and its pulsation frequency range 11

1.6 Elements for the representation of a hydropower plant and the grid 14

3.1 Interpretation of Lyapunov stability and asymptotic stability 30

4.1 Self-inductance for phase a of a salient-pole synchronous machine 42

4.2 Simplified representation of a salient-pole synchronous machine 42

4.3 Procedure flowchart for determination of small-signal models for SIMSEN . . . 45

5.1 Current loops construction in SIMSEN 54

5.2 Synchronous machine connected to an infinite bus 54

5.3 Direct- and quadrature-axis equivalent circuit for the synchronous machine . . 55

5.4 Power fluctuation due to the local mode oscillation 58

5.5 Damping of the excitation current related to the corresponding eigenvalue . . . 58

5.6 Induction connected to an infinite bus 59

5.7 Equivalent circuit of the induction machine 60

5.8 Power fluctuation on induction gen. due to the local mode oscillation 61

5.9 Exponential damping of the aperiodic component in the reactive power 61

5.10 *Yd5*-transformer – generator – infinite bus system 62

5.11 Equivalent circuit of a power transformer 63

5.12 Equivalent circuit of the transformer seen from the magnetizing branch 64

5.13 RLC load 66

5.14 Sinusoidal envelope and its exponential damping for a RLC load 67

5.15 Resistive-inductive transmission line 68

5.16 Three-phase scheme of a π-section transmission line element 69

5.17 IEEE ST1A voltage regulator 70

5.18 Block diagram of the Unitrol® voltage regulator 71

5.19 Example of synchronous generator with automatic voltage regulator 71

5.20 Electrical power pulsation of the system with AVR and short transmission line . 73

5.21 IEEE PSS2B power system stabilizer with filtered inputs 73

5.22 Example of synchronous generator with automatic voltage regulator 74

5.23 Electrical power pulsation with AVR and PSS 76

6.1 Model of a pipe of length dx 78

6.2 Equivalent scheme of a pipe of length dx 80

6.3 Turbine characteristics for different guide vane opening values 81

6.4 Francis turbine model (left) and equivalent scheme (right) 81

6.5 Surge tank model (left) and equivalent scheme (right) 82

6.6 Turbine governor block diagram 83

7.1 Layout of the islanded hydroelectric power plant 90

7.2 Electrical power behavior for different values of short-circuit power 96

7.3 Evolution of local mode with the PSS gain K_{s1}, considering the critical scenario 97

7.4 Electrical power response without and with PSS ($K_{s1} = 20$), in the critical scenario 99

7.5 Most relevant hydraulic mode shapes 100

7.6 Turbine net head and torque for the hydraulic and hydroelectric models 102

7.7 Participation factors color map plot for the hydroelectric system, with enhanced tuning of turbine governor, without PSS 105

7.8 Turbine net head and torque with initial and enhanced tuning of the governor . 106

7.9 Electrical power response with initial and enhanced tuning of the governor . . 106

7.10 Turbine net head and torque with initial and enhanced tuning of the governor, with PSS 108

7.11 Electrical power response with initial and enhanced tuning of the governor, with PSS 109

8.1 Layout of the hydroelectric powerplant 112

8.2 Electrical power swing recorded on-site with active PSS 115

8.3 On-site measurement versus time-domain simulation, without PSS 116

8.4 Frequency and attenuation time constant from time-domain results, without PSS117

8.5 On-site measurement versus time-domain simulation, PSS with reduced gain . 119

8.6 Frequency and attenuation time constant from time-domain results, with PSS . 121

8.7 Mode shapes of the local and intermachine modes, with two generating units . 123

8.8 Mode shapes of the local and intermachine modes, with three generating units 124

8.9 Mode shapes of the local and intermachine modes, with four generating units . 125

8.10 Evolution of local mode with the number of generating units 126

8.11 Mass flow oscillation and gallery 1st elastic pressure mode shapes 127

8.12 Pressure mode shapes of the penstock 1st and 2nd elastic modes 128

8.13 Pressure mode shapes of the draft tube 1st elastic modes 128

8.14 Pressure mode shapes of the draft tube 2nd elastic modes 129

8.15 Forced response of the hydraulic system 130

8.16 Turbine net head and torque response to vortex rope pulsation of 2% H_N 133

8.17 Electrical power swing due to vortex rope pulsation of 2% H_N 133

8.18 Electrical power swing due to vortex rope pulsation of 0.021% H_N 134

A.1 Resistive-inductive transmission line 164

A.2 Three-phase scheme of a π-section transmission line element 164

A.3 IEEE ST1A voltage regulator 168

A.4 Block diagram of the Unitrol® voltage regulator 169

A.5 IEEE PSS2B power system stabilizer with filtered inputs 170

List of Tables

5.1 Synchronous machine ratings 55

5.2 Parameters of the synchronous machine 55

5.3 Eigenproperties of the synchronous machine – infinite bus system 56

5.4 Induction machine ratings 59

5.5 Parameters of the induction machine 60

5.6 Eigenproperties of the induction generator machine – infinite bus system . . . 60

5.7 Power transformer ratings 62

5.8 Parameters of the *Yd5* power transformer 63

5.9 Eigenproperties of the power transformer 63

5.10 Eigenproperties of the transformer – generator – infinite bus system 64

5.11 Parameters of the RLC load 66

5.12 Eigenproperties of the RLC load 66

5.13 Parameters of RL transmission line and voltage regulator 71

5.14 Eigenproperties of the system with AVR and short transmission line 72

5.15 Parameters of the PSS2B 74

5.16 Eigenproperties of the system with PSS, AVR and step-up transformer 75

7.1 Main parameters of the electrical installation 91

7.2 Main parameters of the hydraulic installation 92

7.3 Parameters of the control and regulation elements 92

7.4 Eigenvalues of the electrical system considering the regular scenario 94

7.5 Eigenvalues of the electrical system considering the intermediate scenario . . . 95

7.6 Eigenvalues of the electrical system considering the critical scenario 95

7.7 Evolution of the local mode with the PSS gain, considering the critical scenario 97

7.8 Eigenvalues of the electrical system considering the critical scenario, with PSS ($K_{s1} = 20$) 98

7.9 Most relevant eigenvalues of the hydraulic system 99

7.10 Most relevant eigenvalues of the hydroelectric system with turbine governor, without PSS 101

7.11 Most relevant eigenvalues of the hydroelectric system with enhanced tuning of turbine governor, without PSS 103

7.12 Most relevant eigenvalues of the hydroelectric system with enhanced tuning of turbine governor, with PSS ($K_{s1} = 20$) 107

7.13 Most relevant eigenvalues of the hydroelectric system with initial tuning of turbine governor ($K_p = 1.0$; $T_f = 0.5$ s ; $T_i = 3.7$ s ; $T_d = 1.0$ s), with PSS ($K_{s1} = 20$) 108

8.1 Main parameters of the electrical installation 113

8.2 Main parameters of the hydraulic installation 114

8.3 Eigenproperties of the system with a single machine, without PSS 117

8.4 Eigenproperties of the system with a single machine, PSS with reduced gain . . 120

8.5 Local mode of one generating unit, with and without PSS 122

8.6 Electro-mechanical modes for two generating units, with and without PSS . . . 122

8.7 Electro-mechanical modes for three generating units, with and without PSS. . . 123

8.8 Electro-mechanical modes for four generating units, with and without PSS. . . 124

8.9 Most relevant eigenvalues of the hydraulic system. 127

8.10 Most relevant eigenvalues of the hydroelectric system, with and without PSS. . 131

Curriculum Vitae

Pedro Camilo DE OLIVEIRA E SILVA

Ch. des Ramiers 18
CH-1022 Chavannes-près-Renens
Switzerland

E-mail: pedro.silva@a3.epfl.ch

Nationality: Brazilian
Date of birth: June 1, 1984
Marital status: Single

EDUCATION

04/2012–09/2015 **Ph.D. in Electrical Engineering**
Ecole Polytechnique Fédérale de Lausanne (EPFL), Switzerland

09/2007–02/2009 **M.Sc. in Electrical Engineering**
Ecole Polytechnique Fédérale de Lausanne (EPFL), Switzerland

04/2002–12/2006 **Diploma in Electrical Engineering**
Federal University of Itajubá (UNIFEI), Brazil

PROFESSIONAL EXPERIENCE

04/2012–09/2015 **Teaching and Research Assistant**
Ecole Polytechnique Fédérale de Lausanne (EPFL), Switzerland

- Development of detailed mathematical models for a novel small-signal stability tool (in SIMSEN) applied to hydroelectric systems. Study of transients in hydroelectric power plants and power grids.
- Supervision of two Master projects. Teaching assistant in the courses “Electromechanical Energy Conversion”, “Electrical Machines”, “Transients of Electrical Machines” and “laboratory of Electrical Machines”.

04/2011–03/2012 **Tendering Engineer**
Alstom Renewable Ltd, Brazil

- Responsible for technical tendering of speed governing systems, and for electro-hydraulic drives for hydropower plants lifting and hydromechanical equipment.

09/2009–03/2011 **R&D and Projects Engineer**

Alstom Renewable Ltd, Brazil

- Responsible for the implementation of the standard IEC61850 for hydropower plants control systems, together with a multidisciplinary and multicultural team.
- Responsible for dealing with electrical and mechanical ancillary systems for Foz do Chapecó hydropower plant project (855 MW), in Brazil.

LANGUAGE SKILLS

Portuguese: Mother tongue.

English: Fluent reading, writing and speaking.

French: Fluent reading, writing and speaking.

Spanish: Fair reading, writing and speaking.

German: Basic knowledge.

COMPUTER SKILLS

Technical: Matlab, SIMSEN, language C.

Office tools: MS Office, MS Visio, LaTeX2ε, HTML.

PUBLICATIONS

P.C.O. Silva, S. Alligné, P. Allenbach, C. Nicolet, B. Kawkabani. "A Fully Modular Tool for Small-Signal Stability Analysis of Hydroelectric Systems". In *2014 International Conference on Electrical Machines (ICEM)*, (Berlin, Germany, Sept. 2014), pp. 1697–1703.

S. Alligné, P.C.O. Silva, A. Béguin, B. Kawkabani, P. Allenbach, C. Nicolet, F. Avellan. "Forced Response Analysis of Hydroelectric Systems". *IOP Conference Series: Earth and Environmental Science vol. 22*, issue 4 (Dec. 2014).

P.C.O. Silva, B. Kawkabani, S. Alligné, C. Nicolet, J.-J. Simond, F. Avellan. "Stability Study on Hydroelectric Production Site Using Eigenvalues Analysis Method". *Journal of Energy and Power Engineering vol. 6*, (June 2012), pp. 940–948.

P.C.O. Silva, B. Kawkabani, S. Alligné, C. Nicolet, J.-J. Simond, F. Avellan. "Stability Study of a Complete Hydroelectric Production Site by Eigenvalues Analysis Method Based on Phase Variables". *In 2010 International Conference on Electrical Machines (ICEM)*, (Rome, Italy, Sept. 2010).